ISSN: 3102-0372 (Online)

June 2026

Vol. 3, No. 1

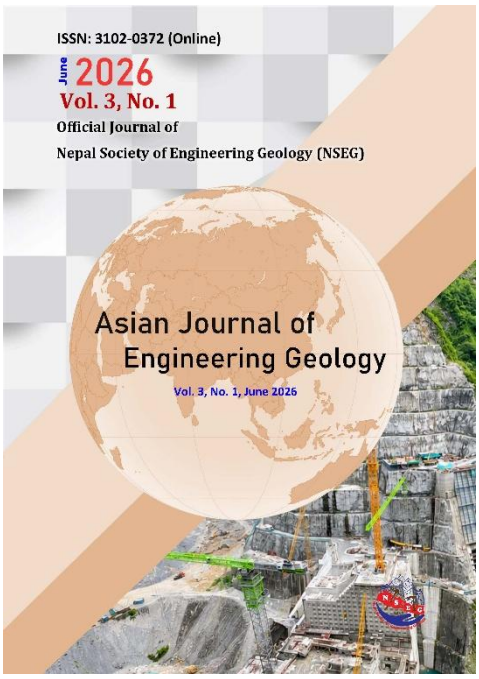
Official Journal of

Nepal Society of Engineering Geology (NSEG)

Asian Journal of Engineering Geology

Vol. 3, No. 1, June 2026





The Official Journal of Nepal Society of Engineering Geology

Asian Journal of Engineering Geology (AJEG)

Concept

The Asian Journal of Engineering Geology (**AJEG**), published by the Nepal Society of Engineering Geology (**NSEG**), is envisioned as a dedicated platform for advancing the understanding and application of engineering geology within the unique geological context of Asia, with a particular focus on the Himalayan region, while also welcoming contributions relevant to other parts of the world.

In recent years, research in engineering geology and related fields has seen significant progress. However, specialized publication platforms remain limited, especially in Asia, hindering the effective dissemination of research findings and knowledge sharing among engineering geologists. To address this gap, NSEG has launched the Asian Journal of Engineering Geology (AJEG), offering a professional and accessible forum for geoscientists, engineers, and environmentalists engaged in landslide studies, environmental geoscience, and engineering geological research.

AJEG aims to be a key resource for stakeholders seeking updated information on the geological challenges and engineering solutions relevant to seismically active and geologically complex regions like the Himalayas and beyond. The journal is committed to publishing original research, case studies, and technical notes that contribute to a deeper understanding of engineering geology in diverse terrains. Under the auspices of **NSEG**, **AJEG** places particular emphasis on:

- Slope stability and landslide hazard assessment
- Earthquake geology and seismic risk analysis
- Engineering geological aspects of infrastructure development
- Environmental and geotechnical investigations
- Integration of geological, geotechnical, and environmental knowledge for sustainable development

The journal actively promotes collaboration among researchers, engineers, and geologists from Asia and around the globe. By engaging regional experts and fostering interdisciplinary dialogue, **AJEG** seeks to address current and emerging challenges in engineering geology through shared knowledge and innovation.

In addition to peer-reviewed articles, **AJEG** will feature updates on conferences, research initiatives, and activities organized by the Nepal Society of Engineering Geology. This will position the journal not only as a scholarly publication but also as a hub for professional exchange and community building within the field of engineering geology in Nepal and across the region.

Aims and Scope

The Asian Journal of Engineering Geology (**AJEG**) serves as a common platform for the publication of integrated research covering all aspects of engineering geology. The journal welcomes original research articles, rapid reports on emerging engineering geology issues, case studies, and technical notes highlighting practical applications. Researchers and practitioners are encouraged to submit original, unpublished contributions. Subject areas include, but are not limited to, the following fields:

- Applied geomorphology
- Structural geology
- Applied geophysics and g
- Geochemistry
- Environmental geology
- Hydrogeology
- Land use planning
- Natural hazards
- Remote sensing techniques
- Soil and rock mechanics
- Applied geotechnical engineering
- Urban Engineering Geology
- Engineering Geology of marine and reservoir.
- Engineering geology in flash floods and tsunami
- Landslide hazard assessment and mapping
- GIS applications in engineering geology
- Landslide monitoring and landslide mitigation
- Engineering geology of the Himalayan slopes
- Rainfall-induced landslides
- Earthquake-induced landslides
- Anthropogenic controls on hazards
- Stability of dams and embankments
- Engineering geology of heritage areas, monitoring and mitigation
- Groundwater monitoring
- Seismic Hazard and Risk
- Disaster Risk Reduction and Management
- Engineering geology of Tunnels and bridges
- Foundations on slopes and plains

- Early warning of multi-hazard risk
- Landslide hazard management at community level
- Physical and numerical modeling in engineering geology
- High altitude engineering geological issues.
- Economics of natural hazards and related climate change
- Agricultural geology
- Snow avalanche
- Engineering geology and infrastructure development
- Snow cover in the Himalaya
- Environment friendly low cost infrastructure development
- Rural infrastructures and engineering geology
- Geotechnical engineering, modeling and ground improvement
- Nature-based solutions for disaster risk reduction

These topics suggest a multidisciplinary approach, encompassing various aspects of geology and engineering that have practical applications in fields such as environmental management, land planning, and geotechnical engineering.

Publication program

The Asian Journal of Engineering Geology (**AJEG**) publishes two issues each year. It is a peer-reviewed journal committed to disseminating the latest developments across various fields of engineering geology. **AJEG** is an open-access online journal, freely available to readers worldwide.

The Nepal Society of Engineering Geology promotes open access publishing to broaden the journal's global reach, enhance the visibility and impact of published research, and improve indexing across major search engines. Researchers and professionals from all relevant disciplines are invited to submit high-quality manuscripts presenting cutting-edge research or innovations in engineering geology and related areas. **AJEG** welcomes both individual and institutional submissions aligned with the journal's aims and scope.

Editorial Team

Editor-in-Chief

Prof. Dr. Kumud Raj Kafle
Kathmandu University, Dhulikhel, Kavre, Nepal

Associate Editor-in-Chief

Dr. Manita Timilsina
Geotech Solutions International, Dhobighat, Lalitpur, Nepal

Associate Editor-in-Chief

Dr. Badal Pokharel
School of Civil and Environmental Engineering, The University of New South Wales, Australia

Editorial Board Members

1. **Dr. Akhilesh Kumar Karna**
Institute of Engineering, Tribhuvan University, Nepal

2. **Prof. Dr. Shuichi Hasegawa**
Kagawa University, Takamatsu, Japan
Former President of Japan Society of Engineering Geology (JSEG)

3. **Prof. Dr. ATM Shakhawat Hoosain**
Jahanirnagar University, Dhaka, Bangladesh
Founding President of IAEG_Bnagladesh National Group

4. **Prof. Dr. Mian Sohail Akram**
University of Punjab, Lahore, Pakistan
Founding Secretary of Association for Engineering Geology, Pakistan – AEGP

5. **P.Geol. Gs. Abd Rasid Jaapar**
CEO of GMTGeos, Malaysia
President of Institute of Geology Malaysia (IGM) and past president of Geological Society of Malaysia (GSM) and Society for Engineering Geology and Rock Mechanics Malaysia, SEGRM (IAEG National Group of Malaysia)

6. **Dr. Kamal Regmi**
School of Mining and Geosciences, Nazarbayev University, Astana 010000, Kazakhstan

7. **Prof. Dr. Dou Jie**
China University of Geosciences, No. 388, Lumo Road, Hongshan District, Wuhan City, Hubei Province, P.R. China

8. **Dr. Debanjan Guha Roy**
Assistant Professor, Dept. of Civil and Infrastructure Engineering
Indian Institute of Technology Jodhpur (IITJ)

9. **Dr. Bingnan Li**
PEXA, Australia

10. **Dr. Mandip Subedi**
Universal Engineering College, Kathmandu, Nepal

11. **Dr. Sweata Sijapati**
GeoHazards International, USA

12. **Dr. Kanchan Chaulagain**
Underground Space Engineering Pvt. Ltd, Nepal

13. Dr. Ashish Acharya
Shimane University, Matsue, Japan

14. Ms. Manvi Kanwar
University of New South Wales, Australia

15. Dr. Sanjeev Regmi
Nepal Electricity Authority, Ratnapark, Kathmandu, Nepal

Editors for online handling

Prof. Dr. Ranjan Kumar Dahal
Tribhuvan University, Central Department of Geology, Kirtipur, Kathmandu, Nepal

Dr. Sunam Kumar Sharma
Geotech Solutions International, Dhobighat, Lalitpur, Nepal

We invite researchers specializing in engineering geology to become part of the editorial board and contribute to our publication. If you are interested in joining, kindly send an email to nsegnepal@gmail.com.

Instructions to Contributors

All manuscripts submitted for publication, including original articles, rapid reports on recent engineering geology issues, case studies, and technical notes, will undergo a rigorous peer review by at least two independent experts in the relevant field. A member of the Editorial Board may also serve as a reviewer when appropriate expertise is required.

Authors' Responsibilities

Only individuals who have made significant intellectual contributions to the content of the manuscript should be listed as authors. Authorship should be based on contributions to the conception and design of the study, active involvement in drafting or critically revising the manuscript, and participation in the final revision process.

The corresponding author is responsible for submitting the final version of the manuscript following the peer review process. Any external support, such as funding, equipment, or institutional assistance, must be clearly acknowledged in the Acknowledgment section.

In the Comments to the Editor section during submission, authors must disclose any prior or duplicate publication of the manuscript's content. All submissions to AJEG are subject to plagiarism screening, and the acceptable similarity index is limited to a maximum of 20%. Author should use given Template in the web site for preparation of manuscript.

Manuscript Preparation Overview

All submissions to the Asian Journal of Engineering Geology (AJEG) must be written in International English. Authors whose first language is not English are strongly encouraged to have their manuscripts reviewed by a native English speaker or to use a professional English editing

service prior to submission. All references, including online sources, must be formatted according to the journal's referencing guidelines outlined in this document. Each submitted article must include an abstract that briefly summarizes the key content and findings of the study. The name, institutional address, and email address of the corresponding author must be clearly indicated on the title page.

Figures and tables should be embedded within the manuscript after the list of references. Original figures should be at least half the size of A4 paper in their longest dimension. Acceptable formats for figures and images are TIFF (TIF) with a resolution of 300–600 pixels per inch (ppi). Monochrome images should be saved in grayscale mode, while color images must be in RGB mode. Only single-layer images are accepted. Authors should make every effort to avoid jargon, clearly define all nonstandard abbreviations upon first use, and present the content in a clear, concise, and accessible manner.

Manuscript Preparation Guidelines for AJEG

Authors must use the official manuscript template available on the AJEG website for preparing their submissions.

Title Page

The **title page** should include the following details:

- **Title** of the article
- **Full name(s)** of all authors (first name, middle initial(s), and surname)
- **Affiliations** of the authors, including department or division, institution or organization, city, and country. Do not use abbreviations for affiliations.
- If multiple authors share the same affiliation, list all authors first, followed by the shared affiliation.
- **Email addresses** of all authors must be included.
- The **corresponding author** should be clearly identified with an asterisk (*).

Abstract and Keywords

The manuscript should begin with an **Abstract** of approximately **300 words**, clearly summarizing:

- The research problem
- The methods used
- Major findings
- Conclusions

Immediately following the abstract, list **up to five keywords or phrases** for indexing purposes as per the template provided.

Figures, Tables, and Symbols

- Special characters, mathematical symbols, and Greek letters not available on a standard keyboard must be created using the **Symbol** font.
- **Figures and tables** should be **embedded** at appropriate locations within the text **after the list of references**.

- After the manuscript is accepted, authors must also submit **figures as separate high-resolution files**.
- Figures should follow the formatting requirements outlined in the submission guidelines (e.g., TIFF format, 300–600 dpi, RGB/grayscale mode, single-layer).

Pagination, Line Numbering, and Equations

- Authors must insert both page numbers and continuous line numbers throughout the manuscript to facilitate the review process. Page numbers should appear in the footer of each page.
- Equations should be left-aligned, with reference numbers aligned to the right margin.
- For long equations, break the right side into approximately equal parts and align to the right. Place the equation number on the last line only.
- All equations must be numbered sequentially as they appear in the text.

Units

Use **SI units** throughout the manuscript. If alternative units are provided, they should appear in parentheses following the SI units.

Acknowledgments

Acknowledgments should be included before the list of References, and the title should read "Acknowledgments." Author/s should obtain a permission to acknowledge from all those mentioned in the Acknowledgements.

References

In the list of references, provide complete information of each reference material. Cite a symposium paper only from published proceedings. Do not cite an article or book only accepted for publication but not published. Do not use ibid. Please avoid excessive referencing.

Unpublished data, unpublished abstracts and personal communications should not be included in the reference list. Footnotes are not acceptable.

AJEG prefers maximum 60 references per article. The journal follows the Harvard system for citation, with author name/s and year of publication in parentheses, such as one author: (Hungr 2003) or Hungr (2003), two authors: (Doe and Morris, 2009) or Doe and Morris (2009), and three authors or more: (Rahardjo et al., 2002) or Rahardjo et al. (2002).

APA-Style Reference (with slightly modified) Examples

Journal article

van Westen, C. J., Rengers, N., and Soeters, R. (2003). Use of geomorphological information in indirect landslide susceptibility assessment. Natural Hazards, 30, 399–419.

Multiple works by same author(s) in same year

Dahal, R. K., Hasegawa, S., Nonomura, A., Yamanaka, M., and Dhakal, S. (2008a). DEM-based deterministic landslide hazard analysis in the Lesser Himalaya of Nepal. Georisk: Assessment and Management of Risk for Engineered Systems and Geohazards, 2(3), 161–178.

Dahal, R. K., Hasegawa, S., Nonomura, A., Yamanaka, M., Dhakal, S., and Paudyal, P. (2008b). Predictive modelling of rainfall-induced landslide hazard in the Lesser Himalaya of Nepal based on weights-of-evidence. Geomorphology, 102(3–4), 496–510.

Journal article with DOI (Please mention DOI, as far as possible)

Hasegawa, S., Dahal, R. K., Yamanaka, M., Bhandary, N. P., Yatabe, R., and Inagaki, H. (2009). Causes of large-scale landslides in the Lesser Himalaya of central Nepal. Environmental Geology, 57, 1423–1434. https://doi.org/10.1007/s00254-008-1420-z

Journal article in press

Dahal, R. K., and Hasegawa, S. (2008). Representative rainfall thresholds for landslides in the Nepal Himalaya. Geomorphology. https://doi.org/10.1016/j.geomorph.2008.01.014 (in press)

Maps and Pamphlets

Amatya, K. M., and Jnawali, B. M. (1994). Geological map of Nepal (Scale 1:1,000,000). Department of Mines and Geology, Kathmandu, Nepal.

Books (authored)

Dahal, R. K. (2006). Geology for technical students. Bhrikuti Academic Publication, Kathmandu.

Same author, multiple books same year

Krahn, J. (2004a). Seepage modeling with SEEP/W: An engineering methodology (1st ed.). Geo-Slope International Ltd., Alberta.

Krahn, J. (2004b). Stability modeling with SLOPE/W: An engineering methodology (1st ed.). Geo-Slope International Ltd., Calgary.

Edited Book

Wohletz, F., and Aaron, G. (Eds.). (1992). Sedimentology. California Press, CA.

Book Chapter

Ward, T. J., Li, R.-M., and Simons, D. B. (1981). Use of a mathematical model for estimating potential landslide sites in steep forested basin. In T. R. H. Davis and A. J. Pearce (Eds.), Erosion and sediment transport in pacific rim steep lands, Institute of Hydrology, Wallingford, Oxon, UK. pp. 21–41.

Proceedings as a Book

Sassa, K. (1998). Recent urban landslide disasters in Japan and their mechanisms. In Proceedings of the 2nd International Conference on Environmental Management, Environmental Management, Australia, 10–13 February. Elsevier, Amsterdam, Vol. 1, pp. 47–58.

Proceedings with an editor, no publisher

Rahardjo, H., Leong, E. C., and Rezaur, R. B. (2002). Studies of rainfall-induced slope failures. In P. Paulus and H. Rahardjo (Eds.), Proceedings of the National Seminar, Slope 2002. Bandung, 27 April 2002, pp. 15–29.

Proceedings without editor, with publisher

Doe, S.-T., and Morris, R. L. (1998). Rainfall-induced slope failures and damming of ravines. In Abstracts of international symposium on water-induced disasters. Tribhuvan University, Kathmandu, 4–9 June 1998.

Proceedings in CD/DVD format

Yatabe, R., Yagi, N., Yokota, K., and Bhandary, N. P. (2000). Influence of expansive chlorite on the strength of weathered Green Rock at Mikabu Belt of Japan. Proceedings of International Conference on Geotechnical and Geological Engineering, Melbourne, Australia, 19–24 November 2000 (CD format).

Publicly Available Unpublished Report

Wagner, A. (1983). The principal geological factors leading to landslides in the foothills of Nepal: A statistical study of 100 landslides – steps for mapping the risk of landslides. HELVETAS-Swiss Technical Cooperation and ITECO-Company for International Cooperation and Development.

Online Document

Hungr, O. (2003). Flow slides and flows in granular soils. In Proceedings of international workshop on occurrence and mechanisms of flows in natural slopes and earth fills, 15 p. Available at: http://www.unina2.it/flows2003/flows2003/articoli/Hungr-Flows.pdf

Dissertation

Khanal, R. K. (1991). Historic landslides of Nepal during 1902–1990 A.D.: Extent and economic significance, M.Sc. dissertation. Central Department of Geology, Tribhuvan University, Nepal. Available at: (*Put web link if available*).

Standard

ASTM D3385-03. (2003). Standard test method for infiltration rate of soils in field using double-ring infiltrometer. ASTM International. Available at: (*Put web link if available*).

Review and Production Process

All manuscripts submitted for publication, including original articles, rapid reports on recent engineering geology issues, case studies, and technical notes, will undergo a rigorous peer review by at least two independent experts in the relevant field. A member of the Editorial Board may also serve as a reviewer when appropriate expertise is required. Accepted materials are subject to copyediting to ensure clarity, consistency, and adherence to journal standards. Authors will receive galley proofs of their article prior to publication and are expected to respond promptly to

any editorial queries. Proof corrections must be limited to typographical or printer's errors; substantial revisions or rewriting at the proof stage will not be permitted.

Page Charges

There is **no page charge/s** for papers submitted to the AJEG. The upper limit on length of a paper is approximately 35 manuscript pages, including tables and references. This limit may be exceeded at the discretion of the Editor-in-chief.

Online Submission

Please note that the online manuscript submission system is available through the journal's official website. This system is essential for preparing and submitting your manuscript electronically to the Asian Journal of Engineering Geology via its web-based peer-review platform.

Manuscripts should be submitted at https://ajeg.nseg.org.np . The submission portal also allows authors to track the progress of their manuscript throughout the peer-review and editorial process.

Author should use given Template in the web site for preparation of manuscript.

Research Article DOI: https://doi.org/10.64862/ajeg.2026.301.01.270 Open Access

Numerical Evaluation of Post-Earthquake Stability and Rehabilitation of Mountain Trails 'Unnat Goreto' in Gorkha and Rasuwa Districts, Nepal

Bikash Adhikari[1], Ram Chandra Tiwari[2*], and Aanchal Tiwari[3]

[1]Department of Environmental Science and Engineering, Kathmandu University, Nepal
[2]Department of Civil Engineering, Institute of Engineering, Pulchowk Campus, Tribhuvan University, Lalitpur, Nepal
[3]Department of Civil Engineering, Institute of Engineering, Pulchowk Campus, Tribhuvan University, Lalitpur, Nepal

(*Corresponding E-mail: rct2075ce_rctiwari@pcampus.edu.np)

Received: November 15, 2025, Accepted: May 15, 2026

Abstract: This study investigates the stability of mountain trails (locally known as *Unnat Goreto*) that were rehabilitated in highly affected communities of Gorkha and Rasuwa Districts following the 2015 Mw 7.8 Gorkha Earthquake in Nepal. The stability of critical trail sections was analyzed using the 2D Finite Element Method (FEM) in Rocscience Phase2 software. This paper presents the stability assessment of one representative critical section from each trail, both rehabilitated in 2017. Stability was evaluated under both best- and worst-case scenarios using the Strength Reduction Method (SRM) based on the Mohr–Coulomb and Hoek–Brown failure criteria.Results indicate that the slope is stable under static conditions and marginally safe under a pseudo-static horizontal seismic coefficient (EQx) of 0.1g, but becomes unstable under higher seismic loading for the trail in Gorkha District. In contrast, the trail in Rasuwa District shows relatively higher stability. The soil-bioengineering slope stabilization techniques applied immediately above and below the trail sections significantly enhance the factor of safety. Additionally, dry stone walls constructed below the trail as retaining structures contribute substantially to slope stability, with their effectiveness varying by wall type (Type 1-3). The analysis also incorporates the influence of mule loads, track components, and stabilization measures. Overall, the study emphasizes the importance of integrating geotechnical design with bioengineering and appropriate structural interventions to ensure the long-term stability and functionality of rehabilitated mountain trails in seismically active, mountainous regions.

Keywords: ***Mule track, Stability analysis, Safety factor, Finite Element Method, Earthquake***

Introduction

This research focuses on the stability analysis of trails in the earthquake-affected areas of Gorkha and Rasuwa Districts that were rehabilitated following the Mw 7.8 Gorkha Nepal Earthquake of 2015. These trails were primarily constructed in regions inaccessible to motorable transport, where existing routes were unsafe and unstable. The study is based on the field-level implementation of trail rehabilitation projects carried out by the National Reconstruction Authority (NRA), Government of Nepal (GoN), which was established in 2015 after the earthquake. The NRA prioritized the construction of safe trails in the most severely affected districts. The construction period spanned from December 2016 to November 2017.

The trail projects were implemented in two districts - three Village Panchayats (VPs) of Gorkha (Manbu, Kashigaun, and Kerauja) and four VPs of Rasuwa (Haku, Saramthali, Yarsa, and Bhorle). Major components of the projects included trail rehabilitation, standardization and upgrading of existing routes, footbridge construction, and establishment of rest areas, and awareness activities for hazard-prone communities, as summarized in Table 1. Figure 1 presents a Google Earth image of the Gorkha trail extending from Dhunchet Majhgaon to Hulchuk village, covering approximately 70 km. Similarly, Figure 2 and Figure 3 illustrate the two trail loops in Rasuwa District — Loop 1 from Malum to Nesing and Loop 2 from Sarsung to Rajang villages — spanning a total length of about 55 km.

Figure 4 provides an overview of the trail construction process, including slope stabilization works, gabion breast walls, and trail construction on steep slopes. Figure 5 and Figure 6 show field-level implementations with different dry stone wall sections designed according to the available slope gradient. Figure 7 and Figure 8 present typical examples of critical trail sections in Gorkha District, characterized by vertical cliffs, narrow passages, and exposed hard rock formations. Figure 9 and Figure 10 illustrate trail conditions before and after the earthquake, showing how the reconstructed trails reduce slope gradient, slow surface runoff, and enhance safety and comfort.

The trail section models were developed based on the identification of critical stretches using Google imagery. Previous studies and guidelines on safe and stable trail construction include USDA (1984), Charles

et al. (2001), Minnesota Guideline (2006), and Trail Design Guidelines (2009). However, based on the literature reviewed for this study, few studies in Nepal have specifically addressed the numerical stability of mountain trails, making this research a novel contribution in this field.

Nepal, being predominantly mountainous, has extensive areas covered by hills and rugged terrain. In many remote villages, constructing motorable roads is not feasible due to safety concerns, high costs, and challenging topography. Therefore, mule trails remain a practical and sustainable transportation solution in such regions.

With this background, the objective of this study is to analyze the stability of mule trails constructed in highly affected communities — particularly in the epicentral zones of the 2015 Gorkha earthquake — within Gorkha and Rasuwa Districts. The stability evaluation was performed using a two-dimensional finite element-based program, Rocscience Phase2 (Rocscience, 2012). A homogenization approach was adopted to incorporate the root-reinforcing effects in the slope. Field identification of soil and rock types was used to estimate geotechnical parameters and develop material models. The effectiveness of slope stabilization measures was then assessed in critical trail sections under both static and seismic conditions.

Although this is a case-based study, the approach can be replicated in other parts of Nepal. Given that thousands of remote settlements still rely on mule trails, such trails will likely remain an essential means of transportation for several decades. Hence, ensuring the stability and safety of these trails is both technically and socioeconomically justified.

Table 1 presents the key components of mule trail construction carried out in the earthquake-affected areas of Gorkha and Rasuwa Districts. A total of 125 km of trails were constructed, with 70 km in Gorkha and 55 km in Rasuwa. The project included the installation of nine foot or truss bridges—five in Gorkha and four in Rasuwa—covering a combined span of 180 meters. To support pedestrians, 15 rest areas or sheds were built, comprising eight in Gorkha and seven in Rasuwa. Safety measures involved the installation of approximately 840 meters of handrails and handholds in critical sections. Furthermore, 8,000 square meters of bioengineering works were implemented on landslide-prone slopes, along with 750 meters of geohazard mitigation structures to enhance the stability and resilience of the trail network.

These works not only restored connectivity but also strengthened the resilience of local communities in the earthquake-affected mountains. The integration of structural measures and bioengineering solutions improved trail safety, accessibility, and sustainability, while the rest areas enhanced traveler comfort. Overall, the project demonstrates a model of resilient and environmentally sensitive trail rehabilitation in Gorkha and Rasuwa.

Table 1, Mule Trail construction in the affected area in Gorkha and Rasuwa Districts

S. No.	Major components of the Trail construction	Detail
1	Trails (km)	125 (Gorkha: 70, Rasuwa: 55)
2	Foot bridge/truss bridge (Total Nos. and Total span in meter)	9 (Gorkha: 5, Rasuwa: 4), 180
3	Rest areas/pedestrian rest shed (Nos.)	15 (Gorkha: 8, Rasuwa: 7)
4	Handrail and handholds in critical sections	840 m
5	Bioengineering works on landslides	8,000 sq. m
6	Geohazard mitigation works	750 m

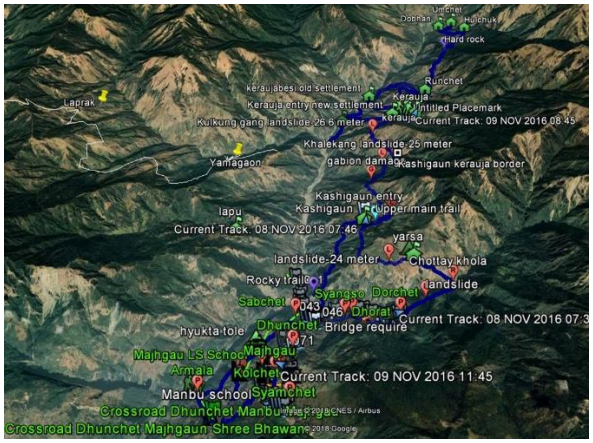


Figure 1, A resilient rehabilitation of trails in highly affected communities of Gorkha Districts

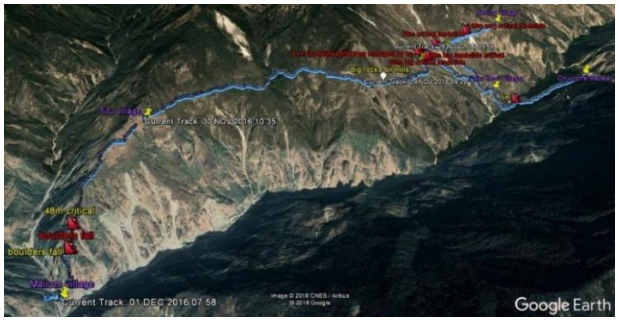


Figure 2, A resilient rehabilitation of trails in highly affected communities of Rasuwa Districts (loop-1)



Figure 3, A resilient rehabilitation of trails in highly affected communities of Rasuwa Districts (loop-2)



Figure 4, General overview of trail construction: (a) Trail with side slope stabilization work, (b) People's participation in trail construction, (c) Typical Gabion works for Breast wall and (d) Trail construction in the steep slope



Figure 5, Field level implementation of trails: (a) Trail with no side slopes, (b) Trail with one side slope. Employed standard dry wall section of Type-2 (mild) and (c) Trail with one side slope (steep). Employed standard dry wall section of Type-3 (steep)



Figure 6, Field level implementation of trails: (a) Trail with Retaining wall and (b) Trail with both Retaining and Breast walls

Figure 4, Figure 5, Figure 6, Figure 7, Figure 8, Figure 9 and Figure 10 collectively highlight the comprehensive approach adopted for resilient trail rehabilitation in the earthquake-affected mountain regions. The designs emphasize terrain adaptability, slope stability, and user safety through appropriate structural and bioengineering measures. By integrating local materials, traditional construction techniques, and modern engineering practices, the project not only restored vital mobility routes but also promoted sustainable development and community ownership in Gorkha and Rasuwa Districts. These reconstructed trails now serve as safe, reliable, and climate-resilient pathways connecting remote settlements and supporting local livelihoods.



Figure 7, Critical sections of Trail (due to vertical cliffs, narrow passage and hard rocks): (a) Closure view of unstable Trail and (b) Overall view of unstable Trail



Figure 8, Widening and stabilizing works at critical sections of Trail (due to vertical cliffs, narrow passage and hard rocks): (a) Widening of existing unstable Trail and (b) Closure view of Rock drilling works



Figure 9, Before and after the construction of Trail, that helps to reduce effective grade and slow water down

and the trail should be comfortable, safe and intact: (a) Before the construction and (b) After the construction



Figure 10, Before and after the construction of dry-stone wall (Gabion walls) for debris fall protection and proper drainage system to ensure longevity of the trails: (a) Before at section-1, (b) After at section-1, (c) Before at section-2 and (d) After at section-2

Stability of trails

The designs of the Trails are based on past practices, experience and reference documents. The Department of Local Infrastructure Development and Agricultural Road norms (DoLIDAR, 2010) to construct Trails are strictly followed by NRA. The Trail construction activities undergo strict engineering procedures, e.g. layout of structures, proper drainage system, proper cut slope, etc. The every kilometer of trail is prepared in the following manner: 1) Minimum width of 1.5m, 2) Extensive erosion control through dry walls and skin walls, 3) Provision of longitudinal and cross drainage structures, 4) Stone balancing approach applied to maximize locally available stones, 5) Geological and Geotechnical assessments to minimize and control hazards, 6) Standard template of dry walls with sectional area in sq. meters are employed and 7) Typical cross section with design, ground level and structure are prepared. These are prepared based on the stability evaluation of the existing Trails. The cross-sectional design and field level implementation (dimensions in meter) of Trails are differed from place to place.

Different types of Tail components were designed and implemented for the sustainability of the trails. The major components of Trails provided were: 1) Flag stone paving, 2) Stone soling, 3) Drainage structures, 4) Retaining and skin walls and 5) Cross drainage structures (scoopers). Besides that, some supplementary structures provided in Trails were: 1) Foot bridges: 9 for Gorkha and Rasuwa, designs based on DoLIDAR/TBSU norms (contractor built), 2) Hand rails: ISMC 75 channel sections and GI pipes used for additional safety and 3) Rest areas: Pedestrian sheds for protection and rest. In addition to these, intensive bioengineering works were planned for post monsoon activities. Bioengineering and slope stabilization works involved were: 1) Cut and fill slope stabilization works practiced maintaining cut and fill slopes, 2) Providing structures as skin walls and toe walls, 3) Landslide debris cleared and minimum passage of 1.5m maintained in landslide areas. Geological and Geo-technical assessment of 41 landslides across 125 kms of trails were carried out and recommendations had been made accordingly. The Trail encountered some critical section such as vertical cliffs, narrow passage, hard rocks, Rock fall, Slope failures and landslides. Table 2 and 3 listed out all 41 landslides in the Trails of both Gorkha and Rasuwa Districts. To minimize the threat, post monsoon activities were planned. A safe cut slope was provided with the help of drilling machines/jack hammers. The mitigation model of landslide slope at critical stretches of Trails can be prepared based on Popescu (2001) and DOR (2007).

Table 2, Landslide at Trails in Gorkha District

S. No.	Landslide Name/Critical Strech (m)	Latitude, Longitude Coordinate (Deg.-Min.-Sec.)
1	Landslide prone zone-1, 30	28-81-41.17N, 84-52-27.83E
2	Biba Kholsa, 50	28-11-43.09N, 84-54-15.24E
3	Dijet, 111.1	28-11-48.22N, 84-54-10.57E
4	Banglang, 86	28-11-49.74N, 84-54-9.45E
5	Khalekang, 25	28-12-50.45N, 84-53-51.61E
6	Kulkung Gang, 26.6	28-13-28.46N, 84-53-32.36E
7	Keranja, 25	28-14-18.29N, 84-53-59.73E
8	Landslide zone-2, 20	28-8-39.37N, 84-52-53.82E
9	Landslide zone-3, 25	28-8-56.66N, 84-52-51.24E
10	Landslide zone-4, 20	28-10-20.42N, 84-55-5.48E
11	Landslide near Yarsa School, 24	28-10-45.28.28N, 84-54-22.88E

Tables 2 and Table 3 mentioned 11 landslide sites in Gorkha and 29 in Rasuwa, several damaged by the 2015 Gorkha earthquake. Their coordinates support precise monitoring and mitigation planning along the reconstructed trails. Figure 11 illustrates the stability condition of the trail near Hyukta Tole in Gorkha District, where a 30 m critical stretch has been affected by landslide.



Figure 11, Stability of trails near to Hyukta Tole in Gorkha Districts (30 m critical stretch due to landslide)

Table 3, Landslide at Trails in Rasuwa District

S. No.	Trail	Landslide Name/Critical Strech (m)	Latitude, Longitude Coordinate (Deg.-Min.-Sec.)
1		Landslide near to cross road Lumbadanda, 12.5	28-6-22.41N, 85-15-4.93E
2	Loop-1	Landslide zone-1, 10	28-6-21.37N, 85-15-6.66E
3		Landslide zone-2, 20	28-6-24.34N, 85-15-14.42E
4		Landslide enlarged by 2015 Gorkha EQ, 91	28-7-7.63N, 85-15-47.91E
5		Landslide zone-3, 85	28-7-28N, 85-15-51.42E
6		Landslide zone-4, 88	28-7-7.33N, 85-15-55.22E
7		Landslide zone-5, 93	28-7-10.09N, 85-15-57.39E
8		Landslide zone-6, 76	28-7-25.10N, 85-16-4.90E
9		Landslide near to Nesing village, 15	28-7-35.76N, 85-16-27.45E
10		Landslide zone-7, 118	28-7-37.43N, 85-16-30.80E
11		Landslide zone-8, 15	28-7-11.28N, 85-16-4.05E
12		Landslide zone-9, 40	28-7-5.64N, 85-16-21.50E
13	Loop-2	Landslide zone-1, 28	28-7-2.55N, 85-16-31.89E
14		Landslide zone-2, 70	28-0-55.92N, 85-15-7.79E
15		Landslide zone-3, 102	28-1-10.58N, 85-15-7.86E
16		Landslide zone-4, 20	28-1-18.80N, 85-15-12.13E
17		Landslide zone-5, 50	28-1-20.12N, 85-15-45.90E
18		Landslide zone-6, 25	28-0-21.43N, 85-15-26.18E
19		Landslide near to Parchyang, 8	28-0-46.82N, 85-16-28.12E
20		Landslide zone-7, 15	28-1-4.59N, 85-16-28.91E
21		Landslide near to 2 alternative trails reaching to Ghichet, 12	28-0-28.98N, 85-16-47.13E
22		Landslide prone zone-8, 15	28-0-26.05N, 85-16-54.56E
23		Landslide near to Ghichet, 7	28-0-19.68N, 85-17-22.65E
24		Landslide prone zone-9, 55	28-1-3.48N, 85-18-41.33E
25		Landslide prone zone-10, 15	28-0-57.61N, 85-18-49.14E
26		Landslide prone zone-11, 12	28-0-44.89N, 85-18-58.59E
27		Landslide prone zone-12, 10.3	28-2-7.31N, 85-18-10.63E
28		Landslide prone zone-13, 25	28-2-3.41N, 85-18-16.96E
29		Landslide prone zone-14, 2 landslides near to Simbandi, 27.2 and 30	28-2-13.82N, 85-18-42.09E

Figures 11, Figure 12, Figure 13 and Figure 14 illustrate representative critical trail sections affected by landslides in Gorkha District, showing the location and extent of vulnerable stretches identified during field investigation. Figures 15, Figure 16, Figure 17, Figure 18, Figure 19 and Figure 20 illustrate the stability conditions of critical trail sections affected by landslides in Gorkha and Rasuwa Districts. The identified stretches, ranging from 5 to 118 meters, include major sites such as Majhgau, Kolchet, Yarsa, Chottay Khola, Lumbadanda, Thulo Haku, Nesing, Haku Besi, and Ghurmu. These figures highlight key areas requiring continuous monitoring and stabilization to ensure safe and resilient trail connectivity. These figures demonstrate the varying severity and distribution of landslide-affected sections along the trails, emphasizing the need for tailored stabilization measures. By documenting critical stretches with precise lengths and locations, the study provides a clear basis for designing site-specific interventions, such as slope reinforcement, bioengineering, and drainage improvements, to enhance trail safety and long-term resilience in the earthquake-prone mountain regions of Gorkha and Rasuwa.



Figure 12, Stability of trails near to Biba Kholsa in Gorkha Districts (50, 111.1 and 86m critical stretches due to Biba Kholsa, Dijet and Bangland landslides)

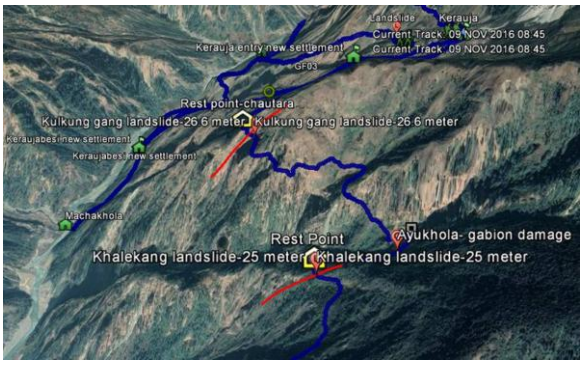


Figure 13, Stability of trails near to Khalekang and Kulkung gang landslides in Gorkha Districts (25 and 26.6m critical stretches due to Khalekang and Kulkung landslides)



Figure 14, Stability of trails near to Kerauja landslide in Gorkha Districts (25m critical stretches due to landslide)



Figure 15, Stability of trails near to Majhgau and Kolchet landslide in Gorkha Districts (20-25m critical stretches due to landslides)



Figure 16, Stability of trails near to Yarsa and Chottay Khola landslide in Gorkha Districts (24 and 20m critical stretches due to landslides)

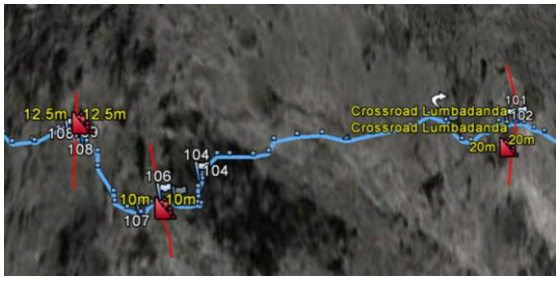


Figure 17, Stability of trails under loop-1 near to Crossroad Lumbadanda landslide in Rasuwa Districts (12.5, 10 and 20m critical stretches due to landslides)



Figure 18, Stability of trails under loop-1 near to Thulo Haku, Nesing Village and Haku Besi village landslide in Rasuwa Districts (88, 91, 76, 118, 15, 40 and 28m critical stretches due to landslides)



Figure 19, Stability of trails under loop-1 near to Haku Besi village (near to Dhunche Bazar) landslide in Rasuwa Districts (5m critical stretch due to landslide)



Figure 20, Stability of trails under loop-2 near to Ghurmu landslide in Rasuwa Districts (70, 102, 20 and 50m critical stretches due to landslides)

Figure 21, Figure 22, and Figure 23 illustrate additional critical trail sections along Rasuwa Loop-2, including the areas around Parchyang, Ghichet, Sangue, Sanguel and Simbandi.



Figure 21, Stability of trails under loop-2 near to Parchyang and Ghichet landslides in Rasuwa Districts (8, 12, 15 and 7m critical stretches due to landslides)



Figure 22, Stability of trails under loop-2 in between Ghichet and Sangue in Rasuwa Districts (55, 15 and 12m critical stretches due to landslides)

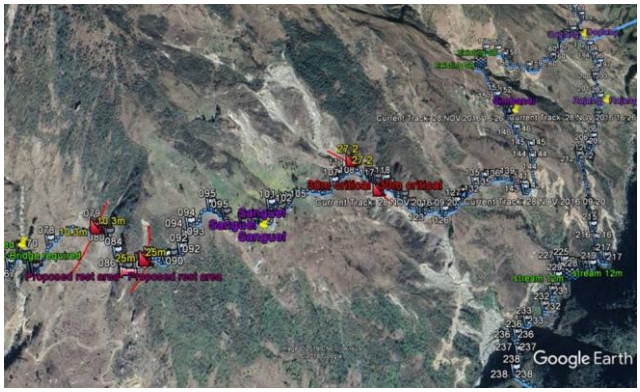


Figure 23, Stability of trails under loop-2 near to Sanguel, Simbandi in Rasuwa Districts (10.3, 25 and 30m critical stretches due to landslides)

Material and method

The soil/rock slope stability analysis is carried out using a finite element formulation provided in the Rockscience Phase2 (Rocscience, 2012). The debris and Rocks in the slopes are modeled as a continuum interface using 2D, plane strain problem. The discontinuities are represented as an interface element in between the Rock wall. The shear strength reduction technique is employed to explore stability of landslide slopes. This method is fully automated and used either Mohr-Coulomb or Hoek-Brown strength parameters. Finite element divide body into small element of 6 noded triangle. Displacement within the element is related to displacement at nodes through shape function. Transmission of internal forces between the edges of adjacent elements is represented by interactions at the nodes of the elements. Fixed boundary conditions are assumed along the lateral side and base of the model such that the displacement is restrained in both the x and y directions. The slope face is kept free. In the loading step, each FE is given both an initial stress and a body force (self-weight). The initial vertical stress is estimated from the weight of the material above the element. Phase2 automatically determines the ground surface above the element and the stress due to the material above the element. The horizontal to- vertical stress ratio σ_H / σ_V is kept as 1.0 according to Pal et al. (2012).

Strength reduction technique is employed here to explore critical safety factor. In Mohr–Coulomb and Hoek-Brown material model, the factored shear strength parameters C_f and ϕ_f are calculated as per Eq. (1) and (2) below.

$$C_f = \frac{C}{SRF} \qquad (1)$$

$$\varphi_f = \tan^{-1}\frac{Tan\varphi}{SRF} \qquad (2)$$

Where SRF is the 'strength reduction factor (SRF).' This method is referred to as the 'shear strength reduction (SSR) technique (Matsui and San, 1992). Four-nodded quadrilateral zero thickness element is used here as a joint element. 1D finite element is designed to simulate shear and normal displacements in the interfaces. The element was originally developed by Goodman et al. (1968). The undulations and asperities on a natural joint surface have a significant influence on its shear behavior. The shear strength in increased in the jointed surface due to shear resistance. Patton (1966) demonstrated the shear tests on saw-tooth specimens according to Eq. (3).

$$\tau = \sigma_n \tan(\varphi_b + i) \qquad (3)$$

The detail material models to explore stability of Mule Tracks in Gorkha District are presented according to Table 4 below. It contains both soil and rock properties. Soil properties are considered as per the field investigation and estimated the soil strength parameter according to Krahenbuhl and Wagner (1983). Similarly, Rock properties are estimated from the literatures such as Griffiths and Lane (1999), Hoek and Diederichs (2006) and Deere and Miller (1966). The step by step procedure to explore the stability of Mule Track includes: 1) Full enclosed boundary is created for the slope section generated from the slope profile in Rocscience Phase2, 2) The next step is adding material to the slope, 3) The failure criterion assigned are Mohr Coulomb for soil/debris and Generalized Hoek and Brown for fractured, jointed bedrock and joint failure criteria by Patton (1966), 4) Then discretization and meshing is done with 6 noded triangular element of 1500 numbers, 5) The boundary condition is fixed at sides and slope face is made free, 6) The gravity loading is assigned as initial effective stress and body force. The first horizontal to vertical stress is assigned as 1 and 7) On completing above procedure the slope stability analysis is ready to run.

Mule load analysis

The Mule load analysis is done accordingly as per Figure 24. An average Mule physical dimensions are presented in Table 5. The average mass (mav) of Mule and load carrying by Mule can be considered as 180+60=240kg (2354 kN weight). Considering an average value of acceleration (aav) of 1 m/s^2 of Mule while walking and neglecting the friction, the inertial force would be 240 N. Based on these calculations, the pulling forces at the flat surface would be, Fa=240/2=120N. For the inclined surface of 15 degrees, pulling force equals to 609N, Fa=240/2+609/2=424.5N, Similarly, for an inclined surface of 30 degrees, pulling force F_p=1177N, Fa=240/2+1177/2=708.5N.

Table 4, Material model *employed to explore the stability of Mule Tracks in Gorkha and Rasuwa Districts*

Material model for soil, according to Krahenbuhl and Wagner (1983)	
Material	Disintegrated debris slope (USCS soil type: CL)
Failure Criteria	Mohr-coulomb
Unit weight (kN/m^3)	17.5 (Gorkha), 18.0 (Rasuwa loop-1) and 19.0 (Rasuwa loop-2)
Elastic Properties	Griffiths and Lane (1999)
Modulus of elasticity (kPa)	10^5
Poisson ratio=0.3	0.3
Shear strength parameters	Field identification of soil types and suggested soil shear strength parameters according to Krahenbuhl and Wagner (1983)
Angle of friction, peak (Degree)	24 (Gorkha), 27.0 (Rasuwa loop-1) and 30.0 (Rasuwa loop-2)
Cohesion, peak (kPa)	10 (Gorkha), 10.0 (Rasuwa loop-1) and 15.0 (Rasuwa loop-2)
Material model for rock (Mule Track critical sections in Gorkha, Rasuwa loop-1 and 2)	
Material	Schist inters bedded with Phyllite
Failure Criteria	Generalized Hoek and Brown
Unit weight (kN/m3)	29
Elastic properties	
Modulus of elasticity	Hoek and Diederichs (2006)
Modulus of elasticity of intact rock (kPa)	54,000,000
Modulus of elasticity of rock mass (kPa)	29,306,428.2
Poisson ratio	0.3
Intact rock uniaxial compressive strength (UCS) according to Deere and Miller (1966), (kPa)	80,000
GSI (Marinos and Hoek, 2000) according to Cai et al. (2004)	60
mi according to Deere and Miller (1966)	7
Disturbance factor (No blasting), D	0
For joint	
Basic friction angle, ϕb (Degree)	20
Roughness angle, i (Degree)	15
Joint normal stiffness (GPa/m)	0.1
Joint shear stiffness (GPa/m)	0.01

The Mule has single hoof so it prefers walking on soft surfaces (soil). Stone soling (15 cm depth) up to 15% longitudinal gradient is not affected by Mules movement. Stairs in length with longitudinal gradient more than 30% are damaged more due to Mule movement. The rocks found in the trail construction area are mostly metamorphic rocks such as Phyllite and Schist. These rocks are weak and undergo breaking with pointed load. The best alternative is to use Meta sandstone and Phamatic Phyllite.

Figure 25 shows the standard template of dry wall along with a typical sectional view of the Trail that are implemented as per the analysis done. Similarly, Figure 26 shows a typical cross-sectional design and the field level implementation of trail.

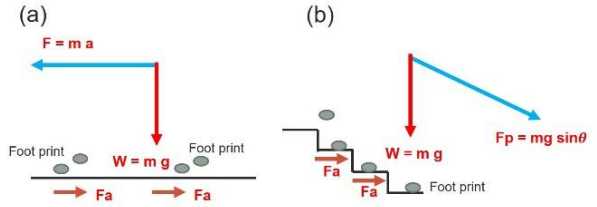


Figure 24, Mule load analysis: (a) Walking in the plain Trail and (b) Walking in the steep Trail

Table 5, Average Mule physical dimensions

S. No.	Parameters	Values
1	Length (m)	1.6-1.8
2	Weight (kg)	120-180
3	Load carrying capacity (kg) and load on each side (kg)	60, 30
4	Load in each leg (if distributed equally) (kg)	45-60
5	Diameter of hoof (cm)	7-9
6	Height of Mule (m)	1.1-1.3
7	Width of mule's waist without load (m)	0.5
8	Width of mule with load (Load pack+Mule body+Load pack)	1.1(0.3+0.5 +0.3)

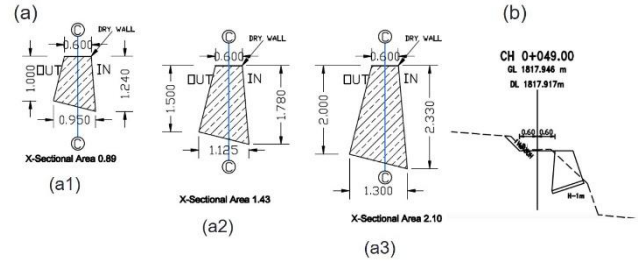


Figure 25, Standard template of dry wall along with typical sectional view of trail: (a) Type of dry stone wall along with sectional area (Sq. meters): (a1) Type-1 with sectional area of 0.89, (a2) Type-2 of sectional area of 1.43, (a3) Type-3 of sectional area of 2.10 and (b) Sectional view with Retaining wall

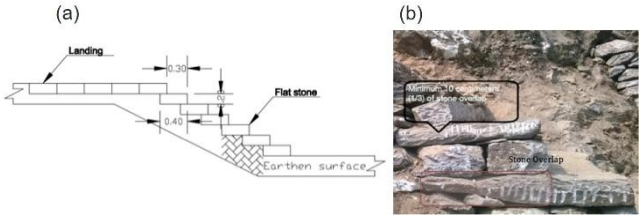


Figure 26, Typical cross-sectional design and field level implementation of trail: (a) Design drawing (dimensions in meter) and (b) Field implementation (Minimum 10 centimeters (1/3) of stone overlap)

Results and discussion

The summary of the computational results of landslide slope stability of 3 critical sections of mountain Trails in Gorkha and Rasuwa Districts of Nepal is presented in Table 6. The results are computed for different seismic coefficient along with dry stone wall and bio-engineering layer. The construction of Mule Trails are successfully completed in the year 2017 in the highly affected communities of Gorkha and Rasuwa. There are altogether 41 critical stretches in Mule Trails that have been identified and rehabilitated after the Gorkha Earthquake. Among them, we have identified the most critical stretches in the Mule Tracks, one from Gorkha and one from each loops of Trails from Rasuwa Districts. The similar numerical and computational scheme can be applied for the remaining landslides identified in the Mule Tracks in Gorkha and Rasuwa Districts.

Figure 27 shows the stability analysis of Mule Trail at Kulkung Gang landslide, Gorkha (28-13-28.46N, 84-53-32.36E) that include landslide slope model, shear strain plots (kN/m^2) and strength Reduction actor, SRF (nos.) vs U_{max}(m). The shear strain plot gives a tentative idea of failure surface. Figure 28 shows the Pseudo-static seismic stability analysis (with variable horizontal seismic coefficient, EQx) of 0.1, 0.2 and 0.3. Similarly, the Figure 29, Figure 30 and Figure 31 respectively show the stability models, shear strain plots (kN/m^2) and strength reduction factor, SRF (Nos.) vs maximum horizontal displacement, Umax (m) of Mule Trail in varying sections of dry-stone wall (Type 1, 2 and 3) and soil-bioengineering (soil-root matrix of 1m).

The Figure 32 and Figure 33 respectively show the landslide model, shear strain plots (kN/m2) and SRF vs U_{max} (m) of the stability analysis of Mule Trail at 118m landslide, Rasuwa loop-1 (28-7-37.43N, 85-16-30.8E) of both barren and vegetated soil slopes (soil-bioengineering in the form of soil-root matrix continuum of 1m layer). Similarly, Fig. 34 and 35 respectively show the landslide model, shear strain plots (kN/m^2) and SRF vs Umax(m) of the stability analysis of Mule Trail at 102 m big landslide, Rasuwa loop-2 (28-1-10.58N, 85-15-7.86E) of both barren and vegetated soil slopes (soil-bioengineering in the form of soil-root matrix continuum of 1m layer).

The results demonstrate that variations in dry stone-wall cross-sections and soil slope conditions, including barren and vegetated surfaces, have a significant influence on the calculated factor of safety. The findings indicate that the slopes along the critical stretches of the Mule Track are stable under static loading conditions for both soil and rock slopes. Under pseudo-static seismic loading with a horizontal seismic coefficient (EQx) of 0.1, the slopes are marginally stable. However, they become unstable when subjected to higher seismic coefficients, indicating increased vulnerability to stronger earthquake shaking.

The critical Strength Reduction Factor (SRF) is identified from the SRF versus maximum displacement (U_{max}) plots by observing the point at which displacement increases abruptly with a small additional increase in SRF. This transition represents the onset of plastic deformation and the progressive loss of material strength. The inflection point indicates the transition from predominantly elastic to elastoplastic behavior. Therefore, an elastoplastic constitutive model is considered appropriate for representing the material behavior and evaluating slope stability in this study.

Table 6, The stability analysis of critical sections of Trails in Gorkha and Rasuwa districts

Landslide slope stability analysis at critical sections of Trails	Static soil/rock slope condition		Seismic soil/rock slope condition					
			0.1 g		0.2 g		0.3 g	
	Without Bio.	With Bio.	Without Bio.	With Bio.	Without Bio.	With Bio.	Without Bio.	With Bio.
Kulkung Gang landslide, Gorkha (28-13-28.46N, 84-53-32.36E)								
Type-1 Dry wall	0.94	0.97	0.78	0.84	0.70	0.76	0.66	0.68
Type-2 Dry wall	1.01	1.10	0.81	0.89	0.75	0.81	0.68	0.71
Type-3 Dry wall	1.06	1.16	0.84	0.91	0.76	0.87	0.70	0.76
118 m landslide, Rasuwa loop-1 (28-7-37.43N, 85-16-30.8E)								
Type-1 Dry wall	0.96	0.99	0.95	1.02	0.92	0.96	0.85	0.91
Type-2 Dry wall	1.02	1.10	0.98	1.08	0.97	1.00	0.88	0.94
Type-3 Dry wall	1.08	1.15	1.01	1.11	0.99	1.05	0.91	0.95
102 m big landslide, Rasuwa loop-2 (28-1-10.58N, 85-15-7.86E)								
Type-1 Dry wall	1.07	1.13	0.99	1.04	0.94	0.95	0.88	0.92
Type-2 Dry wall	1.11	1.17	1.02	1.07	0.97	0.99	0.91	0.96
Type-3 Dry wall	1.16	1.22	1.08	1.11	1.00	1.03	0.93	0.97

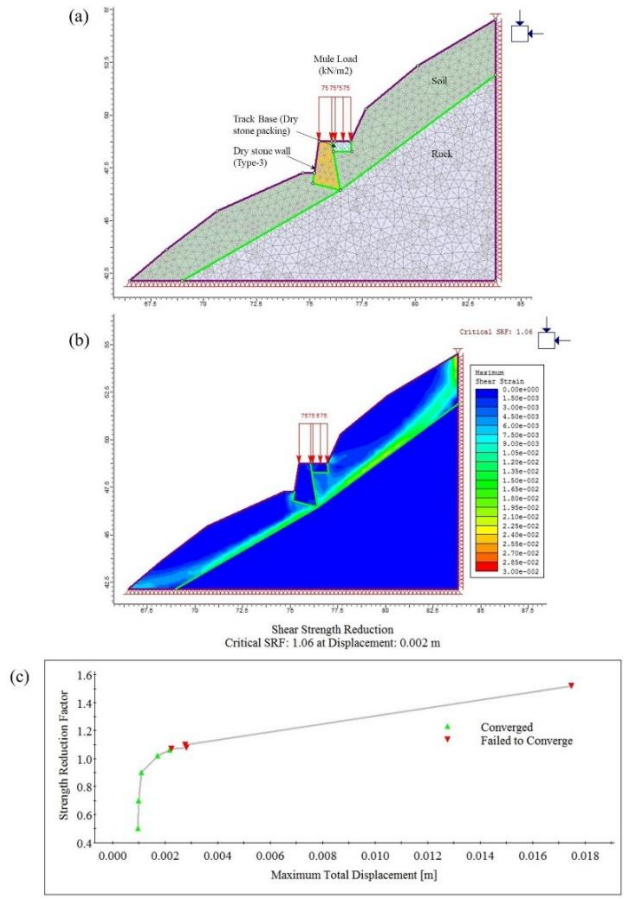


Figure 27, Stability analysis of Mule Trail at Kulkung Gang landslide, Gorkha (28-13-28.46N, 84-53-32.36E): (a) Landslide slope model, (b) Strain plots (kN/m^2) and (c) Strength Reduction Factor, SRF (nos.) vs U_{max} (m)

Table 6 presents the stability analysis of critical trail sections in Gorkha and Rasuwa Districts under both static and seismic conditions. The analysis considers different types of dry-stone walls with and without bioengineering measures. Results show that the inclusion of bioengineering consistently improves slope stability, increasing the factor of safety (FS) under static conditions and across seismic accelerations of 0.1g, 0.2g, and 0.3g. For instance, at the Kulkung Gang landslide in Gorkha, FS values rise from 0.94–1.06 without bioengineering to 0.97–1.16 with bioengineering. Similarly, critical landslides in Rasuwa (118 m in loop-1 and 102 m in loop-2) show notable FS improvements, demonstrating the effectiveness of combined structural and bioengineering interventions in enhancing trail resilience against static and earthquake-induced slope failures.

Figure 27 and Figure 28 illustrate the stability analysis of the Mule Trail at the Kulkung Gang landslide in Gorkha (28-13-28.46N, 84-53-32.36E). Figure 27 presents the landslide slope model, corresponding strain distribution (kN/m^2), and the variation of the Strength Reduction Factor (SRF) with maximum displacement (Umax), providing insights into slope behavior under static conditions. Figure 28 shows the pseudo-static seismic stability analysis for varying horizontal seismic coefficients (EQx = 0.1, 0.2, and 0.3), highlighting the trail's response under different earthquake loading scenarios and demonstrating the effectiveness of mitigation measures in enhancing slope stability.

These figures emphasize the critical role of site-specific analysis in designing resilient trail sections in landslide-prone areas. By combining slope modeling, strain distribution, and seismic response evaluation, the study identifies vulnerable zones and quantifies the benefits of structural and bioengineering interventions.

This approach ensures that the reconstructed trails can withstand both static and seismic stresses, improving safety, durability, and long-term usability for local communities.

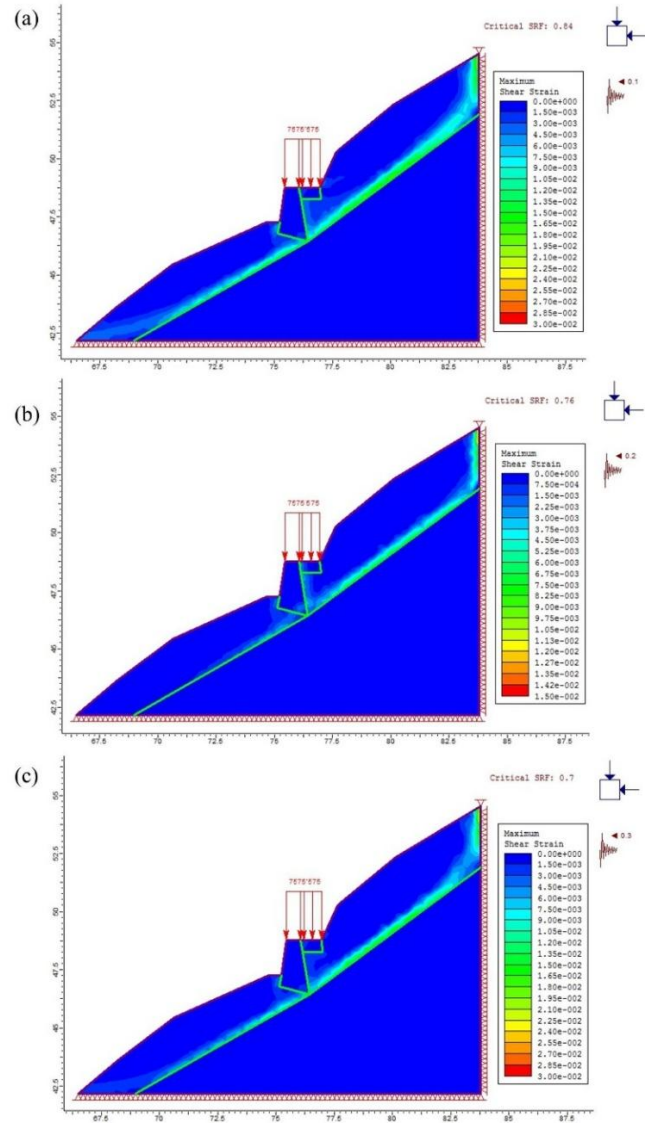


Figure 28, Pseudo-static seismic stability analysis (with variable horizontal seismic coefficient, EQx) of Mule Trail at Kulkung Gang landslide, Gorkha (28-13-28.46N, 84-53-32.36E): (a) EQx of 0.1, (b) EQx of 0.2 and (c) EQx of 0.3

Figure 29 and Figure 30 present the stability models and strain distribution of the Mule Trail at the Kulkung Gang landslide in Gorkha (28-13-28.46N, 84-53-32.36E) for varying dry stone wall designs combined with a 1 m soil-bioengineering (soil-root) matrix. Figure 29 shows the three types of dry wall sections (Type-1, Type-2, and Type-3) integrated with bioengineered soil, illustrating how structural variations influence overall slope stability. Figure 30 complements this by displaying the corresponding strain plots (kN/m^2) for each section, highlighting the areas of maximum stress and potential deformation under loading.

The analysis demonstrates that increasing the complexity and height of the dry-stone wall in combination with the soil-root matrix significantly improves the slope's factor of safety and reduces critical strain concentrations. This approach validates the effectiveness of hybrid structural and bioengineering interventions in mitigating landslide risks, ensuring safer and more resilient trails for the communities in Gorkha District.

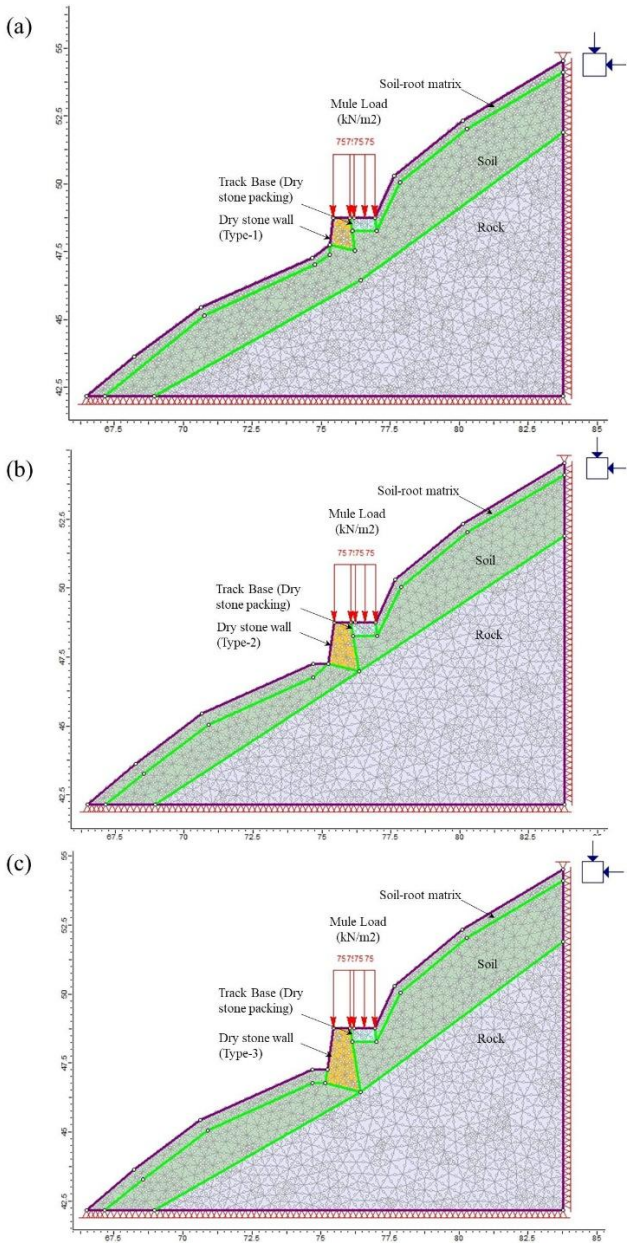


Figure 29, Stability models of Mule Trail at Kulkung Gang landslide, Gorkha (28-13-28.46N, 84-53-32.36E) in varying section of dry-stone wall and soil-bioengineering (soil-root matrix of 1m): (a) Type-1, (b) Type-2 and (c) Type-3

These figures also highlight the importance of optimizing trail design based on local slope conditions and available materials. By comparing the three wall types, it is evident that a tailored combination of dry-stone structures and bioengineered soil can effectively distribute stress, control deformation, and enhance slope resilience. Such targeted interventions not only prevent future landslide occurrences but also contribute to the long-term sustainability and safety of mountain trail networks in earthquake-prone regions.

This approach ensures that reconstructed trails remain stable under both static and seismic conditions. Moreover, it provides a practical model for resilient trail construction in other landslide-prone mountain regions.

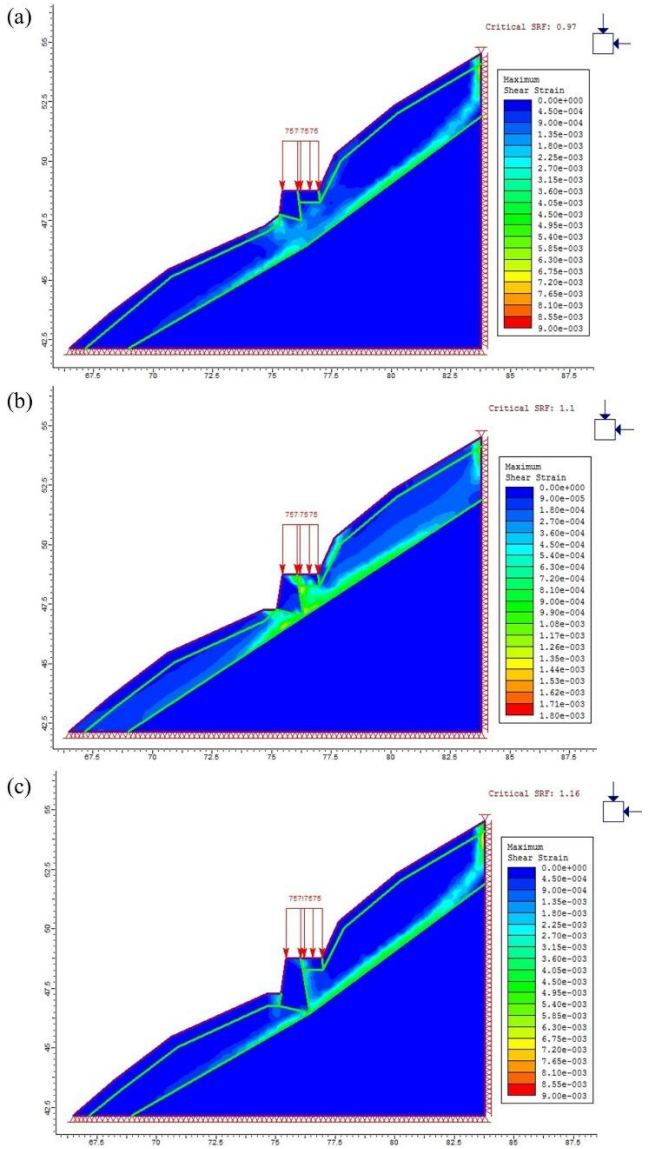


Figure 30, Strain plots (kN/m2) of stability analysis of Mule Trail at Kulkung Gang landslide, Gorkha (28-13-28.46N, 84-53-32.36E) in varying section of dry-stone wall and soil-bioengineering (soil-root matrix of 1 m): (a) Type-1, (b) Type-2 and (c) Type-3

Figure 31 and Figure 32 present detailed stability analyses of critical Mule Trail sections in Gorkha and Rasuwa Districts. Figure 31 shows the variation of the Strength Reduction Factor (SRF) versus maximum horizontal displacement (Umax) for the Kulkung Gang landslide in Gorkha (28-13-28.46N, 84-53-32.36E), comparing three types of dry-stone wall sections combined with a 1 m soil-bioengineering (soil-root) matrix. The plots highlight how different structural designs influence slope stability and deformation, providing insights into optimal mitigation measures.

Figure 32 focuses on the 118 m landslide in Rasuwa loop-1 (28-7-37.43N, 85-16-30.8E), presenting the landslide slope model, corresponding strain distribution (kN/m^2), and SRF versus U_{max} plots. These results illustrate the trail's response under static and pseudo-static conditions, emphasizing the effectiveness of combined structural and bioengineering interventions in enhancing slope resilience and ensuring safer, more stable trails in landslide-prone mountain regions.

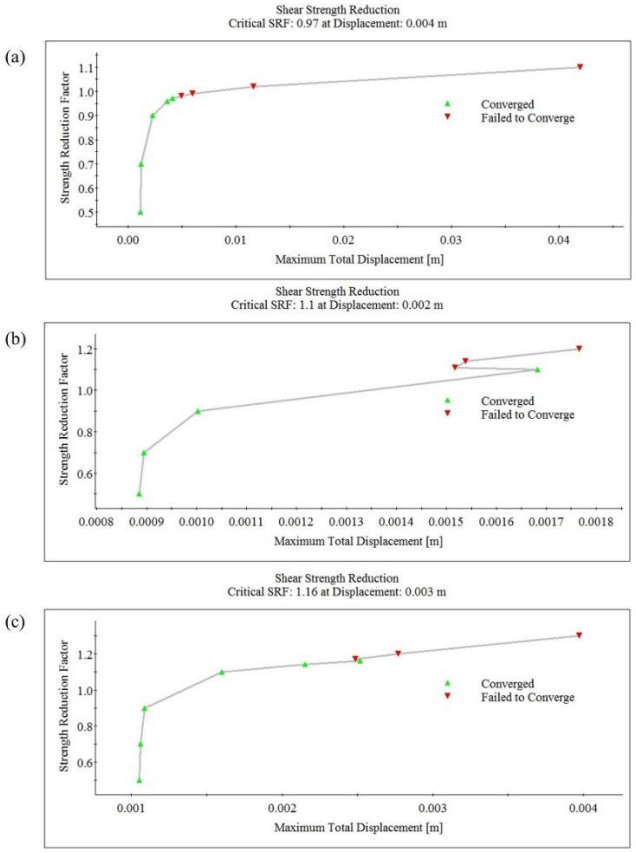


Figure 31, Strength reduction factor, SRF (Nos.) vs Maximum horizontal displacement plots, Umax(m) of stability analysis of Mule Trail at Kulkung Gang landslide, Gorkha (28-13-28.46N, 84-53-32.36E) in varying section of dry-stone wall and soil-bioengineering (soil-root matrix of 1m): (a) Type-1, (b) Type-2 and (c) Type-3

These figures underscore the importance of integrating site-specific structural solutions with bioengineering measures to improve slope stability along critical trail sections. By analyzing SRF and displacement for different wall types and soil-root matrices, the study identifies designs that effectively minimize deformation and distribute stress across the slope. This approach not only enhances trail safety but also prolongs the service life of the infrastructure. Additionally, it provides a replicable framework for resilient trail construction in other landslide-prone mountainous regions.

Moreover, the comparison between the Gorkha and Rasuwa sites highlights the variability in landslide behavior across different terrains. Such analyses enable engineers and planners to prioritize high-risk sections, implement targeted stabilization measures,

and develop resilient trail networks that can withstand future landslide and seismic events, ultimately supporting the mobility and safety of mountain communities. Overall, these findings serve as a valuable reference for future trail rehabilitation projects and disaster risk reduction strategies in the Himalayan region, ensuring safer and more sustainable mountain infrastructure. They also reinforce the importance of combining engineering expertise with local knowledge for effective mountain trail management.

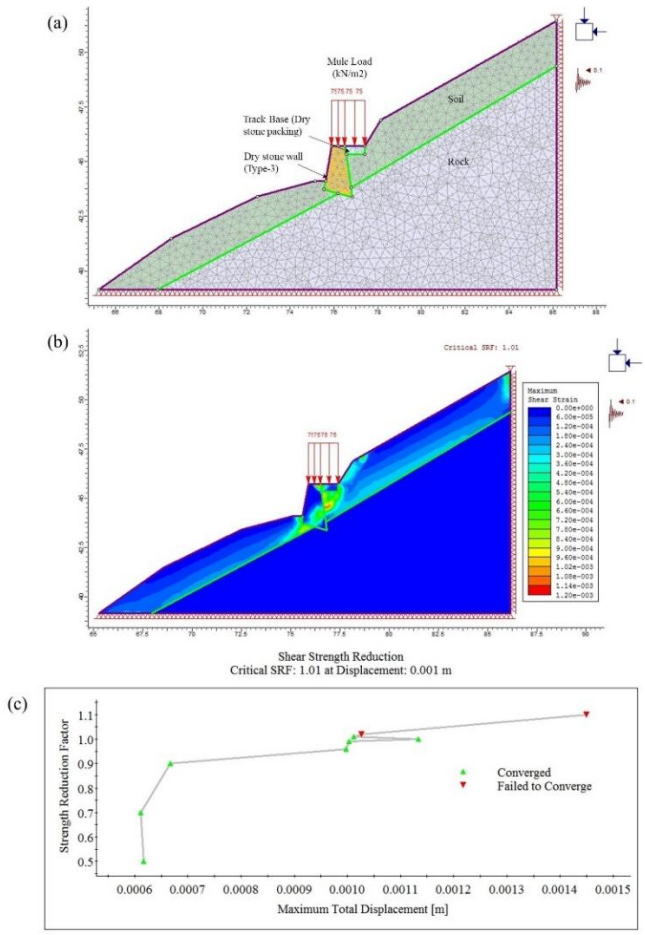


Figure 32, Stability analysis of Mule Trail at 118m landslide, Rasuwa loop-1 (28-7-37.43N, 85-16-30.8E): (a) Landslide slope model, (b) Strain plots (kN/m^2) and (c) Strength Reduction actor, SRF (nos.) vs U_{max}(m)

Figure 33, Figure 34 and Figure 35 present the stability analysis of critical Mule Trail sections in Rasuwa District, focusing on the 118 m landslide in loop-1 (28-7-37.43N, 85-16-30.8E) and the 102 m landslide in loop-2 (28-1-10.58N, 85-15-7.86E). Both analyses incorporate a 1 m soil-bioengineering (soil-root) matrix to evaluate slope behavior. Each figure includes the landslide slope model, corresponding strain distribution (kN/m^2), and the variation of the Strength Reduction Factor (SRF) with maximum horizontal displacement (U_{max}), providing a comprehensive assessment of slope stability under static and pseudo-static conditions.

The results demonstrate that integrating bioengineering measures with structural solutions effectively increases slope stability and reduces critical strain concentrations along the trail. By quantifying the slope response for these large landslides, the analysis supports targeted interventions that enhance safety, resilience, and long-term usability of the trails, ensuring reliable connectivity for communities in landslide-prone areas of Rasuwa District.

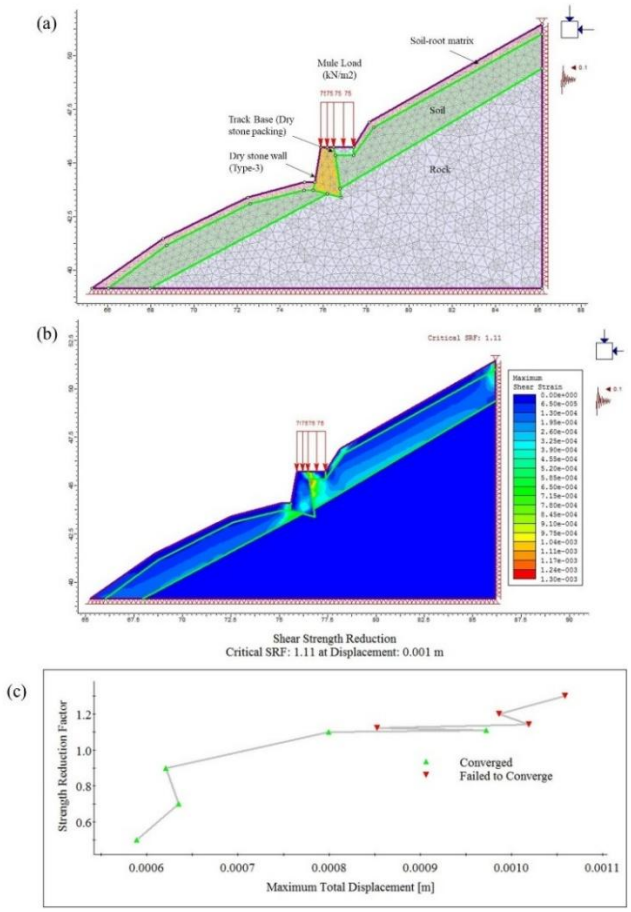


Figure 33, Stability analysis of Mule Trail at 118m landslide, Rasuwa loop-1 (28-7-37.43N, 85-16-30.8E) considering soil-bioengineering (soil-root matrix of 1m): (a) Landslide slope model, (b) Strain plots (kN/m^2) and (c) Strength Reduction actor, SRF (nos.) vs U_{max} (m)

These analyses highlight the significance of combining engineering and ecological approaches for trail stabilization in mountainous terrain. The soil-root matrix not only reinforces the slope but also promotes vegetation growth, which contributes to long-term slope cohesion and reduces erosion. Such integration of structural and bioengineering measures ensures that the trails remain stable under both normal and earthquake-induced loading conditions, minimizing the risk of future landslides.

Furthermore, comparing the 118 m and 102 m landslide sites underscores the need for site-specific designs, as slope geometry, soil conditions, and local topography influence stability outcomes. The findings provide valuable guidance for planning and

implementing resilient trail construction across similar landslide-prone regions, supporting both community mobility and sustainable mountain infrastructure development. These figures also emphasize the importance of continuous monitoring and maintenance of reconstructed trails. By understanding the behavior of slopes under varying conditions, engineers can prioritize critical sections for reinforcement, implement timely mitigation measures, and adapt designs based on observed performance. This proactive approach ensures that trails remain safe, functional, and resilient over time, even in the face of recurring landslides or seismic events.

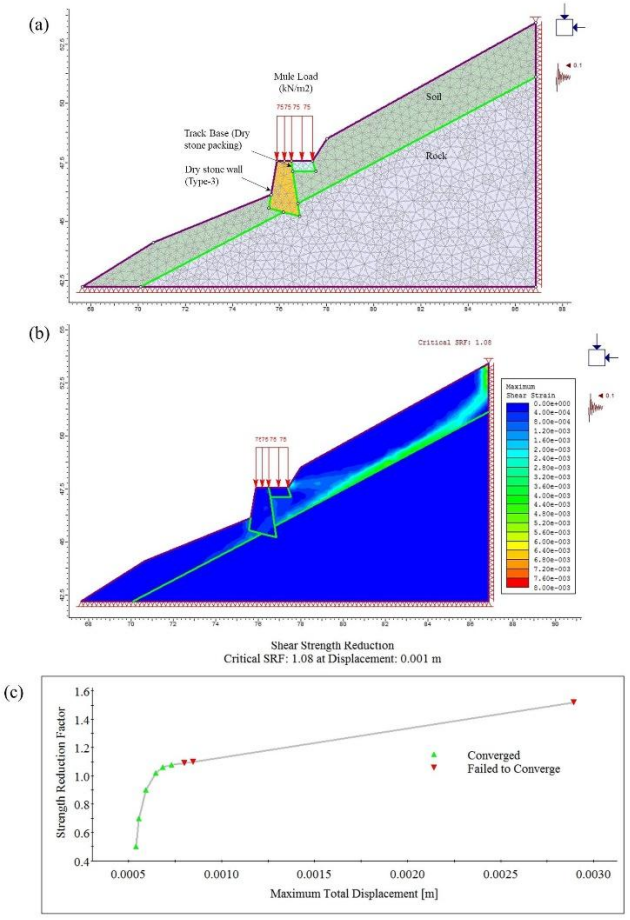


Figure 34, Stability analysis of Mule Trail at 102m big landslide, Rasuwa loop-2 (28-1-10.58N, 85-15-7.86E): (a) Landslide slope model, (b) Strain plots (kN/m^2) and (c) Strength Reduction actor, SRF (nos.) vs U_{max} (m).

Conclusion

The stability assessment of critical Mule Trail sections in Gorkha and Rasuwa demonstrates the importance of incorporating both geotechnical and seismic considerations into the planning and rehabilitation of mountain trails in earthquake-prone terrain. The two-dimensional FEM-based approach adopted in this study provides a useful framework for understanding the overall stability behavior of vulnerable trail sections and for evaluating the suitability of different stabilization strategies.

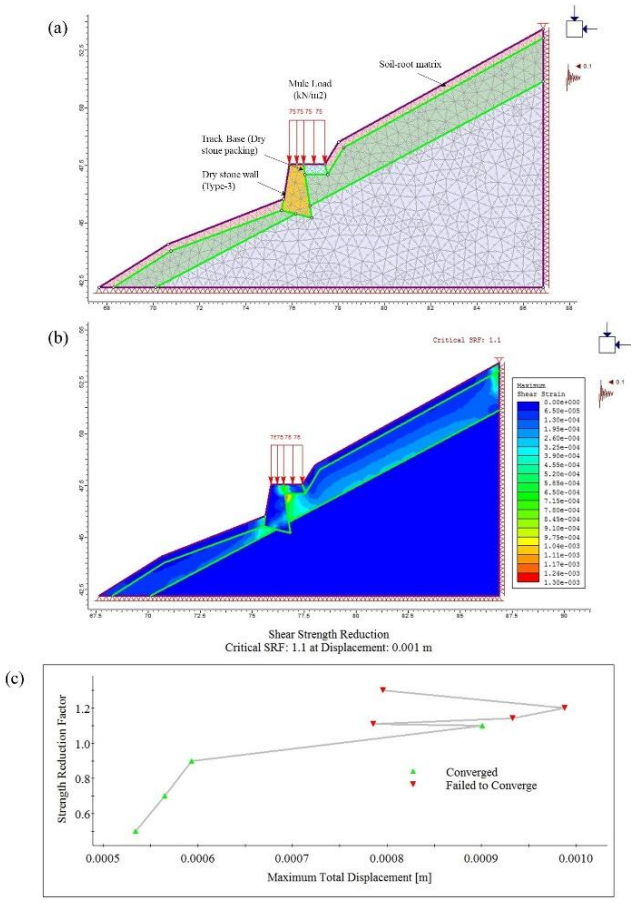


Figure 35, Stability analysis of Mule Trail at 102m big landslide, Rasuwa loop-2 (28-1-10.58N, 85-15-7.86E) considering soil-bioengineering (soil-root matrix of 1m): (a) Landslide slope model, (b) Strain plots (kN/m^2) and (c) Strength Reduction actor, SRF (nos.) vs U_{max} (m)

The study indicates that stability assessment of mountain trails cannot be based solely on static conditions. The additional effects imposed by earthquake-induced loading can substantially alter the stability state of an already vulnerable slope. Therefore, seismic considerations should be an integral part of the design, rehabilitation, and upgrading of mountain trails in the Himalayan region, particularly in areas affected by major earthquakes or located within active seismic zones.

The analysis further demonstrates the value of combining conventional structural stabilization with nature-based slope protection. Dry-stone walls provide immediate structural support, while soil-bioengineering offers an additional mechanism for improving surface reinforcement, reducing erosion, and promoting progressive ecological stabilization of the slope. The combination of these approaches is therefore more appropriate for mountain environments where long-term slope performance depends on both mechanical resistance and control of surface degradation.

An important implication of the study is that stabilization measures should not be implemented as a uniform solution across an entire trail network. Mountain slopes are highly heterogeneous, and their

response is governed by local geological, geomorphological, geometric, and environmental conditions. Consequently, the type and extent of stabilization should be determined through site-specific investigation and stability assessment. The numerical framework used in this study can assist in such prioritization by identifying sections requiring greater structural intervention and by supporting technically justified decisions regarding rehabilitation measures.

The study also highlights the relevance of locally appropriate and environmentally compatible construction practices. The use of dry stone and vegetation-based stabilization is particularly suitable for remote mountain trails, where construction materials, transportation, maintenance facilities, and skilled resources may be limited. Such approaches can reduce the need for heavily engineered solutions while maintaining compatibility with the surrounding natural environment. Their successful application can therefore contribute not only to slope stability but also to the sustainability and social functionality of rural trail infrastructure.

The rehabilitation of Mule Trails should also be considered as a continuing process rather than a one-time construction activity. Even a stable slope at the time of construction can experience progressive deterioration due to intense rainfall, surface erosion, drainage problems, weathering, vegetation changes, and subsequent seismic activity. Regular inspection and maintenance of drainage systems, dry-stone structures, and vegetated slopes are therefore essential for maintaining the performance of the rehabilitated trails. Particular attention should be given to sections identified as critically vulnerable through numerical analysis and field observations.

The methodology developed in this study can be extended beyond the three representative sections examined here. The identification of additional critical stretches along the Mule Trail network provides an opportunity to apply a similar analytical framework for systematic risk assessment and prioritization. Such an approach could support the development of a broader trail-slope management system in which vulnerable sections are assessed according to their geological setting, slope condition, seismic exposure, and required stabilization measures.

Finally, the findings emphasize that resilient mountain infrastructure requires an integration of engineering analysis, appropriate construction practices, ecological measures, and continued field-based management. The experience from the post-earthquake rehabilitation of Mule Trails in Gorkha and Rasuwa provides a useful basis for improving future trail development and disaster-risk reduction initiatives in Nepal. The approach presented in this study can contribute to the development of safer, more durable, and environmentally sustainable mountain transportation networks, particularly in regions where landslides and earthquakes pose recurrent threats to community connectivity.

Acknowledgements

Special thanks to the National Reconstruction Authority, Government of Nepal (NRA, GoN), for providing this opportunity. The Mule Trails (local name: *UNNAT GORETO*) was the rehabilitation project implemented after the M_w 7.8 2015 Gorkha, Nepal Earthquake. We also extend our gratitude to the local communities and field teams for their active participation and support throughout the project. Their cooperation was vital in ensuring the successful restoration and resilience of the mountain trail network.

Article note

This article is a full-length paper developed from **Extended Abstract #209**, entitled "**Post-Earthquake Stability and Rehabilitation of Mountain Trails ('Unnat Goreto') in Gorkha and Rasuwa Districts, Nepal**" which was presented at the 15th Asian Regional Conference of the International Association for Engineering Geology and the Environment (ARC-15 of **IAEG**), held in Kathmandu, Nepal, from 27 to 29 November 2025.

References

Cai, M., Kaiser, P. K., Uno, H., Tasaka, Y., and Minami, M. (2004). Estimation of rock mass deformation modulus and strength of jointed hard rock masses using the GSI system. International Journal of Rock Mechanics and Mining Sciences, 41(1), 3–19. https://doi.org/10.1016/S1365-1609(03)00025-X

Charles, A., Flink, K., Olka, K., and Searns, R. M. (2001). Trails for the Twenty-First Century: Planning, Design, and Management Manual for Multi-Use Trails (2nd ed.). Rails-to-Trails Conservancy. https://doi.org/10.2307/jj.41003685

Deere, D., and Miller, R. (1966). Engineering classification and index properties of rock (Technical Report No. AFNLTR-65-116). Air Force Weapons Laboratory, Albuquerque, NM. https://doi.org/10.21236/ad0646610

Department of Local Infrastructure Development and Agricultural Roads (DoLIDAR), Government of Nepal (GoN). (2010). Revised norms: Working norms for agricultural and rural roads.

DoR (2007). Department of Roads Government of Nepal. Roadside Geotechnical Problems: A Practical Guide to Their Solution.

Goodman, R. E., Taylor, R. L., and Brekke, T. L. (1968). A model for the mechanics of jointed rock. Journal of the Soil Mechanics and Foundations Division, ASCE, 637–659. https://doi.org/10.1061/JSFEAQ.0001133

Griffiths, D.V, and Lane, P.A. (1999). Slope stability analysis by finite elements. Géotechnique, 49(3), 387–403. https://doi.org/10.1680/geot.51.7.653.51390

Hoek, E., and Diederichs, M.S. (2006). Empirical estimation of rock mass modulus. International Journal of Rock Mechanics and Mining Sciences, 43, 203–215. https://doi.org/10.1016/j.ijrmms.2005.06.005

Krahenbuhl, J., and Wagner, A. (1983). Survey, design, and construction of trail suspension bridges for remote areas. SKAT, Swiss Center for Appropriate Technology, St. Gallen, Switzerland.

Marinos, P., and Hoek, E. (2000). GSI: A geologically friendly tool for rock mass strength estimation. In Proceedings of the GeoEng2000 International Conference on Geotechnical and Geological Engineering (pp. 1422–1446). Technomic Publishers, Lancaster.

Matsui, T., and San, K. C. (1992). Finite element slope stability analysis by shear strength reduction technique. Soils and Foundations, 32(1), 59–70. https://doi.org/10.3208/sandf1972.32.59

Minnesota Guideline (2006). Minnesota Department of Natural Resources. Trail Planning, Design, and Development Guidelines: Shared Use Paved Trails, Natural Surface Trails, Winter-Use Trails, Bikeways. Trails and Waterways, Minnesota Department of Natural Resources.

Pal, S., Kaynia, A. M., Bhasin, R. K., and Paul, D. K. (2012). Earthquake stability analysis of rock slopes: A case study. Rock Mechanics and Rock Engineering, 45, 205–215. https://doi.org/10.1007/s00603-011-0145-6

Patton, F. (1966). Multiple modes of shear failure in rock. In Proceedings of the 1st Congress of the International Society for Rock Mechanics, Lisbon, Vol. 1, pp. 509–513.

Popescu, M. E. (2001). A suggested method for reporting landslide remedial measures. IAEG Bulletin, 60(1), 69–74. https://doi.org/10.1007/s100640000084

Rocscience (2012). Phase2: A 2D Finite Element Program for Calculating Stresses and Estimating Support around Underground Excavations. Geomechanics Software and Research, Rocscience Inc., Toronto, Canada. Available at: www.rocscience.com

Trail Design Guidelines. (2009). Regional Trails, Natural Areas and Developed Parks. PP&R Trail Guidelines Coordination Team, Portland Parks & Recreation, Portland, Oregon.

USDA (1984). U.S. Department of Agriculture Standard Specifications for Construction of Trails. USDA Forest Service Engineering Staff.

Research Article DOI: https://doi.org/10.64862/ajeg.2026.301.02.317 Open Access

Engineering Geological Characterization and Mapping of Aleta Wondo Town for Urban Development in Southern Ethiopia

Deginet Tesfaye Youkamo[1*] and Ephrem Getahun Gure[2]

[1]Bonga University, Kaffa, Bonga, Ethiopia
[2]Arba Minch University, Arba Minch, P.O. Box 21, Ethiopia

(*Corresponding E-mail: detesfaye1311@gmail.com)

Received: December 27, 2025, Accepted: May 18, 2026

Abstract: Aleta Wondo town, located in the Sidama Regional State of Ethiopia, lacks comprehensive geotechnical information on its ground conditions. The soils and rocks of the area have not been comprehensively characterized, despite the presence of geotechnical and geo-environmental challenges, including settlement, landslides, and groundwater problems. Comprehensive information on the types, characteristics, and distribution of underlying soils and rocks is essential for the safe and economically feasible construction of engineering structures. The primary objective was to characterize the geological and geotechnical properties of the study area through engineering geological investigations of soil and rock and to prepare a detailed multipurpose engineering geological map. Field investigations and laboratory testing were conducted to achieve this objective. Laboratory tests included natural moisture content, Atterberg limits, grain-size distribution, free swell, and shear strength. Seven traverses were conducted across the town to document exposures along road and river cuts, quarry sites, stream channels, and slope cuts. Discontinuity characteristics were measured and recorded, and Schmidt hammer tests were conducted on exposed rock surfaces. The laboratory and field results were used to classify the soils and rocks for engineering purposes. The Unified Soil Classification System (USCS), British Standard System (BSS), Rock Mass Rating (RMR), and unconfined compressive strength were used for classification. According to the USCS, the soils are classified as CL, representing inorganic clays of low to medium plasticity, and MH, representing inorganic and elastic silts. According to the BSS, the soils are classified as compressible silt and medium-plasticity inorganic clay. Based on RMR, unconfined compressive strength, and degree of weathering, the rocks are classified as good basalt with slight weathering and very high strength, good ignimbrite with slight weathering and high strength, and poor ignimbrite with high weathering and very low strength.

Keywords: ***Engineering geological map, Rock Mass Rating (RMR), Residual soil, Ethiopia.***

Introduction

Structural failures involving buildings, roads, dams, bridges, and other infrastructure have resulted in loss of life and significant economic damage. This is partly attributed to the focus on complex structural design without adequate consideration of the geotechnical characteristics of the ground surface and subsurface (Ayalew et al., 2022). The ground beneath complex structures is naturally anisotropic and heterogeneous, making geotechnical investigations essential for assessing the engineering suitability and economic feasibility of construction sites (Berhane, 2010). These investigations consider both surface and subsurface conditions. Foundation design, construction methods, and the mitigation of geotechnical and engineering geological problems depend on understanding the engineering and geological characteristics of soil and rock (Hunde, 2014).

Geotechnical properties control the suitability of soil and rock for engineering structures. These properties include grain-size distribution, plasticity, hydraulic conductivity, consolidation, shear strength, density, and porosity. Ground suitability can be properly assessed when these geotechnical properties are evaluated together with geo-environmental conditions (Bell, 2007).

Inadequate understanding of the geotechnical characteristics of foundation materials can lead to various foundation problems, including differential settlement of subsoil and masonry, horizontal movement caused by low shear strength, shrinkage resulting from moisture loss beneath foundations, and lateral pressure that may cause structural overturning (Ayalew et al., 2022). Engineering geologists use engineering geological maps to identify problematic areas, determine suitable locations for construction, and assess potential risks associated with poor foundation conditions and geohazards (Gure et al., 2013). These maps are specifically prepared for engineering purposes and provide information on lithology, layer thickness, depth below the ground surface, groundwater-table depth, and significant geomorphological features such as karst formations, landslides, active faults, and sources of construction materials (Price, 2008). In larger towns containing heavy engineering structures such as multistory buildings and roads, detailed knowledge of the geological and geotechnical properties of foundation materials and construction materials is essential (Berhane, 2010).

Ethiopia, a rapidly developing country, is experiencing extensive urbanization and infrastructure development, while many areas are affected by seismic and geotechnical hazards. Therefore, engineering geological investigations are essential to support present and future construction activities. The information obtained from such investigations provides an important basis for land-use planning and for the planning, design, construction, and maintenance of civil engineering projects throughout the country.

In Ethiopia, several studies have investigated the engineering properties of soils and rocks in different towns to assess their suitability for engineering applications. Ayele et al. (2022) used multichannel analysis of surface waves (MASW) to estimate shear-wave velocity for the engineering characterization of soils in Hawassa town, southern Ethiopia. Birhane (2010) investigated the engineering geological characteristics of soil and rock in Mekelle town, northern Ethiopia, and identified expansive clay soils that caused physical damage to buildings. Debebe (2011) investigated the engineering characteristics of soils in Adama town and identified silt and clay soils. Chemeda (2020) conducted an engineering geological investigation of Adama town and identified expansive soils and erosion problems.

Several regional-scale studies have also been conducted in and around the study area, particularly on groundwater, hydrogeology, and Lake Hydrology. Yasin (2002) investigated the hydrogeology of the Upper Gidabo River catchment in southern Ethiopia. Mussie (2007) studied groundwater circulation and hydrochemistry along the Upper Gidabo River and Lake Awassa catchments in the Sidama Zone. Wahid (2007) assessed the suitability of ground conditions for foundation and road construction in Awassa town, southern Ethiopia. Hroch and Megerssa (2018) prepared explanatory notes for thematic geoscientific maps of Ethiopia at a scale of 1:50,000, addressing soil and rock characterization, hydrogeological conditions, exogenous and endogenous geohazards, and possible mitigation measures. Ganole (2010) conducted a GIS-based assessment of surface irrigation potential for river-catchment development in Dale Woreda, Sidama Zone.

Despite previous studies, the engineering properties of the ground in Aleta Wondo town remain inadequately investigated. Civil engineering structures, including single- and multistory buildings and roads, are being developed without sufficient geotechnical investigations. The town also lacks detailed engineering geological and geological maps, while potential geotechnical hazards have not been systematically assessed. These knowledge gaps are reflected in existing infrastructure problems, including building damage and road deterioration along the Hawassa–Yirgalem–Aleta Wondo corridor. Furthermore, substantial areas of the town are vulnerable to flooding, highlighting the urgent need for comprehensive engineering geological investigations to support safe and sustainable urban development.

Therefore, this study investigates the geo-environmental and geotechnical conditions of Aleta Wondo town and prepares multipurpose engineering geological and geological maps to support safer construction, improve design practices, and reduce the risk of infrastructure failure. The study is based on the interpretation of secondary data, collection of primary data through field investigations, and laboratory testing of engineering and index properties of soil and rock. A major limitation of the study is the lack of organized secondary data on the soils and engineering geological conditions of the study area, as many engineering projects have been undertaken without adequate site investigation, standardized data collection, and systematic record keeping.

Study area

Location and accessibility of study area

Aleta Wondo is an autonomous town located in the Sidama Regional State of Ethiopia. Its coordinates range between 43578–43798E and 71799–72500N, with a maximum elevation of 2,008 m and a minimum elevation of 1,879 m above mean sea level. The town is located approximately 337 km south of Addis Ababa and 65 km from the regional capital, Hawassa. It is accessible via the Hawassa–Yirgalem–Aleta-Wondo–Negele Borena asphalt road, as shown in Figure 1.

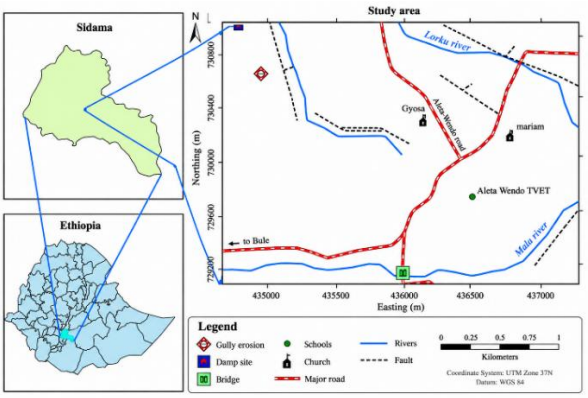


Figure 1, Location map of the study area.

Topography and slope

The topography of the town and its surroundings consists of flat to undulating terrain, deep gorges, river dissections, and steep slopes, resulting from its relatively close proximity to the Rift margin (escarpment), as shown in Figure 2. The larger part of the built-up area is characterized by an average slope ranging from 5% to 15%, while the hilly portions of the town have an average slope greater than 20%. The elevation at the center of the town, near the bus station, is approximately 1,925 m a.s.l. Generally, the elevation increases from the western part of the town toward the east.

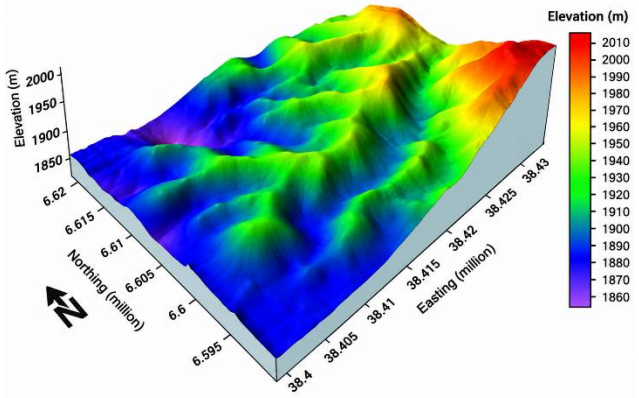


Figure 2, The Physiographic diagram of Alata Wondo Tow.

Drainage

The town is located within the Aleta Chuko watershed, a sub-basin of the Gidabo River Basin. It is bounded by two perennial rivers, the Kola River to the north and the Melebo River to the south. The Melebo River crosses the town, and both rivers ultimately drain into Lake Abaya. The rivers generally follow the major geological structures of the town, with streams flowing from southeast to northwest. The drainage network comprises first-, second-, and third-order streams, labeled 1, 2, and 3, respectively, as shown in Figure 3. The dendritic drainage pattern is strongly controlled by geological structures, indicating that the streams preferentially occupy zones of weakness.

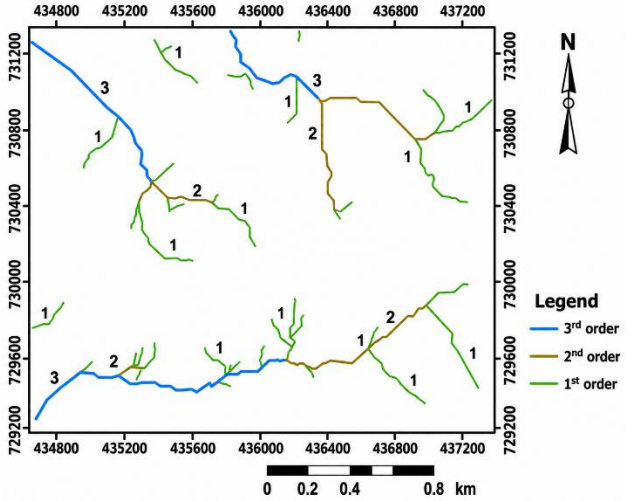


Figure 3, Drainage map of the study area (Aleta Wondo town) the town has third-order Melebo.

Climate

Aleta Wondo town falls within the Woyna-Dega agro-climatic zone, characterized by cool and sub-humid climatic conditions. The town experiences considerable annual and monthly variations in rainfall. The annual rainfall data for Aleta Wondo town over a 22-year period (1987–2008) are presented in Figure 4. During this period, annual rainfall ranged from 1,233 mm to 2,079 mm, with a mean annual rainfall of 1,564 mm.

The seasonal distribution of rainfall in the town indicates a bimodal pattern. The mean monthly rainfall of Aleta Wondo town for the period 1987–2008 is presented in Figure 5. As shown in the figure, low rainfall occurs from November to February, while high rainfall is recorded from April to October.

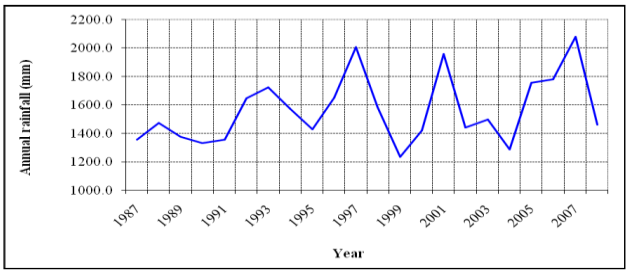


Figure 4, Annual rainfall of Aleta Wondo from 1987-2008 (Data source: Ethiopian Meteorology Agency).

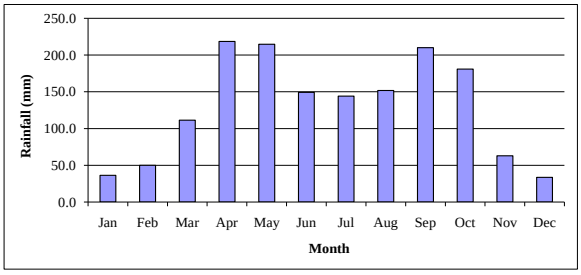


Figure 5, Mean monthly rainfall of Aleta Wondo from 1987-2008 (Data source: Ethiopian Meteorology Agency).

Theoretical concepts

To a civil engineer, soil is any uncemented or weakly cemented accumulation of mineral particles formed through the weathering of rocks, with the void spaces between the particles containing water and/or air.

Because soils and rocks are naturally anisotropic and heterogeneous, geotechnical investigations are essential for assessing the economic feasibility of engineering structures at and around a proposed site (Gure et al., 2013). Geotechnical investigations include both surface and subsurface assessments. Foundation design, construction methods, and the resolution of geotechnical and engineering geological problems begin with determining the engineering and geological characteristics of the soil and rock (Price, 2008). The main objective of geotechnical investigation of soil and rock is to prepare an engineering geological map.

Engineering geological map

Engineering geology is a sub-discipline of applied geology that bridges the professional gap between geology and civil engineering. It is an important field for identifying suitable locations for civil engineering structures (Bell, 2007). Without adequate engineering geological assessment, it may be difficult to identify areas suitable for safe construction and areas affected by poor foundation conditions, geohazards, and unacceptable risks (Gure et al., 2013). These conditions can be evaluated through the preparation of engineering geological maps.

In recent years, considerable attention has been given to the preparation of engineering geological maps. These maps are specifically designed for engineering purposes and provide information on lithology, layer thickness and depth, groundwater-table depth, significant geomorphological features such as karst, landslides and active faults, and the location of construction materials (Price, 2008). An engineering geological map is a type of geological map that provides a general representation of geological environmental conditions relevant to land-use planning, design, construction, and maintenance in civil and mining engineering. The principal factors considered in engineering geological mapping include rock and soil, groundwater, geomorphological conditions, and geodynamic processes. In this context, soil generally refers to materials that can be excavated without explosives or specialized loosening or ripping equipment (Hunde, 2014). According to the survey criteria, areas with soil thickness of less than 1 m are mapped as the underlying bedrock, while soil exceeding 1 m in thickness is considered a separate mapping unit.

The main components of an engineering geological map include the characteristics of rocks and soils, including their description, stratigraphic and structural relationships, genesis, lithology, physical condition, and physical and engineering properties; hydrogeological conditions; geomorphological conditions; and geodynamic phenomena.

Based on purpose, engineering geological maps can be classified into specific-purpose and multipurpose maps. Specific-purpose maps provide information on a particular engineering aspect or purpose, such as dam-site suitability, bearing capacity and settlement, or slope stability. Multipurpose engineering geological maps provide information on multiple aspects of engineering geology for a variety of planning and engineering purposes.

Components of engineering geological maps

Engineering geological maps should include interpretative cross-sections, explanatory text, and a legend. They may also include supporting documentation and data collected during map preparation. At all scales, engineering geological maps should present information in a manner that clearly communicates both the geological conditions and their engineering significance.

A major challenge in multipurpose engineering geological mapping is selecting geological characteristics of rocks and soils that are closely related to important engineering properties such as strength, deformability, durability, and permeability. Determining all these properties quantitatively over large areas, in sufficient detail, and within reasonable time and cost constraints is often difficult. Therefore, geological and index (geotechnical) properties that provide reliable indicators of the physical and engineering geological characteristics are commonly used.

Geotechnical characterization of soil

To assess the suitability of soil for use as a foundation material or construction material, its geotechnical properties must be characterized. Soils are characterized based on their index and engineering (design) properties (Arora, 2008). Index properties are not of primary interest to geotechnical engineers but provide indicators of the engineering properties of soil and are used for classification in engineering practice (Arora, 2008). The index and engineering properties of soil are described in following subsection.

Natural moisture content

The water content of a soil mass is defined as the ratio of the mass of water in the voids to the mass of soil solids. It is usually expressed as a percentage and can range from zero for completely dry soil to several hundred percent for highly saturated soil (Murthy, 2003). Natural moisture content influences soil behavior when used for construction and as a foundation material. It affects settlement and consolidation, shear strength, and the suitability of soil for compaction.

Grain-size analysis

Grain-size analysis determines the particle-size distribution of soil, which influences its engineering properties and is used for soil classification (Arora, 2008). The particle-size distribution curve (gradation curve) represents the distribution of particles of different sizes within a soil mass and indicates the degree of gradation, allowing the soil to be classified as well graded or poorly graded.

Consistency limit

The consistency of soil depends largely on its water content (Arnold, 2001). As the water content of fine-grained soil gradually increases from 0%, the soil passes through different consistency states: brittle solid, semi-solid, plastic, and liquid. The Atterberg limits represent the boundary water contents between these states and include the liquid limit, plastic limit, and shrinkage limit.

Specific gravity

Specific gravity is the ratio of the mass of soil solids to the mass of an equal volume of water at 4°C. It is an important index property of soil and is closely related to its mineralogy and chemical composition (Osuolale et al., 2012). It is also useful for assessing the qualitative behavior of soil (Raj, 2012) and for classifying soil minerals. For example, iron-rich minerals generally have higher specific gravity than silica (Bowles, 1996).

Free swells

The degree of soil swelling depends on clay mineralogy, soil structure and texture, and various physical and

chemical properties. Among clay minerals, montmorillonite has the greatest influence on the swelling magnitude and activity of soils compared with illite and kaolinite (Holtz and Kovacs, 1981). Expansive soils can be identified through mineralogical analysis, indirect index property tests, or direct expansion potential tests (Chen, 1988). The expansivity of soil is primarily governed by the type and proportion of clay minerals present.

Shear strength

The shear strength of soil is its ability to resist sliding along internal surfaces within a soil mass. The stability of cuts, earth dams, foundations, natural slopes, and other structures constructed on soil depends on the shearing resistance of the soil along potential failure surfaces. Cohesion (C) and angle of internal friction (ϕ) are the key parameters of shear strength (Murthy, 2003). The shear resistance of soil results from friction and particle interlocking, as well as possible cementation or bonding at particle contacts.

Permeability and consolidation

Consolidation is the time-dependent settlement of soil resulting from the expulsion of water from its pores. In clay soils, the expulsion of pore water may take considerable time because of their low permeability (Arnold, 2001).

Soil compaction

Soil compaction is a ground improvement technique in which compactive energy is applied to rearrange soil particles into a denser configuration. Compaction increases the shear strength of soil and reduces its compressibility and permeability (Kaniraj, 1988). Compaction is not an index property of soil; rather, it is the densification of soil through the expulsion of air.

Engineering geological classification of soil

From an engineering perspective, soil classification is based on the suitability of soil for use as a foundation or construction material (Arora, 2008). Determining engineering properties in the laboratory can be expensive and time-consuming; therefore, soil classification provides an efficient approach by grouping soils with similar index properties within specified ranges of variation. Soils within these ranges generally exhibit similar engineering qualities for civil engineering applications. A soil classification system should provide an indication of the engineering performance of a soil type and allow rapid identification of soil characteristics (Matula, 1981). Several classification systems are available, each developed for specific applications. For example, the American Association of State Highway and Transportation Officials (AASHTO, 2014) system classifies soils according to their suitability for roads and highways, whereas the Unified Soil Classification System (USCS) and British Standard System were originally developed for airfield construction and later adapted for general engineering applications (Ayalew et al., 2022).

Engineering geological classification and characterization of rock

Rocks exhibit different engineering properties depending on their mode of origin, mineralogical composition, texture, structure, and the presence of primary and secondary structures. Therefore, a qualitative assessment of their engineering properties can often be made based on their genetic type. Rock mass classification provides a quantitative assessment of rock mass quality. Several classification systems are available, among which Rock Quality Designation (RQD) and Rock Mass Rating (RMR) are widely used for engineering characterization.

Geologic setup of the study area

Regional geology

Aleta Wondo town is situated in the southern segment of the Main Ethiopian Rift Valley and represents a transition zone between the Ethiopian Plateau and the Rift Valley, with a poorly defined escarpment. The evolution of the southern segment of the Main Ethiopian Rift has been divided into three stages based on age (Yismaw et al., 2012): pre-rift (32–45 Ma), syn-rift (22–12 Ma), and post-rift (0–5 Ma).

Syn-rift volcanic deposits

Syn-rift volcanic deposits include the Nazareth Formation of Miocene age, consisting of transitional to mildly alkaline and subalkaline basalts and rhyolites, aphyric and porphyritic basalts with lesser vesicular basalt, and minor alkali trachyte flows and tuffs. These deposits cover the areas around Dilla, Wenago, Chinchu, Bedesa, Teferikela, Aleta Wondo, and Kebado. The transitional to mildly alkaline and subalkaline basalt is highly weathered, forms cliffs, and exhibits fractures and joints. It is composed mainly of olivine, pyroxene, and plagioclase and is overlain by rhyolite (Yismaw et al., 2012).

Post-rift volcanic deposits

Post-rift volcanic deposits include pumiceous pyroclastics, ignimbrites, tuffs, water-laid pyroclastics, lacustrine deposits, volcaniclastic sediments, and diatomites. These deposits are exposed in the northern part of the mapped area, covering areas around Midre Genet, Morocho, Yirga Alem, Hawassa, and Chuko.

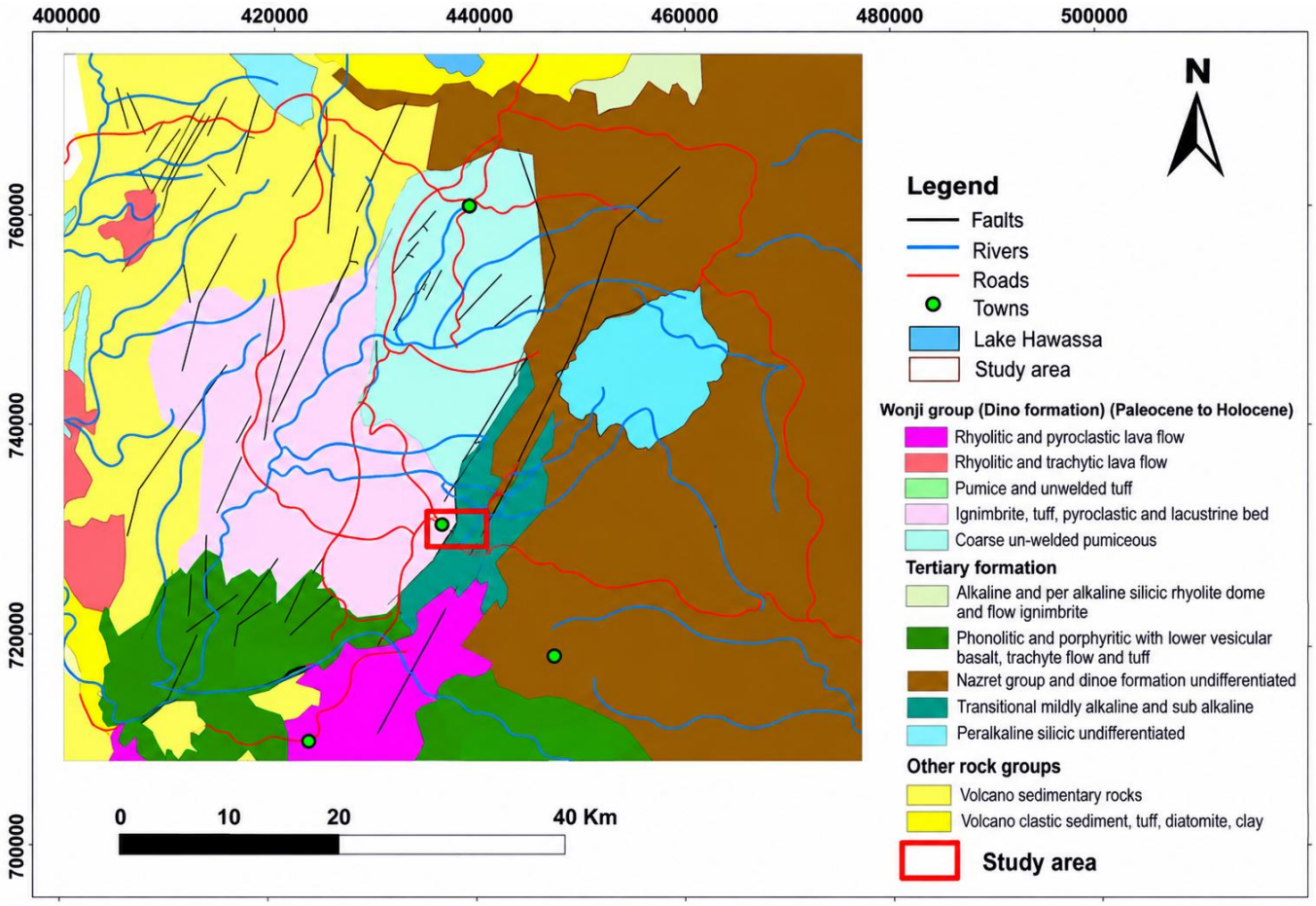


Figure 6, Regional Geologic Map showing location of study area.

Local geology

The geology of the Aleta Wondo area is represented by two volcanic units. The lower unit consists of basaltic lava flows (basalt), which crop out along the river in the eastern to southeastern parts of the town and represent the oldest unit in the area (Figure 11). It consists mainly of sub-horizontal lava flows with thicknesses ranging from a few meters to 20 m. The maximum exposed thickness occurs east of the town along the river. The ignimbrite unit is exposed near Aleta Wondo along the rivers. It overlies the Aleta Wondo basalt and locally covers the products of the composite central volcanoes of Wechecha and Furi. The sequence consists of different flow units, including pale-green to pale-yellow welded and crystal-rich ignimbrites (Figure 7).

Aleta Wondo town is predominantly underlain by thick residual soil. In the southern part of the town, particularly along the slope cuts of the Kibre Mangist Road, thick residual clayey to silty soil deposits ranging in color from white to brown and reddish hues are exposed (Figure 8). The average thickness of the residual soil within the town is approximately 12 m.



Figure 7, Ignimbrite unit deposit along with river "A" and at quarry site "B".

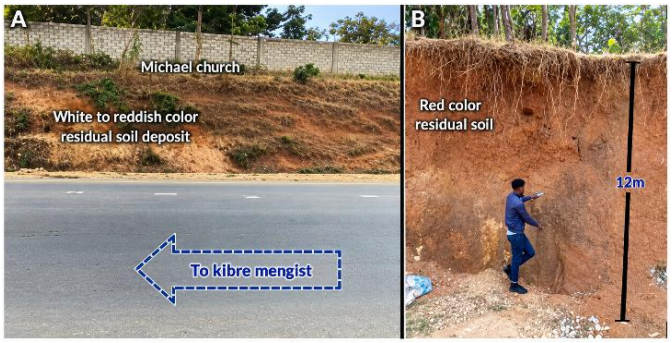


Figure 8, Residual soil deposits.

Geological structures and tectonics

In an engineering context, discontinuities are important factors governing the deformability, strength, and permeability of rock masses. Large and persistent discontinuities can significantly affect the stability of surface and underground excavations. Therefore, understanding the geometric, mechanical, and hydrological properties of discontinuities is essential for rock mechanics and engineering.

The town is located in the southern segment of the Main Ethiopian Rift (MER) system. As shown by the rose net model (Figure 10), the regional fault system and local faults and joints predominantly strike NNW–SSE. However, the southern segment of the MER trends NNE–SSW, indicating that the structural trend of the MER has had limited influence on the structures in the study area. Thus, the strike directions of the MER system and the major fault system in the study area are not similar. The faults in the study area predominantly dip toward the NE and SSW. In the northern part of the town, particularly along stream cuts (Figure 9), minor, persistent joints and two sets of joints dissecting the ignimbrite rock are observed.



Figure 9, Minor local fault and Joints on ignimbrite along to Hawassa route.

Methodology

Climatic, topographic, geomorphological, hydrogeological, geological, and engineering geological data are essential for achieving the objectives of the present study. Based on these data, different methodological stages were designed and implemented in accordance with the intended objectives (Figure 13).

Primary and secondary data obtained from field investigations, previous studies, and laboratory activities were used in this study. The study considers the future expansion of the town boundary as outlined in the current master plan.

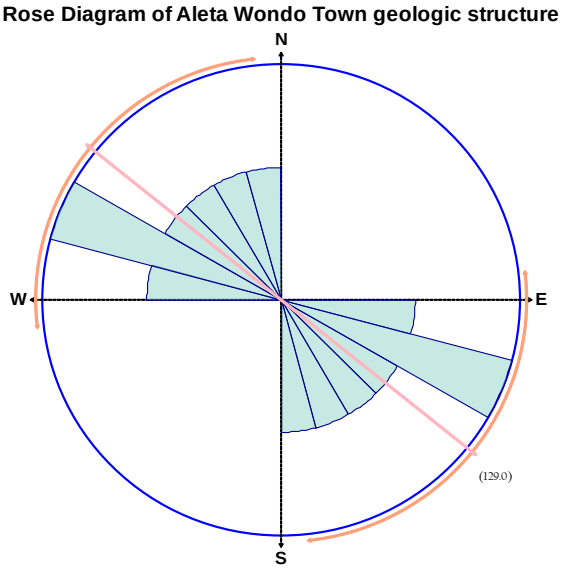


Figure 10, Rose diagram.

Fieldwork included detailed descriptions and observations of exposures along road and river cuts, quarry sites, stream channels, and slope cuts to identify the engineering geological characteristics of the rock. Measurement and recording of discontinuity characteristics were also conducted. Sampling locations and the number of samples were determined based on the geological variations of the soil and bedrock (Figure 12).

Ten test pits were excavated to a maximum depth of 4 m using shovels and other appropriate hand tools. During sampling, vertical variations in the soil profile were carefully observed and recorded. The number of test pits and samples was considered sufficient to characterize the subsurface soil conditions of the study area.

To determine the uniaxial compressive strength (UCS) of the rocks, in-situ tests were conducted on exposed rock surfaces using an N-type Schmidt hammer. The tests were performed on smooth and relatively uniform rock surfaces (Wang et al., 2017). Prior to testing, the rock surfaces were smoothed using the rubbing stone provided with the Schmidt hammer. Rebound values were recorded at each selected test location and converted to unconfined compressive strength (Wang et al., 2017) using the linear relationship presented in Eq. (1).

$$UCS=3.03RN-30.3 \quad (1)$$

The Rock Quality Designation (RQD) was determined using the volumetric joint-count method on exposed rock surfaces. This method estimates RQD based on the number of discontinuities within a defined rock mass volume. The RQD was calculated using the relationship proposed by Deere and Deere (1988).

$$RQD = 115 - 3.3Jv \quad (2)$$

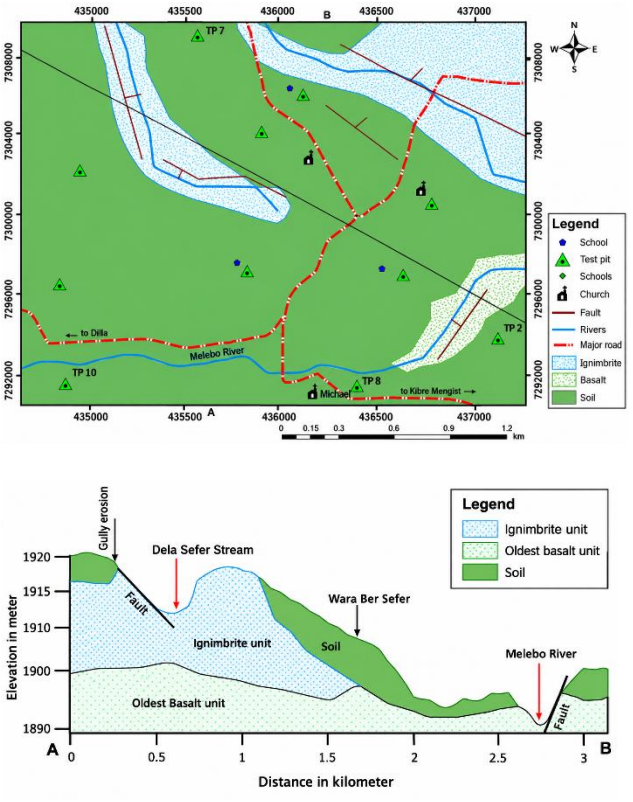


Figure 11, Geologic map and geologic cross section of the study area.

where (Jv) represents the volumetric joint count, defined as the total number of joints per unit length for all joint sets having discontinuity lengths of ≥10 cm. In addition, the condition of the discontinuities and the general groundwater conditions of the exposed rock masses were assessed in the field to evaluate the overall quality of the rock mass.

Finally, the Rock Mass Rating (RMR) was determined using the relevant discontinuity characteristics and RQD as input parameters. The combined assessment of UCS, RQD, discontinuity conditions, groundwater conditions, and RMR provided a basis for evaluating the engineering characteristics and quality of the rock masses in the study area.

Laboratory work included testing the index and engineering properties of soil samples, including natural moisture content (NMC), specific gravity, Atterberg limits (liquid limit and plastic limit), grain-size analysis, pH value, free swell, and shear strength. Laboratory tests were conducted according to ASTM (2018) and AASHTO (2014) standards. The soils of the study area were classified based on their engineering behavior according to the Unified Soil Classification System (USCS) and British Standard System (BSS).

Analysis and interpretation of in-situ and laboratory data were conducted to convert the raw soil and rock data into meaningful information about the study area. Data processing and interpretation were carried out using various software tools, including Microsoft Office for calculation, sorting, and tabulation of raw data; Rose Net projection for geological structural analysis; ArcMap 10.4 and Golden Surfer 9.11 for the preparation and manipulation of maps; and Google Earth Pro for collecting geospatial data.

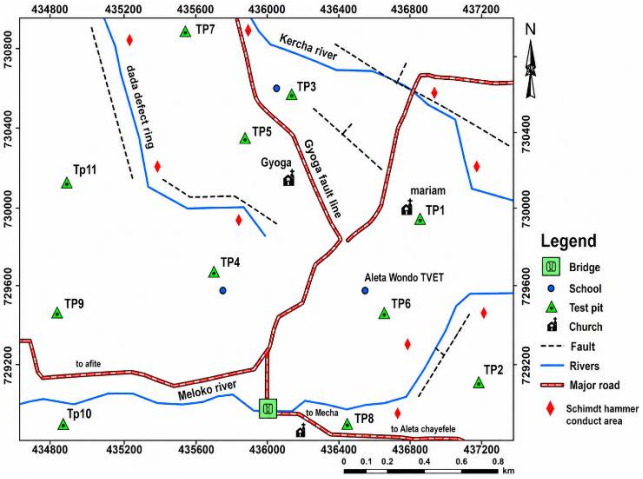


Figure 12, Test-pit and Schmidt hammer test locations.

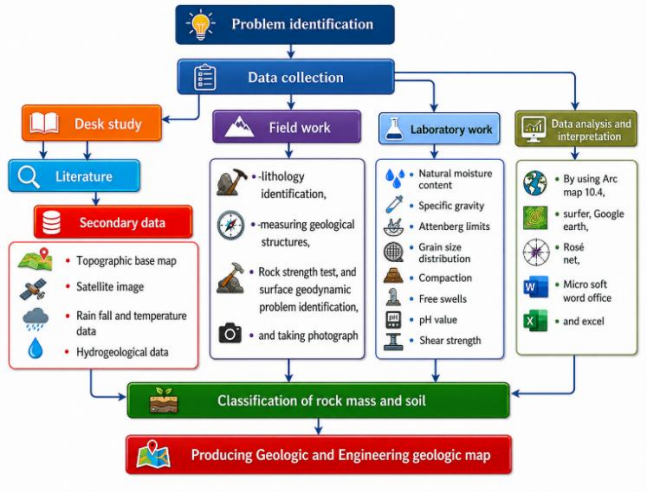


Figure 13, Flow chart of this study.

Results and discussion

Engineering geological characterization and classification of soils

Genetically, the study area is dominated by residual soils formed through in-situ weathering of the parent rock. Characterization of the geotechnical and engineering geological properties of the soils was initiated by describing their genetic, lithological, and textural characteristics, followed by analysis and discussion of the geotechnical laboratory results from the study area.

Index properties

Natural moisture content

For many soils, water content is an important index for establishing the relationship between soil behavior and its properties. The natural moisture content of the soils in the study area ranges from 23.2–48% for silty soil, 39% for clayey silt, and 28.8% for sandy silt. These

results indicate that the soils of the study area generally have medium water-holding capacity, with fine-grained fractions being dominant.

Table 1, Summarized index property test results of study area.

S. No.	Depth (m)	NMC	SG	PD (%)			LL	PL	Soil type		Lithology
				%Sa	%Si	%C			USCS	BSS	
1	10	3	39	2.60	18.7	41.3	40	38.93	CL	CM	Clay
2	7	3	28.8	2.51	47	33.26	13	50.7	SM	SM	Sand
3	1	1.5	31.64	2.47	7.4	61.95	30.65	71.76	MH	MH	Silt
4	1	3	—	2.40	7.61	63.69	28.43	59	MH	MH	Silt
5	2	3	34.9	2.50	10.5	54	36	57	MH	MH	Silt
6	3	3	31.7	2.54	15.65	56.55	27.24	60.8	MH	MH	Silt
7	4	3	27.4	2.52	10	58.8	32	66.7	MH	MH	Silt
8	5	3	23.2	2.48	8.7	63.65	27.64	69.5	MH	MH	Silt
9	6	1.5	30.7	2.55	8.93	73.9	18	62.3	MH	MH	Silt
10	6	3	—	2.50	8.34	70	15	48.3	MH	MH	Silt
11	2	2	48	2.60	22	49.5	28	42.0	CL	MH	Silt
12	8	4	—	2.56	20	42.95	37	58.4	MH	MH	Silt
13	9	3	35	2.52	10.2	64.59	25.21	62.4	MH	MH	Silt

The degree of consolidation of the soil can be estimated by comparing the natural water content (w) with the liquid limit (LL) and plastic limit (PL). If the water content is closer to the liquid limit than to the plastic limit, the soil is likely to be normally consolidated. Conversely, if the water content is closer to the plastic limit than to the liquid limit, the soil is likely to be pre-consolidated (Munsell, 2000). Based on the particle-size analysis, water content, and Atterberg limits, the silt- and sand-dominated soils in most parts of the town have water contents closer to the plastic limit, indicating that they are likely pre-consolidated. However, the southwestern and some parts of the southeastern areas of the town (Figure 14) are dominated by clayey soil, where the natural moisture content is closer to the liquid limit.

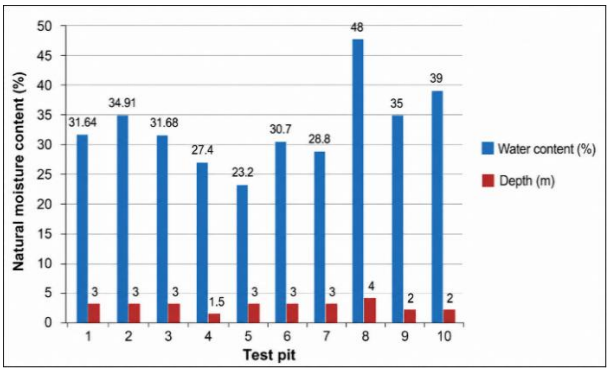


Figure 14, Graph of natural moisture content of soils in the study area.

Specific Gravity (Gs)

The specific gravity of soil is the ratio of the unit weight of soil solids to the unit weight of water. In the laboratory, the specific gravity of soil was determined by placing a known weight of oven-dried soil sample in a pycnometer, which was then partially filled with distilled water. The specific gravity of solids for most natural soils generally ranges from 2.65 to 2.80, with lower values typically observed in coarse-grained soils. Specific gravity is used to determine the void ratio and particle-size characteristics of soils.

The specific gravity laboratory determination followed ASTM D854-23 (ASTM, 2023).

$$Gs = \frac{Unit\ weight\ of\ solid\ soil}{Unit\ weight\ of\ water} \qquad (3)$$

In study area-specific gravity range from 2.47-2.6 for silty soils and 2.61 and 2.55 for clayey and sandy respectively.

Grain size analysis

To determine the index properties of the soils in the study area, thirteen soil samples were collected from ten test pits, as presented in Table 1. Based on grain-size distribution, the soils in the study area were classified into sandy, silty, and clayey types. The sandy soil contains approximately 47% sand, 37.5% silt, and 13% clay. The silty soils contain 37.5%–73.9% silt, 8.7%–15.65% sand, and 18%–30.65% clay. The clayey soil contains approximately 50% clay, 31.6% silt, and 18.4% sand. Overall, the grain-size analysis indicates that the study area is predominantly underlain by silty soils, as illustrated in Figure 15.

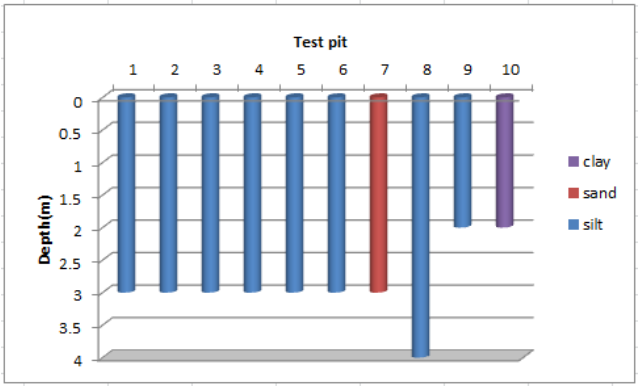


Figure 15, lithological description of grain size distribution.

Atterberg limits and plasticity index

According to Bowles (1996), soils with higher plasticity indices may present greater engineering problems when used as engineering materials, particularly for foundation support and road subgrades. As shown in Table 1, laboratory test results indicate that the clayey soils have liquid limit (LL) and plastic limit (PL) values of 38.93% and 15.8%, respectively. The silty soils have LL values ranging from 57%–71% and PL values from 41%–48.6%, while the sandy soils have LL values ranging from 39.9%–50.7%. The plasticity indices (PI) of the clayey and sandy soils are 23.23% and 10%, respectively, while the PI of the silty soils ranges from 10%–23%.

Soils with higher plasticity indices generally have lower engineering suitability. Soils with PI >35% are classified as very highly plastic, while those with 20% ≤ PI ≤ 35% and 10% ≤ PI < 20% are classified as highly and moderately plastic, respectively. Soils with PI ≤10% are classified as low-plasticity soils (Seed et al., 1962). In the study area, sandy soils have low plasticity, whereas silty and clayey soils have medium to high plasticity. Therefore, special consideration is required during construction, particularly in the southwestern parts of the town, where compressible clay and silt with high plasticity and shallow groundwater conditions are

present. Based on the Casagrande plasticity chart (Figure 16), the soil samples from the study area range from low to high plasticity.

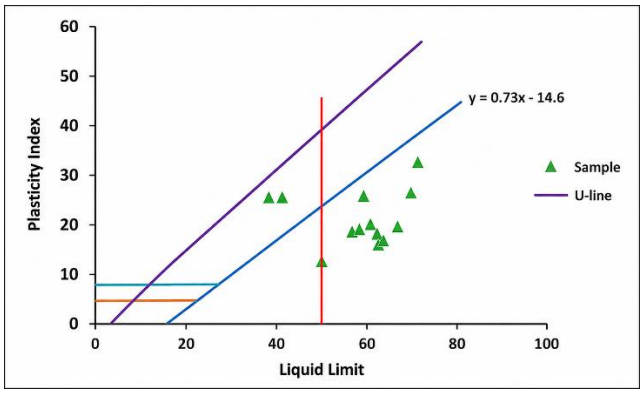


Figure 16, Plots of soils of the study area on Casagrande plasticity chart.

Activity of soils

Activity of soil is as the ratio of the plasticity index and the percentage of clay fraction, i.e. finer than 2μ (Clayton, 1995.)

$$Ac=\frac{PI}{\%\ of\ caly\ fraction} \qquad (4)$$

Eq. 3 illustrates activity and it is a measure of the water-holding capacity of clay soils. The change in volume of clay soil during swelling or shrinkage depends on its activity, which is related to the percentage by weight of soil particles smaller than 2 μm. Based on Table 1, soils with an activity of 0.75 < A < 1.25 are classified as normal clays, A < 0.75 as inactive clays, and A > 1.25 as active clays. Activity is useful for classifying and evaluating the engineering properties of soils, particularly active and inactive clays. It also shows a fair to good correlation with the type of clay mineral.

Laboratory test results indicate that activity, swelling potential, and plasticity index are generally directly related, whereas the percentage of clay fraction does not necessarily have a direct relationship with activity. The swelling potential and activity of clayey soils are strongly influenced by clay mineralogy rather than solely by the percentage of clay fraction. The laboratory data show that the plasticity index has a stronger relationship with soil activity than with the percentage of clay fraction, owing to the influence of clay mineralogy and chemical behavior. Soils containing active minerals such as montmorillonite and smectite generally exhibit higher plasticity and activity, regardless of the clay fraction. In contrast, clay fractions dominated by quartz do not exhibit significant water-absorption behavior because quartz is an inactive mineral. Montmorillonite has an expandable lattice and exhibits a high degree of hydration and cation adsorption. The degree of lattice expansion depends on the nature of the adsorbed cations. Illite is another common clay mineral and exhibits limited expansion due to strong bonding between silica sheets by potassium ions (Holtz and Gibbs, 1956). Therefore, soils with a low clay fraction may have high swelling potential if they contain montmorillonite-group minerals, and vice versa.

Generally, the influence of clay content on soil activity is significant when active clay minerals are present; otherwise, variations in clay fraction may have little effect on activity when the soil is dominated by inactive minerals such as kaolinite. Clay fractions containing kaolinite generally have low activity, whereas those containing montmorillonite have high activity (Rich, 1968). As observed in Table 2 and the activity–soil category plot (Figure 17), the soils of Aleta Wondo town are predominantly classified as inactive to normal. Soil activity in the study area was determined using the plasticity index and grain-size analysis results based on Skempton's classification of soil activity.

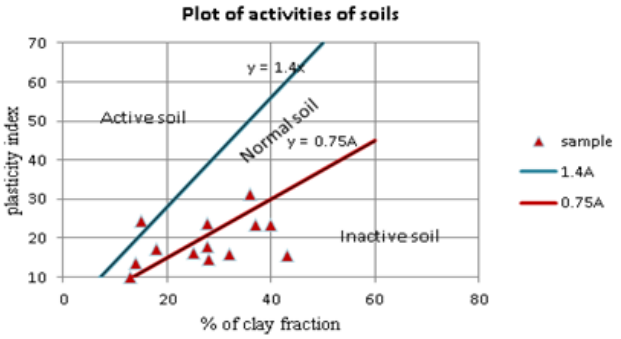


Figure 17, Skempton's chart showing the activity of soils in the study area.

Table 2, Activity of study area soils.

S. No.	Depth (m)	Dominant	PL	LL	PI	Activity	Remark
1	1-2	Clay	15.8	38.93	23.3	0.612	Active
2	1-3	Sand	39.9	50.7	10	0.76	Normal
3	1.5	Silt	41.6	71	31.16	1.016639	Normal
4	3	Silt	35.2	59	23.8	0.837144	Normal
5	1-3	Silt	41	57	16	0.444444	Inactive
6	1-2	Silt	43	60.8	17.8	0.653451	Inactive
7	1-2	Silt	49.5	66.7	17.2	0.5375	Inactive
8	1-3	Silt	45	69.5	24.5	0.886397	Normal
9	1.5	Silt	48.6	62.3	13.7	0.761111	Normal
10	3	Silt	48.3	63	14.7	0.98	Normal
11	2	Silt	19	42	23	0.812143	Normal
12	4	Silt	42.2	58.4	16.2	0.437838	Inactive
13	1-3	Silt	47	62.4	15.4	0.610869	Inactive

Liquidity index (LI), plasticity index and consistency index (CI)

The liquidity index of a soil indicates the proximity of its water content to the liquid limit. At the liquid limit, the liquidity index is 100%, and the soil behaves as a liquid, whereas at the plastic limit, it is zero. Negative liquidity index values indicate a water content below the plastic limit (Arora, 2008). These indices are determined from the natural moisture content, liquid limit, and plastic limit using mathematical formulae (Eq. 5).

$$LI = \frac{w-PL}{PI} \qquad (5)$$

The liquidity index of soils in Aleta Wondo town, determined from ten test pits, ranges from −1.26 to 1.285. As presented in Table 3, most soil samples have

negative liquidity index values, except TP10 and TP8, which have liquidity index values of 1.003 and 1.26, respectively. Similarly, the consistency index of the soils in the study area is presented in Table 4. The consistency index indicates the firmness of soil and its proximity to the plastic limit. Soil with water content equal to the plastic limit has a consistency index of 100%, indicating relatively firm soil.

The consistency index values in the study area range from −0.003 to 1.779. Most soils in the study area are firm, except those at TP10 and TP8. Overall, the liquidity and consistency index results indicate that the majority of the soils in the study area are hard to stiff and firm in consistency.

Table 3, The liquidity, plasticity and consistency index of Aleta Wondo Town.

TP	Depth (m)	Dominant	PL	LL	PI	CI	LI
10	1-2	Clay	15.8	38.93	23.3	-0.003	1.003
7	1-3	Sand	39.9	50.7	10	2.028	-1.028
1	1.5	Silt	41.6	71	31.16	1.339	-0.339
	3		35.2	59	23.8	1.109	-0.109
2	1-3		41	57	16	1.381	-0.381
3	1-2		43	60.8	17.8	1.636	-0.636
4	1-2		49.5	66.7	17.2	2.285	-1.285
5	1-3		45	69.5	24.5	1.890	-0.890
6	1.5		48.6	62.3	13.7	2.307	-1.307
	3		48.3	63	14.7	2.109	-1.109
8	2		19	42	23	-0.26	1.26
	4		42.2	58.4	16.2	0.747	0.253
9	1-3		47	62.4	15.4	1.779	-0.779

Free swell

The free swell test is one of the simplest and essential index tests for fine-grained soils, as it indicates the presence of swelling clay minerals based on soil mineralogy. The swelling potential of soil is related to its activity, which is associated with the plasticity index. Free swelling or expansion of clayey soils can cause failure of engineering structures (Holtz and Gibbs, 1956).

Soils having a free swell value below 50% rarely exhibit extensive volume changes, even under very light loadings (Prakash et al., 2004). However, soils with free swell values of about 100% or higher may cause considerable damage to lightly loaded structures.

The free swell values in the study area range from 15.9% to 60% for silty soils, and from 19.5% to 54% for sandy and clayey soils, respectively (Table 4).

According to the IS soil classification system based on the free swell index, Aleta Wondo is characterized by a low to medium degree of expansion. Therefore, samples with free swell values greater than 50% require consideration during the design of civil structures founded on such soils, as they exhibit significant swelling potential. In particular, TP1, TP10, and TP5 require special consideration.

Table 4, Free swell chart of study area.

TP	Depth (m)	Dominant	PL	LL	PI	FS
10	1-2	Clay	15.8	38.93	23.3	47
7	1-3	Sand	39.9	50.7	10	34.5
1	1.5	Silt	41.6	71	31.16	60
	3		35.2	59	23.8	
2	1-3		41	57	16	13.9
3	1-2		43	60.8	17.8	18
4	1-2		49.5	66.7	17.2	27.5
5	1-3		45	69.5	24.5	50
6	1.5		48.6	62.3	13.7	21.7
	3		48.3	63	14.7	
8	2		42	65.3	23.3	15.9
	4		42.2	58.4	16.2	
9	1-3		47	62.4	15.4	18.2

PH (power of hydrogen)

Soil pH is a measure of its acidity or alkalinity, expressed numerically on a scale of 0–14. The geotechnical properties of soil can be significantly affected by changes in pH; therefore, determining soil aggressiveness is essential for assessing its potential effects on engineering structures. Dissolution reactions are more pronounced under highly acidic and alkaline pH conditions, which can deteriorate or corrode concrete in engineering structures (Yadeta, 2020).

The consistency limits generally decrease with changes in pH. Changes in pH can also induce cation exchange, weakening the electrostatic attraction between soil particles and consequently reducing the strength of lateritic soil (Osuolale et al., 2012). In the study area, the pH values range from 7.11 to 7.31 (Table 5), indicating slightly alkaline conditions. Therefore, the soil is not expected to pose significant adverse effects that could lead to the failure of civil engineering structures.

Table 5, pH value of study area.

TP	Depth (m)	Dominant	PL	LL	PI	FS
10	1-2	Clay	15.8	38.93	23.3	47
7	1-3	Sand	39.9	50.7	10	34.5
1	1-5	Silt	41.6	71	31.16	60
	3		35.2	59	23.8	
2	1-3		41	57	16	13.9
3	1-2		43	60.8	17.8	18
4	1-2		49.5	69.7	17.2	27.5
5	1-3		45	69.5	24.5	50
6	1.5		48.6	62.3	13.7	21.7
	3		48.3	63	14.7	
8	2		42	65.3	23.3	15.9
	4		42.2	58.4	16.2	
9	1-3		47	62.4	15.4	18.2

Compaction

Laboratory measurements of the bulk mass of compacted soil were obtained for each trial, and the corresponding moisture content values were determined. The optimum moisture content and maximum dry density results for the study area are presented in Table 6.

Table 6, Compaction test result of study area.

TP	Depth	ρd (kg/m³)	Wopt%
1	1.5	1.562	32.8
2	3	1.604	28.5
3	3	1.38	33
5	3	1.22	30.5
7	3	1.424	31
8	2	1.487	28.8

Geotechnical engineers assess field soil compaction based on the relative compaction value. According to Arora, the dry density achieved in the field is compared with the maximum dry density obtained in the laboratory. The ratio of field dry density to maximum dry density is known as relative compaction.

According to Arora, cohesive soils should attain at least 95% relative compaction to minimize geotechnical problems. Since the study area is dominated by cohesive silty clay soil, the field compaction value of Aleta Wondo soil should be greater than 95% when compared with the laboratory results.

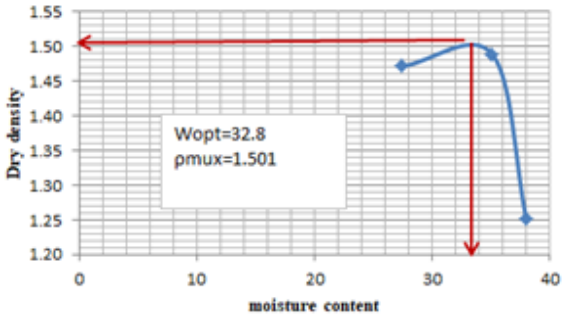


Figure 18, Compaction test result of TP1.

Direct shear test

In this study, six representative samples from different engineering soil classes were selected. The engineering properties and shear strength parameters of the selected samples are presented in Table 7. The results indicate that the cohesion of compressible silt varies from 22.86 to 49.37 kPa, while the angle of shearing resistance ranges from 19° to 22.88°. For low-plasticity clay with silt, the cohesion and angle of internal friction are 54 kPa and 18°, respectively.

Soil classification

Based on the Unified Soil Classification (USCS), Aleta Wondo town is characterized by compressible silt and low- to medium-plasticity clay. According to the British Standard Soil Classification System, the study area soils are classified as compressible silt and medium-plasticity inorganic clay.

Table 7, Shear strength test result of study area.

TP	Lithology	Engineering class (USCS)	Depth	Shear strength	
				Cohesion (kPa)	Internal friction angle
1	Silty	Compressible Silt with clay	1 m	21	22.88
2	Silty	Compressible Silt with clay	3 m	38.4	22.5
6	Silty	Compressible Silt with clay	1.5 m	49.73	20.56
7	Sandy	Compressible Silt with clay	3 m	21.16	22.88
8	Silty	Compressible Silt with clay	4 m	36	19
10	Clayey	Low plasticity Clay with silt	3 m	54	18
11	Sandy	Compressible Silt with clay	3 m	22.12	22.99

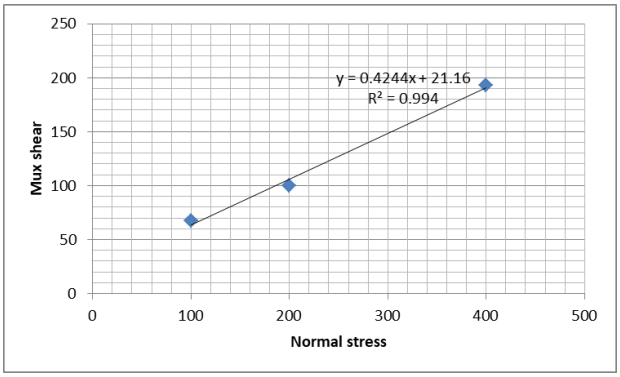


Figure 19, Shear strength test result of TP7.

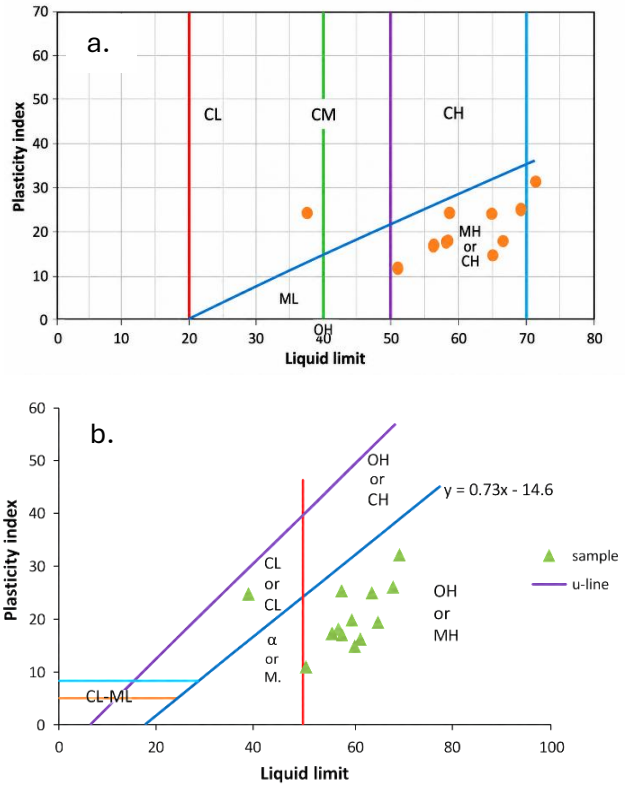


Figure 20, Soil classification according to (a) British Soil Classification System (BSCS) and (b) Unified Soil Classification System (USCS).

Engineering geological characterization and classification of rocks

In the study area, nine testing locations were identified to determine the Schmidt rebound value of the rock, and an average of ten readings was taken at each location. Schmidt hammer rebound values were recorded for each rock type at different locations to classify rock quality. The Schmidt rebound values were converted to unconfined compressive strength using the formula Unconfined Compressive Strength (UCS) = 3.03RN – 30.3 (Wang et al., 2017).

Rock Quality Designation was determined using the volumetric count method, while weathering conditions and discontinuity characteristics were assessed through visual observations. Finally, the rock mass quality in the study area was calculated by summing the ratings of the five basic parameters (Bieniawski, 1989).



Figure 21, Conducting Schmidt hammer test on ignimbrite, the northern part of town at the quarry site.

Table 8, Uniaxial Compressive Strength of rocks of the study area.

No	Northing	Easting	Rock genesis	Rebound value	UCS (MPa)	Description
1	729619	437136	Basalt	45.6	107.868	High Strength
2	729306	436795		42.9	99.687	High Strength
3	729823	437267		42.4	98.172	High Strength
4	729107	436596		40.5	92.415	High Strength
5	730932	435868	Ignimbrite	42.1	97.21	High Strength
6	730312	435323		25	45.45	Medium Strength
7	730568	435965		22	36.36	Medium Strength
8	730312	437125		10	12.12	Medium Strength
9	730919	436008		6	3.03	Very Low Strength

RQD determination by volumetric count method

RQD related to drill core is determined from the summation of discontinuities having lengths greater than 10 cm divided by the total core run. However, where drill core data are unavailable, Rock Quality Designation (RQD) can be determined using the joint volumetric count method. The volumetric count method is more advantageous than the drill-core method because it reduces directional dependence (Palmström, 1982). Therefore, since no rock core drilling data were available for the study area, Rock Quality Designation (RQD) was estimated using the joint volumetric count method (Eq. 6).

$$RQD=115-3.3Jv \quad (6)$$

Where Jv is the total number of discontinuities more than 10 cm long in 1 m x 1 m exposed rock face (volumetric count).

A joint trace exposed on ignimbrite rock at UTM coordinates (X = 436087, Y = 730949) is shown in Figure 22. The total number of discontinuities with lengths greater than 10 cm is 12; therefore, Jv = 12. The average joint spacing is 33 cm, and the joint condition is slightly rough and slightly weathered, with a separation of less than 1 mm. The groundwater condition is completely dry. Therefore, RQD = 115 – 3.3 × 12 = 75.4%.

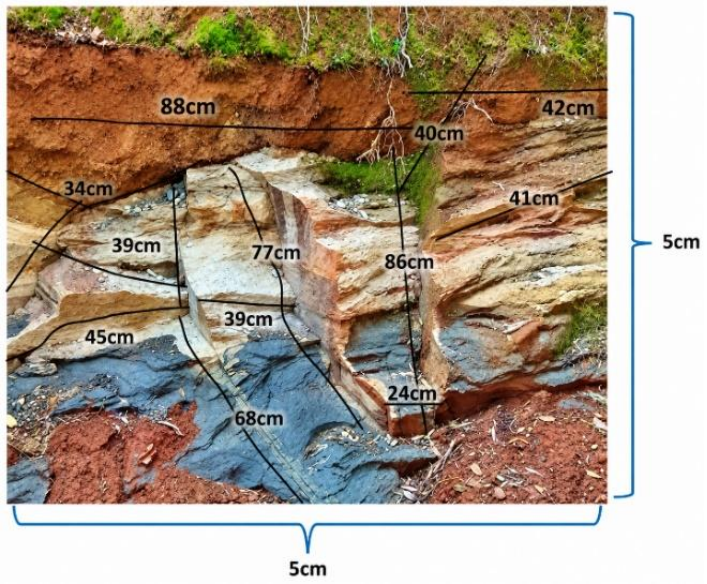


Figure 22, Joint trace exposed in study area.

The remaining seven UTM locations are determined in similar way and presented on the following Table 9.

Meaning and description of RMR

Based on the above-mentioned chart, Aleta Wondo Town is characterized by rock mass classes “B” and “C”. The rock mass quality in the study area for engineering purposes ranges from Good to Fair, as described by Bieniawski (1989).

Relationship of RQD and UCS with RMR

The RMR system provides a numerical value ranging from 0 to 100. Determining the RMR value of the rock mass in the study area is important because RMR provides a more comprehensive representation of actual ground conditions than RQD and UCS alone.

Table 9, RQD and RMR of rocks of the study area. (SW=slightly weathered, HW=highly weathered, SR=slightly rough, CCS=continuous slickenside, R=rating, JSc=joint space, GWC=ground water condition, CD=condition of discontinuity, RQD= rock quality designation, RMR=rock mass rating, D= description, Dr=dripping).

No	Northing	Easting	Rock genesis	USC	R	RQD	R	JS (cm)	R	CD	R	GWC	R	RMR	D
1	730070	435767	Basalt	107.868	12	69	13	35	10	SR and SW	25	Dry	10	70	Good
2	730366	435298		99.687	7	66	13	39	10	SR and SW	25	Dry	15	70	Good
3	730870	435065		98.172	7	71.3	13	38	10	SR and SW	25	Dry	10	65	Good
4	729107	436596	Ignimbrite	92.415	7	65.4	13	33	10	SR and SW	25	Dry	15	70	Good
5	730932	435868		97.263	7	74	13	24	10	SR and SW	25	Dry	10	65	Good
6	730312	435323		45.45	4	66	13	18	8	CSS	10	Wet	7	42	Fair
7	730568	436965		36.36	4	48	8	19	8	SR and HW	20	Wet	7	47	Fair
8	730312	437125		12.12	4	58	13	17	8	SR and HW	20	Dry	10	55	Fair
9	730919	436008		3.03	2	42	8	13	8	SR and HW	20	Dr	4	42	Poor

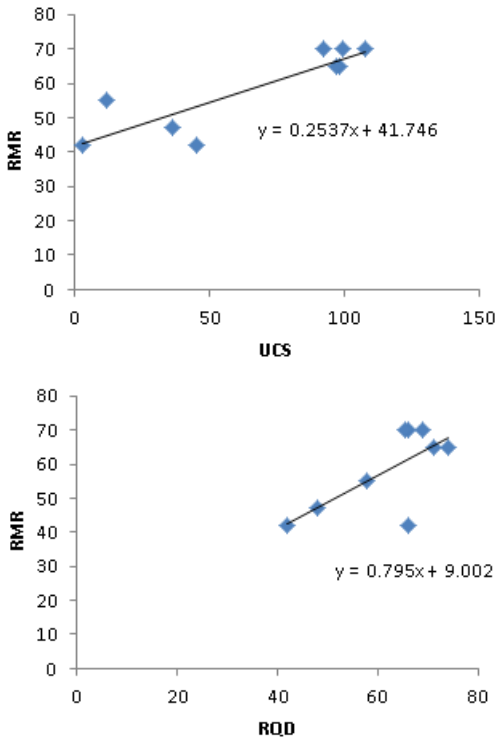


Figure 23, Relationships between RMR, RQD and UCS.

Rock-mass classification based on RMR is therefore a reliable approach for assessing the engineering quality of the rock mass. Where RMR classification is not available, rock quality may be assessed using RQD and UCS. To evaluate the relative reliability of these parameters, a comparison between RMR–RQD and RMR–UCS was conducted. The analysis shows that RQD has a stronger positive correlation with RMR, with a correlation coefficient of 0.795 (Figure 23). UCS also exhibits a positive correlation with RMR, although it is weaker than that of RQD. Overall, rock-mass quality classification based on RMR and RQD appears to better represent actual ground conditions. The authors recommend further analysis using a larger dataset to validate these findings.

Assessment of hydrogeological, geomorphological, and geodynamic hazards

Hazard-related earth processes are broadly classified as geohazards. A geohazard is a geological condition or process that may result in loss of life, damage to property, and disruption of socioeconomic activities. Geohazards may involve short- or long-term geological and environmental processes. They can range from relatively small features to large-scale phenomena, such as submarine or terrestrial landslides, and can significantly affect local and regional socioeconomic conditions. Other major geohazards include earthquakes, volcanic eruptions, avalanches, and floods (Derbyshire et al., 2001). Aleta Wondo town is located in the southwestern part of the Main Ethiopian Rift, within the transitional zone between the Main Ethiopian Rift System and the Ethiopian Plateau. Consequently, significant volcanic and earthquake hazards are not prominent in the town. Landslides, gully erosion, and shallow groundwater are the most commonly observed geodynamic and hydrogeological processes responsible for damage to engineering structures and modification of the surficial features of the study area.

Landslide

A landslide, also called a landslip, the downslope movement of a rock mass, debris, earth, or soil (soil being a mixture of earth and debris). Landslides occur when gravitational and other types of shear stress within a slope exceed the shear strength (resistance to shearing) of the materials that form the slope. Shear stresses can be built up within a slope by some processes. These include over steepening of the base of the slope, by natural erosion or excavation, and loading of the slope, such as by an inflow of water, a rise in the groundwater table, or the accumulation of debris on the slope's surface. Landslides are generally classified by type of movement (slides, flows, spread, topple, or fall) and type of material (rock, debris, or earth). Sometimes more than one type of movement occurs within a single landslide. At study area, small and medium scale soil slide observed specially along slop cut of north eastern and southern part of town (Figure 24). This process damages the asphalt road of town. Landslide phenomena in the study area were documented on the engineering geological map by extracting polygonal landslide features from Google Earth Pro.

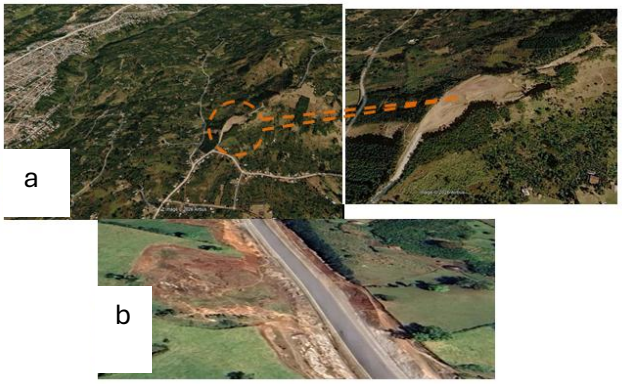


Figure 24, (a) Landslides of study area north eastern part of town and (b) damages of road due to small scale landslide southern parts of town. Source: Google Earth Pro.

Erosion and weathering

The northwestern part of the town experiences gully erosion due to steep topographic slopes. Consequently, roads and residential houses are frequently affected by flooding. In the study area, topography, parent materials, and the degree of weathering govern the type and development of soils. In humid regions, temperature and moisture content control the degree and rate of weathering.

Residual soil dominates the study area, indicating that in situ chemical weathering is more prevalent than mechanical weathering. Highly to slightly weathered ignimbrite rock (Figure 25) is also observed along the river cut in the northern part of the town.

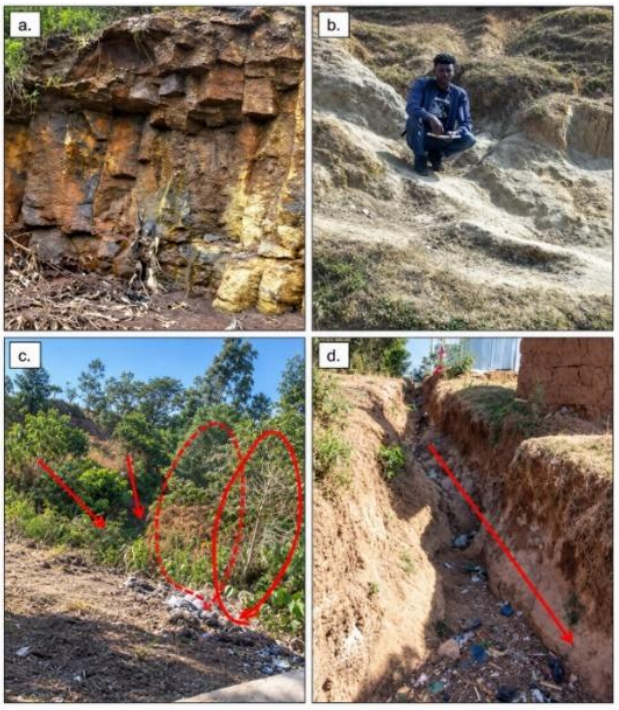


Figure 25, Weathered ignimbrite rock units: (a) erosion of white clay soil, (b) gully erosion in an area covered by trees and grasses (c), lateral erosion (d).

Groundwater

The flow of groundwater below the ground surface is a fundamental factor controlling the strength and compressibility of soil, thereby affecting its ability to support structural loads. When soil becomes saturated, it develops specific physical characteristics due to the relative incompressibility of water. These characteristics are particularly significant below the groundwater table.

Common groundwater issues during construction include unstable subgrades, unstable excavations, water seepage, construction delays, and cost overruns. Common groundwater problems after construction include water leakage, wet basements, mold growth, cracked and uneven floors, cracked and uneven walls, and instability of slopes and retaining walls.

Aleta Wondo town is characterized by shallow groundwater, particularly in the southwestern and south-central parts of the town. Field surveys indicate that the groundwater depth is less than 4 m in the southeastern part of the town, allowing residents to easily access groundwater through boreholes (Figure 26).

The groundwater depth increases to approximately 12 m toward the northern part of the town. Borehole data indicate that the groundwater level gradually increases from south to north. The regional groundwater level of Aleta Wondo Town was estimated using data collected from nine boreholes (Table 10). Groundwater-level contours indicate a general groundwater flow direction from north to south (Figure 27).



Figure 26, Groundwater image captured from Southeastern part of town.

Table 10, Static water level and groundwater level in the study area.

Northing	Easting	Elevation (m)	GWL (m)	SWL (m)
435411	729454	1905	1901.5	3.5
435489	729374	1901	1896.2	4.8
435463	729336	1902	1899	3
436141	729445	1908	1905.5	2.5
436182	729440	1906	1904.3	1.7
436359	729446	1906	1903.8	2.2
436722	729781	1927	1916.8	10.2
435561	720495	1991	1979	12
436892	720022	1920	1905	15

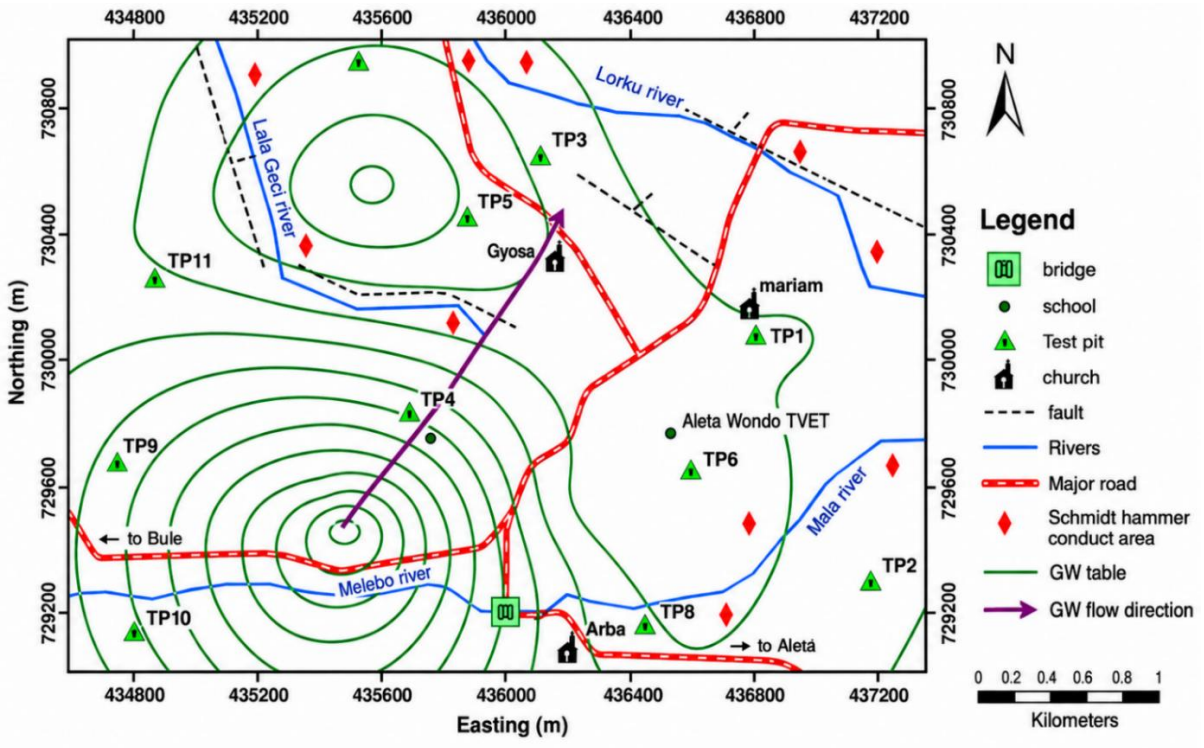


Figure 27, Groundwater level and flow direction in Aleta Wondo Town.

Preparation of multipurpose engineering geologic map

For the current study, a multipurpose engineering geological map (EGM) was prepared using the engineering properties of soils and rocks, including strength (unconfined compressive strength) and degree of weathering. To map rock units on the engineering geological map, seven Schmidt hammer test areas were used (Figure 12). These areas exhibit similar RMR and UCS values, indicating consistent engineering properties, and their contacts were identified based on these parameters. Geological units with similar RMR and UCS values were grouped and mapped as single engineering geological units.

Similarly, soil units were mapped based on laboratory test results from test pits, and their contacts were delineated by interpolating the results using ArcGIS software. Therefore, similar lithological units were mapped as different engineering geological units based on their engineering properties. In addition, geodynamic phenomena, including gully erosion and flood risk, as well as groundwater conditions, were documented on the engineering geological map (Figure 28).

Engineering geological map units

The engineering geological map contains different engineering soil and rock units. Similar geological units are mapped as different engineering unit based on their engineering properties and quality.

High strength ignimbrite unit

The rock unit in this category is exposed along the small stream in the central part of the town and northeast of the quarry site. The intact rock strength of this rock mass

ranges from approximately 92.415 to 97.21 MPa. The Schmidt hammer rebound values generally range from 41.0 to 42.1, indicating very strong rock that cannot be easily broken with a geological hammer. The intact rock strength class of this unit is highly strong, and the rock is slightly weathered. The discontinuities are closely to widely spaced and have very narrow apertures.

Very high to high strength basaltic rock unit

This unit represents the geologically oldest basement rock and occurs at considerable depth below the ground surface. Consequently, it is not well exposed in the study area. A few outcrops are observed along the Melebo River in the southeastern part of the town, where the rock is slightly weathered, groundwater conditions are dry, and the discontinuities are free of infilling materials. The intact rock strength of this unit ranges from approximately 98.172 to 107.868 MPa. The Schmidt hammer rebound values generally range from 42.4 to 45.6. The intact rock strength class of this unit is highly strong.

Medium strength ignimbrite rock unit

This unit is exposed in the northwestern corner of the study area and has less favorable engineering properties compared with the other exposed rock units. The Schmidt hammer rebound values generally range from 10 to 25, indicating medium-strength rock. The groundwater conditions range from wet to dry, and the joint spacing is 13 to 19 mm. The discontinuity surfaces range from slickensided to highly weathered. This rock unit is moderately to highly weathered.

Low strength to very low strength

This category of rock is exposed north of the town near the Hawassa route and is highly weathered, with wet groundwater conditions. Extensive discoloration of the rock is observed due to weathering. The intact rock strength of this rock mass is less than 10 MPa. The Schmidt hammer rebound value is approximately 3 MPa, and the rock can be easily broken with a geological hammer. The intact rock strength class of this unit is very weak, highly weathered, and characterized by discontinuities with wide apertures.

Compressible silt with clay (MH)

Inorganic silts, micaceous or diatomaceous fine sandy or silty soils, and elastic silts. This unit covers a large part of the town. The general engineering characteristics of this soil category are semi-pervious to pervious, highly compressible, and fair to poor for engineering works.

Lean clay with silt (CL)

Inorganic clays of very low to medium plasticity, gravelly clays, sandy clays, silty clays, and lean clays. This unit is exposed in the southwestern part of the town. According to the USCS classification, this soil is impervious, has medium compressibility, and is considered fair for engineering works.

Significance of engineering geologic map at study area

An engineering geological map is a predictive document that answers the question: Is the ground suitable for construction?

The primary use of an engineering geological map in the study area is to support urban land-use planning and development. It identifies zones of relative suitability for construction, ranging from low-risk areas to areas that are unsuitable without major remediation. For instance, the southern parts of the town are relatively unsuitable for large masonry buildings due to shallow groundwater. Similarly, the southern and northeastern parts of the town are prone to geological hazards such as landslides and erosion. These areas are considered inappropriate for urban expansion because infrastructure, such as pipelines routed through active debris-flow channels, may be damaged, resulting in ruptures, spills, and significant economic and environmental losses.

Conclusions and recommendations

Conclusion

The main objective of this study was to characterize the geological and engineering geological conditions of Aleta Wondo town and to prepare an engineering geological map for identifying geotechnically problematic areas and guiding the selection of suitable sites for engineering construction. Based on detailed field investigations, laboratory testing, and engineering geological assessment, geological and engineering geological maps of the town were prepared at a scale of 1:20,000.

The study identified two major lithological units, namely ignimbrite and basalt, along with residual soils. The rock units were further subdivided into engineering geological units according to their engineering properties, weathering conditions, and rock strength. The identified rock engineering units include good-quality, slightly weathered, very high-strength basalt; good-quality, slightly weathered, high-strength ignimbrite; and poor-quality, highly weathered, very low-strength ignimbrite. These variations demonstrate that lithologically similar rocks may exhibit substantially different engineering behavior depending on their degree of weathering and mechanical properties.

The groundwater table is generally shallow in the study area, particularly in the southern parts of the town, and therefore represents an important constraint for construction and urban development. The major geological structures consist of faults and small-scale joints, predominantly striking NNW-SSE, with dip directions toward the NE and SSW. These structural features may influence groundwater movement, rock mass stability, and engineering performance.

Laboratory investigations indicate that the soil moisture content ranges from 23.27% to 48%. Grain-size analysis shows that the soils are predominantly fine-grained. The soils exhibit low to medium swelling potential. The optimum moisture content ranges from 28% to 32.8%, while the maximum dry density ranges from 1.21 to 1.60 kg/m^3. Shear-strength testing indicates cohesion values of 38.4 to 49.37 kPa and friction angles of 19° to 22.99° for compressible silt (silty clay), while sandy silt exhibits cohesion of 22.73 to 25.86 kPa and friction angles of 22.88° to 22.99°. Clayey silt has a cohesion of approximately 54 kPa and a friction angle of 18°.

Based on the Unified Soil Classification System (USCS), the clayey soils are classified as CL, representing inorganic clays of low to medium plasticity, whereas the silt and sandy silt soils are classified as MH, representing inorganic and elastic silts. The field-based lithological descriptions and soil classifications are generally consistent with the laboratory test results, supporting the reliability of the engineering geological characterization.

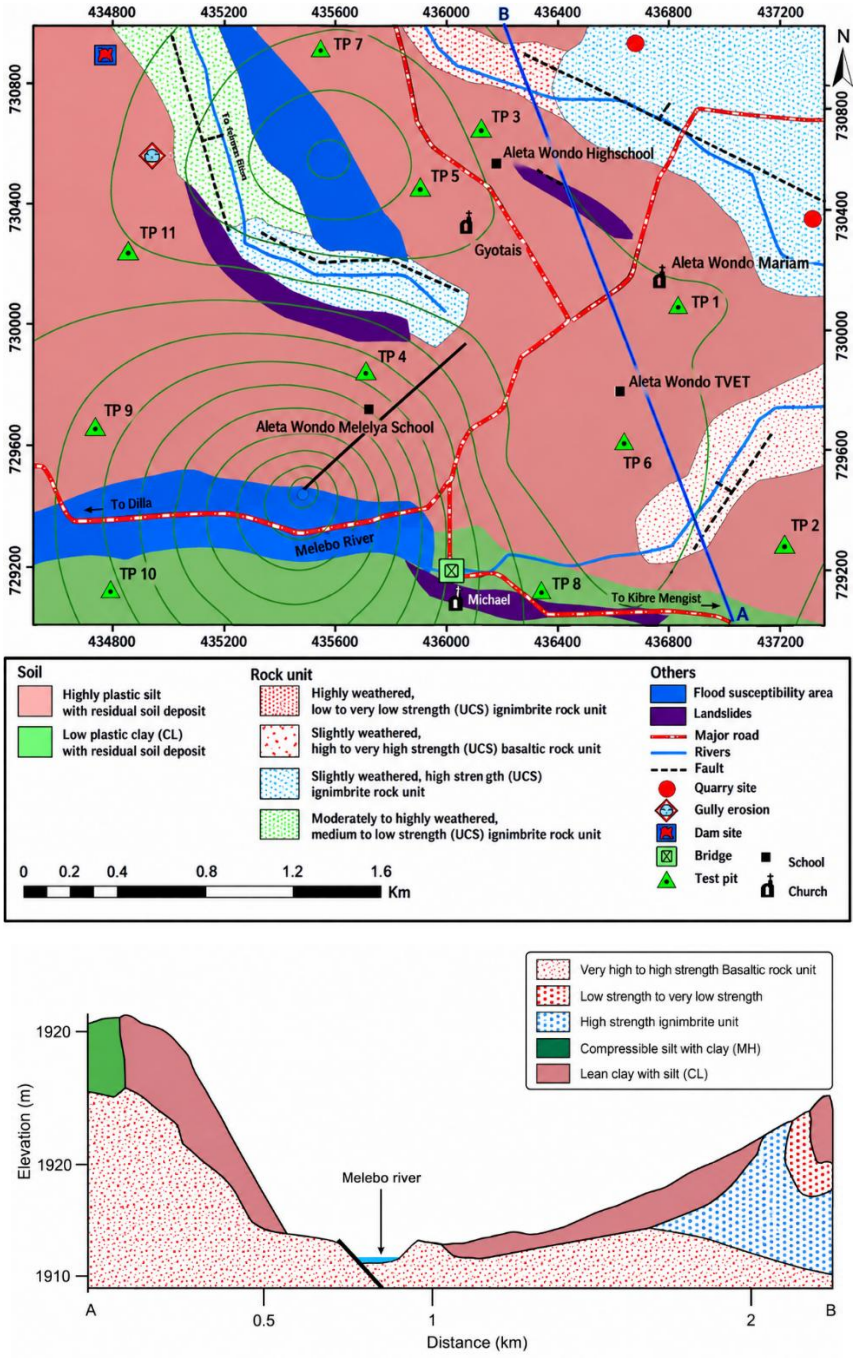


Figure 28, Engineering geologic map and cross section

Overall, the engineering geological conditions of Aleta Wondo town are highly variable and are controlled by lithology, weathering, soil properties, geological structures, groundwater conditions, and geodynamic processes. The resulting engineering geological map provides a practical basis for identifying relatively

suitable and problematic areas for construction and urban expansion. Areas affected by shallow groundwater, highly weathered and weak rock, erosion, and other geohazards require detailed site-specific investigation and appropriate engineering measures before development. Thus, the engineering geological map serves as an essential planning tool for safer and more sustainable urban development in Aleta Wondo town.

Recommendations

The following recommendations are provided for the study area:

- The study area is dominated by compressible silt, which is unfavorable for civil engineering works. Therefore, special design considerations and detailed site investigations are required before construction.
- Potentially medium-expansive soils were identified in the southwestern part of the town. Therefore, appropriate precautions should be taken when constructing civil engineering structures on these soils.
- Detailed subsurface investigations using geophysical methods are recommended to better understand subsurface conditions, including overburden thickness.
- Further research should be conducted by increasing the number of test pits within the study area and extending investigations to additional areas not covered by the present study.

Acknowledgements

Special thanks and sincere appreciation to two anonymous reviewers and editors of AJEG for extensive editorial comments and suggestions.

Availability of data and materials

The datasets supporting the findings of this study are available from the corresponding author upon reasonable request via email.

Competing interests

The authors declare that they have no conflict of interest regarding the publication of this paper.

References

AASHTO (2014). Standard Specifications for Transportation Materials and Methods of Sampling and Testing and 2014 AASHTO Provisional Standards (34th ed.). American Association of State Highway and Transportation Officials (AASHTO). 1023p.

Arnold, V. (2001). Soil Mechanics. Standard Publishers Distributors, Delft University of Technology.

Arora, K. R. (2008). Soil Mechanics and Foundation Engineering (Geotechnical Engineering): In SI Units. Standard Publishers, New Delhi.

ASTM (2018). Standard test methods for liquid limit, plastic limit, and plasticity index of soils (D4318-10). ASTM International. https://doi.org/10.1520/D4318-10

ASTM (2023). Standard test methods for specific gravity of soil solids by the water displacement method (ASTM D854-23). ASTM International. https://doi.org/10.1520/D0854-23

Ayalew, A., Balabathina, V. N., Birhane, G., Shano, L., Demise, T., and Tadese, A. (2022). Engineering geological characterization of soils and rocks in Arba Minch Town, Southern Ethiopia: Implication for building cracks and road failures. International Journal for Modern Trends in Science and Technology, 8(7), 102–117. https://doi.org/10.46501/IJMTST0807017

Ayele, A., Woldearegay, K., and Meten, M. (2022). Multichannel analysis of surface waves (MASW) to estimate the shear wave velocity for engineering characterization of soils at Hawassa town, Southern Ethiopia. International Journal of Geophysics, Article ID 7588306. https://doi.org/10.1155/2022/7588306

Bell, F. G. (2007). Engineering Geology (2nd ed.). Butterworth-Heinemann, Elsevier.

Berhane, G. (2010). Engineering geological soil and rock characterization in the Mekelle Town, Northern Ethiopia: Implications to engineering practice. Momona Ethiopian Journal of Science, 2(2), 64–86.

Bieniawski, Z. T. (1989). Engineering Rock Mass classifications: A complete manual for engineers and geologists in mining, civil, and petroleum Engineering. John Wiley & Sons.

Bowles, J.E. (1996). Engineering properties of soils and their measurement. (4thed.) McGraw-Hill, New York.

Chemeda, Y. C. (2020). Engineering geological investigation of Adama town: Implication to engineering practice. Ethiopian Journal of Science and Sustainable Development, 7(2), 103–116. https://doi.org/10.20372/ejssdastu:v7.i2.2020.281

Chen, F.H. (1988). Foundations on expansive soils (2nd ed.). Developments in Geotechnical Engineering, 54. Elsevier.

Clayton, C. R. I. (1995). The standard penetration test (SPT): Methods and Use. CIRIA Report 143. Construction Industry Research and Information Association, London.

Debebe D. (2011). Investigation on some of engineering characteristics of soils in Adama town, Ethiopia (Msc. Thesis, Addis, Addis Ababa University). http://etd.aau.edu.et/handle/12345678/3082

Deere, D. U., and Deere, D. W. (1988). The rock quality designation (RQD) index in practice. In L. Kirkaldie (Ed.), Rock classification systems for engineering purposes (ASTM STP 984, pp. 91–101). ASTM International. https://doi.org/10.1520/STP48465S

Derbyshire, E., 2001. Geological hazards in loss terrain, with particular reference to the loess regions of China. Earth-Science Rev. 54, 231–260. https://doi.org/10.1016/ S0012-8252(01)00050-2

Ganole, K., (2010). GIS Based Surface Irrigation Potential Assessment of River Catchments for Irrigation Development in Dale Woreda Sidama Region. M.Sc. Thesis, Haramaya University. Available at: https://cgspace.cgiar.org/bitstreams/483328b2-7fe1-4615-9ae9-8b012f1dc00c/download

Gure, E. G., Weldearegay, K., and Birhane, G. (2013). Engineering geological and geotechnical appraisal of Northern Mekelle town, Tigray, Northern Ethiopia. American Scientific Research Journal for Engineering, Technology, and Sciences, 5(1), 23–56. Available at: https://asrjetsjournal.org/American_Scientific_Journal/article/view/532

Holtz, R. D., and Kovacs, W. D. (1981). An introduction to geotechnical engineering. Prentice-Hall, Englewood Cliffs, New Jersey.

Holtz, W. G., and Gibbs, H. J. (1956). Engineering properties of expansive clays. Transactions of the American Society of Civil Engineers, 121(1), 641–663. https://doi.org/10.1061/TACEAT.0007325

Hroch, T., Megerssa, L., Buriánek, D., Verner, K., Martínek, K., Mihret, Y., Janderková, J., Šíma, J., Kryštofová, E., Gebremariyam, H., Tadesse, E., Legesse, F., Valenta, J., Pécskay, Z., and Hejtmánková, P. (2018). Explanatory notes to the thematic geoscientific maps of Ethiopia at a scale of 1:50,000, Map Sheet 0638-A2 Leku. Czech Geological Survey, Prague.

Hunde, B. (2014). Investigation on some of engineering properties of soils found in Ambo Town, Ethiopia, Ph.D. Thesis. Addis Ababa University. Available at: http://etd.aau.edu.et/handle/12345678/2402

Kaniraj, S. R. (1988). Design aids in soil mechanics and foundation engineering. Tata McGraw-Hill Publishing Company, New Delhi.

Matula, M. (1981). Rock and soil description and classification for engineering geological mapping: Report by the IAEG Commission on Engineering Geological Mapping. Bulletin of the International Association of Engineering Geology, 24, 235–274. https://doi.org/10.1007/BF02595273

Munsell A. H. (2000). Munsell soil color charts (Year 2000 revised washable ed.). Munsell Color, New Windsor, New York.

Murthy, V. N. S. (2003). Geotechnical engineering: Principles and practices of soil mechanics and foundation engineering. Marcel Dekker, New York.

Mussie, M. (2007). Groundwater Circulation and Hydrochemistry of the Corridor (Upper Gidabo River and Lake Awassa Catchments), Sidama Zone, Snnprs. M.Sc. Thesis, Addis Ababa University. Available at: http://10.90.10.223:4000/handle/123456789/7379

Osuolale, O. M., Falola, O. D., and Ayoola, M. A. (2012). Effect of pH on geotechnical properties of laterite soil used in highway pavement construction. Civil and Environmental Research, 2(10), 23–28. https://www.iiste.org/Journals/index.php/CER/article/view/3536

Palmström, A. (1982). The volumetric joint count: A useful and simple measure of the degree of rock mass jointing. In Proceedings of the 4th International Congress of the International Association of Engineering Geology, pp. 221–228.

Prakash, K., and Sridharan, A. (2004). Free swell ratio and clay mineralogy of fine-grained soils. Geotechnical Testing Journal, 27(2), 220–225. https://doi.org/10.1520/GTJ10860

Price, D. G. (2008). Engineering geology: Principles and practice. Edited and compiled by M. H. de Freitas. Springer, Berlin, Heidelberg. https://doi.org/10.1007/978-3-540-68626-2

Raj, P. P. (2012). Soil mechanics and foundation engineering. Dorling Kindersley (India) Pvt. Ltd., New Delhi.

Rich, C. I. (1968). Mineralogy of soil potassium. In V. J. Kilmer, S. E. Younts, and N. C. Brady (Eds.), The role of potassium in agriculture (pp. 79–96). American Society of Agronomy, Crop Science Society of America, and Soil Science Society of America. https://doi.org/10.2134/1968.roleofpotassium.c5

Seed, H. B., Woodward, R. J., Jr., and Lundgren, R. (1962). Prediction of swelling potential for compacted clays. Journal of the Soil Mechanics and Foundations Division, 88(3), 53–87. https://doi.org/10.1061/JSFEAQ.0000431

Wahid, M. G. (2007). Suitability of Ground condition for building and road in Hawassa town, Southern Ethiopia. MSc Thesis. Addis Ababa University, Ethiopia, 97p.

Wang, H, Lin, H., and Cao, P. (2017). Correlation of UCS rating with Schmidt hammer surface hardness for rock mass classification. Rock Mechanics and Rock Engineering, 50(1), 195–203. https://doi.org/10.1007/s00603-016-1044-7

Yasin, K., (2002). Hydrogeology of upper Gidabo river catchment, Southern Ethiopia, M.Sc. Thesis. Addis Ababa University, Ethiopia.

Yismaw, A., Besufikad, A., Dure, T., Ersido, A., Kebede, E., Wondfraw, T., and Ababa, A. (2012). Geology, geochemistry and gravity survey of Megalo Map Sheet. Geological Survey of Ethiopia, Basic Geoscience Mapping Directorate.

Research Article DOI: https://doi.org/10.64862/ajeg.2026.301.03.308 Open Access

Landslide Susceptibility Assessment along the Hilly Coastal Corridor of Cox's Bazar-Teknaf, Bangladesh

Muqit Ajmain Shahriyar[1*], Md. Abdul Malek[1], Md. Younus Hider[1], Tasmim Banu[1], and Md. Mahedi Hasan[1]

[1]Department of Geology and Mining, University of Rajshahi, Rajshahi 6205, Bangladesh

(*Corresponding E-mail: muqit.ajmain2001@gmail.com)

Received: December 20, 2025, Accepted: May 28, 2026

Abstract: **The southeastern coastal cliffs of Bangladesh, extending from Cox's Bazar to Teknaf, are highly susceptible to landslides due to steep terrain, intense monsoonal rainfall, and increasing anthropogenic disturbances. This study presents an integrated landslide susceptibility assessment by combining the knowledge-based Analytic Hierarchy Process (AHP) and the data-driven Frequency Ratio (FR) model to identify spatial patterns of landslide. A landslide inventory comprising 55 documented landslide locations was prepared using NASA Global Landslide Catalog data and high-resolution Google Earth imagery. Ten conditioning factors- elevation, slope, aspect, curvature, soil type, geomorphology, rainfall, drainage density, distance from roads, and Normalized Difference Vegetation Index (NDVI) were derived from satellite imagery and geospatial datasets and synthesized within a Geographic Information System (GIS) environment to generate susceptibility maps. Model performance was evaluated using Receiver Operating Characteristic (ROC) curves and the Area Under the Curve (AUC) metric. The AHP model demonstrated strong predictive capability with an AUC value of 0.859, classifying 63.48% of the study area as moderate susceptibility and identifying 1.06% as high-susceptible zones, primarily along the Teknaf hill tracts. In contrast, the FR model exhibited moderate accuracy (AUC = 0.688) and produced a more detailed five-class susceptibility map, delineating 4.35% of the area as high to very high susceptible. Both models consistently indicate that critical landslide susceptibility is concentrated along the coastal cliffs of Teknaf and parts of the hilly terrain in Ukhiya. These findings have important implications for infrastructure safety, particularly the Marine Drive corridor, and for the densely populated Rohingya refugee settlements, where unstable slopes pose significant hazards. The comparative application of AHP and FR framework offers a cost-effective and transferable approach for landslide susceptibility assessment and disaster mitigation in data-scarce, high-hazard region.**

Keywords: ***Analytic Hierarchy Process (AHP), Frequency Ratio, Landslide Inventory, Multi-Criteria Decision Analysis, Disaster Risk Reduction.***

Introduction

Landslides are the gravity-driven movements of soil and rock on slopes. Most modern geomorphology sources say, a landslide as the movement of a mass of rock, debris, or earth down of a slope under gravity (Turner, 2018; Wubalem, 2021). They are among the most frequent geo-hazards in mountainous regions and cause substantial loss of life and property worldwide.

Global Study says that, about 4862 fatal non-seismic landslides killed 55997 people in 2004-2016, heavily concentrated in Asia (Froude et al., 2018). In the USA, estimated annual landslide frequencies range from ~0.002 to 29 landslides per 1000 km^2 per year (Luna et al, 2025). This hazard occurs with a family of gravity-driven movements that include falls, topples, slides, spreads, flows, and their complex combinations, acting through stages of failure, movement and deposition (Varnes, 1978). Shear failure happens along a surface or in a shear zone when driving stress exceeds shear strength (Petley et al., 2002; Cuomo, 2020). Post failure movement occurs acceleration, possible transition from slide to flow and entrainment of more material (Cuomo, 2020; Tian et al., 2020).

Most of the landslides occur in mountainous topography on moderate-steep, concave mid-upper slopes, especially in zones dissected by rivers or roads; in flatter or low-relief terrain, landslides are much less common. A global analysis of fatal landslides shows that ~70% of natural landslides and ~44% of human-triggered ones occur in mountainous areas in tropical and temperate regions (Fidan et al., 2024). Most of the cases natural-factor landslides tend to initiate in the higher parts of the topographic profile, at higher elevations and steeper slopes with little human disturbance (Carrara, 1983; Fidan et al., 2024). Some studies also find that while steeper slopes are more susceptible, extremely steep slopes may have thinner, more stable soils, so landslide erosion can peak on near-threshold but not the very steepest slopes (Prancevic et al., 2020).

Bangladesh comprises up a large portion of the Bengal Basin, and its coastal areas undergo landslides of any dimension (Rahman et al., 1995). In Bangladesh, landslide-vulnerable areas mainly concentrated in the southeastern and some northeastern hilly districts, especially around Chattogram and Cox's Bazar which are identified as landslide-prone districts based on 2000-2018 catalog (Sultana, 2020). Steep, deforested slopes (often 12-30° or more, 60-200 m elevation) with sandy/loamy soils in Cox's Bazar and Chattogram are

the most vulnerable factor for landslide hazard (Chowdhury et al., 2023; Nahar et al., 2025; Islam et al., 2024). Intense monsoon rainfall saturates weak sandy soils on steep, cut, and deforested slopes, especially around roads, camps, and informal settlements accelerate landslide. In Cox's Bazar (Ramu-Ukhiya-Teknaf), June rainfall shows a strong statistical correlation with monthly landslide incidence (Nahar et al., 2025). High topographic wetness and stream power indices (areas where runoff converges) are strongly associated with failures because they focus infiltration and erosion (Islam et al., 2024; Fuad et al., 2024). Between Cox's Bazar and Teknaf (the Teknaf Peninsula), the land is a narrow ridge of low hills flanked by the Bay of Bengal to the west and the Naf River/floodplains to the east. These hills form a dissected, erosion-prone landscape with strong relief over short distances. In Cox's Bazar district, most hills are ~100-300 m high (Ahmed et al., 2020) and the Ramu-Ukhiya-Teknaf belt, high landslide vulnerable sites are typically at ~90-180 m elevation (Nahar et al., 2025). Hill materials make the area influencing for its unconsolidated or weakly cemented sand, silt and shale, giving high erodibility and frequent shallow landslides when disturbed (Nahar et al., 2025; Kamal et al., 2022; Ahmed et al., 2020).

Recent devastating landslides between Cox's Bazar and Teknaf have concentrated on the Ukhiya-Teknaf Rohingya camp corridor and neighboring host villages, particularly in 2017, 2019, and 2021, displacing thousands and claiming multiple lives throughout each major monsoon season. At June 2017, landslides occur at least 160 deaths in Cox's Bazar district and adjacent hills (Ahmed et al., 2020). At July 2019, 355 mm rain happened over 72 hours and causes 26 landslides, 1 death, ~4,500 people left homeless (Sami et al., 2024). Besides geologic factors, road cuts, building platforms, and quarrying over-steepen slopes and remove support at the toe, making failure much more likely during rain (Skilodimou et al., 2018).

At 2024, regional assessment integrating hazard (susceptibility) and social vulnerability for all southeast Bangladesh finds landslide risk highest in Teknaf, Ukhiya and Ramu upazilas; Cox's Bazar district is second only to Chattogram in overall risk (Sultana et al., 2024). Although numerous landslide susceptibility studies have been conducted in the Chattogram Hill Tracts and surrounding regions (Rabby et al., 2020), relatively few investigations have specifically focused on the Cox's Bazar-Teknaf coastal hill corridor, where rapid infrastructure development, extensive road-cutting activities, and the establishment of large refugee settlements have substantially altered slope stability conditions. Previous studies have commonly applied either statistical or knowledge-based approaches independently; however, a comparative assessment of the Analytic Hierarchy Process (AHP) and Frequency Ratio (FR) models for this coastal environment remains limited. Furthermore, recent changes in land use, vegetation cover, and anthropogenic disturbances necessitate updated susceptibility assessments. Therefore, this study contributes by (i) developing updated landslide susceptibility maps using recent geospatial datasets, (ii) comparing the predictive performance of expert-based and data-driven approaches, and (iii) identifying critical landslide hotspots that directly threaten transportation corridors, settlements, and refugee camps within southeastern Bangladesh to support disaster preparedness and land-use planning.

Geographic and environmental settings

The study area is situated in the southeastern part of Bangladesh along the longest sea beach and the Marine Drive extending roughly between 20°52'-21°25'N latitude and 91°58'-92°18'E longitude shown in Figure 1. It encompasses selected coastal and hilly terrain within the Ramu, Ukhiya, and Teknaf upazilas of Cox's Bazar district. In this area, the exposed hill rocks belong to the Cenozoic Tertiary succession of the Chittagong-Tripura Folded Belt. Regionally, it includes Bhuban Formation (Miocene), Boka Bil (Miocene), Tipam Sandstone + Girujan Clay (Pliocene), Dupi Tila (Plio-Pleistocene), and Recent alluvium (Khanam et al, 2020; Hossain et al., 2025). The Cox's Bazar-Teknaf cliff is mainly dominated by sandstone and shale. Tertiary sandstone-shale successions, weathered at some part of the folded belt that continues into Cox's Bazar area (Hossain et al., 2025). The hilly terrain rises progressively eastward to hundreds of meters in the regional hill belt. (Saddam et al., 2025). In Ramu, Ukhiya and Teknaf upazilas, high landslide-vulnerable hillslopes commonly have steep slopes of about 12-21° and elevations of 89-177 m (Nahar et al., 2025). The natural hilly terrain mostly from gentle 6-12° slopes to steeper 12-21° slopes, but human-modified camp and cut slopes often reach 40-60°, where stability problems and landslides are common (Kamal et al., 2023; Sami et al., 2024). Drainage density in this area is high enough to strongly control erosion, landslides, and water availability. Such networks are mainly dendritic and dominated by numerous short 1st- 3rd order streams on steep slopes that rapidly convey runoff (Chowdhury, 2024). Streams in nearby Chattogram basins (Sangu-Matamuhuri) have high wet-season peak flows and low dry-season baseflow; over a 25-year period, wet-season runoff has increased and dry-season flow has decreased, suggesting flashier behavior and an increasing danger of water scarcity (Rudra et al., 2023).

This hilly zone of Bangladesh lies in humid tropical monsoon belt. It has a marked seasonal cycle with very high rainfall and warm temperatures year-round, and both rainfall and temperature are increasing over recent decades. The Teknaf peninsula is very wet, with typical annual rainfall around 3000-4000 mm, with ~15 °C in winter and ~33 °C in summer (Moslehuddin et al., 2018). Long-term analyses (1950–2023) show increasing annual and seasonal rainfall at Cox's Bazar and Teknaf, though seasonal trends can be irregular and partly non-significant (Suhan et al., 2025). Vegetation in the

Cox's Bazar-Teknaf hill zone ranges from natural semi-evergreen hill forests and coastal Casuarina belts to species-rich homestead agroforests and mangrove-wetland mosaics. Himchari National Park of Cox's Bazar contains 88 tree species (961 stems, 457 stems/ha), with high diversity but dominance of plantation/introduced trees like Acacia auriculiformis, Tectona grandis, Gmelina arborea, Casuarina equisetifolia alongside native species (Hossen et al., 2020). In Teknaf 73 plant species and very high densities (~4000 plants/ha) have been recorded, providing timber, fuelwood, fruits and cyclone protection and storing substantial carbon (117 Mg C/ha) (Nath et al., 2015).

Population growth is highly concentrated in Ukhiya and Teknaf, especially around refugee settlements and growth corridors along roads and upazila centers. Geospatial evidence suggests the regional population-density dimension increased at about 9431 persons/year, alongside a rural-to-urban transition driven by refugee settlement expansion. More than one million refugees have settled mainly in rural and forested areas because of their proximity to the Myanmar border and accessible transport routes (Islam et al., 2023). This population growth has accelerated infrastructure development along secondary highways, camp areas, and modified hill slopes, increasing exposure to landslides, flooding, and heat stress. Development for camps, roads, sanitation, and markets has expanded into environmentally sensitive terrain (Mohiuddin et al., 2025), resulting in the conversion of forest-dominated landscapes into settlements, camps, roads, and other built-up areas (Hossain et al., 2021; Mazumder et al., 2024).

Overall, the Cox's Bazar-Teknaf hilly region is characterized by clustered population growth, infrastructure concentrated in hazard-prone corridors, and extensive forest conversion to settlement and camp-related land uses.

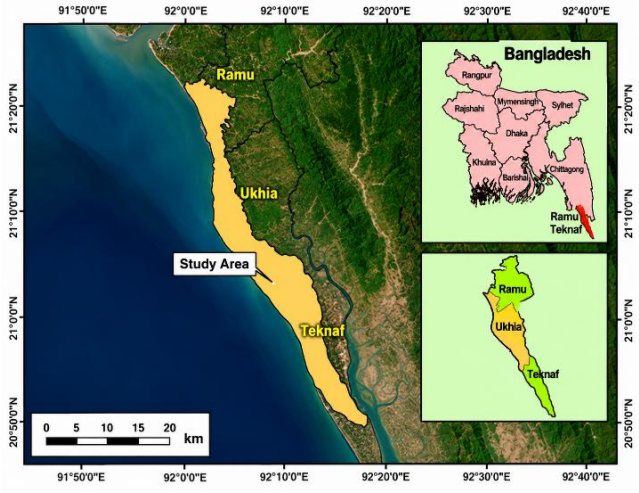


Figure 1, Location map of the study area showing the Cox's Bazar-Teknaf coastal hill corridor and major administrative boundaries.

Methodology

The study maps the landslide susceptibility of the Cox's Bazar-Teknaf coastal cliff using the Analytic Hierarchy Process (AHP) and Frequency Ratio (FR) approach. An outline of the methodological approach is given in (Figure 2). The Analytic Hierarchy Process (AHP) was used to assess the relative weights of the landslide conditioning factors based on expert judgment and their contribution to the occurrence of landslides. At first a hierarchical structure with the objective, criteria, and possibilities was created. The selected conditioning factors included elevation, slope, aspect, curvature, drainage density, soil type, distance from road, annual rainfall, geomorphology, and NDVI. Then, a weighted overlay technique was applied using ArcGIS 10.8 to generate the AHP-based landslide susceptibility map, which was subsequently classified into different susceptibility zones. To ensure the reliability of expert judgments, the consistency of the pairwise comparisons was evaluated using the Consistency Index (CI) and Consistency Ratio (CR) (Yang et al., 2022). On the other hand, Frequency Ratio (FR) method is a widely used bivariate statistical technique for landslide susceptibility assessment and other natural hazard studies (Lee et al., 2006). It evaluates the spatial relationship between historical landslide occurrences and landslide conditioning factors such as slope, aspect, geology, soil type, drainage characteristics, geomorphology, rainfall, and vegetation indices. The frequency ratio for each class was calculated as the ratio of the percentage of landslide pixels within a given class to the percentage of the area occupied by that class. Finally, the FR values of all factor classes were spatially assigned and summed to generate the FR-based landslide susceptibility map using ArcGIS 10.8. After generating the AHP- and FR-based models, the landslide susceptibility results were analyzed and validated using the receiver operating characteristic (ROC) curve and the area under the curve (AUC).

Dataset for the study

The landslide susceptibility analysis incorporated a set of topographic, environmental, climatic, and anthropogenic conditioning factors. The datasets included both raster and vector data acquired from USGS Earth Explorer, Landsat 8, and other relevant and authoritative sources. The selected datasets, their respective sources, spatial resolutions/scales, and classification methods are summarized in Table 1.

Topographic conditioning factors, including elevation, slope, aspect, curvature, and drainage density, were derived from the Digital Elevation Model (DEM). Environmental and anthropogenic factors, including soil type, geomorphology, and distance from roads, were prepared from relevant ancillary vector datasets. Annual rainfall data were obtained from the Climatic Research Unit (CRU) gridded climate dataset in NetCDF format, provided by the University of East

Anglia, with a spatial resolution of 0.5° × 0.5° (approximately 50 km). Landsat 8 imagery was used to derive the Normalized Difference Vegetation Index (NDVI), which was incorporated as an additional conditioning factor in the landslide susceptibility analysis.

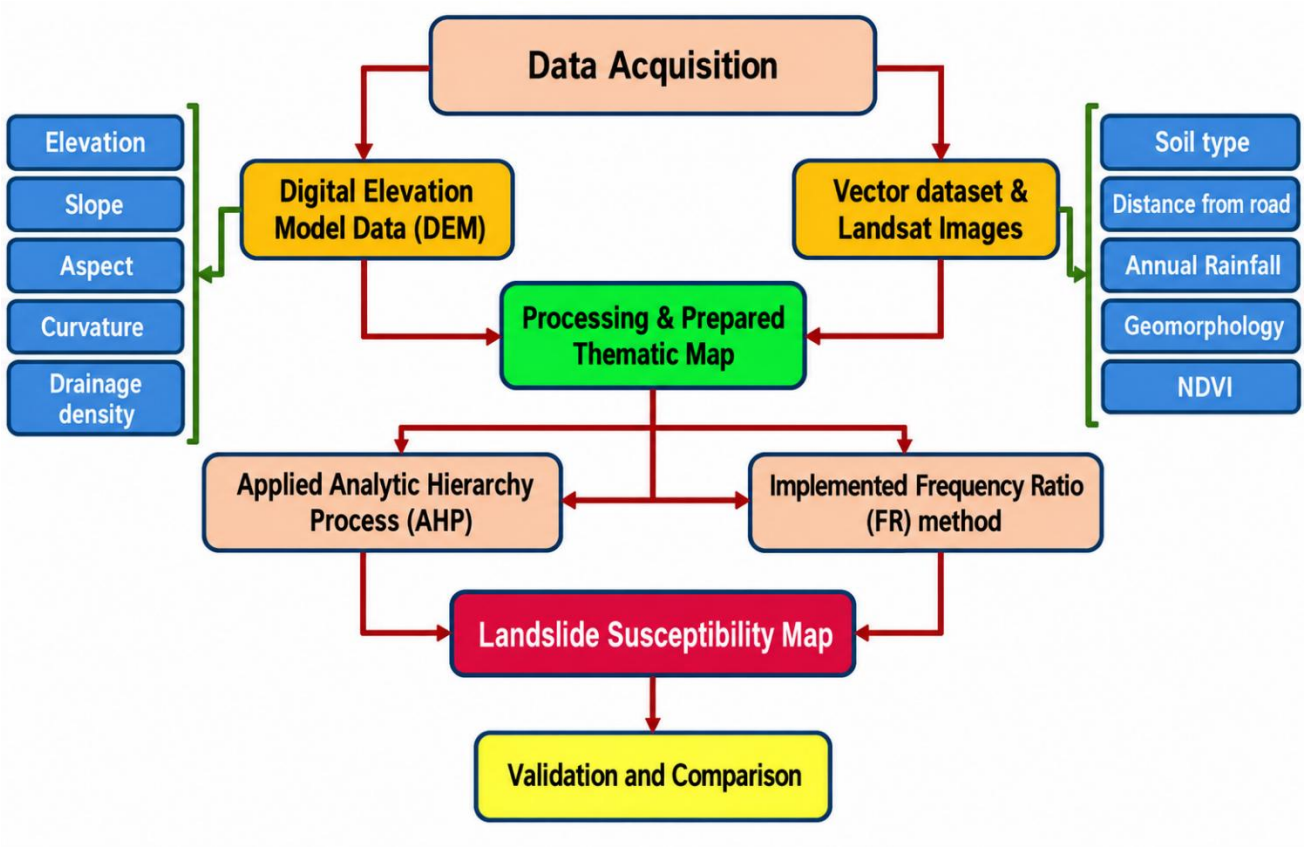


Figure 2, Methodological framework of the study.

Table 1, Datasets and parameters used for landslide susceptibility mapping.

Datasets	Parameters	Source	Acquisition Date	Scale	Classification method
Digital Elevation Model (DEM)	Elevation	USGS Earth Explorer	2014/09/23	30m×30m	Natural break
	Slope				
	Aspect				
	Curvature				
	Drainage Density				
Vector Datasets	Soil type	Open Source data	2023/09/04		Natural break
	Distance form road				
	Geomorphology				
NetCDF	Annual Rainfall	Climatic Research Unit (CRU)	Temporal coverage: January-December 2024		
Landsat Image	NDVI	USGS Earth Explorer	2025/03/13		

Before thematic layer generation, all spatial datasets were preprocessed within the ArcGIS 10.8 environment to ensure spatial consistency. All raster and vector datasets were projected to the World Geodetic System 1984 (WGS 84), Universal Transverse Mercator (UTM) Zone 46N coordinate reference system, clipped to the

study area boundary, and converted to a uniform raster format with a spatial resolution of 30 × 30 m. Topographic parameters, including elevation, slope, aspect, curvature, and drainage density, were derived from the Digital Elevation Model (DEM) using standard Spatial Analyst tools. The Euclidean Distance tool was used to generate the distance-from-road layer, while NDVI was calculated from Landsat imagery using the standard normalized difference equation.

Continuous variables were classified using the Jenks Natural Breaks method to preserve inherent data variability, whereas categorical variables such as soil type and geomorphology retained their original thematic classes. All thematic layers were subsequently standardized to ensure compatibility for AHP and FR-based landslide susceptibility modelling.

Landslide inventory database

A comprehensive landslide inventory database was prepared by integrating landslide occurrence records from the NASA Global Landslide Catalog with additional landslide locations identified through visual interpretation of high-resolution Google Earth imagery. The final inventory comprised 55 verified landslide locations, obtained from the NASA Global Landslide Catalog and supplemented by landslide locations interpreted from Google Earth imagery. All inventory points were carefully examined to eliminate duplicate records and ensure positional consistency before being incorporated into the GIS database. The landslide inventory served as the basis for susceptibility modelling, while model performance was evaluated using Receiver Operating Characteristic (ROC) analysis. The spatial distribution of the inventoried landslides covers the major hilly areas of the Cox's Bazar–Teknaf coastal corridor and provides the fundamental database for landslide susceptibility modelling.

Landslide conditioning factors

For this study, ten conditioning factors were selectively chosen based on a review of the literature, reliability, data accessibility, and their importance to the prevalence of landslides illustrated into (Figure 3 and Figure 4). Identifying and analyzing landslide conditioning factors is a crucial step in landslide susceptibility assessment, as these factors control slope instability and determine the spatial distribution of landslide occurrences.

Conditioning factors do not directly trigger landslides but create favorable conditions that increase the likelihood of failure when triggering events. Each conditioning factor was compiled into a raster format with a spatial resolution of 30 × 30 m in order to assure consistency in data analysis (Fuad et al., 2024).

To categorize the data, we employed the Jenks natural breaks method in the ArcGIS software. This approach facilitates the objective identification of important trends and clusters.

The ten conditioning factors were selected based on their widespread application in previous landslide susceptibility studies, their physical relevance to slope instability, and the availability of reliable spatial datasets for the study area. These factors collectively represent the major topographic, hydrological, environmental, and anthropogenic controls influencing landslide occurrence in the Cox's Bazar-Teknaf coastal hills. Although additional factors such as lithology, land use/land cover (LULC), Topographic Wetness Index (TWI), Stream Power Index (SPI), and lineament density have been employed in other studies, they were not included in the present analysis because of limitations in obtaining consistent, high-resolution datasets and to minimize redundancy among highly correlated variables. The selected conditioning factors provide a comprehensive representation of the dominant processes governing landslide susceptibility within the study area while maintaining model reliability and reducing uncertainty.

Elevation

Elevation plays an important role in landslide susceptibility by controlling potential energy, micro-climate, weathering, and vegetation; many studies find landslides concentrated in specific elevation bands (Chang et al., 2019; He et al., 2012).

In this study, elevation was classified into four classes ranging from 11 to 261 m. Higher elevations are mainly concentrated in the southern Teknaf hills, with elevation values ranging from 135 to 261 m. Lower elevations are primarily located in the valley between the Cox’s Bazar and Teknaf hill ranges.

Slope

Slope angle is consistently one of the most influential predictors and are top-ranked in logistic regression, jackknife and global reviews (Conforti et al., 2021; Saleem et al., 2019). Steeper slopes generally exhibit higher gravitational stress and reduced shear strength, increasing the likelihood of mass movement.

Landslide frequency typically increases with slope angle up to a threshold beyond which material availability may decrease. For this study, slope angle was classified into five classes. Extreme slope angles are mainly concentrated in the Teknaf hills and extend toward the Cox’s Bazar region, with values ranging from 25.59° to 63.95°. Higher slope angles (15.56°–25.58°) are also concentrated in the Teknaf hills, surrounding areas of extreme slope.

Aspect

Aspect affects the potential of landslides by regulating soil moisture levels, vegetation density, evapotranspiration rates, and sun radiation exposure.

Slope failure is more likely to occur on slopes that face particular directions because they can retain more moisture or weather.

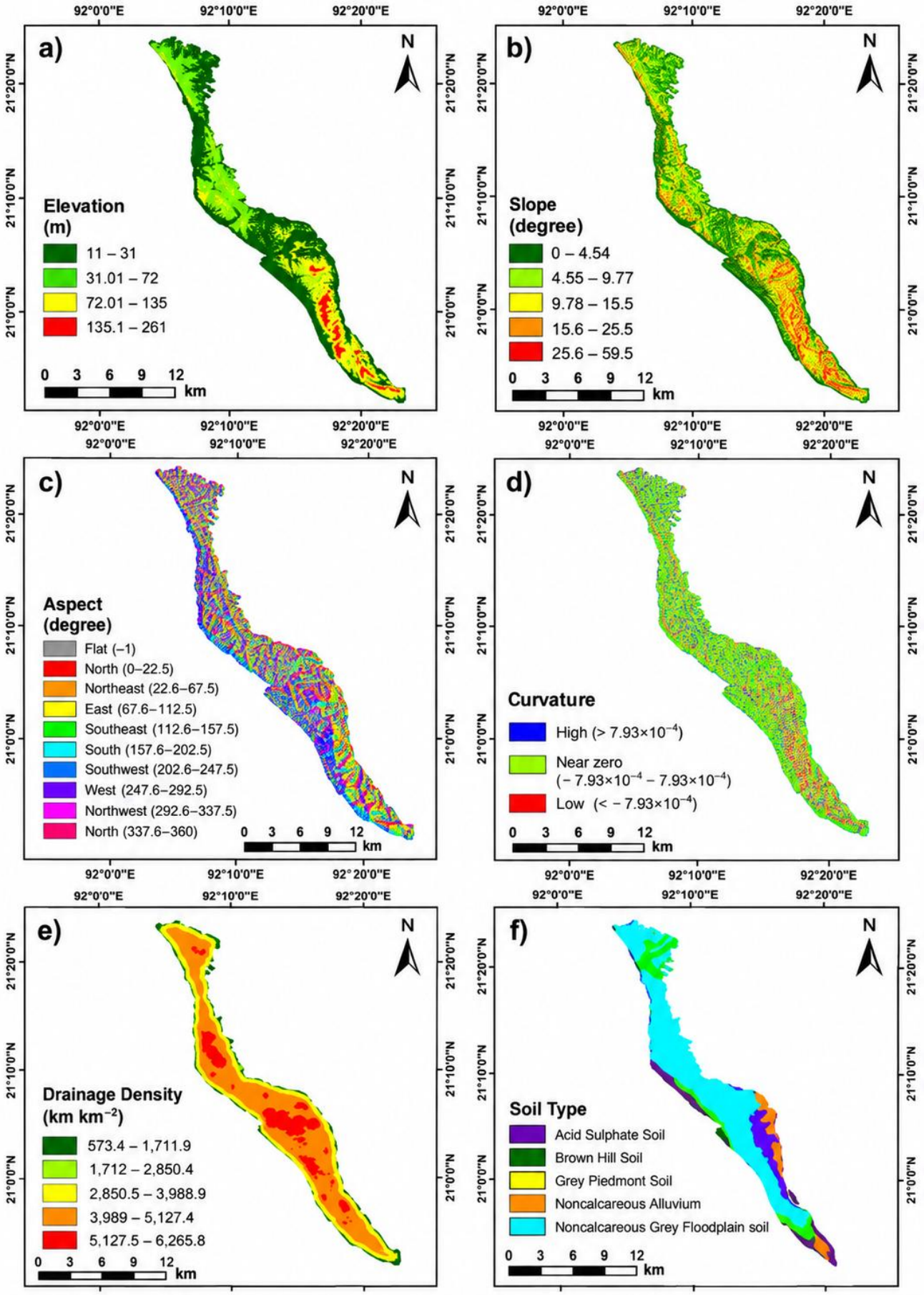


Figure 3, Landslide Conditioning Factor (a) Elevation, (b) Slope, (c) Aspect, (d) Curvature, (e) Drainage Density, (f) Soil Type

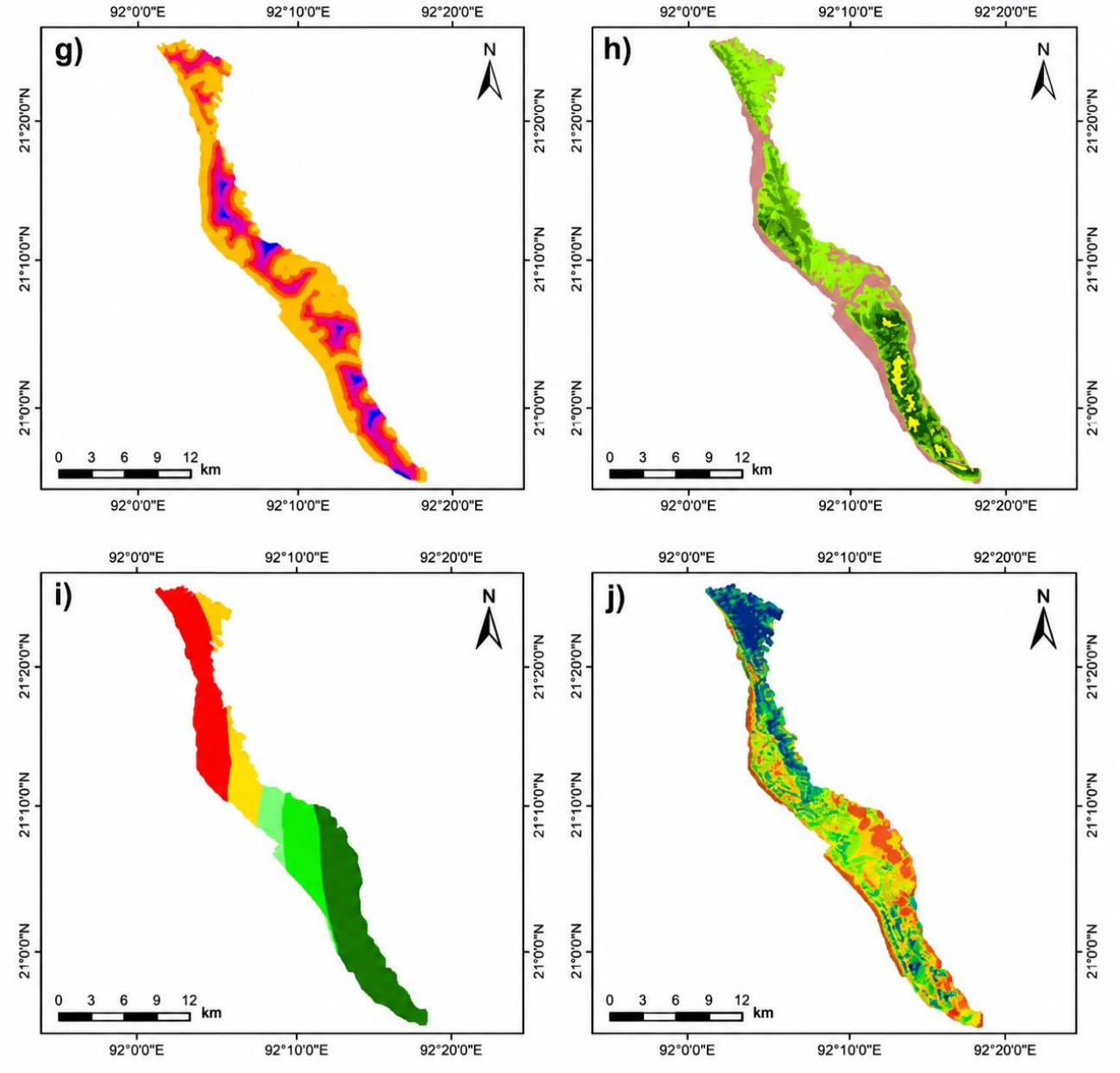


Figure 4, Landslide Conditioning Factors, contd: (g) Distance from Road, (h) Geomorphology, (i) Rainfall Map, (j) NDVI Map.

Aspect was classified into ten directional classes. Slopes facing southeast, south, and southwest are more windward and therefore receive higher monsoonal rainfall, leading to enhanced weathering, increased soil moisture, and pore-water pressure buildup, which increase landslide susceptibility. East and west facing slopes show intermediate susceptibility, whereas north-facing slopes are relatively leeward and generally exhibit lower landslide susceptibility. In parts of Cox's Bazar and Teknaf, slopes exposed to the southwest monsoon from the Bay of Bengal are particularly vulnerable to landslide occurrence.

Curvature

Curvature reflects the geometric form of the terrain and affects the convergence or divergence of surface runoff, modulating erosion and pore-pressure build-up (Huang et al., 2022). Concave slopes tend to accumulate water and sediments, increasing pore-water pressure and landslide susceptibility, whereas convex slopes generally promote runoff dispersion and exhibit comparatively lower instability. In this research, Curvature values span from approximately -1.99×10^{11} to 2.81×10^{11}, indicating alternating concave and convex surfaces across the hilly terrain.

Drainage density

Drainage density represents the degree of surface dissection by stream networks and is closely related to erosion intensity and subsurface hydrological processes. Areas with high drainage density are often characterized by intense surface runoff, channel erosion and slope undercutting which weaken Slope materials and enhance landslide susceptibility (Conforti et al., 2021). Here, Drainage density ranges from 573.4 to 6,265.8 m/km^2, with higher densities concentrated in the central and southern hill tracts where runoff channels are more frequent.

Soil type

Soil type plays a critical role in landslide susceptibility by influencing shear strength, permeability, and water-holding capacity (Moon et al., 2024). The study area is characterized by several soil types, including acid sulphate soil, brown hill soil, grey piedmont soil, noncalcareous alluvium, and noncalcareous grey floodplain soil. Brown hill soils and noncalcareous soils, which dominate the hilly and piedmont regions, are generally more prone to landslides due to their loose texture, moderate-to-high permeability, and susceptibility to saturation during intense rainfall. In contrast, floodplain and alluvial soils, predominantly distributed in low-lying areas, exhibit comparatively lower landslide susceptibility mainly due to gentler slopes and reduced gravitational driving forces.

Distance from road

Distance from road is an important anthropogenic factor influencing slope stability, as road construction often involves slope cutting, vegetation removal, and modification of natural drainage patterns (He et al., 2025). Areas closer to roads exhibit higher landslide susceptibility due to increased slope undercutting, altered runoff pathways, and reduced soil cohesion.

In the study area, distances from roads range from 0-0.023 km, highlighting zones in close proximity to major road corridors where landslide-prone areas are concentrated. Landslide susceptibility generally decreases with increasing distance from roads, reflecting reduced anthropogenic disturbance.

Geomorphology

Geomorphological units represent the surface appearance of geological structure and erosional-depositional processes, which have a significant effect on the occurrence of landslides. The study area comprises hilltops, hill slopes, lower hills, valleys, and barren land. Hill slopes and lower hill units are particularly susceptible to landslides due to steep gradients, active erosion, and weathered materials. Valleys and low-relief areas generally show lower susceptibility because of reduced slope angles and sediment accumulation, while barren lands may exhibit localized instability depending on slope conditions and surface exposure.

Rainfall

Rainfall is an important conditioning and triggering factor for landslides, especially in humid tropical and monsoon-dominated regions. It softening soils and raising pore pressure (He et al., 2025). The spatial variation in annual rainfall across the study area reflects the influence of the southwest monsoon from the Bay of Bengal, with rainfall ranging from 2399 to 2593 mm and gradually increasing from the northern belt toward the southern hilly region. Areas receiving higher rainfall experience enhanced infiltration, elevated pore-water pressure, and reduced shear strength, which collectively increase landslide susceptibility. Consequently, the southern and coastal portions of the study area, which receive relatively higher rainfall, exhibit greater vulnerability compared to regions with lower precipitation.

Normalized Difference Vegetation Index (NDVI)

Vegetation cover, represented by the Normalized Difference Vegetation Index (NDVI), plays an important role in landslide susceptibility by influencing root reinforcement, surface runoff, and soil moisture conditions (Gao et al., 2022). Low NDVI values generally indicate sparse or degraded vegetation, resulting in reduced root cohesion, greater surface exposure, and increased susceptibility to erosion and slope failure. In contrast, higher NDVI values are commonly associated with denser vegetation, which can enhance slope stability through stronger root reinforcement and reduced runoff.

In the study area, NDVI values range from −0.0573 to 0.458, reflecting spatial variation in vegetation cover. Sparse vegetation occurs mainly in the southeastern region, whereas denser vegetation is concentrated toward the northern and eastern hilly areas, including Himchari National Park.

Landslide susceptibility modeling

Analytic Hierarchy Process (AHP) based model

A structured multi-criterion decision-making (MCDM) method developed by Saaty (1977) called the Analytic Hierarchy Process (AHP) is frequently used in landslide susceptibility assessments to ascertain the relative significance of causal elements. It features a methodical framework for evaluating complicated issues involving several qualitative and quantitative criteria.

All conditioning factor layers were prepared and standardized to a common spatial resolution and coordinate system. The pairwise comparison matrix for the Analytic Hierarchy Process (AHP) was developed following Saaty's (1980) fundamental 1-9 scale (Table 2) under the guidance of a geotechnical engineering expert with extensive experience in slope stability assessment and geotechnical investigations.

The relative importance assigned to each conditioning factor was determined based on published literature, the geomorphological characteristics of the study area, and expert judgment. The preliminary weighting scheme was further reviewed through consultation with additional faculty members specializing in geology and geotechnical engineering to ensure its scientific validity and consistency. Subsequently, the pairwise comparison matrix and the corresponding weights were computed by the research team following the expert guidance, and the final matrix was verified and approved by the supervising expert.

Table 2, Saaty's Factor Ranking Scale

Importance Scores	Definition
1	Equal importance
3	Moderate importance
5	Strong importance
7	Very strong importance
9	Extreme importance
2, 4, 6, 8	Intermediate values
Reciprocals	Inverse comparison

For ensuring the accuracy of judgments, AHP employs a Consistency Ratio (CR), which rates the logical structure of the comparisons. A CR score of less than 0.10 indicates acceptable consistency, whereas greater levels suggest that judgments need to be revised. For landslide susceptibility analysis, ten factors were used as inputs. To perform the AHP calculations, pairwise comparison matrices were prepared based on the priority scale shown in Table 3.

The pairwise comparison matrix presented in Table 3 was first processed by summing the values within each column. These column totals were then used to normalize the matrix (Table 4), where each element of the original comparison matrix was divided by the sum of its respective column. This normalization step allowed the relative contribution of each factor to be expressed on a comparable scale. To derive the final weight of each landslide-conditioning factor, the average value of each row in the normalized matrix was calculated, resulting in the weights vector shown in the final column of Table 4. The results indicate that elevation received the highest weight (29%), followed by slope (21%) and soil type (15%), highlighting their dominant influence on landslide susceptibility in the study area. Distance from roads accounted for 11%, while NDVI contributed 8%. Lower weights were assigned to curvature (5%), drainage density (4%), geomorphology (3%), aspect (2%), and rainfall (2%), reflecting their comparatively smaller influence in the model. The comparatively higher weights assigned to elevation and slope are supported by expert opinion, previous studies and the geomorphological characteristics of the study area. Elevation controls terrain relief, weathering intensity, drainage development, and gravitational potential, whereas slope directly influences shear stress and slope stability, making it one of the most influential factors governing landslide occurrence. Previous studies conducted in the Chattogram Hill Tracts have consistently identified elevation and slope as the dominant conditioning factors associated with rainfall-induced landslides.

Table 3, The Pairwise Comparison Matrix and relative importance scores for Landslide susceptibility Mapping

Atributes	Elevation	Slope	Soil type	Distance from road	NDVI	Curvature	Drainage density	Geomorphology	Aspect	Rainfall
Elevation	1	2	3	4	5	6	7	8	9	9
Slope	0.5	1	2	3	4	5	6	7	8	9
Ssoil type	0.333	0.5	1	2	3	4	5	6	7	8
Distance from road	0.25	0.333	0.5	1	2	3	4	5	6	7
NDVI	0.2	0.25	0.333	0.5	1	2	3	4	5	6
Curvature	0.167	0.2	0.25	0.333	0.5	1	2	3	4	5
Drainage density	0.143	0.167	0.2	0.25	0.333	0.5	1	2	3	4
Geomorphology	0.125	0.143	0.167	0.2	0.25	0.333	0.5	1	2	3
Aspect	0.111	0.125	0.143	0.167	0.2	0.25	0.333	0.5	1	2
Rainfall	0.111	0.111	0.125	0.143	0.167	0.2	0.25	0.333	0.5	1

Table 4, The Normalization matrix and corresponding criteria weights of the landslide conditioning factors

Conditioning factors	Class											Criteria Weight
	1	2	3	4	5	6	7	8	9	10	11	
Elevation	0.340127	0.414167	0.388709	0.345040	0.303951	0.289260	0.240688	0.271795	0.197802	0.168667	0.288361	0.151769
slope	0.170063	0.207084	0.259139	0.258780	0.243161	0.224383	0.206304	0.190045	0.175824	0.168667	0.129570	0.210145
soil type	0.113376	0.103542	0.129570	0.172520	0.182371	0.179506	0.171920	0.162896	0.153846	0.148148	0.151769	0.151769
Distance from road	0.085032	0.069028	0.064785	0.086260	0.121581	0.134630	0.137536	0.135747	0.131868	0.129630	0.109609	0.109609
NDVI	0.068025	0.051771	0.043190	0.043130	0.060790	0.089753	0.103152	0.108597	0.109890	0.111111	0.078941	0.078941
Curvature	0.056688	0.041417	0.032392	0.028753	0.030395	0.044877	0.068768	0.081448	0.087912	0.092593	0.056524	0.056524
Drainage Density	0.048590	0.034514	0.025914	0.021565	0.020263	0.022438	0.034384	0.054299	0.065934	0.074074	0.040197	0.040197
Geomorphology	0.042516	0.029583	0.021595	0.017252	0.015198	0.014959	0.017192	0.027149	0.043956	0.055556	0.028496	0.028496
Aspect	0.037792	0.025885	0.018510	0.014377	0.012158	0.011219	0.011461	0.013575	0.021978	0.037037	0.020399	0.020399
Rainfall	0.037792	0.023009	0.016196	0.012323	0.010132	0.008975	0.008596	0.009050	0.010989	0.018519	0.015558	0.015558

After deriving the weight vector, the consistency of the pairwise comparisons were assessed to ensure the reliability of the expert judgments. The analysis yielded a maximum eigenvalue (λ_{max}) of 10.56, from which a Consistency Index (CI) of 0.063 was calculated. Using the corresponding Random Index (RI) value of 1.50, the Consistency Ratio (CR) was determined to be 0.042. As the CR value is well below the commonly accepted threshold of 0.10, it indicates a high level of consistency in the pairwise comparisons, confirming the reliability of the AHP-derived weights.

Therefore, the pairwise comparison matrix is considered logically consistent and suitable for application in the final landslide susceptibility assessment. Based on the derived criteria weights, the final AHP-based landslide susceptibility map was produced.

Frequency Ratio (FR) based model

The frequency ratio (FR) method is based on the fundamental assumption that future landslides are more likely to occur under environmental conditions similar to those associated with past landslide events. This approach quantifies how much more or less frequently landslides occur within each class of a conditioning factor compared to what would be expected by random chance. In this study, a landslide inventory map was prepared using historical landslide records obtained from NASA's global landslide database, complemented by visual interpretation of high-resolution imagery from Google Earth is shown in Figure 5.

This inventory served as the dependent variable in the FR analysis. The independent variables comprised ten selected landslide-conditioning factors. Each conditioning factor was classified into several thematic classes based on its spatial characteristics.

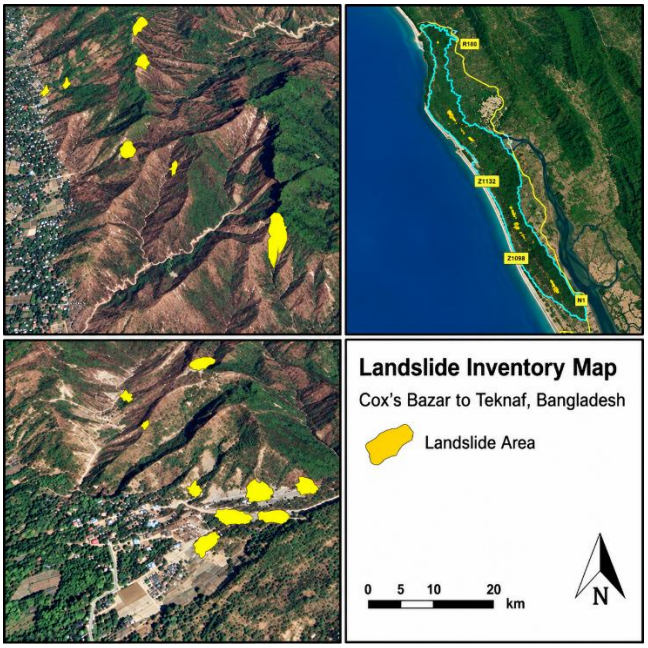


Figure 5, Landslide inventory map of the Cox's Bazar–Teknaf region, Bangladesh, showing mapped landslide locations (yellow).

The frequency ratio value for each class was calculated by dividing the percentage of landslide pixels occurring within that class by the percentage of the total study area occupied by the same class. The Frequency Ratio (FR) values were calculated using Eq. (1), and the corresponding FR calculations for all conditioning factor classes are presented in Table 5.

$$FR = \frac{\left(\frac{Number\ of\ landslide\ pixels\ in\ a\ class}{Total\ number\ of\ landslide\ pixels}\right)}{\left(\frac{Number\ of\ pixels\ in\ a\ class}{Total\ number\ of\ pixels\ in\ the\ study\ area}\right)} \quad (1)$$

The calculated Frequency Ratio (FR) values indicate the degree of association between each conditioning factor class and historical landslide occurrence. An FR value greater than 1.0 indicates that landslides occur more frequently than expected within a particular class

and therefore exhibit a positive relationship with landslide susceptibility, whereas FR values less than 1.0 indicate comparatively lower susceptibility. The results demonstrate that higher elevation and steeper slope classes generally exhibit higher FR values, confirming their dominant influence on landslide occurrence. Likewise, higher FR values associated with areas of sparse vegetation, shorter distances from roads, and specific geomorphological units highlight the combined influence of topographic, environmental, and anthropogenic factors on slope instability.

These FR values were subsequently used to assign class weights for the preparation of the FR-based landslide susceptibility map.

After preparation of the landslide-conditioning factor layers, all datasets were converted to raster format and standardized to a common spatial resolution, projection, and spatial extent to ensure consistency. Each conditioning factor was reclassified into susceptibility classes using the Reclassify tool in ArcGIS 10.8, based on its relative contribution to landslide occurrence as determined by the applied susceptibility models (Addis, 2023).

Landslide susceptibility mapping was carried out using a raster-based weighted overlay approach implemented through the Raster Calculator tool within the Spatial Analyst extension of ArcGIS 10.8. In this process, each reclassified factor raster was multiplied by its corresponding weight, and the weighted raster were summed to generate the Landslide Susceptibility Index (LSI), by the following equation 2 (Pradhan, 2010).

$$LSI = \Sigma(Wi \times Ri) \qquad (2)$$

Where, Wi denotes the weight assigned to the i^{th} conditioning factor and Ri represents its reclassified raster value.

The generated Landslide Susceptibility Index (LSI) raster effectively captures the spatial variability of landslide susceptibility across the study area, highlighting zones with differing levels of potential landslide occurrence (Rasyid et al., 2016). Higher LSI values represent areas with greater susceptibility, whereas lower values indicate comparatively stable regions. To produce the final landslide susceptibility map, the continuous LSI values were classified using the Natural Breaks (Jenks) classification method. This approach groups values by minimizing within-class variance and maximizing between-class differences, allowing for an objective delineation of susceptibility patterns. The classified map was divided into five susceptibilities zones- very low, low, moderate, high, and very high to clearly represent the spatial distribution of landslide-prone areas and support effective hazard assessment and land-use planning.

Model validation

The predictive performance of the landslide susceptibility maps produced using the Analytic Hierarchy Process (AHP) and Frequency Ratio (FR) models was evaluated through a standard model validation procedure based on the Receiver Operating Characteristic (ROC) curve and the Area under the Curve (AUC) (Panchal & Shrivastava, 2021; Ali et al., 2025). Validation was carried out using the landslide inventory dataset, which represents the observed spatial distribution of past landslide events within the study area (Wang et al., 2017).

The ROC-AUC approach is a threshold-independent statistical method widely used to assess the reliability and robustness of susceptibility models. It measures the ability of a model to correctly distinguish between landslide-prone and non-landslide areas across a range of classification thresholds (Chen et al., 2019; Ali et al., 2025). In this study, the ROC curves were generated using Python 2.7.16 with the Scikit-learn, Pandas, NumPy, and Matplotlib libraries by comparing the landslide susceptibility values at the inventoried landslide locations with those at the non-landslide locations. Model performance was evaluated using a validation dataset consisting of 55 landslide points and 30 non-landslide points. The true positive rate (landslide locations) and false positive rate (non-landslide locations) were calculated across a range of threshold values to construct the ROC curves and determine the Area Under the Curve (AUC).

The AUC value, which ranges from 0.5 to 1.0, provides a quantitative measure of model accuracy (Dahal et al., 2008a; Dahal et al., 2008b; Chen et al., 2019; Kusuma et al., 2025). An AUC value close to 1.0 indicates excellent predictive capability, while values near 0.5 suggest random prediction. Generally, AUC values between 0.9-1.0 represent very high accuracy, 0.8-0.9 indicate good performance, 0.7-0.8 reflect moderate accuracy, and values below 0.7 imply poor classification. Conditioning factors with AUC values greater than 0.6 are considered to have a meaningful contribution to landslide occurrence (Kusuma et al., 2025).

The ROC curves and corresponding AUC values demonstrate that both the AHP and FR models perform well in capturing the spatial relationship between landslide occurrences and controlling factors. A higher AUC value indicates stronger agreement between predicted susceptibility classes and observed landslide locations, confirming the reliability of the developed landslide susceptibility maps for hazard assessment and planning purposes (Wubalem, 2020).

Result and discussion

The assessment of landslide susceptibility in the study area was conducted using two distinct modeling approaches, the knowledge-based Analytic Hierarchy Process (AHP) and the data-driven Frequency Ratio (FR) model illustrated in Figure 6.

AHP-based results show that the study area is predominantly classified as moderate susceptible, accounting for about 63.48% of the total area, followed by low susceptibility (35.45%) and a very limited high-susceptibility zone (1.06%). Spatially, high- susceptible areas are mainly concentrated along the southeastern hill slopes of Teknaf, where steep slopes and geomorphic instability prevail. Moderate-susceptible zones extend widely across Ramu, Ukhiya, and Teknaf Upazila, reflecting transitional terrain conditions. In contrast, low- susceptible areas are largely distributed over the coastal plains and relatively flat regions, where slope instability potential is minimal.

Table 5, Frequency Ratio (FR) calculation for the conditioning factor classes used in landslide susceptibility assessment.

Parameter	Classes	Class Pixels	%Class Pixels	Landslide Pixels	%Landslide Pixels	FR	RF	RF (non%)	RF (INT)	Min RF	Max RF	Max-Min RF	(Max-Min)/ Min RF	PR
Slope	0 – 4.514	128613	39.903	1.000	3.125	0.0000	0.003	0.284817	0					
	4.515 – 9.279	100762	31.262	9.000	28.125	0.0001	0.033	3.271872	3					
	9.28 – 15.55	60202	18.678	4.000	12.500	0.0001	0.024	2.433883	2					
	15.56 – 25.58	27286	8.466	5.000	15.625	0.0002	0.067	6.712445	6					
	25.59 – 63.95	5455	1.692	13.000	40.625	0.0024	0.873	87.29698	87					
	Total	**322318**		32.000		0.0027				0.002848	0.87297	0.870122	0.202983	4.286667
Elevation	(-)11 – 24	125628	38.389	1.000	3.125	0.0000	0.005	0.454787	0					
	24.01 – 50	119221	36.432	7.000	21.875	0.0001	0.034	3.354591	3					
	50.01 – 90	52131	15.930	4.000	12.500	0.0001	0.044	4.383875	4					
	90.01 – 149	20917	6.392	9.000	28.125	0.0004	0.246	24.58314	24					
	149.1 – 261	9349	2.857	11.000	34.375	0.0012	0.672	67.22361	67					
	Total	**327246**			32.000	0.0018				0.004548	0.672236	0.667688	0.202983	3.289376
Soil Type	Acid Sulphate Soil	24707	8.470	1.000	3.226	0.0000	0.046	4.596086	4					
	Brown Hill Soil	31277	10.722	5.000	16.129	0.0002	0.182	18.15319	18					
	Grey Piedmont Soil	17290	5.927	6.000	19.355	0.0003	0.394	39.40619	39					
	Noncalcareous Aluvium	22478	7.706	6.000	19.355	0.0003	0.303	30.3111	30					
	Noncalcareous Grey Floodplain soil	195956	67.175	13.000	41.935	0.0001	0.075	7.533433	7					
	Total	291708			31.000	0.0009				0.046	0.394062	0.3481	0.202983	1.714925
Geomorphology	Baren land	124286	53.390	4.000	12.500	0.0000	0.021	2.128362	2					
	Hill Slopes	69453	29.835	8.000	25.000	0.0001	0.148	14.81715	14					
	Hilltops	26779	11.503	6.000	18.750	0.0002	0.076	7.617398	7					
	Valleys	12273	5.272	14.000	43.750	0.0011	0.754	75.43709	75					
	Total	232791			32.000	0.0015				0.021284	0.754371	0.733087	0.202983	3.611565
Rainfall	2,399 – 2,437	91026	45.954	6.000	18.750	0.0001	0.213	21.34692	21					
	2,555 – 2,593	107055	54.046	26.000	81.250	0.0002	0.787	78.65308	78					
	Total	198081			32.000	0.0003				0.213469	0.786531	0.573062	0.202983	2.823197
Drainage Density	1,712 – 2,850.4	48953	16.690	3.000	9.375	0.0001	0.185	18.45309	18					
	2,850.5 – 3,988.9	70143	23.915	1.000	3.125	0.0000	0.043	4.29282	4					
	3,989 – 5,127.4	117487	40.057	26.000	81.250	0.0002	0.666	66.63626	66					
	5,127.5 – 6,265.8	56718	19.338	2.000	6.250	0.0000	0.106	10.61784	10					
	Total	293301			32.000	0.0003				0.042928	0.666363	0.623434	0.202983	3.071358
Distance From Road	0 – 0.00459	116236	35.494	2.000	6.250	0.0000	0.028	2.806812	2					
	0.0046 – 0.00918	80036	24.440	5.000	15.625	0.0001	0.102	10.19081	10					
	0.00919 – 0.0138	63798	19.481	10.000	31.250	0.0002	0.256	25.56919	25					
	0.0139 – 0.0184	45692	13.953	13.000	40.625	0.0003	0.464	46.41167	46					
	0.0185 – 0.023	21719	6.632	2.000	6.250	0.0001	0.150	15.02153	15					
	Total	327481			32.000	0.0006				0.028068	0.464117	0.436049	0.202983	2.148199
NDVI	(-)0.0573 – 0.106	37867	11.573	3.000	9.375	0.0001	0.159	15.94784	15					
	0.107 – 0.169	80503	24.604	10.000	31.250	0.0001	0.250	25.00515	25					
	0.17 – 0.223	98303	30.044	5.000	15.625	0.0001	0.102	10.2387	10					
	0.224 – 0.286	60130	18.377	11.000	34.375	0.0002	0.368	36.82503	36					
	0.287 – 0.458	50395	15.402	3.000	9.375	0.0001	0.120	11.98327	11					
	Total	327198			32.000	0.0005				0.102387	0.36825	0.265863	0.202983	1.309779
Aspect	Flat (-1)	39127	13.653	1.000	3.125	0.0000	0.029	2.891633	2					
	North (0–22.5)	35523	12.395	4.000	12.500	0.0001	0.127	12.74002	12					
	Northeast (22.5–67.5)	35782	12.486	7.000	21.875	0.0002	0.221	22.13365	22					
	Southeast (112.5–157.5)	36406	12.704	3.000	9.375	0.0001	0.093	9.323263	9					
	South (157.5–202.5)	39031	13.620	8.000	25.000	0.0002	0.232	23.18996	23					
	Southwest (202.5–247.5)	37953	13.243	4.000	12.500	0.0001	0.119	11.92432	11					
	West (247.5–292.5)	32074	11.192	4.000	12.500	0.0001	0.141	14.10998	14					
	Northwest (292.5–337.5)	30685	10.707	1.000	3.125	0.0000	0.037	3.687173	3					
	Total	286581			32.000	0.0009				0.028916	0.2319	0.202983	0.202983	1
Curvature	High	121622	37.166	19.000	59.375	0.0002	0.547927	54.79267	54					
	Moderate	113603	34.716	6.000	18.750	0.0001	0.185243	18.52433	18					
	Low	92012	28.118	7.000	21.875	0.0001	0.26683	26.683	26					
	Total	327237			32.000	0.0003				0.185243	0.547927	0.362683	0.202983	1.786765

In comparison, the FR-based model provides a more detailed zonation by dividing the area into five susceptibility classes. The results indicate dominance of very low susceptibility (44.75%) and low susceptibility (38.39%) zones, together covering more than 80% of the study area. Moderate- susceptibility areas (12.51%) appear as scattered patches, mainly within the hill tracts of Teknaf and parts of Ukhiya.

Importantly, the FR model identifies high-susceptibility (3.91%) and very high-susceptibility (0.44%) zones, which form distinct and continuous clusters along the steep southeastern slopes of Teknaf,

highlighting zones of pronounced terrain instability. A comparison of spatial extent reveals notable differences between the two models. The AHP model allocates a larger proportion of land to the moderate-susceptibility category, suggesting a more generalized classification. In contrast, the FR model concentrates most of the area within very low and low- susceptibility classes, while simultaneously identifying a higher combined percentage of high and very high-Susceptibility zones (4.35%). This indicates that the FR approach is more sensitive in distinguishing unstable terrain and capturing localized high- susceptible areas.

Area-based analysis further supports this distinction. While AHP assigns only 2.73 km^2 to the high-susceptibility category, the FR model identifies approximately 11.14 km^2 as high to very high susceptibility combined shown in Table 6. The differences in the spatial patterns of the AHP and FR models arise from their methodological approaches.

The AHP model produces more generalized susceptibility patterns based on expert-assigned weights, whereas the FR model identifies more localized high-susceptibility zones by statistically relating historical landslides to conditioning factor classes.

The ROC-AUC validation results demonstrate clear differences in predictive capability between the two models in Figure 7. The AHP model achieved an AUC value of 0.859, indicating strong predictive performance and a high level of agreement between predicted susceptibility and observed landslide locations. Conversely, the FR model yielded an AUC value of 0.688, representing moderate predictive capability.

The susceptibility patterns identified in the present study are generally consistent with previous landslide susceptibility investigations conducted in the Chattogram Hill Tracts and southeastern Bangladesh, where elevation, slope, rainfall, and anthropogenic activities have been recognized as the dominant controls on slope instability (Sultana et al., 2024; Islam et al., 2024; Nahar et al., 2025). Similar studies employing AHP, Frequency Ratio, and other GIS-based approaches have likewise reported that steep hill slopes, higher elevations, and road-cutting activities significantly increase landslide susceptibility (Chowdhury et al., 2023; Rabby and Li, 2020). The concentration of high and very high susceptibility zones in the Teknaf and Ukhiya hill regions observed in this study therefore agrees well with earlier investigations, confirming the strong influence of both geomorphological conditions and human-induced landscape modifications. The higher predictive performance of the AHP model also supports previous findings that expert knowledge can effectively represent complex terrain characteristics in data-limited environments, whereas the FR model provides greater spatial detail by directly incorporating the statistical relationship between historical landslide occurrences and conditioning factors.

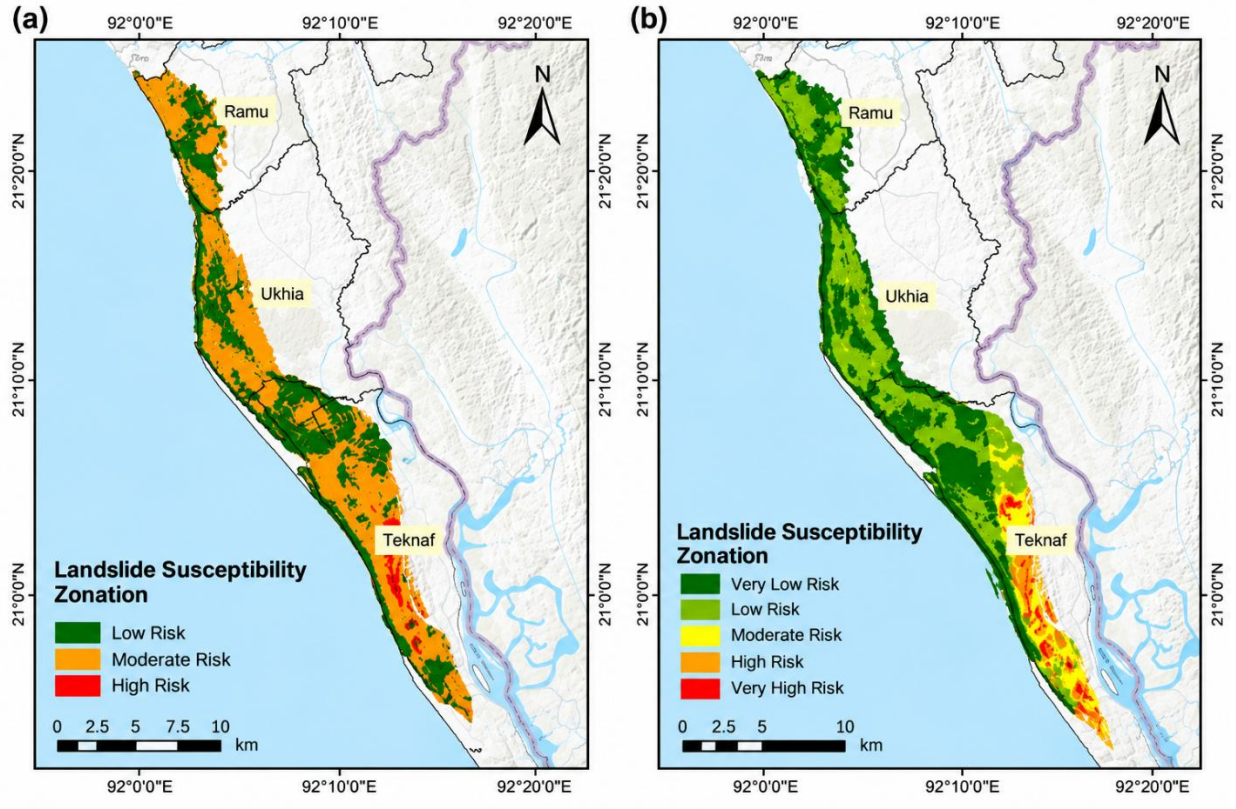


Figure 6, Landslide Susceptibility mapping of the study area, (a) AHP based susceptibility mapping and (b) FR based susceptibility mapping.

The generated landslide susceptibility maps and identified high- and very high-susceptibility zones can assist government agencies and local authorities in prioritizing slope stabilization, regulating hill-cutting activities, and guiding infrastructure development in vulnerable areas. The maps also provide valuable information for emergency preparedness, land-use planning, and humanitarian management, particularly in the Ukhiya–Teknaf corridor where transportation infrastructure, settlements, and refugee camps are exposed to recurrent landslide hazards.

Table 6, Spatial Extent of Susceptibility Class in AHP and FR Models

AHP Based Model		
Susceptibility Class	**Area (Km²)**	**Percentage (%)**
Low	90.87	35.45
Moderate	162.72	63.48
High	2.73	1.06
FR Model		
Susceptibility Class	**Area (Km²)**	**Percentage (%)**
Very Low	114.62	44.75
Low	98.33	38.39
Moderate	32.04	12.51
High	10.03	3.91
Very High	1.11	0.44

Despite these encouraging results, the present study relied primarily on ROC-AUC analysis for model validation. Although ROC-AUC is a robust and widely accepted metric for evaluating landslide susceptibility models, incorporating additional validation measures, such as confusion matrix-based indices (e.g., precision, recall, F1-score, and overall accuracy), the Kappa coefficient, and Success Rate Curves, would provide a more comprehensive assessment of model performance and predictive reliability.

Limitations and future research

This study has several limitations that should be considered when interpreting the results. The landslide inventory was compiled from the NASA Global Landslide Catalog and Google Earth imagery; therefore, some undocumented landslide events may not have been captured. In addition, the input datasets differ in source, spatial resolution, and acquisition time, introducing unavoidable uncertainties. The AHP model relies on expert judgment, whereas the FR model assumes that future landslide occurrence follows historical spatial patterns. The pairwise comparison matrix satisfied the recommended consistency criterion (CR < 0.10); however, a formal sensitivity analysis was not performed. Furthermore, the susceptibility maps represent the relative likelihood of landslide occurrence rather than deterministic predictions. Despite these limitations, the ROC-AUC validation (Figure 7) results indicate that the models provide a reliable basis for regional landslide hazard assessment. Future research should incorporate sensitivity analysis, field-based validation, higher-resolution datasets, and additional statistical and machine-learning approaches, such as Logistic Regression (LR), Random Forest (RF), Support Vector Machine (SVM), and Extreme Gradient Boosting (XGBoost), to further improve model robustness and predictive performance. In addition, future studies should include systematic field investigations and independent validation datasets to verify the identified susceptibility zones and further improve the reliability of landslide susceptibility assessments.

Conclusion and recommendations

This study applied AHP and FR-based landslide susceptibility models to identify and compare spatial patterns of landslide susceptibility in the study area. The findings demonstrate the effectiveness of integrating expert-based and data-driven approaches to identify landslide-prone areas and provide a scientifically reliable framework for regional hazard assessment. The generated susceptibility maps contribute valuable spatial information to support evidence-based planning, infrastructure development, and disaster risk management in one of Bangladesh's most landslide-prone regions. The complementary performance of these models demonstrates that their combined application can improve landslide susceptibility assessment by integrating expert knowledge with statistically derived spatial relationships.

Based on the findings, the following recommendations are proposed to support risk reduction and sustainable land management.

1. Risk-sensitive land-use planning

High and very high landslide susceptibility zones, especially along the steep slopes of Teknaf, should be strictly regulated. New settlements, road construction, and slope cutting activities should be avoided or minimized in these areas.

2. Rohingya refugee camp management

Several refugee camps are located in or adjacent to moderate- to high-susceptibility zones. Immediate attention should be given to relocating shelters away from high-risk slopes, enforcing slope setbacks, and limiting hill cutting for fuelwood or shelter expansion. Temporary stabilization measures, such as surface drainage control and bioengineering techniques, should be implemented where relocation is not immediately feasible.

3. Slope stabilization along marine drive and coastal cliffs

The marine drive corridor, which runs along steep coastal cliffs, is highly vulnerable to slope failure due to combined effects of steep gradients, rainfall, and

coastal erosion. Regular geotechnical inspections, controlled drainage systems, retaining structures, and vegetation-based slope reinforcement are strongly recommended to reduce landslide risk and ensure road safety.

4. Integrated use of susceptibility models

For practical applications, it is recommended to use AHP for regional-scale planning and FR for site-specific risk identification, as their combined application provides a more comprehensive understanding of landslide susceptibility.

Overall, the results of this study provide a valuable scientific basis for disaster risk reduction strategies, infrastructure planning, and humanitarian management in a highly vulnerable and socio-environmentally sensitive region.

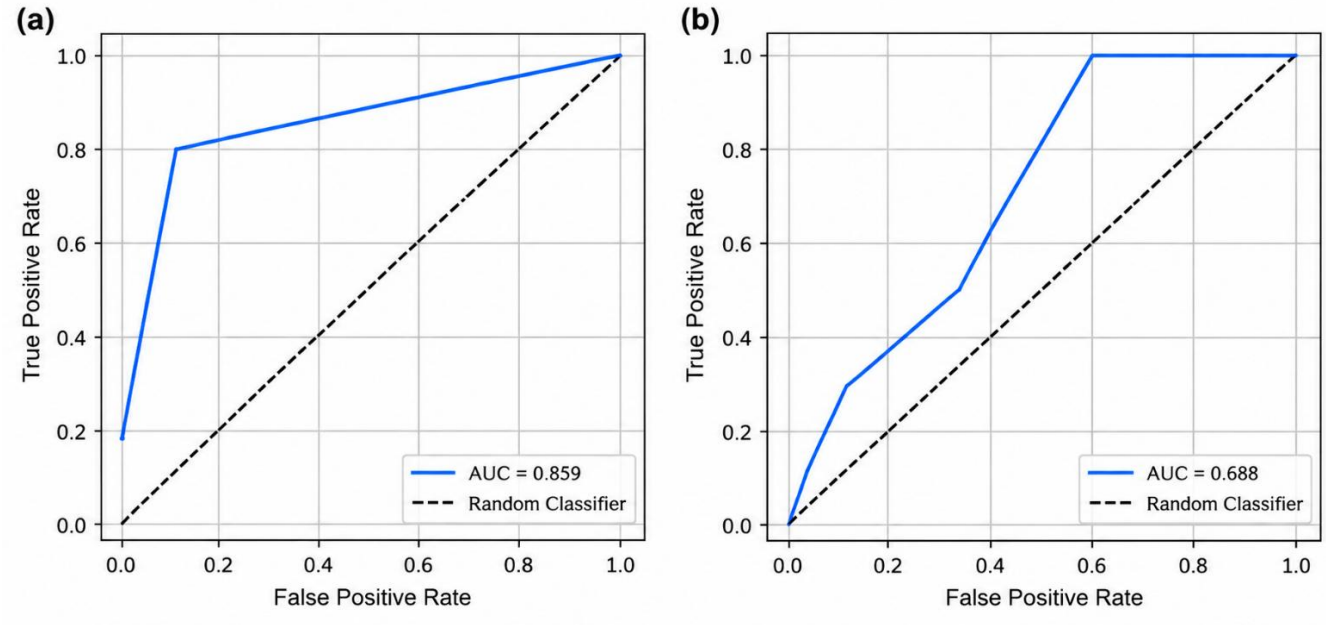


Figure 7, ROC–AUC curves of the (a) AHP and (b) FR landslide susceptibility models.

Acknowledgements

Special thanks to Prof. Dr. Younus Ahmed Khan for his insightful ideas and academic support. The author further thanks the IAEG YEG, University of Rajshahi (UR), Bangladesh team for fostering an enthusiastic research environment and creating a festive academic spirit during the 15th ARC Conference.

Author contributions

Muqit Ajmain Shahriyar conceived the research idea, conducted data analysis, prepared the figures, and wrote the original manuscript. Dr. Md. Abdul Malek supervised the study and provided continuous guidance in structuring the research framework and methodology.

Md. Yunus Hider, Tasmim Banu, and Md. Mahedi Hasan contributed to manuscript writing, critical revision, and overall improvement of the paper. Tasmim Banu also presented the research at the 15th ARC Conference, Nepal. All authors reviewed and approved the final version of the manuscript.

Data availability

The data used in this study are not publicly available. The datasets and analytical outputs generated during the study are available from the corresponding author upon reasonable request.

Declarations

The authors declare that they have no known competing financial interests or personal relationships that could have influenced the work reported in this article.

Article note

This article is a full-length paper developed from **Extended Abstract #091**, entitled "**Integrating AHP and Remote Sensing Method for Landslide Susceptibility Mapping of the Coastal Cliffs in Southeastern Bangladesh**" which was presented at the 15th Asian Regional Conference of the International Association for Engineering Geology and the Environment (ARC-15 of **IAEG**), held in Kathmandu, Nepal, from 27 to 29 November 2025.

Reference

Addis, A. (2023). GIS-Based Landslide Susceptibility Mapping Using Frequency Ratio and Shannon Entropy Models in Dejen District, Northwestern Ethiopia. Journal of Engineering. https://doi.org/10.1155/2023/1062388

Ahmed, B., Rahman, M., Sammonds, P., Islam, R., and Uddin, K. (2020). Application of geospatial technologies in developing a dynamic landslide early warning system in a humanitarian context: the Rohingya refugee crisis in Cox's Bazar, Bangladesh. Geomatics, Natural Hazards and Risk, 11, 446 - 468. https://doi.org/10.1080/19475705.2020.1730988

Ali, A., Teku, D., Sisay, T., and Mihret, B. (2025). A combined analysis of frequency ratio and analytical hierarchy process for landslide susceptibility assessment in Tenta, South Wollo, Ethiopia. Scientific Reports, 15. https://doi.org/10.1038/s41598-025-94611-z

Carrara, A. (1983). Multivariate models for landslide hazard evaluation. Journal of the International Association for Mathematical Geology, 15, 403-426. https://doi.org/10.1007/bf01031290

Chang, K., Merghadi, A., Yunus, A., Pham, B., and Dou, J. (2019). Evaluating scale effects of topographic variables in landslide susceptibility models using GIS-based machine learning techniques. Scientific Reports, 9. https://doi.org/10.1038/s41598-019-48773-2

Chen, W., Sun, Z., and Han, J. (2019). Landslide Susceptibility Modeling Using Integrated Ensemble Weights of Evidence with Logistic Regression and Random Forest Models. Applied Sciences, 9(1), 171. https://doi.org/10.3390/app9010171

Chowdhury, M. (2024). Morphometric analysis of Halda River basin, Bangladesh, using GIS and remote sensing techniques. Heliyon, 10. https://doi.org/10.1016/j.heliyon.2024.e29085

Chowdhury, M., Rahman, M., Sheikh, M., Sayeid, M., Mahmud, K., and Hafsa, B. (2023). GIS-based landslide susceptibility mapping using logistic regression, random forest and decision and regression tree models in Chattogram District, Bangladesh. Heliyon,10. https://doi.org/10.1016/j.heliyon.2023.e23424

Conforti, M., and Ietto, F. (2021). Modeling Shallow Landslide Susceptibility and Assessment of the Relative Importance of Predisposing Factors, through a GIS-Based Statistical Analysis. Geosciences, 11(8), 333. https://doi.org/10.3390/geosciences11080333.

Cuomo, S. (2020). Modelling of flowslides and debris avalanches in natural and engineered slopes: a review. Geoenvironmental Disasters, 7, 1-25. https://doi.org/10.1186/s40677-019-0133-9

Dahal, R. K., Hasegawa, S., Nonomura, A., Yamanaka, M., Masuda, T., and Nishino, K. (2008a). GIS-based weights-of-evidence modelling of rainfall-induced landslides in small catchments for landslide susceptibility mapping. Environmental Geology, 54(2), 311–324. https://doi.org/10.1007/s00254-007-0818-3

Dahal, R. K., Hasegawa, S., Nonomura, A., Yamanaka, M., Dhakal, S., and Paudyal, P. (2008b). Predictive modelling of rainfall-induced landslide hazard in the Lesser Himalaya of Nepal based on weights-of-evidence. Geomorphology, 102(3–4), 496–510. https://doi.org/10.1016/j.geomorph.2008.05.041

Fidan, S., Tanyaş, H., Akbaş, A., Lombardo, L., Petley, D.N., and Görüm, T. (2024). Understanding fatal landslides at global scales: a summary of topographic, climatic, and anthropogenic perspectives. Natural Hazards, 120, 6437 - 6455. https://doi.org/10.1007/s11069-024-06487-3

Froude, M.J., and Petley, D. (2018). Global fatal landslide occurrence from 2004 to 2016. Natural Hazards and Earth System Sciences, 18, 2161-2181. https://doi.org/10.5194/nhess-18-2161-2018

Fuad, N., Meandad, J., Haque, A., Sultana, R., Anwar, S., and Sultana, S. (2024). Landslide vulnerability analysis using frequency ratio (FR) model: a study on Bandarban district, Bangladesh. ArXiv, abs/2407.20239. https://doi.org/10.48550/arxiv.2407.20239

Gao, J., Shi, X., Li, L., Zhou, Z., and Wang, J. (2022). Assessment of Landslide Susceptibility Using Different Machine Learning Methods in Longnan City, China. Sustainability, 14(24), 16716. https://doi.org/10.3390/su142416716

He, Q., Wu, S., Zhao, X., Hui, Z., Wang, Z., Tsangaratos, P., Ilia, I., Chen, W., Chen, Y., and Hao, Y. (2025). Evaluation of landslide susceptibility of mountain highway based on RF and SVM models. Scientific Reports, 15. https://doi.org/10.1038/s41598-025-08774-w

He, S., Pan, P., Dai, L., Wang, H., & Liu, J. (2012). Application of kernel-based Fisher discriminant analysis to map landslide susceptibility in the Qinggan River delta, Three Gorges, China. Geomorphology, 171, 30-41. https://doi.org/10.1016/j.geomorph.2012.04.024

Hossain, F., and Moniruzzaman, D. M. (2021). Environmental change detection through remote sensing technique: A study of Rohingya refugee camp area (Ukhiya and Teknaf sub-district), Cox's Bazar, Bangladesh. Environmental Challenges,100024. https://doi.org/10.1016/j.envc.2021.100024

Hossain, S., Tushar, M., Islam, S., Razzak, M., Alve, A., and Junayed, T. (2025). Investigating the role of rock weathering and clay mineralogy in landslide occurrences within the exposed Tertiary Formations in Rangamati area. Geoenvironmental Disasters, 12. https://doi.org/10.1186/s40677-025-00324-w

Hossen, S., Hossain, M., Hossain, M., and Uddin, M. (2020). Quantitative assessment of tree species diversity of Himchari National Park (HNP) in Cox's Bazar, Bangladesh. Asian Journal of Forestry, 5(1), 1-7. https://doi.org/10.13057/asianjfor/r050101

Huang, F., Tao, S., Li, D., Lian, Z., Catani, F., Huang, J., Li, K., and Zhang, C. (2022). Landslide Susceptibility Prediction Considering Neighborhood Characteristics of Landslide Spatial Datasets and Hydrological Slope Units Using Remote Sensing and GIS Technologies. Remote. Sens., 14(18), 4436. https://doi.org/10.3390/rs14184436

Islam, M. T., Sikder, S. K., Charlesworth, M., and Rabbi, A. (2023). Spatial transition dynamics of urbanization and Rohingya refugees' settlements in Bangladesh. Land Use Policy, 133, 106874. https://doi.org/10.1016/j.landusepol.2023.106874

Islam, S., Miah, M., Jubaer, A., Mondal, K., and Mahmud, M. (2024). An Assessment of the Causes and Consequences of Landslides (2017) Occurred in the Southeastern Areas of Bangladesh. Journal of Science and Technology Research, 5(1). https://doi.org/10.3329/jscitr.v5i1.74011

Kamal, A., Hossain, F., Ahmed, B., Rahman, M., and Sammonds, P. (2023). Assessing the effectiveness of landslide slope stability by analysing structural mitigation measures and community risk perception. Natural Hazards, 117, 2393 - 2418. https://doi.org/10.1007/s11069-023-05947-6

Kamal, A., Hossain, F., Rahman, M., Ahmed, B., and Sammonds, P. (2022). Geological and soil engineering properties of shallow landslides occurring in the Kutupalong Rohingya Camp in Cox's Bazar, Bangladesh. Landslides, 19, 465-478. https://doi.org/10.1007/s10346-021-01810-6

Khanam, F., Rahman, M., Alam, M., and Abdullah, R. (2020). Sedimentology and basin-fill history of the Cenozoic succession of the Sylhet Trough, Bengal Basin, Bangladesh. International Journal of Earth Sciences, 110, 193-212. https://doi.org/10.1007/s00531-020-01946-1

Kusuma, R., Meilano, I., and Fitri, I. (2025). Landslide Susceptibility Assessment using Analytical Hierarchy Process in West Java. IOP Conference Series: Earth and Environmental Science, 1472, 1-13. https://doi.org/10.1088/1755-1315/1472/1/012035

Lee, S., and Pradhan, B. (2006). Probabilistic landslide hazards and risk mapping on Penang Island, Malaysia. Journal of Earth System Science, 115(6), 661-672. https://doi.org/10.1007/s12040-006-0004-0

Luna, L., Woodard, J., Bytheway, J., Belair, G., and Mirus, B. (2025). Constraining landslide frequency across the United States to inform county-level risk reduction. Natural Hazards and Earth System Sciences, 25, 3279–3304. https://doi.org/10.5194/nhess-25-3279-2025

Mazumder, A., Sarkar, A., Sikder, M., Tabassum, A., Islam, S. T., and Barua, E. (2024). Impact of Land Conversion on Land Surface Temperature Over the Coastal Area: A Spatiotemporal Study of Cox's Bazar District, Bangladesh. Journal of Geovisualization and Spatial Analysis, 8, 38. https://doi.org/10.1007/s41651-024-00196-y

Mohiuddin, M., Hossain, M., Islam, M. Y., Nowreen, S., and Sultana, N. (2025). Assessing the impact of Land Use Land Cover change after Rohingya forced migration on elephant route in Cox's Bazar district, Bangladesh. Landscape and Ecological Engineering, 21, 303 - 319. https://doi.org/10.1007/s11355-025-00642-z

Moon, S., Noh, J., Kim, H., Kang, S., and Seo, Y. (2024). Comparison of factors influencing landslide risk near a forest road in Chungju-si, South Korea. Geoenvironmental Disasters, 11, 1-17. https://doi.org/10.1186/s40677-024-00267-8

Moslehuddin, A., Rahman, M., Moriyama, M., and Tani, M. (2018). Physiography, Forests, and People in Teknaf. , 11-40. https://doi.org/10.1007/978-981-10-5475-4_2

Nahar, N., Mohiuddin, M., Nowreen, S., and Hossain, M. (2025). Influential Factors of Landslide Occurrence in the South-Eastern Part of Bangladesh. IDRiM Journal. https://doi.org/10.5595/001c.143100

Nath, T., Aziz, N., and Inoue, M. (2015). Contribution of Homestead Forests to Rural Economy and Climate Change Mitigation: A Study from the Ecologically Critical Area of Cox's Bazar—Teknaf Peninsula, Bangladesh. Small-scale Forestry, 14, 1-18. https://doi.org/10.1007/s11842-014-9270-x

Panchal, S., and Shrivastava, A. (2021). A Comparative Study of Frequency Ratio, Shannon's Entropy and Analytic Hierarchy Process (AHP) Models for Landslide Susceptibility Assessment. ISPRS Int. J. Geo Inf., 10, 603. https://doi.org/10.3390/ijgi10090603

Petley, D., Bulmer, M., and Murphy, W. (2002). Patterns of movement in rotational and translational landslides. Geology, 30, 719-722. https://doi.org/10.1130/0091-7613(2002)030<0719:pomira>2.0.co;2

Pradhan, B., and Lee, S. (2010). Delineation of landslide hazard areas using frequency ratio, logistic regression and artificial neural network models. https://doi.org/10.1007/s12665-009-0245-8

Prancevic, J., Lamb, M., McArdell, B., Rickli, C., and Kirchner, J. (2020). Decreasing Landslide Erosion on Steeper Slopes in Soil-Mantled Landscapes. Geophysical Research Letters, 47. https://doi.org/10.1029/2020gl087505

Rabby, Y., and Li, Y. (2020). Landslide Susceptibility Mapping Using Integrated Methods: A Case Study in the Chittagong Hilly Areas, Bangladesh. Geosciences. https://doi.org/10.3390/geosciences10120483

Rahman, H., and Khan, Y. A. (1995). Landslides and stability of coastal cliffs of Cox's Bazar area, Bangladesh. Natural hazards, 12(2), 101-118.

Rasyid, A., Bhandary, N., and Yatabe, R. (2016). Performance of frequency ratio and logistic regression model in creating GIS based landslides susceptibility map at Lompobattang Mountain, Indonesia. Geoenvironmental Disasters, 3, 1-16. https://doi.org/10.1186/s40677-016-0053-x

Rudra, A., and Alam, A. (2023). Streamflow characteristics of Sangu-Matamuhuri watershed in the southeastern part of Bangladesh. Heliyon, 9. https://doi.org/10.1016/j.heliyon.2023.e14559

Saaty, T.L. (1977). A Scaling Method for Priorities in Hierarchical Structures. Journal of Mathematical Psychology, 15, 234-281. https://doi.org/10.1016/0022-2496(77)90033-5

Saaty, T. L. (1980). The Analytic Hierarchy Process: Planning, Priority Setting, Resource Allocation. McGraw-Hill.

Saddam, M., Hossain, K., Mollick, P., Salauddin, M., Roy, S., Ahmad, A., Bhowmick, R., and Rony, M. (2025). Shoreline dynamics in response to sea-level changes on the eastern coast of Bangladesh. Environmental Monitoring and Assessment, 197. https://doi.org/10.1007/s10661-025-14375-x

Saleem, N., Huq, M., Twumasi, N., Javed, A., and Sajjad, A. (2019). Parameters Derived from and/or Used with Digital Elevation Models (DEMs) for Landslide Susceptibility Mapping and Landslide Risk Assessment: A Review. ISPRS Int. J. Geo Inf., 8(12), 545. https://doi.org/10.3390/ijgi8120545

Sami, M., Hoque, M., Moniruzzaman, M., and Pradhan, B. (2024). Spatial landslide risk assessment in a highly populated Rohingya refugee settlement area of Cox's Bazar, Bangladesh. Asian Geographer, 42, 79 - 100. https://doi.org/10.1080/10225706.2024.2362638

Skilodimou, H., Bathrellos, G., Koskeridou, E., Soukis, K., and Rozos, D. (2018). Physical and Anthropogenic Factors Related to Landslide Activity in the Northern Peloponnese, Greece. Land, 7(3), 85. https://doi.org/10.3390/land7030085

Suhan, M., and Adhikary, S. (2025). Exploring Climate Change Trends in Temperature and Rainfall across the Southeastern Coastal Area of Bangladesh. Journal of Engineering Science, 15(2), 51-67. https://doi.org/10.3329/jes.v15i2.82162

Sultana, N. (2020). Analysis of landslide-induced fatalities and injuries in Bangladesh: 2000-2018. Cogent Social Sciences, 6. https://doi.org/10.1080/23311886.2020.1737402

Sultana, N., Tan, S., and Hossen, M. (2024). Landslide risk assessment by integrating hazards and vulnerability indices in Southeast Bangladesh. International Journal of Disaster Risk Reduction. https://doi.org/10.1016/j.ijdrr.2024.104991

Tian, H., Gan, J., Jiang, H., Tang, C., Luo, C., Wan, C., Xu, B., Gui, F., Liu, C., and Liu, N. (2020). Failure Mechanism and Kinematics of the Deadly September 28th 2016 Sucun Landslide, Suichang, Zhejiang, China. Advances in Civil Engineering. https://doi.org/10.1155/2020/8828819

Turner, A. (2018). Social and environmental impacts of landslides. Innovative Infrastructure Solutions, 3, 1-25. https://doi.org/10.1007/s41062-018-0175-y

Varnes, D. (1978). SLOPE MOVEMENT TYPES AND PROCESSES. Transportation Research Board Special Report, 11-33.

Wang, Q., and Li, W. (2017). A GIS-based comparative evaluation of analytical hierarchy process and frequency ratio models for landslide susceptibility mapping. Physical Geography, 38, 318 - 337. https://doi.org/10.1080/02723646.2017.1294522

Wubalem, A. (2020). Landslide susceptibility mapping using statistical methods in Uatzau catchment area, northwestern Ethiopia. Geoenvironmental Disasters, 8, 1-21. https://doi.org/10.1186/s40677-020-00170-y

Wubalem, A. (2021). Landslide Inventory, Susceptibility, Hazard and Risk Mapping. Landslide. https://doi.org/10.5772/intechopen.100504

Yang, W. C., Kang, H. S., Ri, G. S., and Kim, J. S. (2022). Consistency improvement method of pairwise matrix based on consistency ratio decreasing rate and attribute weighting method considered decision makers' levels in analytic hierarchy process: application to hip joint prosthesis material selection. Mathematical Problems in Engineering, 2022(1), 1463006. https://doi.org/10.1155/2022/1463006

Research Article DOI: https://doi.org/10.64862/ajeg.2026.301.04.305 Open Access

Fuzzy Overlay-Based Groundwater Quality Assessment for Drinking and Irrigation Purposes, Hydro geochemical Evaluation and Health Risk Assessment in the Coastal Aquifer of Lakshmipur District, Bangladesh

Md. Mahedi Hasan[1*], Khondaker Emamul Haque[1], Shamim Ahmed[2], and Md. Nazmul Islam Hasan[1]

[1]Department of Geology and Mining, University of Rajshahi, Rajshahi 6205, Bangladesh
[2]Institute of Environmental Science, University of Rajshahi ,Rajshahi 6205, Bangladesh

(*Corresponding E-mail: mdmahedihasan107190@gmail.com)

Received: December 18, 2025, Accepted: May 27, 2026

Abstract: In the coastal region of Bangladesh, groundwater is the main source of irrigation and drinking water; however, both natural and anthropogenic processes are progressively threatening groundwater quality. Using hydro geochemical analysis, the Water Quality Index (WQI), GIS-based fuzzy overlay modeling, Principal Component Analysis (PCA), the Na^+/Cl^- ratio, and the Chloro-Alkaline Index (CAI), this study assessed the hydro geochemistry and groundwater quality of the Lakshmipur coastal aquifer. The findings show that a number of groundwater samples were unfit for drinking without treatment because they had levels of arsenic, salinity, total dissolved solids, and some heavy metals that were higher than those allowed by the Department of Environment (DoE) and the World Health Organization (WHO). The Na^+/Cl^- ratios and CAI value further supported the roles of ion exchange, water–rock interaction, and localized saline water influence in groundwater evolution. PCA showed that salinity enrichment, mineralization, and geogenic processes dominate groundwater chemistry. A non-carcinogenic health risk assessment revealed that 70% of samples exceeded the Hazard Index (HI > 1) for adults and 75% for children, indicating significant health threats, particularly from arsenic and iron contamination through oral ingestion. While irrigation appropriateness varied throughout the study area, the WQI and fuzzy overlay analyses revealed a number of places with low water quality for drinking. In addition to highlighting the necessity of ongoing monitoring and sustainable groundwater management to guarantee safe drinking water and agricultural viability, these findings offer an integrated picture of groundwater evolution and quality in the Lakshmipur Coastal Aquifer.

Keywords: ***Hydro geochemistry, Rock-water interaction, Water quality index, Fuzzy overlay, Coastal aquifers.***

Introduction

Groundwater is a vital resource for agriculture, industry, and human use, particularly in areas where surface water is scarce. In recent years, growing population pressure, intensive agricultural methods, urbanization, and industrial expansion have caused serious issues with groundwater supply and quality. Understanding the physicochemical parameters of groundwater is essential for evaluating its quality, identifying potential contamination sources, and ensuring sustainable management. To fully explain the chemical properties and determine the main elements affecting water quality, this study focused on the groundwater quality evaluation of Lakshmipur.

To protect this important resource, it is necessary to study the chemical properties of groundwater. This helps us understand whether the water is safe to use and what factors might be polluting it. This study examined the groundwater in Lakshmipur to determine its quality and understand the natural and human-made factors that affect it. The goal is to use this knowledge to manage groundwater safely and sustainably in the future. According to the United Nations, approximately two-thirds of the world's population may be living in water-stressed conditions by 2025 (United Nations, 2016).

Bhuiyan et al. (2016) conducted a comprehensive study on the assessment of water quality in Lakshmipur district of Bangladesh using water quality indices, geo statistical methods, and multivariate analysis. Their research indicated that groundwater evaluation indices, multivariate statistical techniques, and geo statistical models were applied to assess the source apportionment and spatial variability of groundwater pollutants in the Lakshmipur district of Bangladesh. A total of 60 groundwater samples were collected from wells (shallow to deep wells, i.e., 10–375 m) in the study area. This study has multiple implications for the quality assessment and spatial variability of groundwater as an effort toward more effective water quality management.

Tens of millions of Bangladesh is who consume groundwater contaminated with as are at risk of developing serious health issues. A detailed geochemical study of groundwater was conducted to understand the role of various elements in groundwater aquifers, including all major ions such as Na, K, Ca, Mg,

Zn, Cu, Pb, As, Cd, NO^{3-}, SO_4^{2-}, PO_4^{3-},CO_3^{2-}, HCO_3^{-}, F^{-}, Br^{-}, I^{-}, Cl^{-}, Fe^{2+}, Mn^{2+}, B^{+}, Si^{+}, Al^{3+}, Cu^{2+}, and Cr^{3+}, and how the elemental fluxes are exchanged through atmospheric, terrestrial, and aquatic interactions. Groundwater geochemical studies help identify potential quality changes as development advances (Gupta et al., 2009). Geochemistry is the science that uses the tools and principles of chemistry to explain the mechanisms behind major geological systems, such as the Earth's crust and oceans. This study assessed the chemical characteristics and major influencing factors of water quality in the Lakshmipur area.

Study area

This is a location map (Figure 1) of the Lakshmipur District in southeastern Bangladesh. The district is bordered by the Meghna River to the west and south, which influences its coastal geography. It is geographically positioned between 90°40'E and 91°10'E longitude and 22°45'N and 23°10'N latitude. The region is bounded by Ramganj to the north, Kamalnagar and Ramgati to the south, Roypur to the west, and Meghna River to the southwest.

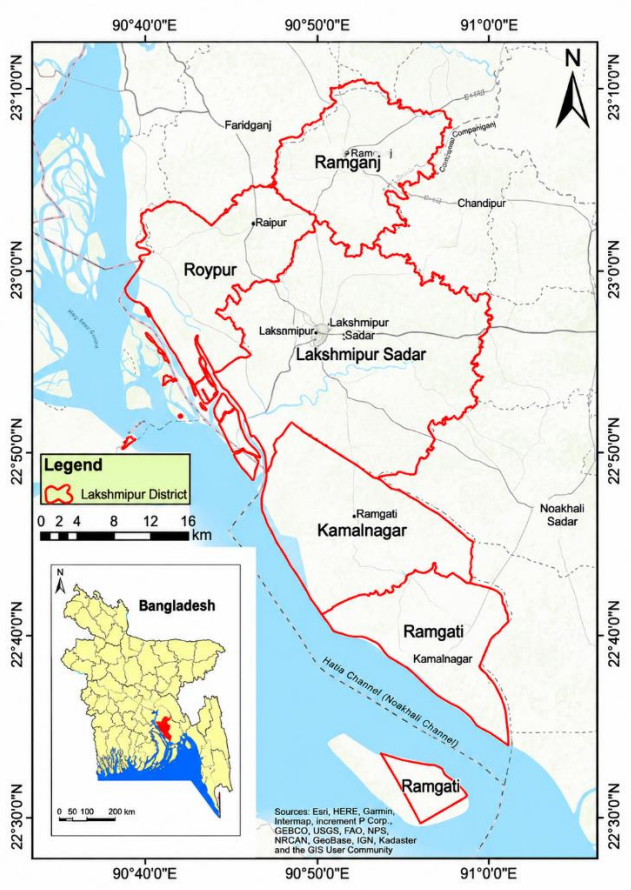


Figure 1, Location map of the study area.

Lakshmipur includes flat alluvial plains formed by sediments deposited by the Meghna River and its tributaries. This makes the region agriculturally fertile and heavily reliant on groundwater for irrigation, domestic use, and small-scale industry. The climate is typically tropical, with high humidity, significant rainfall during the monsoon season, and mild winter.

Methodology

Twenty groundwater (GW) samples were collected in 2021 from the Bangladesh Water Development Board in five Upazilas in the district of Lakshmipur, as depicted in Figure 2. The given chart was used for the research (Figure 3).

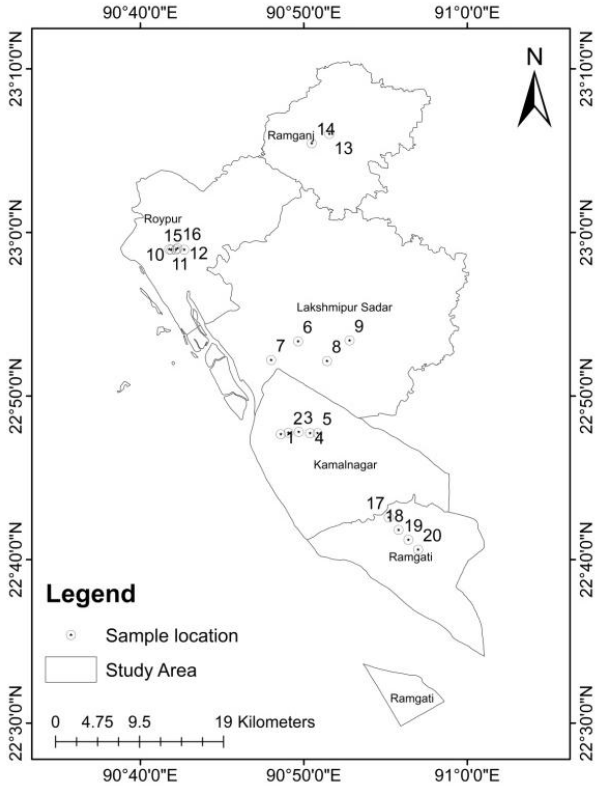


Figure 2, Shows the locations of the groundwater samples.

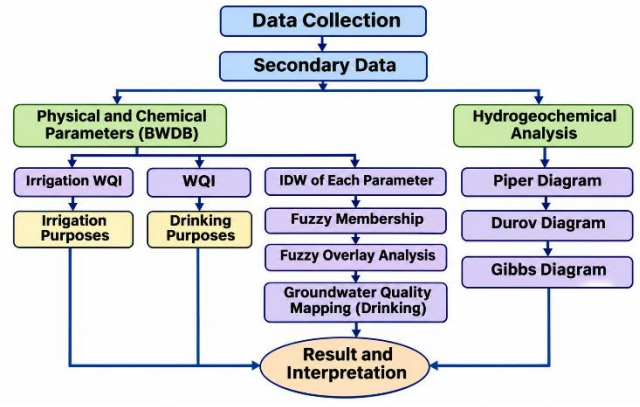


Figure 3, Methodology flow-chart.

WQI for drinking water

The WQI is an effective method for providing exact and comprehensive information about the overall quality of water for human consumption/drinking (Su et al., 2018). This method was first developed from thermodynamics to information systems (Shannon, 2001). The base of the entropy weight method is the volume of information used to calculate the index's weight, which is similar to the main objective of fixed-weight methods (Li et al., 2011). The WQI was measured

using the weighted arithmetic water quality index, which was first proposed by Horton (1965) and improved by Brown et al. (1972). Table 1 presents the Water Quality Index (WQI) classification categories based on the criteria adopted in this study.

The WQI is calculated as Eq. 1.

$$WQI = \frac{\sum_{i=1}^{n} w_i q_i}{\sum_{i=1}^{n} w_i} \qquad (1)$$

Where n is the number of parameters, w_i is the relative weight of the i^{th} parameter, and q_i is the water quality rating of the i^{th} parameter.

Here, the q_i value can be calculated by the following Equation 2 (Brown et al., 1972):

$$q_i = \left(\frac{v_i - v_{id}}{s_i - v_{id}}\right) \times 100 \qquad (2)$$

Where, v_i = Observed value of i^{th} parameter, s_i = Standard permissible limit of i^{th} parameter, v_{id} = Ideal value of i^{th} parameter in pure water.

The unit weight (w_i) of the i^{th} parameters is inversely proportional to the values of the recommended standards (s_i) and it can be calculated as Equation 3:

$$w_i = \frac{K}{S_i} \qquad (3)$$

Where, $K = \frac{1}{\sum_{i=1}^{n} \frac{1}{s_i}}$

Here, K is the constant and S_i is the sstandard permissible limit of i^{th}parameter.

Table 1, Classification categories of WQI (Sahu and Sikdar, 2008; Ketata-Rokbani et al., 2011) are given as follows:

WQI	Category
< 50	Excellent water
50–100	Good water
100–200	Poor water
200–300	Very poor water
> 300	Water unsuitable for drinking

WQI for irrigation

Sodium percentage (Na %)

The percentage of sodium water determines the presence of sodium in water as a soluble form. It is expressed as Na% and measured using the following Equation (4) (Wilcox, 1955):

$$Na\% = \frac{Na^+ + K^+}{Ca^{2+} + Mg^{2+} + Na^+ + K^+} \times 100 \qquad (4)$$

All the concentration are measured in meq/L.

Sodium Absorption Ratio (SAR):

SAR is the most significant parameter for determining the acceptability of groundwater for irrigation purposes. The SAR can be calculated as following Eq. 5 (Richards, 1954).

$$SAR = \frac{Na^+}{\sqrt{\frac{Ca^{2+} + Mg^{2+}}{2}}} \qquad (5)$$

Where all ionic concentrations are expressed in meq/L

Residual Sodium Carbonate (RSC):

The equation for RSC calculation was proposed by Eaton (1950). The Equation 6 is as follows:

$$RSC = (HCO_3^- + CO_3^{2-}) - (Ca^{2+} + Mg^{2+}) \qquad (6)$$

Where all ionic concentrations are expressed in meq/L.

Magnesium Hazard (MH):

MH for irrigation water can be determined with the following Equation 7 (Szabolcs and Darab, 1964):

$$MH = \frac{Mg^{2+}}{Ca^{2+} + Mg^{2+}} \times 100 \qquad (7)$$

Where the concentrations are expressed in meq/L.

Kelly's ratio:

Kelly's ratio is determined by (Eq.8) dividing concentrations of sodium ions by the sum of calcium and magnesium ions (Kelly, 1940).

$$KR = \frac{Na^{2+}}{Ca^{2+} + Mg^{2+}} \qquad (8)$$

Where, concentrations of all ions were expressed in meq/l.

Permeability Index:

The permeability index is calculated by the following Equation 9:

$$PI = \frac{Na^+ + \sqrt{HCO_3^-}}{Ca^{2+} + Mg^{2+} + Na^+} \times 100 \qquad (9)$$

Here, concentrations of all ions were expressed in meq/l.

Total Dissolved Solids (TDS):

TDS is calculated with the following Equation (10):

$$TDS = (\sum Cations) + (\sum Anions) \qquad (10)$$

Where the concentrations are expressed in mg/L.

Statistical and hydro geochemical analyses

Principal Component Analysis, Na/Cl ratio analysis, and the Chloro-Alkaline Index were carried out to improve the understanding of groundwater evolution. Standardized data were used to perform PCA to determine the primary factors influencing groundwater composition. Scree and PCA biplots were used to evaluate the data (Cloutier et al., 2008). The Kaiser criterion (Kaiser, 1960) was used to retain components with eigenvalues greater than 1.0. The relative contributions of silicate weathering, evaporation, and salty water effect were assessed using the Na/Cl molar ratio, while the cation exchange processes between

groundwater and aquifer materials were evaluated using the Chloro-Alkaline Index (CAI).

Na/Cl ratio

To assess the origins of salinity and differentiate between seawater intrusion, mineral weathering, and ion exchange processes, the Na/Cl molar ratio was calculated (Appelo and Postma, 2005) using Equation 11:

$$\mathrm{Na/Cl} = \frac{\mathrm{Na^+}}{\mathrm{Cl^-}} \qquad (11)$$

where Na^+ and Cl^- represent the molar concentrations (meq/L) of sodium and chloride, respectively. Na/Cl >1 generally indicates silicate weathering or cation exchange, whereas Na/Cl <1 suggests chloride enrichment due to evaporation or saline water influence (Appelo and Postma, 2005).

Chloro Alkaline Index (CAI)

It is crucial to understand how the chemical composition of groundwater and subsurface flow channels varies over time (Jamal et al., 2024). To comprehend how the chemical composition of groundwater varies depending on its flow, chloro alkaline indicators were examined (Schoeller, 1977). To understand the ion exchange mechanisms between shallow aquifers and their surrounding environment, he proposed using the chloro-alkaline indices (Equation12):

$$\mathrm{CAI} = \frac{\mathrm{Cl-(Na+K)}}{\mathrm{Cl}} \qquad (12)$$

Where all ionic concentrations are expressed in meq/L. Positive CAI values indicate reverse ion exchange, whereas negative values indicate direct ion exchange between groundwater and aquifer materials.

Health risk assessment

An essential part of a thorough groundwater investigation is the evaluation of health concerns. Specifically, evaluating the possible impacts on human health is a crucial way to find harmful consequences in both adults and children (Takeya et al., 2025). Standard equations for calculating the overall health risk indices were suggested by USEPA (2021). The potential health risks associated with both ingestion and cutaneous exposure were estimated in this study using the United States Environmental Protection Agency (USEPA, 1989), which has been widely utilized in hydro-environmental risk assessments. The chronic daily intake through ingestion (CDI_{oral}) and dermal absorption (CDI_{dermal}) was determined using the following Equation (13),(14):

$$CDI_{oral} = (CW \times IR \times EF \times ED) / (BW \times AT) \qquad (13)$$

$$CDI_{dermal} = (CW \times SA \times ED \times EF \times ET \times CF \times KP \times 10\text{-}3)/(BW \times AT) \qquad (14)$$

The exposure parameters used in the human health risk assessment for adults and children are summarized in Table 2. The accepted values, which were based on established risk assessment standards, were used to determine both carcinogenic and non-carcinogenic health dangers. USEPA (1989) provided all of the parameters. According to NCR, the hazard quotient (HQ) assesses non-carcinogenic risk (USEPA, 1989). The total potential for non-carcinogenic consequences resulting from exposure to various pollutants is shown by the hazard index, which is calculated by adding the HQs. Equation 15 used to calculate HQ:

$$HQ = CDI / RfD \qquad (15)$$

Table 2, Exposure parameters used for human health risk assessment

Parameter	Description	Adult	Child	Unit
CW	Concentration of contaminants in groundwater	Measured value	Measured value	µg/L
IR	Ingestion rate	2.2	1.0	L/day
EF	Exposure frequency	365	365	days/year
ED (NCR)	Exposure duration (non-carcinogenic risk)	70	10	years
ED (CR)	Exposure duration (Carcinogenic risk)	70	70	years
BW	Body weight	70	25	kg
AT (NCR)	Averaging time (non-carcinogenic risk)	25,550	3,650	days
AT (CR)	Averaging time (Carcinogenic risk)	25,550	25,550	days
SA	Exposed skin surface area	18,000	6,600	cm^2
Kp	Skin permeability coefficient	0.001	0.001	cm/h
CF	Conversion factor	0.001	0.001	L/cm^3

The maximum acceptable level of exposure to an element through oral or dermal routes is indicated by the reference dose (RfD). The hazard index (HI), which is computed as the sum of all individual hazard quotients (HQs) and is determined by Equation 16, was used to evaluate the cumulative non-carcinogenic risk from these elements.

$$HI = HQ_1 + HQ_2 + HQ_3 + \ldots\ldots\ldots + HQ_n \qquad (16)$$

Human health is considered to be safeguarded when both HQ and HI levels are less than 1. When the hazard index (HI) is greater than 1, residents are at risk of non-carcinogenic health effects. Trace metals including as, Cr, Ni, and Pb may also increase the risk of cancer in addition to these non-carcinogenic problems. The carcinogenic risks related to skin contact and oral ingestion are calculated using the following Equation 17, 18:

$$CR_{oral} = CDI_{oral} \times SF_{oral} \quad (17)$$

$$CR_{dermal} = CDI_{dermal} \times SF_{dermal} \quad (18)$$

$$CR = CR_{oral} + CR_{dermal} \quad (19)$$

The term "carcinogenic risk" (CR) in Equation 19. According to USEPA, the acceptable limit for CR is 1.0×10-4. The slope factor (SF), expressed in $(mg/kg/day)^{-1}$, indicates the degree of a carcinogenic contamination. The related dermal slope factors (SF_{dermal}) are 3.66, 20, and 42 for as, Cr, Ni, and Pb, whereas the corresponding oral slope factors (SF_{oral}) are 1.50, 0.5, 1.7, and 0.0085. Five. CR readings above this cutoff point suggest a lifelong cancer risk for the affected group.

Water quality index development using fuzzy-GIS

It is challenging to make accurate estimations because the evaluation of the earth system is prone to ambiguity and uncertainty (Jha et al., 2020). In these situations, the researcher and other interested parties could employ Fuzzy Operation (FO) to convince people that human knowledge and expertise are sufficient for the accurate evaluation of the natural system (Zadeh, 1965). The Inverse Distance Weighting (IDW) interpolation technique in ArcGIS 10.8 was used to create spatial distribution maps of the water quality metrics. IDW is a deterministic interpolation method that uses the weighted influence of adjacent observations to estimate values at unsampled locations, with closer sampling points having a greater impact than those farther away. This approach was chosen because of its ease of use, computational effectiveness, and applicability for spatial interpolation of water quality parameters from a comparatively small number of sampling locations. However, prediction uncertainty may increase in regions with reduced sample density, similar to other deterministic interpolation techniques, and the interpolated maps should be interpreted appropriately.

Fuzzification of water quality parameter

It is challenging to make accurate estimations because the evaluation of the earth system is prone to ambiguity and uncertainty (Jha et al., 2020). In these situations, the researcher and other interested parties could employ Fuzzy Operation (FO) to convince people that human knowledge and expertise are sufficient for the accurate evaluation of the natural system (Zadeh, 1965). The Inverse Distance Weighting (IDW) interpolation technique in ArcGIS 10.8 was used to create spatial distribution maps of the water quality metrics. IDW is a deterministic interpolation method that uses the weighted influence of adjacent observations to estimate values at unsampled locations, with closer sampling points having a greater impact than those farther away. This approach was chosen because of its ease of use, computational effectiveness, and applicability for spatial interpolation of water quality parameters from a comparatively small number of sampling locations. However, prediction uncertainty may increase in regions with reduced sample density, similar to other deterministic interpolation techniques, and the interpolated maps should be interpreted appropriately.

Fuzzy overlay and fuzzy-GIS based water quality index map:

Every raster that was fuzzified was superimposed using fuzzy overlay techniques. Fuzzy AND, fuzzy OR, fuzzy SUM, fuzzy PRODUCT, and fuzzy GAMMA are the five fuzzy overlay choices accessible in ArcGIS. Using the fuzzy AND overlay function, the fuzzy raster returns the minimum value of the sets contained. When all input conditions are met, the least common denominator is determined using this method. The fuzzy OR overlay function returns the largest value of the sets in the fuzzified raster, in contrast to the fuzzy AND overlay function. For any input criterion, this is helpful in determining the highest membership values (Tiwari et al., 2023). A fuzzy overlay operation was used to identify the strictly suitable water quality zones in the study area.

Validation of the fuzzy-GIS groundwater quality map

The anticipated and actual WQI classes at 20 sampling locations were compared in order to validate the fuzzy-GIS groundwater quality map. To assess the categorization performance, a confusion matrix was created. The agreement between the observed and predicted groundwater quality classes was evaluated using Cohen's Kappa coefficient (κ) and Overall Accuracy (OA) (Wan et al., 2015).

The validation results give a clear measure of how reliable and accurate the fuzzy GIS map is in predicting groundwater quality. Comparing the actual results with the expected water quality index categories helped determine how well the different groundwater quality groups matched each other. The confusion matrix shows how well different sampling locations were correctly identified, while the Overall Accuracy (OA) tells us the general percentage of all samples that were correctly classified. Cohen's kappa coefficient (κ) shows how much agreement there is between the actual classifications and the predicted ones, taking into account the agreement that might happen just by chance. When OA and κ are higher, it means the classification is better and there is more agreement between the predicted groundwater quality map and the actual water quality index measurements. So, these validation metrics helped figure out how well and how

dependable the fuzzy-GIS method was for classifying groundwater quality in the study area.

Results and discussion

Physico-chemical assessment of groundwater

Results of physical parameters

The physical properties of groundwater in the research area indicate low water quality. Although the measured pH ranged from 5.5 to 7.2, indicating slightly acidic to nearly neutral conditions, several samples fell below the WHO-recommended range (6.5–8.5), rendering the water unsafe for drinking and agriculture. The usual shallow aquifer conditions are reflected in the groundwater temperature range of 25.8–29.4 °C. Elevated ionic concentrations were indicated by electrical conductivity (EC) values between 516 and 2130 µS/cm, with many samples surpassing the WHO limit of 1000 µS/cm.

Hem's (1970) categorization and WHO recommendations state that most samples with total dissolved solids (TDS) between 331 and 13,320 mg/L are unfit for irrigation or drinking. The WHO limit of 5 NTU was significantly exceeded by turbidity values (4.7–271 NTU), suggesting a high load of suspended particles and the need for treatment before home use. The extremely low dissolved oxygen (DO) content (0.044–1.03 mg/L), which may imply lowering circumstances linked with elevated levels of iron, manganese, or arsenic, further restricts drinking acceptability. Salinity ranges from 0.21 to 12.18 ppt, and higher values significantly exceed the allowable limits for drinking and irrigation, endangering both agricultural productivity and human health. As further shown by the regional distribution maps (Figure 4), the evaluation of field-based physical factors indicates that groundwater in the research area is typically unsuitable for residential, drinking, and irrigation use.

The overall physical parameters indicate high spatial variability of groundwater quality in the study area. High EC, TDS, turbidity, salinity and low DO together indicate significant hydrochemical stress on the aquifer system. These conditions may restrict the use of groundwater for drinking and irrigation purposes without proper treatment. Therefore, ongoing surveillance and proper water management practices are necessary to mitigate the potential risks to human health and agricultural productivity.

Results of chemical parameters

The principal ions and trace elements in the groundwater of the studied area exhibited a general deterioration in water quality and were indicative of complex anthropogenic and geogenic processes. Among the trace metals with high quantities that present serious health risks are iron (0.14–14.3 mg/L), manganese (0.07–3.09 mg/L), and arsenic (0–0.161mg/L), particularly when aquifer conditions deteriorate. Overall, the hydro chemical composition and spatial distribution patterns (Figure 5) demonstrate that groundwater in the study area is largely unsuitable for drinking and irrigation without appropriate treatment.

Comparison with drinking water quality standards

Water quality is widely above allowable limits throughout the research region when compared to WHO (2011) and DoE (2016) drinking water regulations. High hardness and salinity are indicated by increasing concentrations of major ions such calcium, magnesium, sodium, and potassium in a considerable number of samples (Table 3).

Arsenic, iron, manganese, and aluminum are among the trace and dangerous elements that, in the majority of samples, surpass both WHO (2011) and DoE (2016) criteria, raising grave implications for public health. Arsenic and Iron concentrations are far above permissible limits exceeding in all (16) samples. pH, electrical conductivity, total dissolved solids, and turbidity are examples of physical characteristics that routinely surpass recommended values, especially EC, TDS, and turbidity. Chloride and Salinity values are slightly above standard limits in some cases. Rather than direct human inputs, natural geochemical processes are probably in charge of the high arsenic contents found in several groundwater samples. Arsenic is frequently mobilized in coastal aquifers by the reductive breakdown of iron oxyhydroxides in reducing circumstances, which releases adsorbed arsenic into groundwater.

Furthermore, prolonged water-rock contact and competitive desorption by phosphate ions may increase arsenic mobility. The current study's finding of a correlation between iron and arsenic concentrations lends credence to iron mineral dissolution as a possible mechanism regulating arsenic release in the aquifer. Bangladesh’s sedimentary aquifers have significantly higher trace-element concentrations than crystalline basement aquifers (Ahmed et al., 2004; Bhattacharya et al., 2002; Nwankwo et al., 2020).

Elevated levels of arsenic, iron, manganese, aluminum, salinity, EC, and TDS all point to the necessity of routine groundwater monitoring and efficient water-treatment techniques. These findings highlight how crucial it is to find safe substitute water sources, especially for areas who rely significantly on groundwater for household and drinking needs.

Water Quality Index (WQI)

WQI readings and associated water quality status for groundwater samples taken from various sites in Bangladesh's Lakhsmipur district are displayed in Table 4. The study area's WQI values, which vary greatly throughout the district, range from 63.51 to 1922.51.

Table 3, Comparison of the groundwater quality in the study area with WHO, DoE standards.

Parameters	Units	WHO standards (2011)	DoE Standard (2016)	Concentration in the study area		Number of samples Exceeding	
				Max.	Min.	WHO	DoE
Calcium	mg/L	200	75	858.9	24.4	7	14
Magnesium	mg/L	150	35	362.5	23.0	5	18
Sodium	mg/L	200	200	2149.9	48.1	13	13
Potassium	mg/L	1.2	12	157.2	8.1	20	20
Arsenic	µg/mL	0.01	0.005	0.2	0	16	16
Iron	mg/L	0.3	0.3-1	14.3	0.1	16	16
Manganese	mg/L	0.4	0.1	3.1	0.07	6	18
Aluminium	mg/L	0.2	0.2	0.98	0.02	16	16
Chloride	mg/L	500	600	5900	135	13	13
Salinity	ppt	-	1	12.2	0.2	0	12
P^H		6.5-9.2	6.5-8.5	7.2	5.4	12	12
Temperature	°C	25	20-30	29.5	25.8	20	20
EC	µs/cm	1400	-	20200	509	14	0
TDS	mg/L	1500	1000	13260	326	13	14
Turbidity	NTU	5	10	273	4.1	19	14

The majority of the samples are classified as "unsuitable" by WQI, indicating significant deterioration of water quality in numerous areas. Samples with exceptionally high WQI values, such as Roypur (GQHS51580010), where the WQI is 1922.508, Roypur (GQHS5158004), where the WQI is 1252.774, and others, indicate that these water sources are highly contaminated and unfit for human consumption.

A small number of groundwater samples, meanwhile, exhibit somewhat higher quality. Sample GQHS5158002 (Roypur), for example, has a WQI score of 63.51, which is in the "Good" category and indicates that the drinking water quality is adequate there. In a similar vein, samples GQHS5133005 from Kamalnagar and GQHS5158001 from Ramganj are classified as "Good" and "Poor," respectively.

These results imply that although the majority of the Lakhsmipur district's groundwater is extremely unfit for human consumption, there are a few isolated areas with comparatively higher water quality.

The district-wide spatial variance in WQI indicates localized sources of contamination, which could be brought on by anthropogenic activity, inadequate sanitation, geogenic causes, and agricultural runoff. The findings show that in order to increase groundwater safety in the area, routine monitoring and focused mitigation measures are desperately needed.

Irrigation water quality

Groundwater's appropriateness for irrigation is important because of the impact that water's mineral components have on soil and plants. Since this mineral component (impurities) of water can affect osmotic pressures and produce metabolic reactions due to toxic elements, they can also impact on plant growth. Additionally, they might alter the permeability, aeration and structure of the soil.

Sodium percentage (Na%)

The Na% of the groundwater of the study area ranges from 31.71 to 88.12 (Table 11), which concluded that the groundwater is “Permissible” to the maximum station and “Unsuitable” (Table 5) in two sample. Most samples fall in the “Permissible” and “Doubtful” categories suggesting moderate to high sodium hazards for irrigation. The two “Unsuitable” samples show high sodium hazard and should not be used for irrigation without appropriate management.

Table 4, WQI values with pre-determined categories.

Sample ID	Location	WQI	Water quality Status
GQHS5133001	Kamalnagar	330.9	unsuitable
GQHS5133002	Kamalnagar	310.3	unsuitable
GQHS5133003	Kamalnagar	298.3	Very poor
GQHS5133004	Kamalnagar	275.6	Very poor
GQHS5133005	Kamalnagar	78.5	Good
GQHS5143001	Lakshmipur Sadar	581.8	unsuitable
GQHS5143002	Lakshmipur Sadar	670.9	unsuitable
GQHS5143003	Lakshmipur Sadar	704.1	unsuitable
GQHS5143004	Lakshmipur Sadar	864.7	unsuitable
GQHS5158001	Ramganj	122.1	poor
GQHS5158002	Ramganj	63.5	Good
GQHS5158003	Raipur	449	unsuitable
GQHS5158004	Raipur	1252.8	unsuitable
GQHS5158005	Raipur	538	unsuitable
GQHS5158007	Raipur	651.1	unsuitable
GQHS5158010	Raipur	1922	unsuitable
GQHS5165001	Ramgati	338.8	unsuitable
GQHS5165002	Ramgati	210.9	Very poor
GQHS5165003	Ramgati	313.8	unsuitable
GQHS5165004	Ramgati	428.9	unsuitable

Sodium percentage (Na%)

The Na% of the groundwater of the study area ranges from 31.71 to 88.12 (Table 11), which concluded that the groundwater is "Permissible" to the maximum station and "Unsuitable" (Table 5) in two sample. Most samples fall in the "Permissible" and "Doubtful" categories suggesting moderate to high sodium hazards for irrigation. The two "Unsuitable" samples show high sodium hazard and should not be used for irrigation without appropriate management.

Table 5, Classification of Sodium Percentage for Groundwater (Deshmukh and Pawar, 2001)

Water Class	Na%	Number of Samples
Excellent	<20	Nil
Good	20-40	4
Permissible	40-60	9
Doubtful	60-80	5
Unsuitable	>80	2

Sodium Absorption Ration (SAR)

The SAR values in the groundwater of the study area ranges from 1.33 to 28.5. In dry season (Table 11), which stands the groundwater is "Excellent" to "Good" for irrigation and GQHS5133003 station is "Bad" for irrigation. The quality of the Groundwater for irrigation purpose depends upon SAR (Raghunath, 1987) is given below (Table 6).

Table 6, Classification of groundwater depending upon SAR.

Water Class	SAR	Number of Samples
Excellent	<10	11
Good	10-18	8
Medium	18-26	Nil
Bad	>26	1

Residual Sodium Carbonate (RSC)

The RSC values in the groundwater of the study area ranges from (-10.12 to 48.70) meq/L (Table 11), which stands the groundwater is "Good" for irrigation and Nine samples is "Unsuitable" for irrigation (Table 7)

Table 7, Residual Sodium Carbonate (RSC) classification of the groundwater samples in the study area according to Eaton, 1950.

Water Class	RSC (meq/L)	Number of Samples
Good	<1.25	11
Doubtful	1.25-2.5	Nil
Unsuitable	>2.5	9

Magnesium Hazard (MH)

The MH values in the groundwater of the study area ranges from (23.61 to 75.46) % (Table 11), which stands most of the groundwater sample is "Suitable for irrigation" and Seven samples is "Unsuitable for irrigation" (Table 8).

Table 8, Magnesium hazard classification of the groundwater samples in the study area according to Szabolcs and Darab (1964).

Water Class	MH%	Number of Samples
Suitable for Irrigation	<50	13
Unsuitable for Irrigation	>50	7

Kelly's Ratio (KR)

The KR values in the groundwater of the study area ranges from (0.42 to 7.19) (Table 11), which stands most of the groundwater sample is "Unsuitable" for irrigation and nine samples is "suitable" for irrigation (Table 9).

Table 9, Kelly's Ratio (KR) classification of the groundwater samples in the study area according to Kelly, 1940.

Water Class	KR	Number of Samples
Suitable	<1	9
Unsuitable	>1	11

Permeability Index (PI)

The PI values in the groundwater of the study area ranges from (42 to 89.8) (Table 11), which stands most

of the groundwater sample is “Good” for irrigation and two samples is “Excellent” for irrigation (Table 10).

Table 10, Permeability index (PI) classification of the groundwater samples in the study area according to (Raghunath, 1987).

Water Class	PI	Number of Samples
Unsuitable	<25	Nil
Good	25-75	18
Excellent	>75	2

The evaluation of irrigation water quality has significant effects on the sustainability of agriculture in the research region. Reduced soil permeability, deterioration of soil structure, and limited water infiltration might occur from groundwater with high salinity and poor irrigation indices gradually raising soil salinity and sodicity. These modifications may restrict the availability of nutrients, hinder the uptake of water by plants, and eventually lower crop output. Therefore, continuous use of low-quality groundwater for irrigation may hasten soil degradation and jeopardize long-term agricultural sustainability, especially in Bangladesh's coastal agricultural districts. To reduce these negative effects and maintain agricultural output, appropriate irrigation management techniques, regular soil monitoring, and the concurrent use of alternate water sources are advised.

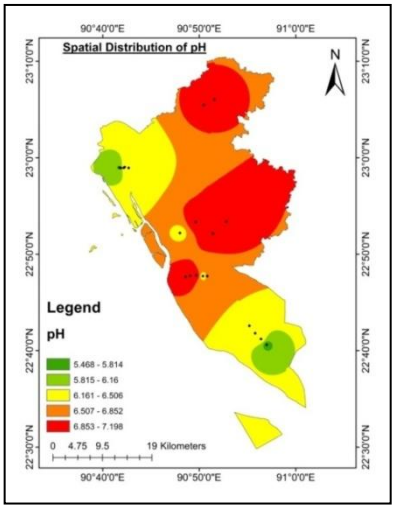
Fuzzy-GIS based groundwater quality index mapping

As stated in the methodology section, the coefficient of correlation approach was used to determine the optimal fuzzy overlay technique for creating the Fuzzy-GIS based Groundwater Quality Index (FGWQI) map.

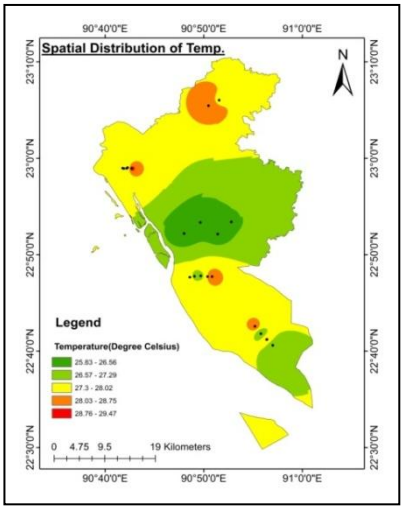
The most successful technique for this was the Fuzzy-AND overlay method. Each technique's fuzzy membership maps are shown in Figure 6. The FGWQI map of the study area is shown in Figure 7.

Table 11, Statistical results of groundwater for irrigation purposes.

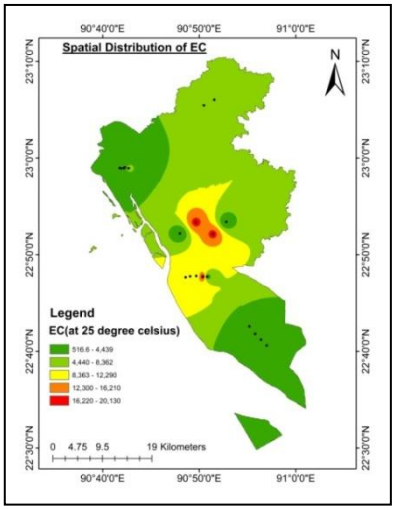
Sample ID	SAR	MH	RSC (meq/L)	Na%	PI	KR
GQHS5133001	10.1	52.4	-3.1	50.4	49.9	0.9
GQHS5133002	10.2	41.0	-10.1	47.2	47.1	0.9
GQHS5133003	28.5	67.8	48.7	88.1	89.8	7.2
GQHS5133004	16.4	37.7	28.3	59.8	59.8	1.4
GQHS5133005	2	66.7	-3.8	34.9	51.2	0.5
GQHS5143001	17.4	38.4	35.7	62.4	62.5	1.6
GQHS5143002	1.3	75.5	-2.9	32.7	51.1	0.4
GQHS5143003	12.7	38.1	10.7	54.7	55.3	1.2
GQHS5143004	2.7	70.3	-1.5	46.0	64.5	0.7
GQHS5158001	2.6	46.6	-1.0	45.7	66.1	0.8
GQHS5158002	2.3	48.2	-0.6	47.0	73.9	0.8
GQHS5158003	12.7	28.0	20.2	68.7	68.9	2.1
GQHS5158004	11.1	23.6	14.7	62.7	65.1	1.6
GQHS5158005	17.3	53.6	28.0	80.3	86.6	4
GQHS5158007	2.3	33.5	-7.7	31.7	42.0	0.4
GQHS5158010	8.5	30.7	8	60.4	65.8	1.5
GQHS5165001	4.6	50.7	1.1	53.8	54.9	1.1
GQHS5165002	6.0	45.7	3.8	60.1	65.5	1.4
GQHS5165003	4.4	48.4	0.5	52.4	61.7	1.1
GQHS5165004	1.9	41.7	-3.9	35.0	48	0.5
Maximum	**28.5**	**75.5**	**48.7**	**88.1**	**89.8**	**7.2**
Minimum	**1.3**	**23.6**	**-10.1**	**31.7**	**42.0**	**0.4**
Average	**8.75**	**46.93**	**8.2**	**53.7**	**61.5**	**1.5**
Standard Deviation	**7.02**	**14.0**	**15.6**	**16.0**	**12.1**	**1.52**



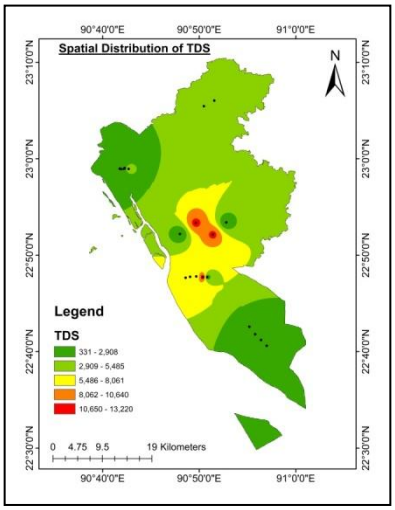
a)



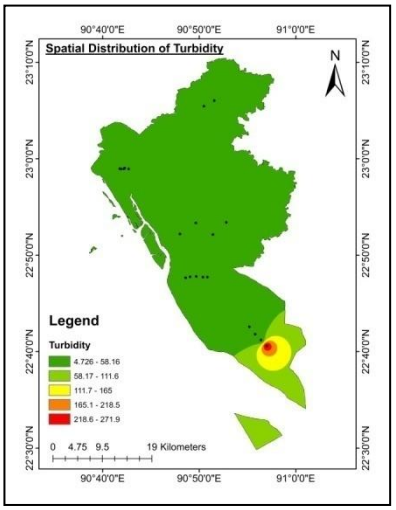
b)



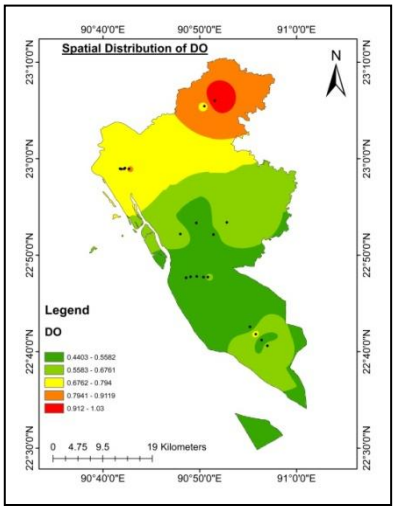
c)



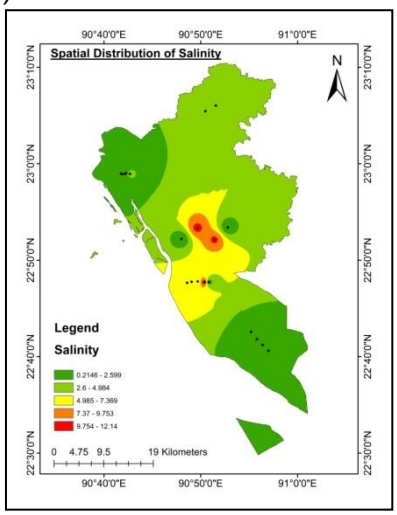
d)



e)

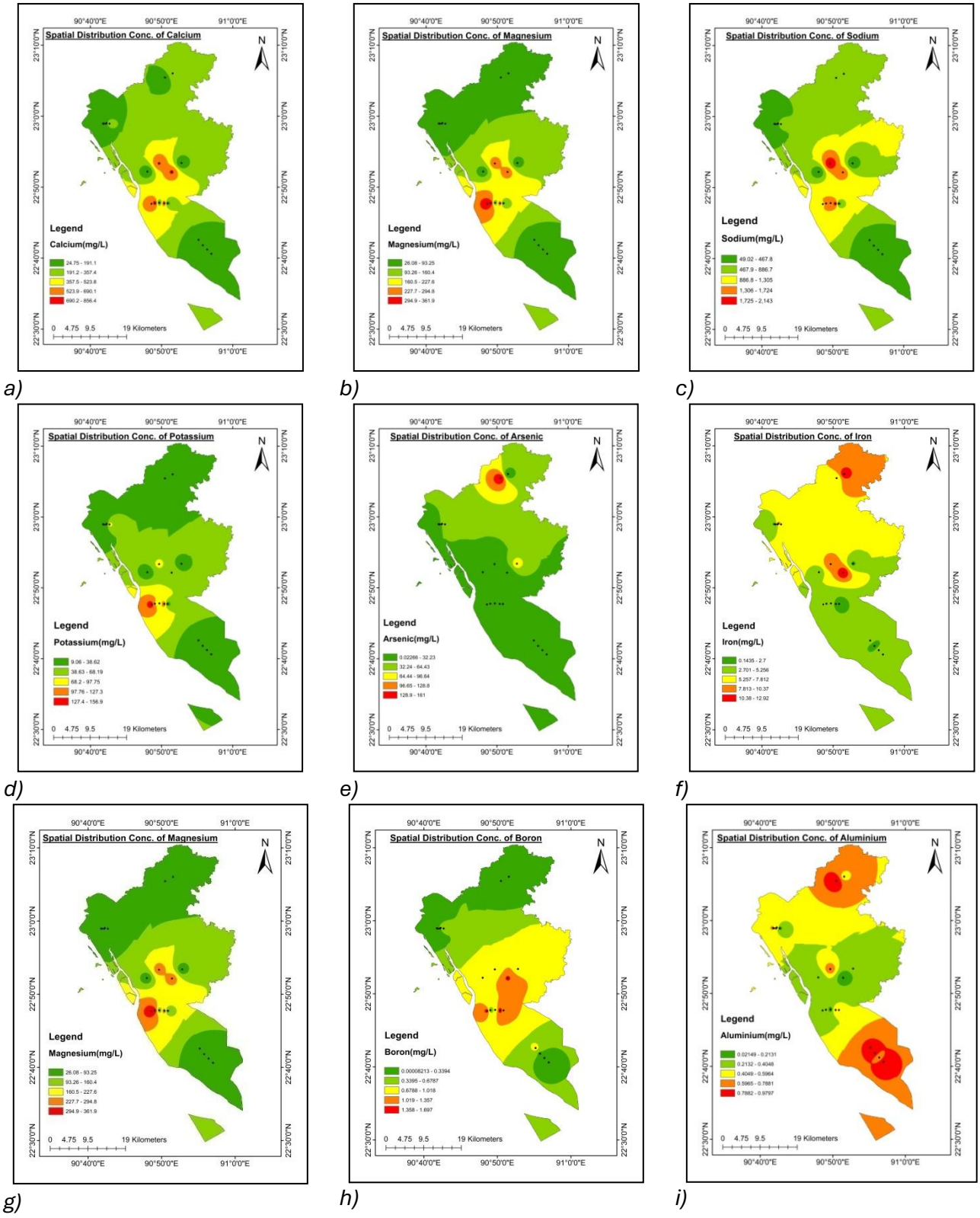


f)



g)

Figure 4, Spatial distribution map of (a) pH (b) Temperature (°C) (c) EC (µS/cm) (d) TDS (mg/L) (e) Turbidity (NTU) (f) DO (mg/L) (g) Salinity (ppt).

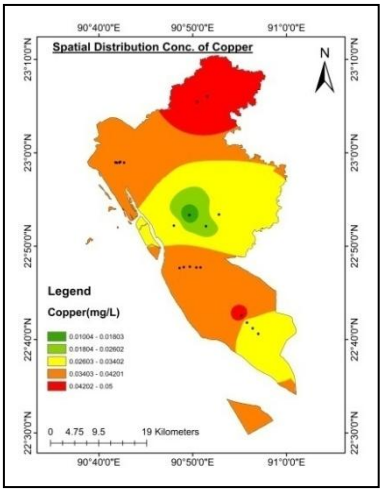


a) b) c)

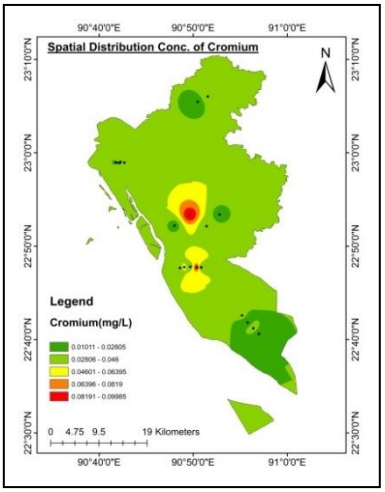
d) e) f)

g) h) i)

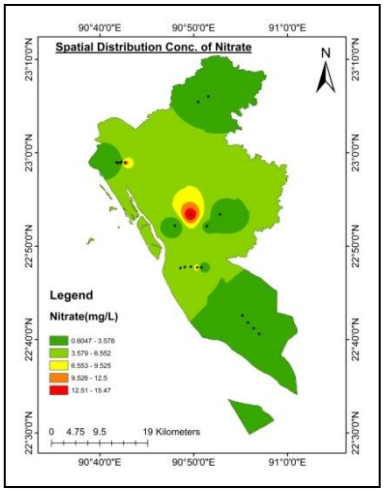
Figure 5, Spatial distribution map of (a) Calcium (mg/L) (b) Magnesium (mg/L) (c) Sodium(mg/L) (d) Potassium (mg/L) (e) Arsenic (µg/L) (f) Iron (mg/L) (g) Manganese (mg/L) (h) Boron (mg/L) (i) Aluminum(mg/L).



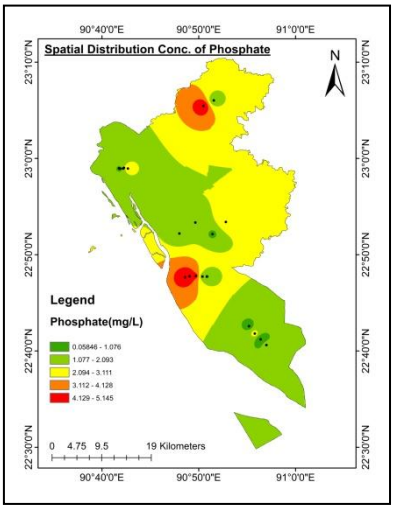
j)



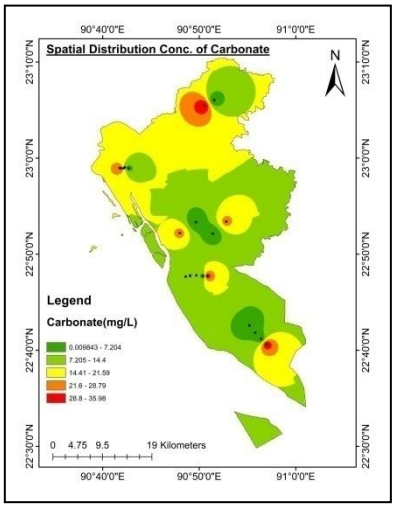
k)



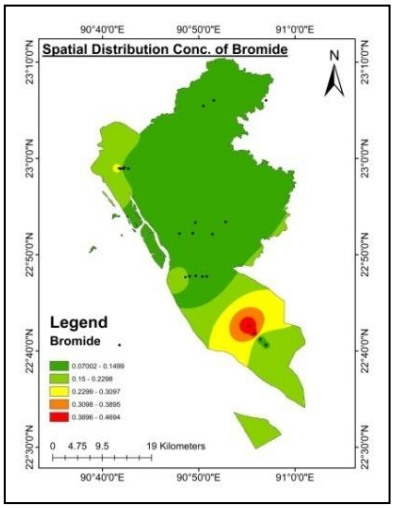
l)



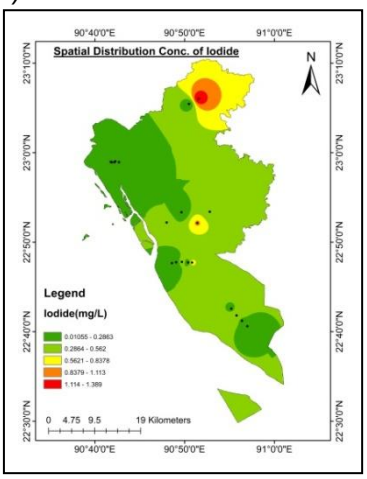
m)



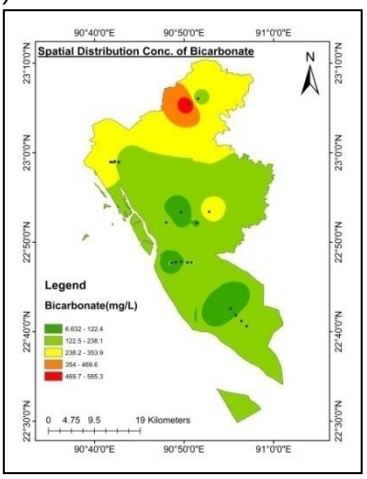
n)



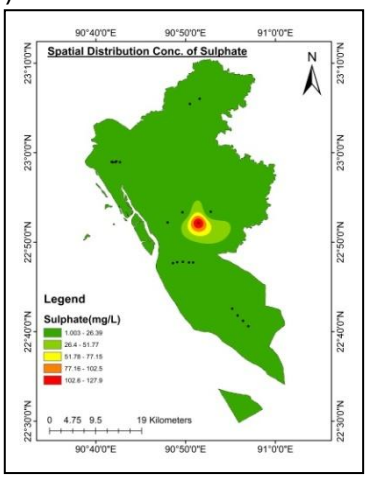
o)



p)



q)



r)

Figure 5 contd., Spatial distribution map of (j) Copper (mg/L) (k) Chromium (mg/L) (l) Nitrate (mg/L) (m) Phosphate (mg/L) (n) Carbonate (mg/L) (o) Bromide (mg/L) (p) Iodide (mg/L) (q) Bicarbonate (mg/L) (r) Sulphate (mg/L).

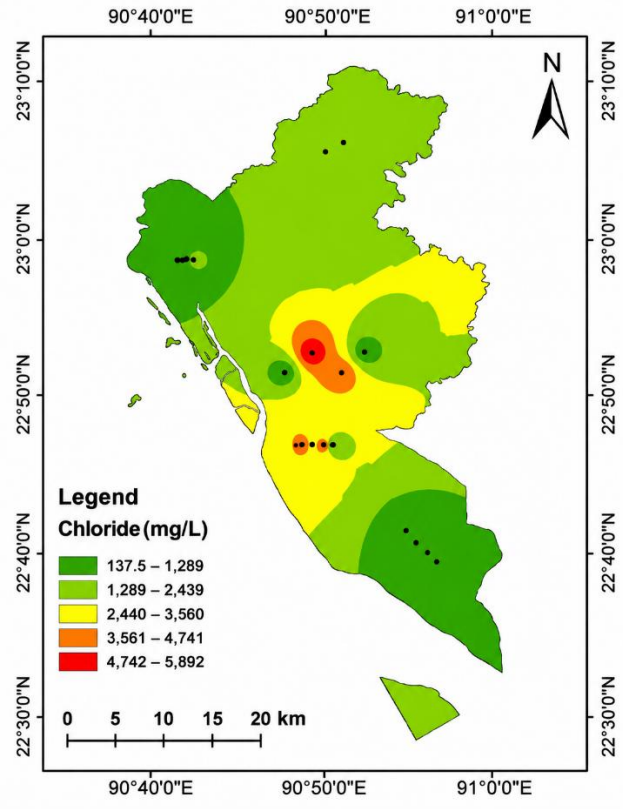


Figure 5 contd., Spatial distribution map of (s) Chloride(mg/L).

The research area's southern and western regions, which are closer to the Meghna estuary and more vulnerable to the effects of saline water, are where the highest concentrations of EC, TDS, salinity, Na^+, and Cl^- are found, according to the geographical distribution maps. While localized NO_3^- and PO_4^{3-} enrichment may be a result of domestic inputs and agricultural activity, higher Fe and as concentrations are probably linked to geogenic release from alluvial sediments under decreasing aquifer conditions. These geographical differences show that the combined effects of regional geology, coastal processes, and land-use practices regulate water quality.

Groundwater quality index mapping

Water Quality Map by Fuzzy Overlay represents the spatial variation in water quality across different upazilas (sub-districts) of the Lakshmipur district in Bangladesh (Figure7). The map uses a fuzzy overlay analysis, a GIS-based technique for integrating multiple water quality parameters to assess overall quality levels. The analysis categorizes water quality into five classes: Very Poor, Poor, Moderate, High, and Very High, each indicated by a specific color ranging from red (very poor) to bright green (very high).

The majority of the red-marked (Very Poor, 0–0.00357) areas are located in the district's western (Roypur) and southern (Ramgati) regions. These areas show serious problems with water quality, which could be brought on by pollution, saline intrusion, or heavy metal contamination. Water quality conditions in the orange zones (Poor, 0.00358 – 0.00912), which include portions of Ramganj and Kamalnagar, are marginally better but still cause for worry.

Particularly in central Lakshmipur Sadar and portions of Kamalnagar, yellow (Moderate, 0.00913 – 0.0129) and light green (High, 0.013 – 0.0159) areas indicate intermediate water quality, which is neither optimal nor significantly deteriorated. These areas can be undergoing mild anthropogenic influences or seasonal variations. Bright green (Very High, 0.016 – 0.0202), which is mostly seen in the central and northeastern zones, indicates the best water quality and is thought to be comparatively unpolluted and safe water resources.

Graphical representation of chemical analysis

Graphical representation of chemical analysis is very effective to understand the result of analysis and to provide means for comparing the analysis with each other, or to emphasize differences and similarities. To make the interpretation and description of the water quality variation and geochemical character of groundwater the results of chemical analysis of ground samples are represented in various graphical forms-

Piper diagram

For crucial investigations into the origins of the dissolved elements in water, the Piper Trilinear Diagram (Piper, 1944) is a useful tool for sorting hydro chemical analysis results. For critical investigations concerning the sources of dissolved constituents (major cations, Ca, Mg, Na, K and major anions, HCO_3^{2-}, Cl^-, SO_4^{2-}) in waters, changes in the character of water as it moves through an area, and associated geochemical issues, it is a useful tool for separating hydro-chemical analysis data. The areas make up the trilinear diagram's central plotting field (diamond shape), and water is categorized into nine types based on which area the analysis results fall into. The alkali cations (Na and K) are referred to as primary constituents, while the alkaline earth cations (Ca^{2+} and Mg^{2+}) are referred to as secondary constituents. $CO_3^{2-}$and HCO_3^{2-} are regarded as weak anions, while the strong anions (SO_4^{2-}, Cl^-) are regarded as saline components. The chemical makeup of water is determined by the approximate balance of these cations and anions (Figure 8).

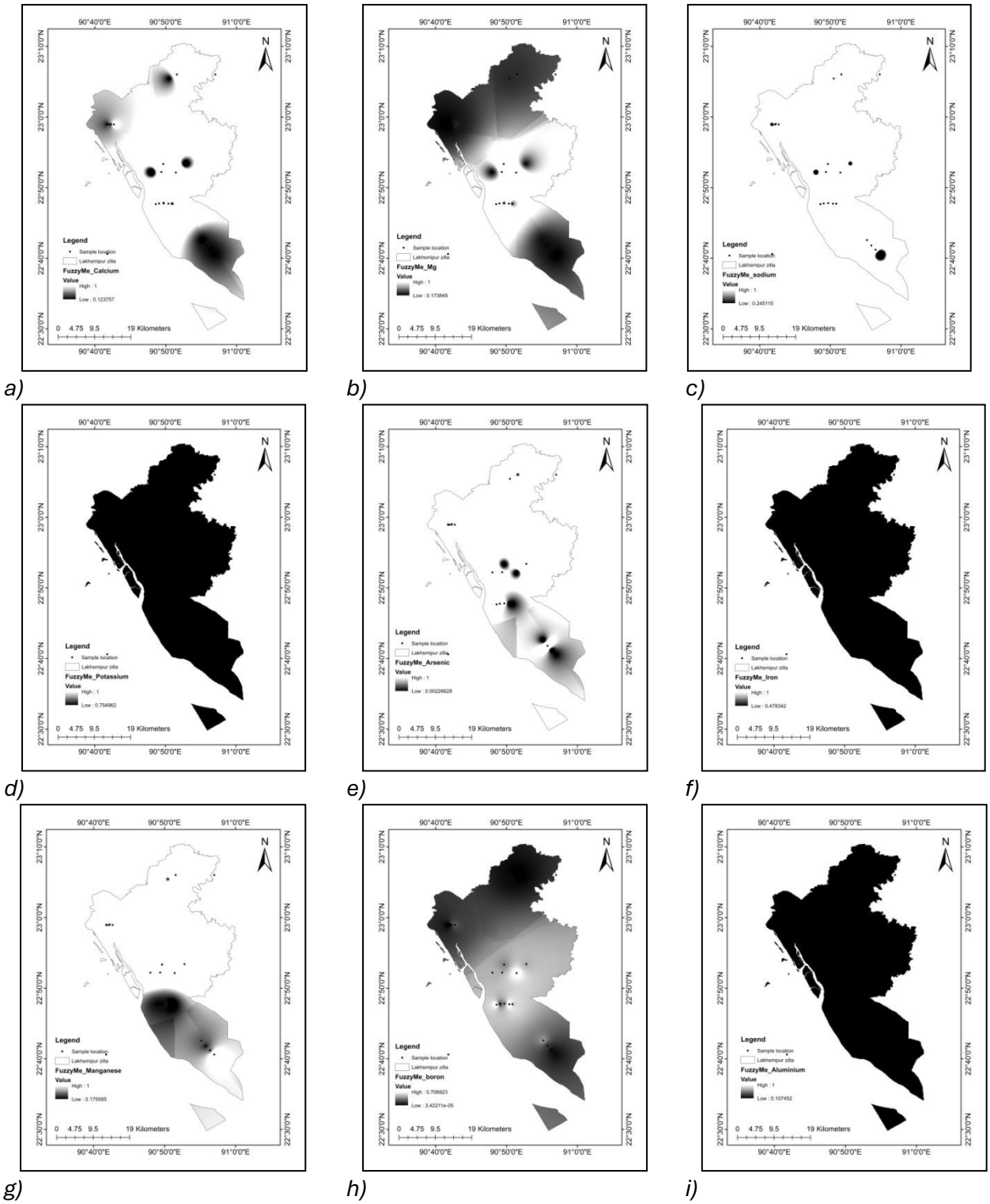
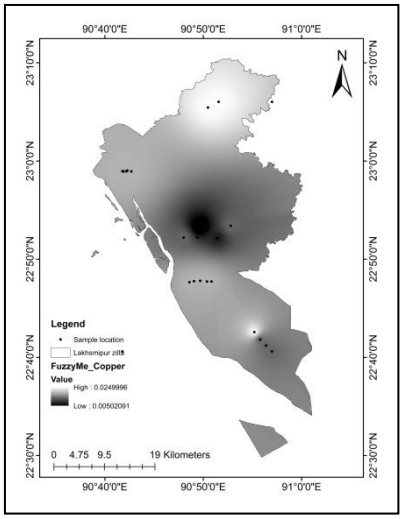
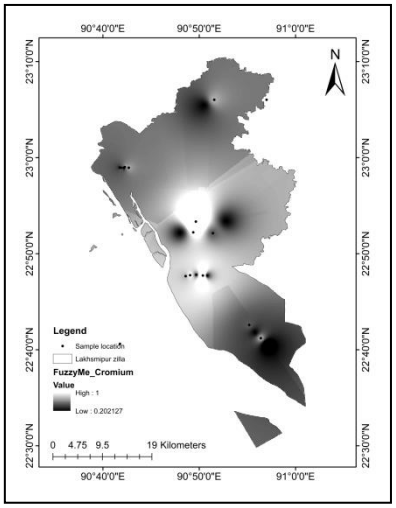


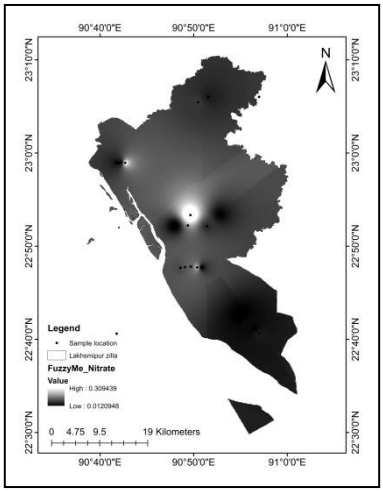
Figure 6, Fuzzy linear membership map of (a) Calcium (mg/L) (b) Magnesium (mg/L) (c) Sodium(mg/L) (d) Potassium (mg/L) (e) Arsenic (mg/L) (f) Iron (mg/L) (g) Manganese (mg/L) (h) Boron (mg/L) (i) Aluminum (mg/L).



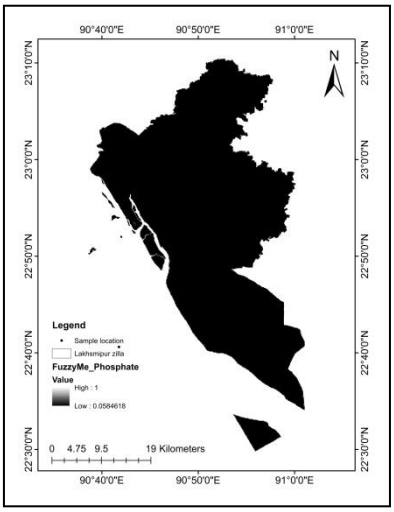
j)



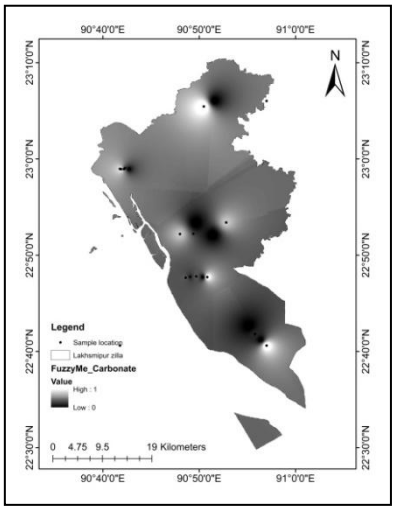
k)



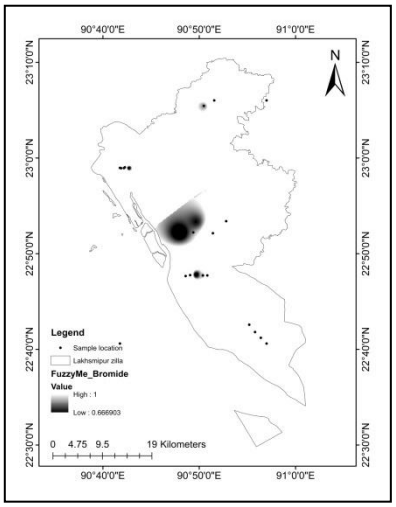
l)



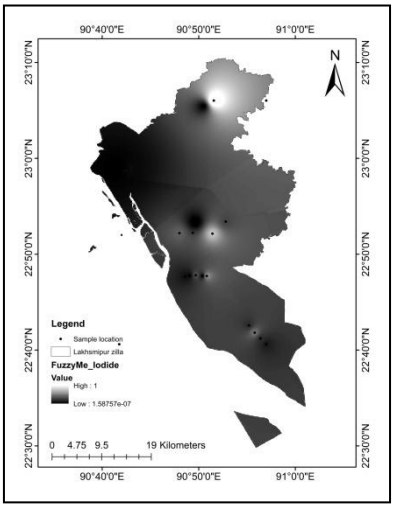
m)



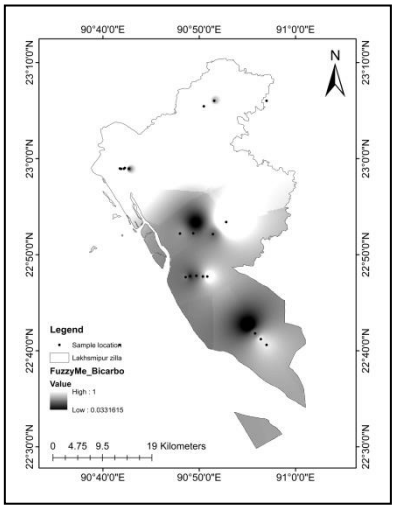
n)



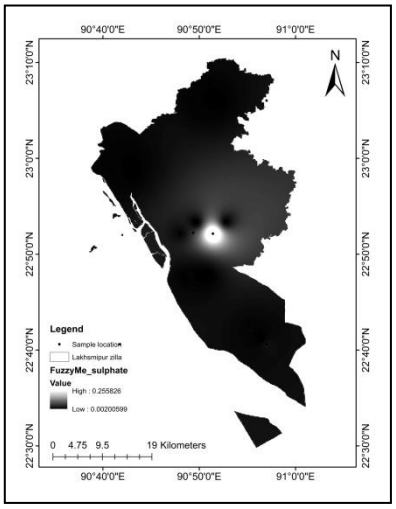
o)



p)



q)



r)

Figure 6 contd., Fuzzy linear membership map of (j) Copper (mg/L) (k) Chromium (mg/L) (l) Nitrate (mg/L) (m) Phosphate (mg/L) (n) Carbonate (mg/L) (o) Bromide (mg/L) (p) Iodide (mg/L) (q) Bicarbonate (mg/L) (r) Sulphate (mg/L).

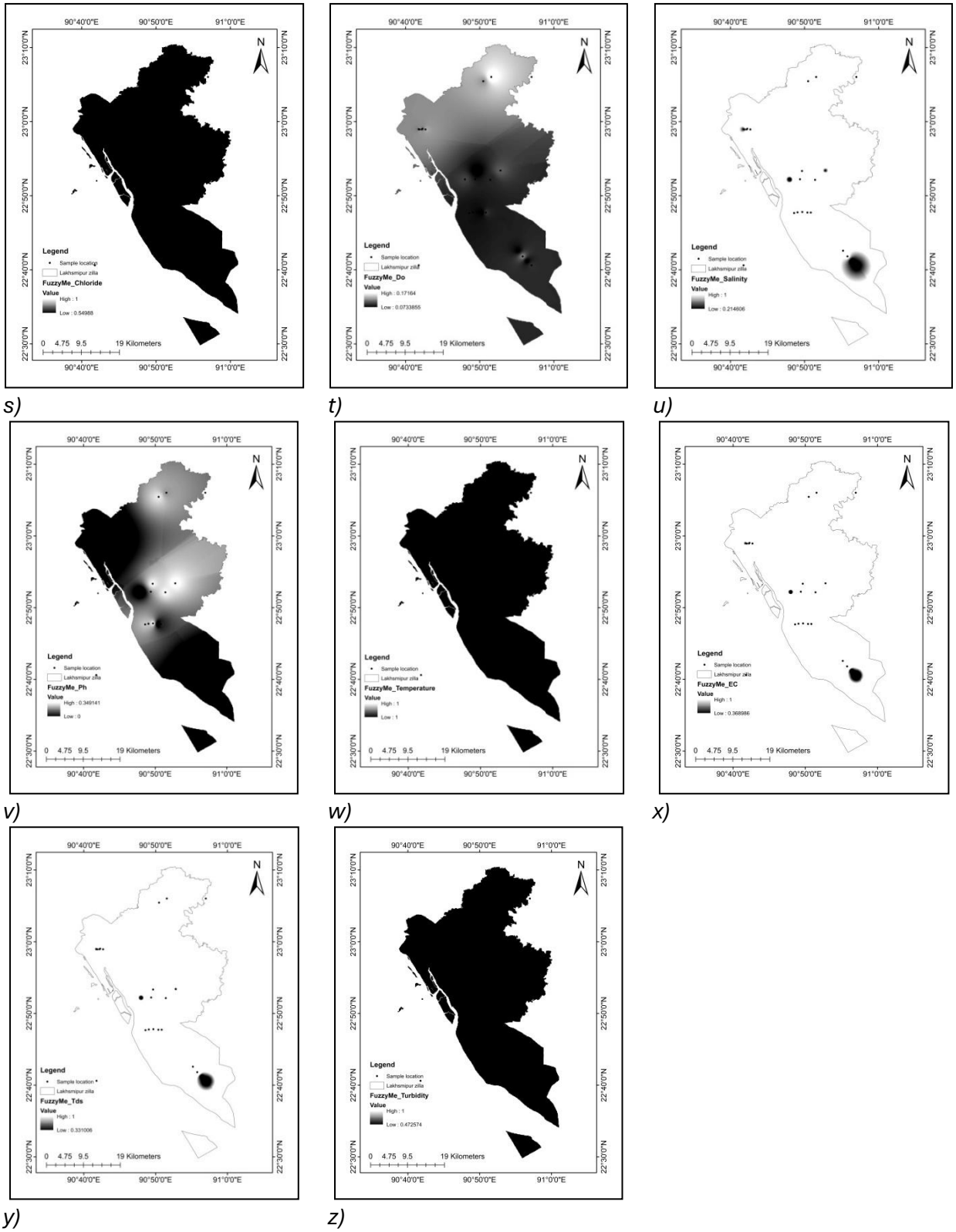


Figure 6 contd., Fuzzy linear membership map of (s) Chloride (mg/L) (t) DO (mg/L) (u) Salinity (ppt) (v) Lead (mg/L) (w) Temperature (°C) (x) EC (µs/cm) (y) TDS (mg/L) (z) Turbidity (NTU).

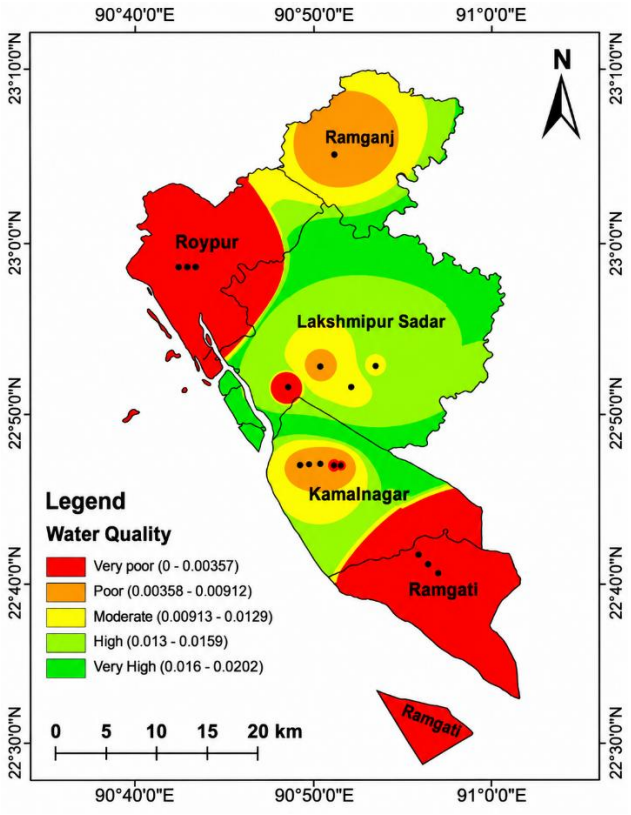


Figure 7, Groundwater Quality Index map by fuzzy overlay of the study area.

In this diagram, samples from Kamalnagar, Lakshmipur Sadar, Ranganj, Raipur, and Ramgati are plotted using different symbols. Most samples cluster in the $Na^{+}+K^{+}$-$Cl^{-}+SO_4^{2-}$ dominant zone, indicating a saline or marine-influenced water type, common in coastal regions. This suggests ion exchange or seawater intrusion may influence groundwater chemistry, especially near the coast. Such analysis is crucial for understanding water quality and planning for drinking and irrigation suitability.

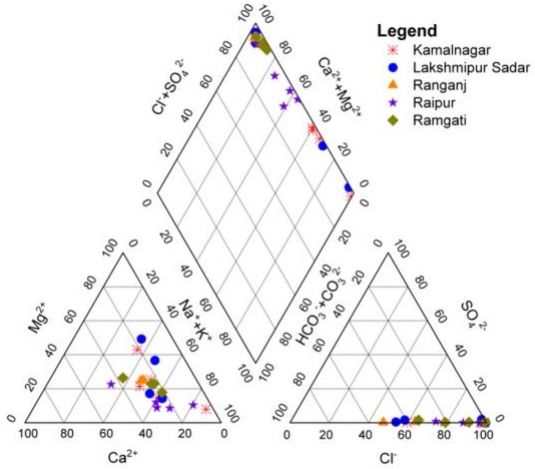


Figure 8, Piper's Trilinear Diagram of groundwater of the study area.

Durov diagram

The Durov diagram is used to reveal hydro geochemical processes associated with the chemical composition of water, such as cation exchange, reverse cation exchange, mixing, and simple dissolution (Durov, 1948; Ravikumar et al., 2015). It consists of a central square figure bounded on the left by a cation triangle, on the top by an anion triangle, on the right by a TDS (Total Dissolved Solids) rectangle, and on the bottom by a pH rectangle (Durov, 1948; Chen et al., 2020, Yu et al., 2021). The milliequivalent per liter concentrations of the total cations and anions are transformed into percentages and scaled on the diagram. According to the classification of Lloyd and Heathcote (1985), the central rectangular figure is subdivided into nine zones representing different hydro geochemical processes, including mixing and reverse cation exchange waters (Ca-Cl type water), mixing and reverse cation exchange reactions, mixing with seawater or halite, calcite and gypsum dissolution, mixing reactions from various origins, mixing and cation exchange waters, infiltration (Ca-HCO_3 type water), cation exchange reactions, and cation exchange waters (Na-HCO_3 type water).

In this plot (Figure 9), groundwater samples from Kamalnagar, Lakshmipur Sadar, Ranganj, Raipur, and Ramgati are color-coded and symbolized. Most samples plot toward the $Na^{+}+K^{+}$ and Cl^{-} dominant zones, indicating saline water influence or ion exchange processes, which are typical in coastal aquifers. The dominance of Mg^{2+} over Ca^{2+} in many samples also suggests cation exchange reactions. The clustering in the lower-right central square indicates Cl^{-}-Na^{+} water type, often linked with seawater intrusion or anthropogenic contamination. This type of analysis helps in understanding the groundwater evolution and suitability for drinking and agricultural use.

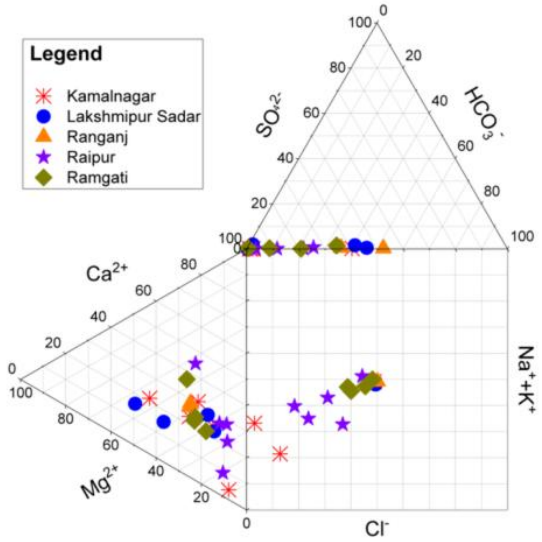


Figure 9, Durov diagram for hydrogeochemical types of the study area.

Gibbs diagram

For evaluating dominant hydro geochemical processes, such as hydrochemistry formation interactions, compositional change trends, and the hydro geochemical evolution of analyzed groundwater based on its chemical composition, the Gibbs diagram is

another useful tool (Liu et al., 2021; Lyu et al., 2019; Nazzal et al., 2014, Gibbs, 1970). Additionally, it shows how aquifer lithology characteristics and groundwater composition are related (Gibbs, 1970). The Gibs diagram was first used to assess the hydro-chemical processes that predominate in surface water, but it is also used to assess the hydro-chemical processes in groundwater (Palmer and Cherry, 1984; Barica, 1972).

Evaporation is less significant in groundwater chemistry (Marandi et al., 2018), and the dominance of the rock is more significant than other components in the Gibs diagram (Palmer and Cherry, 1984). Anthropogenic activities can occasionally affect how rocks weather (Pradhan et al., 2022). The plot of Total Dissolved Solids (TDS) against ($Na^+/Na^+ + Ca^{2+}$) and TDS against ($Cl^-/Cl^- + HCO_3^-$) is depicted in Figure 10 by the Gibbs diagram. The Na/Cl ratio, CAI, and PCA results provide additional support for the hydro chemical facies found in the Piper and Durov diagrams. The prevalence of Na–Cl facies, along with Na/Cl ratios that show chloride enrichment and positive CAI values, demonstrate that ion exchange, rock–water interaction, and salinity enrichment, rather than seawater intrusion alone, have an impact on groundwater evolution.

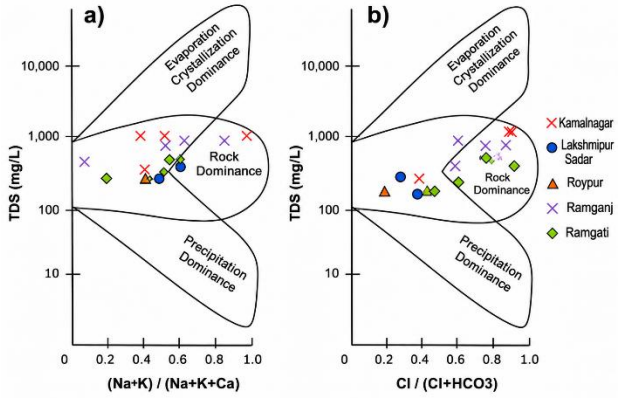


Figure 10, Gibbs diagram for representation of Hydogeochemical evolution of the study area.

Additionally, salinity-related variables (EC, TDS, salinity, Na^+, Ca^{2+}, and Mg^{2+}) were found to be the primary contributors to groundwater chemistry by PCA, which quantitatively supported the hydro chemical processes deduced from the facies study.

In both plots, most groundwater samples cluster within the "Rock Dominance" field, indicating that rock-water interactions, such as mineral weathering and dissolution, are the primary processes influencing groundwater chemistry. A few samples trend toward the Evaporation-Crystallization dominance field, suggesting possible salinization from evaporation effects, especially in coastal areas. These interpretations are crucial for understanding geochemical processes and ensuring sustainable groundwater management in the Lakshmipur region.

Principal Component Analysis (PCA)

Principal Component Analysis (PCA) was applied to identify the major processes controlling groundwater chemistry in the study area. Three principal components with eigenvalues greater than one were extracted, explaining 79.09% of the total variance (Table 12). The scree plot also indicates that the first three principal components account for most of the variability in the dataset. PC1 explained 52.54% of the total variance and showed strong positive loadings for EC, TDS, salinity, Na^+, Ca^{2+}, and Mg^{2+}, indicating that groundwater chemistry is mainly controlled by salinity enrichment and mineralization processes. PC2 accounted for 16.56% of the total variance and was primarily associated with HCO_3^-, As, Fe, and Mn, suggesting the influence of geogenic processes on water quality. PC3 explained 10.00% of the total variance and was mainly related to NO_3^- and SO_4^{2-}, indicating a comparatively minor contribution from anthropogenic activities (Figure 11a). The PCA biplot (Figure 11b) further illustrates the relationships among the hydro chemical parameters and confirms the dominant influence of salinity-related variables on water quality. Overall, the PCA results are consistent with the interpretations derived from the Piper, Durov, and Gibbs diagrams, providing additional evidence for the hydro geochemical evolution of groundwater in the coastal aquifer.

The comprehensive hydro geochemical analyses show that geogenic processes dominate groundwater chemistry in the studied area. According to the PCA, hydro chemical facies, Na^+/Cl^- ratio, and CAI-I analyses, the main processes controlling the evolution of groundwater chemistry are water–rock interaction, mineral dissolution, ion exchange, and localized saline water effect. Natural geochemical processes, such as mineral weathering and the reductive dissolution of iron-bearing minerals, are primarily responsible for elevated concentrations of Fe, Mn, and As. On the other hand, nitrate enrichment, which is probably related to home wastewater, agricultural fertilizer application, and other human activities, is the main indicator of localized anthropogenic impacts. Overall, the findings imply that while anthropogenic inputs locally contribute to groundwater degradation, geogenic processes are the primary regulators of water quality.

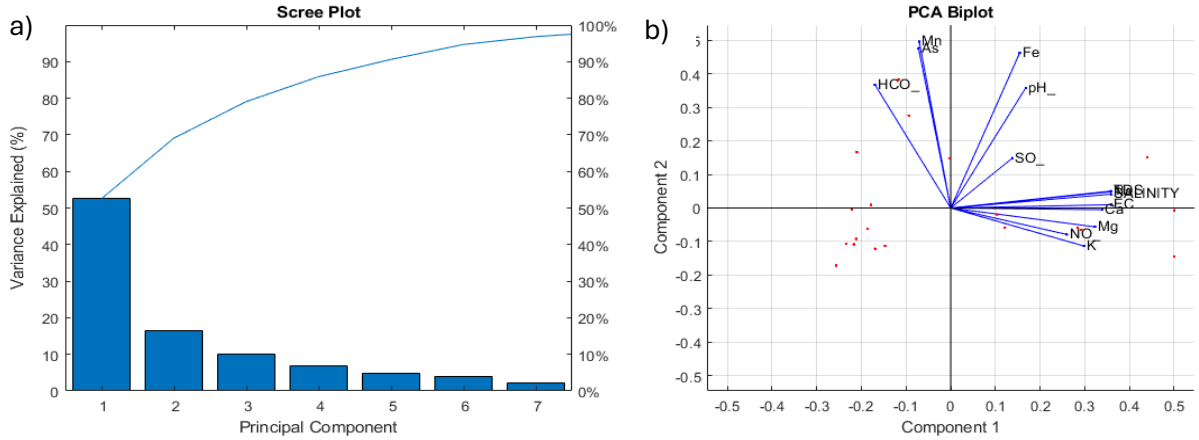


Figure 11, (a) Standard Scree Plot (b) PCA Biplot

Table 12, PCA Loading (PC1-PC3)

	PC1	PC2	PC3
pH	0.17	0.36	-0.05
EC	0.36	0.01	-0.004
TDS	0.36	0.05	-0.005
SALINITY	0.36	0.04	-0.002
Na	0.36	0.05	-0.108
K	0.30	-0.11	-0.305
Ca	0.34	-0.005	0.069
Mg	0.32	-0.06	-0.015
NO	0.26	-0.08	-0.31
SO	0.14	0.15	0.58
HCO_3^-	-0.17	0.37	-0.34
As	-0.07	0.48	-0.467
Fe	0.15	0.46	0.298
Mn	-0.07	0.50	0.177

Na/Cl ratio

The Na/Cl ratio increased marginally from 0.35 to 1.03 due to ongoing cation exchange and water-rock interaction through monsoonal recharge (Figure 12), demonstrating partial dilution of chloride through recharge. All other ratios that are less than unity (Na/Cl < 1) exhibit persistent chloride enrichment. Salinity has an impact on groundwater, and the Na/Cl ratios guarantee this. Additionally, the Na/Cl ratios show how groundwater salinity is affected by the combined actions of groundwater mineralization, cation exchange, evaporation, and localized saline groundwater mixing.

Numerous hydro geochemical processes, such as weathering, evaporation, and localized saline water mixing, contribute to groundwater salinity. This has been documented using Na/Cl ratio measurements in coastal aquifers on Hatiya Island and Bhola (Tajwar et al., 2023; Shaibur et al., 2023).

Chloro-Alkaline Index (CAI)

The evolution of groundwater is influenced by both concomitant cation exchange and mineral weathering, according to geochemical data from the CAI. Na^+ and K^+ in groundwater are exchanged with Ca^{2+} and Mg^{2+} adsorbed on aquifer materials, according to the consistently CAI values, which range from -0.05 to 0.63 (Table 13).

Table 13, Chloro-Alkaline Index (CAI) values of groundwater samples during the pre-monsoon and post-monsoon seasons.

Sample ID	CAI	Sample ID	CAI
GQHS5133001	0.39	GQHS5158002	0.16
GQHS5133002	0.47	GQHS5158003	0.22
GQHS5133003	0.23	GQHS5158004	0.43
GQHS5133004	0.36	GQHS5158005	-0.05
GQHS5133005	0.41	GQHS5158007	0.63
GQHS5143001	0.43	GQHS5158010	0.43
GQHS5143002	0.37	GQHS5165001	0.57
GQHS5143003	0.47	GQHS5165002	0.4
GQHS5143004	0.23	GQHS5165003	0.22
GQHS5158001	0.45	GQHS5165004	0.42
Average	0.36		
Standard Deviation	0.15		

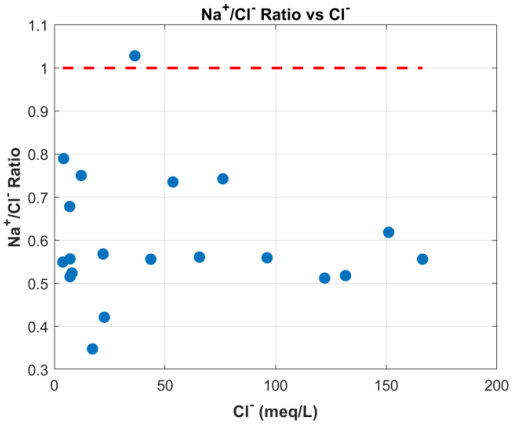


Figure 12, Seasonal variation of Na/Cl ratios

Because ion-exchange activities also significantly contribute to Na enrichment in the groundwater, elevated sodium concentrations should not be taken only as proof of seawater incursion.

Multiple hydro geochemical processes, as opposed to only exceeding drinking water requirements, regulate the degradation of groundwater quality. The main

processes controlling groundwater chemistry are rock–water contact, mineral dissolution, ion exchange, and salinity enrichment, according to the combined interpretation of the Piper, Durov, Gibbs diagrams, and PCA. Furthermore, the enrichment of Fe and As is probably linked to geogenic processes under decreasing aquifer conditions, but the higher amounts of Na^+, Cl^-, EC, and TDS indicate the influence of saline water. The observed decline in groundwater quality in the coastal aquifer is better explained by these findings.

Aquifer features and groundwater depth also affect groundwater chemistry in coastal aquifers. While deeper aquifers are frequently regulated by long-term water-rock interaction and geogenic processes, shallow aquifers are generally more vulnerable to surface contamination and salinity intrusion. The observed regional variability in groundwater chemistry may partially reflect variations in aquifer conditions and groundwater flow, even though groundwater depth measurements were not available for this investigation. A more thorough knowledge of the changes in groundwater quality in the study area might be possible with future research that incorporates comprehensive data and aquifer features. The hydro geochemical features found in the coastal aquifer of Lakshmipur are mostly in line with earlier research done in other coastal areas of Bangladesh, such as Bhola, Noakhali, Satkhira, and Hatiya. According to similar research, the main mechanisms governing groundwater chemistry in these coastal aquifers are increased salinity, Na^+–Cl^- dominant water types, ion exchange, and rock–water interaction (Bhuiyan et al., 2016; Shaibur et al., 2023; Tajwar et al., 2023). However, the comparatively greater concentrations of Fe and as found in this study suggest that geogenic processes contribute significantly to the degradation of groundwater quality in addition to salinity enrichment (Bhuiyan et al., 2016). These parallels show that geogenic pollution and salinity enrichment are prevalent hydro geochemical traits in Bangladesh's coastal aquifers.

Health risk assessment

The Hazard Index (HI) for groundwater drinking and cutaneous exposure ranged from 0.22 to 4.21 for adults and from 0.24 to 4.60 for children, according to the health risk assessment (Table 14). Oral intake is the main exposure channel, as demonstrated by the fact that HQ_{Total} (ingestion) consistently exceeded HQ_{dermal} across all samples. 14 out of 20 samples (70%) and 15 out of 20 samples (75%) surpassed the threshold for adults and children, respectively, according to USEPA recommendations (HI > 1 indicates potential non-carcinogenic risk), suggesting significant health concerns in the research area.

Sample No. 6 had the highest health hazards (HI: 4.21 adult, 4.60 child), followed by Samples No. 12 and 16. Sample No. 5 had the lowest risk. Due to their lower body weight and higher relative water intake, children showed noticeably greater sensitivity than adults in every location.

Table 14, Health risk of groundwater samples collected from Lakhsmipur district

Sample No	HQ_{oral}		HQ_{dermal}		HI	
	Adult	Children	Adult	Children	Adult	Children
1	0.97	1.24	0.56	0.44	1.54	1.68
2	1.06	1.35	0.62	0.48	1.68	1.83
3	1.09	1.39	0.63	0.50	1.73	1.89
4	1.19	1.51	0.69	0.54	1.88	2.05
5	0.14	0.18	0.08	0.06	0.22	0.24
6	2.66	3.39	1.55	1.21	4.21	4.60
7	0.59	0.75	0.34	0.27	0.93	1.02
8	1.68	2.14	0.98	0.76	2.66	2.90
9	0.54	0.69	0.32	0.25	0.86	0.94
10	0.24	0.30	0.14	0.11	0.38	0.41
11	0.18	0.23	0.10	0.08	0.28	0.31
12	2.16	2.75	1.26	0.98	3.42	3.74
13	1.71	2.18	0.99	0.78	2.70	2.95
14	1.05	1.33	0.61	0.48	1.66	1.81
15	0.94	1.20	0.55	0.43	1.49	1.63
16	2.00	2.54	1.16	0.91	3.16	3.45
17	0.72	0.92	0.42	0.33	1.14	1.24
18	0.30	0.38	0.18	0.14	0.48	0.52
19	0.71	0.90	0.41	0.32	1.12	1.22
20	0.76	0.97	0.44	0.34	1.20	1.31

The "Very Poor" groundwater quality zones found in Raipur and Ramgati are spatially correlated with the elevated HI values, highlighting the critical need for targeted arsenic/iron removal technologies and alternate safe water sources in these high-risk areas.

Validation of the fuzzy-GIS groundwater quality map

Table 15 and Figure 13 provide the validation results. An Overall Accuracy (OA) of 45.0% and a Kappa coefficient (κ) of 0.056 were found when the observed and projected WQI classes were compared, suggesting a small degree of agreement between the two classifications. The Very Poor group accounted for the majority of correctly identified samples, although misclassification mostly happened between adjacent quality classes. Uncertainties related to the fuzzy categorization approach and regional variability in groundwater quality could be the cause of these discrepancies.

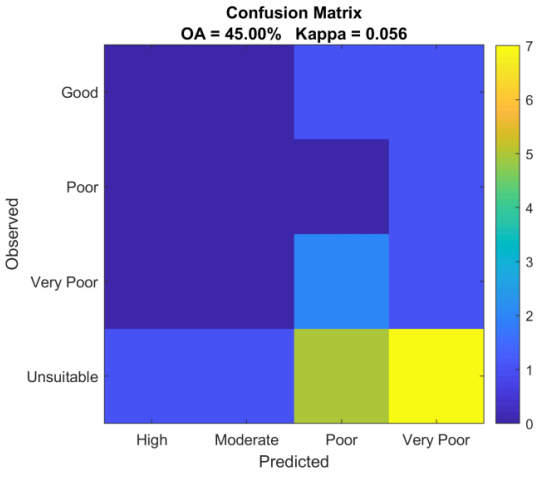


Figure 13. Confusion matrix showing the validation of the fuzzy-GIS groundwater quality map based on observed and predicted WQI classes.

Table 15, Observed and predicted WQI classes used for validation of the fuzzy-GIS groundwater quality map.

Sample ID	Sample No	Location	WQI Status	Fuzzy WQI
GQHS5133001	1	Kamalnagar	unsuitable	Poor
GQHS5133002	2	Kamalnagar	unsuitable	Poor
GQHS5133003	3	Kamalnagar	Very poor	Poor
GQHS5133004	4	Kamalnagar	Very poor	Poor
GQHS5133005	5	Kamalnagar	Good	Poor
GQHS5143001	6	Lakshmipur Sadar	unsuitable	Poor
GQHS5143002	7	Lakshmipur Sadar	unsuitable	Very Poor
GQHS5143003	8	Lakshmipur Sadar	unsuitable	moderate
GQHS5143004	9	Lakshmipur Sadar	unsuitable	High
GQHS5158001	10	Ramganj	poor	Very Poor
GQHS5158002	11	Ramganj	Good	Very Poor
GQHS5158003	12	Raipur	unsuitable	Very Poor
GQHS5158004	13	Raipur	unsuitable	Poor
GQHS5158005	14	Raipur	unsuitable	Poor
GQHS5158007	15	Raipur	unsuitable	Very Poor
GQHS5158010	16	Raipur	unsuitable	Very Poor
GQHS5165001	17	Ramgati	unsuitable	Very Poor
GQHS5165002	18	Ramgati	Very poor	Very Poor
GQHS5165003	19	Ramgati	unsuitable	Very Poor
GQHS5165004	20	Ramgati	unsuitable	Very Poor
FWQI (Predicted)	**WQI (Observed)**	-	-	-
Very High	Excellent water	-	-	-
High	Good water	-	-	-
moderate	Poor water	-	-	-
Poor	Very poor water	-	-	-
Very Poor	Water unsuitable for drinking	-	-	-

Study limitations and future research

Several limitations should be noted, despite the fact that the current study offers insightful information about the hydro geochemistry and groundwater quality of the Lakshmipur coastal aquifer. The groundwater data used for the analysis came from 20 BWDB monitoring sites, which might not accurately reflect the spatial diversity of groundwater quality throughout the district. Additionally, seasonal fluctuations in groundwater chemistry could not be assessed because the study was carried out using data from a single monitoring period. Furthermore, prediction uncertainty affects the spatial distribution maps produced by the IDW interpolation technique, especially in regions with comparatively low sampling density.

One disadvantage is the lack of a thorough conceptual hydro geological model that incorporates salinity patterns, chemical properties, and quality classifications. The existing dataset lacks the aquifer geometry, hydraulic gradient, and seasonal water-level data needed for development, which restricts interpretation to descriptive geographical analysis. To create such a model for the Lakshmipur coastal aquifer, future studies including hydro geophysical surveys, multi-level piezometric monitoring, and stable isotopes ($\delta^{1}{}_{2}O$, $\delta^{2}H$) are advised. To enhance the spatial and temporal representation of groundwater quality, future research should combine multi-season groundwater sampling with a bigger and denser monitoring network. The comprehension of groundwater evolution, contaminant transport, and groundwater quality prediction in coastal aquifers would be further improved by integrating hydro geochemical modeling, geochemical speciation, groundwater flow and solute transport modeling, isotope techniques, and machine learning approaches.

Conclusion

Some groundwater samples exceeded permissible limits (WHO, 2011; DoE, 2016) for parameters such as arsenic, TDS, salinity, and certain heavy metals, making them unsuitable for drinking without treatment. The results of Water Quality Index (WQI) and fuzzy-overlay map indicate that a significant portion of the groundwater in Lakshmipur district falls unsuitable for drinking purposes. The health risk assessment further revealed that 70% of the samples posed non-carcinogenic risks for adults (HI > 1) and 75% for children, with children being more vulnerable due to higher relative water intake. Oral ingestion was identified as the primary exposure pathway, with the highest risks concentrated in the western and southern regions (Raipur and Ramgati), correlating with the "Very Poor" groundwater quality zones. The irrigation water quality indices, including Na%, SAR, RSC, MH, KR, and PI, show varying suitability across the district. While some areas are excellent for irrigation, others are unsuitable. The findings highlight the urgent need for continuous monitoring, appropriate treatment, and sustainable groundwater management practices to ensure safe water for drinking and irrigation. It should be mentioned that these conclusions should not be applied to the entire Lakshmipur District because they are based on groundwater samples that were taken from the places under investigation throughout the research period. In order to enhance the geographical and temporal representation of groundwater quality and to support more comprehensive groundwater management methods, future research with a greater

number of sampling points and multi-season monitoring is advised.

Acknowledgements

Special thanks to two anonymous reviewers for their comments and suggestions, which helped to rectify the manuscript. The author also expresses sincere gratitude to University of Rajshahi for its continuous support.

Author contributions

Md. Mahedi Hasan contributed to data analysis and drafted the main manuscript, Khondaker Emamul Haque was responsible for visualization, supervision, and conceptualization of the study, Shamim Ahmed handled the software-related tasks and Md. Nazmul Islam Hasan revised the article. All authors also reviewed it.

Data availability

The data will be available upon request to the corresponding author.

Declarations

The authors declare that they have no known competing financial interests or personal relationships that could have appeared to influence the work reported in this article.

Article note

This article is a full-length paper developed from **Extended Abstract #091**, entitled "**Assessment of Hydro Geochemistry and Groundwater Quality for Drinking and Irrigation purposes in Coastal Aquifer of Lakshmipur district, Bangladesh: Using Fuzzy Overlay**" which was presented at the 15th Asian Regional Conference of the International Association for Engineering Geology and the Environment (ARC-15 of **IAEG**), held in Kathmandu, Nepal, from 27 to 29 November 2025.

References

Ahmed, K. M., Bhattacharya, P., Hasan, M. A., Akhter, S. H., Alam, S. M., Bhuyian, M. H., Imam, M. B., Khan, A. A., and Sracek, O. (2004). Arsenic enrichment in groundwater of the alluvial aquifers in Bangladesh: An overview. Applied Geochemistry, 19(2), 181–200. https://doi.org/10.1016/j.apgeochem.2003.09.006

Appelo, C. A. J., and Postma, D. (2005). Geochemistry, groundwater and pollution (2nd ed.). Balkema, Rotterdam. https://doi.org/10.1201/9781439833544

Barica, J. (1972). Salinization of groundwater in arid zones. Water Research, 6(8), 925–933. https://doi.org/10.1016/0043-1354(72)90044-9

Bhattacharya, P., Jacks, G., Ahmed, K. M., Routh, J., and Khan, A. A. (2002). Arsenic in groundwater of the Bengal Delta Plain aquifers in Bangladesh. Bulletin of Environmental Contamination and Toxicology, 69(4), 538–545. https://doi.org/10.1007/s00128-002-0095-5

Bhuiyan, M. A. H., Bodrud-Doza, M., Islam, A. R. M. T., Rakib, M. A., Rahman, M. S., and Ramanathan, A. L. (2016). Assessment of groundwater quality of Lakshmipur District of Bangladesh using water quality indices, geostatistical methods, and multivariate analysis. Environmental Earth Sciences, 75, 1020. https://doi.org/10.1007/s12665-016-5823-y

Brown, R. M., McClelland, N. I., Deininger, R. A., and Tozer, R. G. (1972). A water quality index: Do we dare? Water and Sewage Works, 117(10), 339–343.

Chen, G., Sun, Z., Nie, F., Li, C., Zhen, Y., and Zhou, Z. (2020). Hydrogeochemical characteristics of the sandstone-hosted uranium mineralization in northern Ordos Basin, China. Ore Geology Reviews, 126, 103769. https://doi.org/10.1016/j.oregeorev.2020.103769

Cloutier, V., Lefebvre, R., Therrien, R., and Savard, M. M. (2008). Multivariate statistical analysis of geochemical data as indicative of the hydrogeochemical evolution of groundwater in a sedimentary rock aquifer system. Journal of Hydrology, 353(3–4), 294–313. https://doi.org/10.1016/j.jhydrol.2008.02.015

Department of Environment. (2016). Surface and ground water quality report. Available at: https://doe.gov.bd/site/publications/5132a8d7-68e9-469d-a9af-8981306b3b9f/Surface-and-Ground-Water-Quality-Report-2016

Deshmukh, K. K., and Pawar, N. J. (2001). Impact of irrigation on the chemistry of the soils and groundwater from Sangamner area, Ahmednagar District (M.S.) Ph.D. Thesis. University of Pune, India.

Durov, S. A. (1948). Classification of natural waters and graphical representation of their composition. Doklady Akademii Nauk SSSR, 59(1), 87–90.

Eaton, F. M. (1950). Significance of carbonates in irrigated waters. Soil Science, 69, 127–128.

Gibbs, R. J. (1970). Mechanisms controlling world water chemistry. Science, 170(3962), 1088–1090. https://doi.org/10.1126/science.170.3962.1088

Gupta, S., Rao, K. S., Ranganathan, K., Padma, T. V., Kumar, R., and Krishnamurthy, V. (2009). Geochemical assessment of groundwater around Macherla-Karempudi area, Guntur District, Andhra Pradesh. Journal of the Geological Society of India, 73(2), 202–212. https://doi.org/10.1007/s12594-009-0076-y

Hem, J. D. (1970). Study and interpretation of the chemical characteristics of natural water (Water-

Supply Paper No. 1473). U.S. Government Printing Office.

Horton, R. K. (1965). An index number system for rating water quality. Journal of the Water Pollution Control Federation, 37(3), 300–306.

Jamal, A. S. I. M., Jhumur, N. T., Shaikh, M. A. A., Moniruzzaman, M., Uddin, M. R., Siddique, M. A. B., Al-Mansur, M. A., Akbor, M. A., Tajnin, J., Ahmed, S., and Mahmud, R. (2024). Spatial distribution and hydrogeochemical evaluations of groundwater and its suitability for drinking and irrigation purposes in Kaligonj Upazila of Satkhira District of Bangladesh. Heliyon, 10(7), e27857. https://doi.org/10.1016/j.heliyon.2024.e27857

Jha, M. K., Shekhar, A., and Jenifer, M. A. (2020). Assessing groundwater quality for drinking water supply using hybrid fuzzy-GIS-based water quality index. Water Research, 179, 115867. https://doi.org/10.1016/j.watres.2020.115867

Kaiser, H. F. (1960). The application of electronic computers to factor analysis. Educational and Psychological Measurement, 20(1), 141–151. https://doi.org/10.1177/001316446002000116

Kelly, W. P. (1940). Permissible composition and concentration of irrigated waters. Proceedings of the American Society of Civil Engineers, 66, 607–613.

Ketata-Rokbani, M., Gueddari, M., and Bouhlila, R. (2011). Use of geographical information system and water quality index to assess groundwater quality in El Khairat Deep Aquifer (Enfidha, Tunisian Sahel). Iranian Journal of Energy and Environment, 2, 133–144.

Li, P., Qian, H., Wu, J., Zhang, Y., and Zhang, H. (2011). Major ion chemistry of shallow groundwater in the Dongsheng coalfield, Ordos Basin, China. Environmental Earth Sciences, 64, 563–574. https://doi.org/10.1007/s12665-010-0863-9

Liu, H., Tang, J., Zhang, X., Wang, R., Zhu, B., Li, N., and Zhao, P. (2021). Seasonal variations of groundwater recharge in a small subtropical agro-forestry watershed with horizontal sedimentary bedrock. Journal of Hydrology, 596, 125703. https://doi.org/10.1016/j.jhydrol.2020.125703

Lloyd, J. W., and Heathcote, J. A. A. (1985). Natural inorganic hydrochemistry in relation to groundwater. Clarendon Press.

Lyu, M., Pang, Z., Yin, L., Zhang, J., Huang, T., Yang, S., and Gulbostan, T. (2019). The control of groundwater flow systems and geochemical processes on groundwater chemistry: A case study in Wushenzhao Basin, NW China. Water, 11(4), 790. https://doi.org/10.3390/w11040790

Marandi, A., and Shand, P. (2018). Groundwater chemistry and the Gibbs Diagram. Applied Geochemistry, 97, 209–212. https://doi.org/10.1016/j.apgeochem.2018.07.009

USEPA (1989). Risk assessment guidance for Superfund: Volume I, human health evaluation manual (Part A). U.S. Environmental Protection Agency, Office of Emergency and Remedial Response, Washington, DC, EPA/540/1-89/002. https://www.epa.gov/sites/default/files/2015-09/documents/rags_a.pdf

Nazzal, Y., Ahmed, I., Al-Arifi, N. S., Ghrefat, H., Zaidi, F. K., El-Waheidi, M. M., and Zumlot, T. (2014). A pragmatic approach to study the groundwater quality suitability for domestic and agricultural usage, Saq Aquifer, northwest of Saudi Arabia. Environmental Monitoring and Assessment, 186, 4655–4667. https://doi.org/10.1007/s10661-014-3728-3

Nwankwo, C. B., Hoque, M. A., Islam, M. A., and Dewan, A. (2020). Groundwater constituents and trace elements in the basement aquifers of Africa and sedimentary aquifers of Asia: Medical hydrogeology of drinking water minerals and toxicants. Earth Systems and Environment, 4(2), 369–384. https://doi.org/10.1007/s41748-020-00151-z

Palmer, C. D., and Cherry, J. A. (1984). Geochemical evolution of groundwater in sequences of sedimentary rocks. Journal of Hydrology, 75(1–4), 27–65. https://doi.org/10.1016/0022-1694(84)90045-3

Piper, A. M. (1944). A graphic procedure in the geochemical interpretation of water-analyses. Transactions, American Geophysical Union, 25(6), 914–928. https://doi.org/10.1029/TR025i006p00914

Pradhan, R. M., Behera, A. K., Kumar, S., Kumar, P., and Biswal, T. K. (2022). Recharge and geochemical evolution of groundwater in fractured basement aquifers (NW India): Insights from environmental isotopes (δ18O, δ2H, and 3H) and hydrogeochemical studies. Water, 14(3), 315. https://doi.org/10.3390/w14030315

Raghunath, H. M. (1987). Groundwater (2nd ed.). Eastern Limited, New Delhi.

Ravikumar, P., Somashekar, R. K., and Prakash, K. L. (2015). A comparative study on usage of Durov and Piper diagrams to interpret hydrochemical processes in groundwater from SRLIS River Basin, Karnataka, India. Elixir Earth Science, 80, 31073–31077.

Richards, L. A. (1954). Diagnosis and improvement of saline and alkali soils (Agriculture Handbook No. 60). U.S. Government Printing Office.

Sahu, P., and Sikdar, P. K. (2008). Hydrochemical framework of the aquifer in and around East Kolkata wetlands, West Bengal, India. Environmental Geology, 55, 823–835. https://doi.org/10.1007/s00254-007-1034-x

Schoeller, H. (1977). Geochemistry of groundwater. In Groundwater studies: An international guide for research and practice, UNESCO, Paris, pp. 1–18.

Shaibur, M. R., Ahmmed, I., Sarwar, S., Karim, R., Hossain, M. M., Islam, M. S., Shah, M. S., Khan, A. S., Akhtar, F., Uddin, M. G., and Rahman, M. M. (2023). Groundwater quality of some parts of coastal Bhola District, Bangladesh: Exceptional evidence. Urban Science, 7(3), 71. https://doi.org/10.3390/urbansci7030071

Shannon, C. E. (2001). A mathematical theory of communication. ACM SIGMOBILE Mobile Computing and Communications Review, 5(1), 3–55.

Su, L., Xiao, M., Zhou, M., Wang, F., and Zhang, Y. (2018). Assessment of groundwater quality using water quality index (WQI) and GIS in a rural area of China. Ecological Indicators, 87, 22–29. https://doi.org/10.1016/j.ecolind.2017.12.001

Szabolcs, I., and Darab, C. (1964). The influence of irrigation water of high sodium carbonate content on soils. In I. Szabolics (Ed.), Proceedings of the 8th International Congress of Soil Science: Sodic soils. Research Institute of Soil Science and Agricultural Chemistry, Hungarian Academy of Sciences, pp. 802–812.

Tajwar, M., Uddin, A., Lee, M. K., Nelson, J., Zahid, A., and Sakib, N. (2023). Hydrochemical characterization and quality assessment of groundwater in Hatiya Island, southeastern coastal region of Bangladesh. Water, 15(5), 905. https://doi.org/10.3390/w15050905

Takeya, L. A., Haque, K. E., Ahmed, S., Siddique, M. A. B., Moniruzzaman, M., Uddin, M. R., and Rahman, M. S. (2025). Hydrochemistry, quality, and potential health risk appraisal of arsenic-enriched groundwater in central-west Bangladesh using the integrated water quality index and Monte Carlo simulation. Science of the Total Environment, 1003, 180707. https://doi.org/10.1016/j.scitotenv.2025.180707

Tiwari, A., Kumar, M., Thakur, S., Singh, P., Yadav, A., and Mehra, R. (2023). Groundwater quality assessment for drinking purpose using traditional and fuzzy-GIS-based water quality index in Gurugram District of Haryana, India. Environmental Geochemistry and Health. https://doi.org/10.1007/s10653-023-01783-6

United Nations Department of Economic and Social Affairs. (2016). The sustainable development goals report 2016. United Nations.

U.S. Environmental Protection Agency. (2021). Regional screening levels (RSLs): Equations. https://www.epa.gov/risk/regional-screening-levels-rsls-equations

Wan, T., Jun, H., Pan, W., and Hua, H. (2015). Kappa coefficient: A popular measure of rater agreement. Shanghai Archives of Psychiatry, 27(1), 62. https://doi.org/10.11919/j.issn.1002-0829.215010

World Health Organization. (2011). Guidelines for drinking-water quality (4th ed.). World Health Organization, Geneva, Switzerland. https://apps.who.int/iris/bitstream/10665/44584/1/9789241548151_eng

Wilcox, L.V. (1955). Classification and Use of Irrigation Water. US Department of Agriculture, Circular 969, Washington DC.

Yu, J., Jiao, Y., Yang, W., Yang, J., and Liu, L. (2021). Hydrogeochemical characterization of a possible carbon sink from shallow saline-alkaline groundwater in the eastern Hetao Basin of Inner Mongolia in China. Environmental Science: Processes and Impacts, 23(2), 344–356. https://doi.org/10.1039/d0em00415d

Zadeh, L. A. (1965). Fuzzy sets. Information and Control, 8(3), 338–353.

Research Article DOI: https://doi.org/10.64862/ajeg.2026.301.05.306 Open Access

Spatiotemporal Analysis and Forecasting of Groundwater Level Fluctuations with Sectoral Water Demand Assessment in Shahjadpur, Sirajganj, Bangladesh

Md. Nazmul Islam Hasan[1*], Khondaker Emamul Haque[1], Shamim Ahmed[2], and Md. Mahedi Hasan[1]

[1]Department of Geology and Mining, University of Rajshahi, Rajshahi 6205, Bangladesh
[2]Institute of Environmental Science, University of Rajshahi, Rajshahi 6205, Bangladesh

(*Corresponding E-mail: hasanjunaid48@gmail.com)

Received: December 18, 2025, Accepted: June 12, 2026)

Abstract: Groundwater is a vital freshwater source sustaining agriculture, domestic use, and industry across north-central Bangladesh, yet its sustainability is increasingly threatened by over-extraction and climate variability. This study integrates statistical (parametric and non-parametric) and geostatistical approaches to evaluate long-term spatiotemporal groundwater dynamics in Shahjadpur Upazila, Sirajganj District, from 2000 to 2024. Linear regression, Mann–Kendall, and Sen's slope analyses were employed to detect temporal trends, while spatial interpolation using Inverse Distance Weighting (IDW) and Ordinary Kriging characterized spatial variability. ARIMA-based forecasting was further applied to predict future water-level fluctuations through 2030. Results reveal a significant declining trend (–0.01 to -0.45 m year^{-1}) in most observation wells, with deeper aquifers showing the steepest depletion. Kriging interpolation achieved higher predictive accuracy (RMSE = 0.23 m) than IDW and delineated zones of critical groundwater stress in the southern and eastern sectors. Forecasts indicate an additional -1.5 to -2.0 m decline by 2030 if current abstraction rates persist. The integrated analytical framework provides a replicable tool for trend detection, spatial mapping, and forecasting in groundwater-stressed floodplain aquifers, supporting data-driven management and sustainable water policy development in Bangladesh and similar hydrogeological settings.

Keywords: ***Groundwater depletion, Trend analysis, Mann–Kendall test, Geostatistics, ARIMA forecasting.***

Introduction

Groundwater plays an essential role in ensuring water security, particularly in densely populated and agriculturally dependent regions such as Bangladesh. Globally, groundwater provides nearly 50% of drinking water and 40% of irrigation supplies (Gleeson et al., 2012). In South Asia, rapid population growth, agricultural intensification, and unregulated abstraction have resulted in alarming groundwater declines and aquifer depletion (Taylor et al., 2013; Rodell et al., 2018). Bangladesh, situated within the Ganges–Brahmaputra–Meghna (GBM) basin, relies heavily on groundwater for both irrigation and domestic consumption, with abstraction rates increasing sharply since the 1980s (Edmunds et al., 2015; MacDonald et al., 2016).

Within Bangladesh, regional hydrogeological variations have led to spatially heterogeneous patterns of groundwater depletion (Monir et al., 2024; Fahim et al., 2023, Faruqa et al., 2025). The Sirajganj District, located in the north-central floodplain region, represents a particularly dynamic hydrological setting due to its proximity to the Jamuna River and associated floodplain deposits. Over-extraction, compounded by reduced recharge during dry seasons, has produced measurable groundwater declines in many upazilas, including Shahjadpur (de Silva et al., 2024; Rahman et al., 2022). Understanding the temporal and spatial variability of groundwater levels is therefore essential for regional water policy, irrigation scheduling, and aquifer sustainability planning.

Previous studies on groundwater trends in Bangladesh have primarily relied on either parametric technique, such as regression analysis (Zar, 2010; Todd and Mays, 2005), or non-parametric tests, such as the Mann–Kendall (Mann, 1945; Ribeiro and Macedo, 1995) and Sen's slope estimator (Sen, 1968; Hirsch et al., 1982). However, integrating these approaches with geostatistical models (Goovaerts, 1997; Júnez-Ferreira et al., 2023) and time-series forecasting tools such as ARIMA (Box and Jenkins, 1976; Hyndman and Athanasopoulos, 2018) enhances analytical robustness, enabling both descriptive and predictive insights. Such an integrated framework can provide not only the identification of historical trends but also spatial delineation of recharge–discharge zones and future scenario forecasting (Kumar et al., 2019; Thakur et al., 2021; Mahammad et al., 2026).

The present study aims to quantify long-term and short-term trends in groundwater levels using parametric (linear regression) and non-parametric (MK and Sen's slope) techniques. Evaluate the spatial variability of groundwater levels using IDW and Kriging interpolation. Assess future groundwater fluctuations using ARIMA forecasting models.

This integrated methodological approach contributes to the growing body of groundwater monitoring and modeling literature and provides actionable insights for sustainable water management in the Shahjadpur region.

Although numerous studies have investigated groundwater depletion in Bangladesh, most have relied on a single analytical technique, such as linear regression, Mann–Kendall trend analysis, geostatistical interpolation, or time-series forecasting, providing only a partial understanding of groundwater dynamics. Comprehensive studies integrating these complementary approaches within a unified framework remain limited, particularly for floodplain aquifer systems where groundwater availability is simultaneously influenced by climatic variability, intensive irrigation, industrial abstraction, and increasing domestic demand. Furthermore, previous investigations have rarely linked groundwater trend analysis with sector-specific water demand, limiting their applicability for sustainable resource management and policy development.

The principal novelty of this study lies in the development of an integrated analytical framework that combines parametric statistical analysis, non-parametric trend detection, geostatistical spatial modelling, ARIMA-based groundwater forecasting, and quantitative sectoral water-demand assessment within a single workflow. This multi-method approach not only improves the reliability of groundwater trend detection through methodological cross-validation but also provides spatial identification of groundwater-stressed zones, forecasts future groundwater conditions, and evaluates the anthropogenic pressures driving groundwater depletion. By combining historical analysis with predictive modelling and water-use assessment, this study provides a more comprehensive evaluation of groundwater sustainability than previous studies conducted in Bangladesh.

Therefore, this research contributes both methodologically and practically by presenting a reproducible framework that can be applied to groundwater monitoring, vulnerability assessment, and evidence-based groundwater management in Shahjadpur and other alluvial floodplain regions of Bangladesh and South Asia.

Study area

The study area, Shahjadpur Upazila, is located in the Sirajganj District of north-central Bangladesh, between latitudes 24°05'04"–24°15'25" N and longitudes 89°34'03"–89°45'10" E, covering an area of approximately 324.15 km^2 (Figure 1). It lies within the active floodplain of the Jamuna River, bounded by Ullahpara and Belkuchi Upazilas to the north, Enayetpur and Chauhali to the south, Tangail District to the east, and Santhia Upazila (Pabna District) to the west.

Topographically, the region is characterized by low-lying alluvial plains formed through sediment deposition by the Jamuna and its distributaries. Elevations range from 10 to 20 meters above mean sea level, producing gentle undulations conducive to irrigation and settlement. The area experiences a tropical monsoonal climate, with annual rainfall exceeding 1,800 mm, concentrated from June to September, and average monthly temperatures ranging between 12°C and 34°C.

Geologically, Shahjadpur forms part of the Bengal Fore-deep, consisting of unconsolidated Holocene and Pleistocene alluvial deposits. The upper stratigraphic sequence comprises fine to medium sands interbedded with silty clay and occasional gravel lenses, forming multi-aquifer systems. Groundwater occurs under both unconfined and semi-confined conditions, primarily within shallow alluvial formations (Mondal et al., 2022; Fahim et al., 2023).

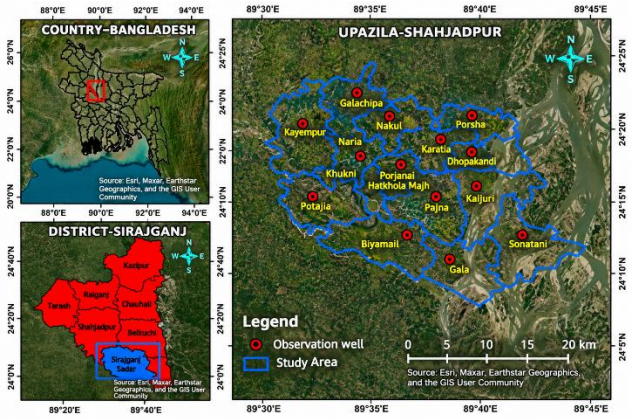


Figure 1, Location map of the study area showing observation well positions and administrative boundaries.

Groundwater abstraction is dominated by shallow and deep tube-wells serving both irrigation and domestic uses. Increasing demand, particularly from the textile and dairy industries in Shahjadpur, has accelerated aquifer stress over the past two decades.

Data collection

Groundwater-level (GWL) data from fourteen observation wells were collected from the Bangladesh Water Development Board (BWDB) for the period 2000–2024. These wells are spatially distributed across Shahjadpur Upazila to ensure comprehensive coverage of hydrogeological variations across floodplain, terrace, and lowland zones (Figure 1). The well network includes locations such as Kayempur, Shahjadpur Pourashava, Beltail, Porjana, Rupabati, Potajia, Narnia, Khukni, Kajjuri, Habibullah Nagar, Jalalpur, Gala, Garadaha, and Sonatani, representing varying hydrostratigraphic and land-use settings.

Measurements were taken quarterly from 2000–2010 and monthly thereafter, yielding a consistent 24-year record of seasonal and interannual fluctuations. The observation wells range in depth from 20 to 40 meters,

screened across shallow to semi-confined aquifers. Data preprocessing included outlier detection, missing-value interpolation, and conversion to mean annual depth-to-water levels (in meters below ground surface).

The groundwater-level dataset was obtained from fourteen observation wells operated by the Bangladesh Water Development Board (BWDB). Detailed metadata for the observation wells, including well identification number, geographic coordinates, total well depth, screened interval (where available), aquifer type, monitoring period, and data completeness, are provided in Supplementary Table S1.

Meteorological data (rainfall, evapotranspiration) were cross-referenced from the Bangladesh Meteorological Department (BMD) to contextualize hydrological variability.

Observation well characteristics

The study utilized groundwater-level records from 14 BWDB observation wells distributed throughout Shahjadpur Upazila. The wells have depths ranging from 20 to 40 m bgl and monitor shallow to semi-confined alluvial aquifers. The groundwater-level dataset covers 2000–2024, with quarterly observations before 2011 and monthly observations thereafter. Data quality was assessed through consistency checks, outlier screening, and interpolation of limited missing observations before statistical analysis. Because the BWDB groundwater-level database used in this study does not include complete well-construction logs, well-specific screened intervals were available.

Influence of temporal sampling resolution

Groundwater levels were measured quarterly during 2000–2010 and monthly from 2011 onward, reflecting improvements in the Bangladesh Water Development Board (BWDB) groundwater monitoring program. To ensure methodological consistency throughout the study period, all observations were aggregated into annual mean groundwater levels prior to statistical analysis. This standardization minimized potential biases arising from differences in sampling frequency and provided a uniform temporal resolution for linear regression, the Mann–Kendall test, Sen's slope estimator, and ARIMA modelling.

Although monthly observations collected after 2010 capture seasonal fluctuations more effectively than the earlier quarterly records, the use of annual averages reduces the influence of unequal sampling frequency on long-term trend estimation. Consequently, the reported long-term groundwater trends are considered robust. Nevertheless, the higher temporal resolution available after 2010 may better represent intra-annual groundwater variability, and this limitation should be considered when interpreting seasonal groundwater responses.

Source and reliability of industrial activity data

The industrial and agricultural activity data used for groundwater demand estimation were compiled from official government statistics and published institutional reports to ensure data reliability and consistency. Information on the number of handloom and textile units was obtained from the Bangladesh Bureau of Statistics (BBS) and the Bangladesh Handloom Board (BHB). Data on textile dyeing and finishing industries were collected from records of the Bangladesh Small and Cottage Industries Corporation (BSCIC) and relevant local government offices. Livestock population statistics were obtained from the Department of Livestock Services (DLS), whereas information on electricity generation facilities was compiled from the Bangladesh Power Development Board (BPDB). Agricultural land-use statistics and crop areas were obtained from the Bangladesh Bureau of Statistics (BBS) and the Department of Agricultural Extension (DAE).

Where recent upazila-level statistics were unavailable, activity data were cross-checked against district statistical yearbooks and official sectoral reports to ensure consistency. Sector-specific unit water-use coefficients were adopted from published peer-reviewed literature, national engineering guidelines, and relevant technical reports. Although some activity data may vary slightly among reporting years, the compiled datasets represent the most reliable information currently available for Shahjadpur Upazila and are considered appropriate for regional-scale groundwater demand assessment.

Methodology for data analysis

Parametric methods were employed to quantify long-term linear relationships between groundwater levels and time (Zar, 2010).

Annual groundwater-level data (2000–2024) from each of the 14 observation wells were analyzed separately. Linear regression was used to estimate the annual rate of groundwater-level change, while the Mann–Kendall test evaluated the significance of monotonic trends. Sen's slope estimator was subsequently calculated to quantify the magnitude of the detected trends. The regression slope, Mann–Kendall statistics (Z and p values), and Sen's slope values reported in Tables 1 and 2 were derived independently for each observation well.

Non-parametric tests were employed to detect monotonic trends that do not assume normal data distribution or homoscedasticity (Hirsch et al., 1982; Helsel et al., 2020).

Parametric statistical analysis

Linear regression

A least-squares regression model was used to estimate the slope (m) and intercept (c) of groundwater level trends as:

$$m = \frac{\sum_{i=1}^{n}(X_i - \bar{X})(Y_i - \bar{Y})}{\sum_{i=1}^{n}(X_i - \bar{X})^2} \quad (1)$$

$$c = \bar{y} - m\bar{x} \quad (2)$$

$$Y_i = mx_i + c \quad (3)$$

$$r = \frac{\sum_{i=1}^{n}(X_i - \bar{X})(Y_i - \bar{Y})}{\sqrt{\sum_{i=1}^{n}(X_i - \bar{X})^2 \sum_{i=1}^{n}(Y_i - \bar{Y})^2}} \quad (4)$$

where Y_i denotes the observed groundwater level, and X_i represents the corresponding time (year). The slope (m) indicates the annual rate of change in groundwater level (m year^{-1}), n denotes number of observations, r is the Pearson Correlation Coefficient.

Mean short-term slope

The Pearson correlation coefficient (r) was computed to assess the strength and direction of the linear association between groundwater level and time:

$$Slope_i = \frac{Y_{i+1} - Y_i}{X_{i+1} - X_i}, i = 1,2, \dots, n-1 \quad (5)$$

Statistical significance ($p < 0.05$) was used to validate the consistency of temporal trends (Pearson, 1895).

Non-parametric trend analysis

Mann–Kendall (MK) test

We use the nonparametric Mann–Kendall test (Mann, 1945; Ribeiro and Macedo, 1995) to determine whether (Yi) exhibits a monotonic trend (increasing or decreasing) over time, independent of linearity (i.e., no assumption of constant slope), because hydrologic time series frequently deviate from parametric regression assumptions because of non-normal residuals, outliers, or seasonality (Hirsch et al., 1982; Suter, 2008).

The Mann-Kendall S_m Statistic may be represented as follows:

$$Sm = \sum_{i=1}^{n-1}\sum_{j=i+1}^{n} sign(X_j - X_i)$$

with the sign function:

$$\text{Sign}(T_j - T_i) = \begin{cases} 1 \; if \; X_j - X_i > 0 \\ 0 \; if \; X_j - X_i > 0 \\ -1 \; if \; X_j - X_i > 0 \end{cases} \quad (6)$$

The variance (σ) for the S_m statistic is defined by:

For data without ties

$$\sigma = \frac{[n(n-1)(2n+5)]}{18} \quad (7)$$

For tied observations

$$\sigma = \frac{n(n-1)(2n+5) - \sum t_p(t_p-1)(2t_p+5)}{18} \quad (8)$$

The standard test statistic Z_S is calculated as follows:

$$ZS = \begin{cases} \frac{S_m - 1}{\sqrt{\sigma}} \; for \; S_m > 0 \\ 0 \; for \; S_m = 0 \\ \frac{S_m + 1}{\sqrt{\sigma}} \; for \; S_m < 0 \end{cases} \quad (9)$$

The two-tailed p-value is obtained from the standard normal distribution. A positive Z_S indicates an upward trend, a negative Z_S a downward trend (Hirsch et al., 1982; Suter, 2008). If the data exhibit significant autocorrelation, a modified Mann–Kendall or pre-whitening correction may be necessary (Hamed and Rao, 1998).

The variance of SSS was estimated, and the standardized Z statistic determined trend direction:

Z > 0: increasing trend

Z < 0: decreasing trend

|Z| > 1.96: significant at 95% confidence level

Prior to the Mann–Kendall test, lag-1 serial autocorrelation (AR (1)) was evaluated. Time series with significant autocorrelation were corrected using the Trend-Free Pre-Whitening (TFPW) method (Yue and Wang, 2002) before applying the Mann–Kendall test and Sen's slope estimator, thereby minimizing the influence of serial dependence on trend significance.

Sen's slope estimator

While the MK test assesses statistical significance of a trend, it does not estimate its magnitude. We therefore compute Sen's slope estimator (Sen, 1968), also called the Theil–Sen estimator, which is a robust nonparametric slope estimator (median of pairwise slopes) (Hirsch et al., 1982; Helsel et al., 2020).

$$Qi = \frac{X_j - X_k}{j-k} \; where \; (j > k) (for \; i=1,2,3...n) \quad (10)$$

where X_j and X_k are the data values at times *j* and *k(j>k)*, respectively.

Sens slope estimator can then be calculated as

$$Q_{med} = \text{Median}(Q_i) \quad (11)$$

$$Q_{med} = \begin{cases} Q\left[\frac{n+1}{2}\right] if \; n \; is \; odd \\ \frac{Q_{n/2} + Q_{(n+2)/2}}{2} \; if \; n \; is \; even \end{cases} \quad (12)$$

The Q_{med} sign reflects data trend, while its value indicates the steepness of the trend.

Spatial analysis

Inverse distance weighting

Spatial interpolation and contour mapping of groundwater levels were performed using Python (PyCharm IDE) to visualize the spatiotemporal variability of groundwater across Shahjadpur Upazila (Figure 2).

Groundwater level data obtained from observation wells were first preprocessed using NumPy and Pandas libraries for statistical consistency checks and missing data handling. Subsequently, SciPy's grid data and Matplotlib's contour functions were applied to generate continuous spatial surfaces from the discrete well data. The interpolation employed an Inverse Distance Weighting (IDW) approach to estimate groundwater levels at unsampled locations, ensuring smooth spatial transitions across the study area. The resulting contour maps depict the distribution and gradient of groundwater depth, facilitating the identification of recharge and discharge zones. All spatial analyses and visualizations were executed within a Python-based geospatial workflow, which provides reproducibility, computational efficiency, and flexibility compared to conventional GIS software.

In order to characterize the spatial distribution of groundwater levels across the study area, the observation-well data were interpolated and contoured within a Python environment (using e.g., NumPy, Pandas, SciPy, and Matplotlib). Initially, the discrete groundwater-depth values at known coordinates (x_i, y_i) were assembled and cleaned for missing or erroneous entries. A regular grid covering the study extents (longitude 89°34'03" E to 89°45'10" E, latitude 24°05'04" N to 24°15'25" N) was then generated. The interpolation was performed using the deterministic Inverse Distance Weighting (IDW) method, where for any grid cell at location $r = (x_i, y_i)$ the estimated groundwater-level $Z(r)$ is given by:

$$Z(r) = \frac{\sum_{k=1}^{n} w(r_k) Z(r_k)}{\sum_{k=1}^{n} w(r_k)} \text{ with } w(r_k) = \frac{1}{d(r,r_k)^p} \qquad (13)$$

$$Z(x) = \frac{\sum_{i=1}^{n} \frac{z_i}{d_i^p}}{\sum_{i=1}^{n} \frac{1}{d_i^p}} \qquad (14)$$

where Z (r_k) is the measured value at known point r_k ; d(r, r_k) is the Euclidean distance between the grid node and the known point (i.e., $d = \sqrt{(x - x_k)^2 + (y - y_k)^2}$; and p is the power parameter controlling the rate at which influence decreases with distance. Following the interpolation, contour lines of equal groundwater-depth were derived (e.g., via Matplotlib's contour/contour functions or a dedicated geospatial library) to visualize recharge/discharge zones and gradients. Cross-validation or error metrics such as root-mean-square error (RMSE) were used to assess interpolation performance. Where spatial autocorrelation and variogram structure (nugget, sill, range) were identified, optional geostatistical approaches (such as Ordinary Kriging) were also considered in parallel.

By scripting the workflow in Python, the interpolation, contouring and mapping steps become reproducible, flexible, and automatable—allowing for systematic comparison of temporal maps and sensitivity analyses of the power parameter p, grid resolution, and spatial sampling density.

Data preparation

Following processes are used to prepare data.

1. Imported the observation-well dataset (coordinates in longitude/latitude, groundwater depth Z) using pandas.read_csv() (or read_excel()).
2. Checked for missing/erroneous values and removed or imputed as needed (e.g., df.dropna(subset=['Z'])).
3. Converted geographic coordinates to a projected system (e.g., UTM zone) using pyproj or geopandas.to_crs() to compute Euclidean distances.
4. Defined the output grid domain covering the study extents (longitudes 89°34'03" E to 89°45'10" E, latitudes 24°05'04" N to 24°15'25" N) and created a regular grid of nodes (e.g., using numpy.meshgrid()) at a chosen cell size (for example 1 m or 20 m).

Kringing

The Kriging interpolation included into the ArcGIS program was used to conduct the geographical analysis of WT levels (Figure 3) and groundwater EC (Johnston et al., 2001). In geostatistics, kriging is a common interpolation method. It is predicated on a spatial linear model for the data that establishes a geographic dependence structure and parametric spatial mean function (Berke, 1999). Kriging weights each observation in the estimation process based on the direction and distance between that point and the point that needs to be estimated.

$$Z^*(x_0) = \sum_{i=1}^{n} \lambda_i Z(x_i) \qquad (15)$$

Subjected to

$$\sum_{i=1}^{n} \lambda_i = 1 \ldots\ldots\ldots\ldots (xvi) \qquad (16)$$

Where, $\lambda_i = Kriging\ weights$

Kriging employs the spatial data configuration, the fitted model from the variogram, and the values of the measured sample points surrounding the prediction site to forecast an unknown value for a particular position (Mustapha, 2013). The current work used Ordinary Kriging (OK), one of the different types of Kriging (Obaje, 2009).

To evaluate data consistency and uniformity, a preliminary exploratory data study comprising trend analysis and data distribution analysis was carried out.

We were able to find patterns in the input datasets and obtain a three-dimensional view of the data thanks to the trend analysis. There is no trend if the line is flat (Cay and Uyan, 2009). Kriging makes the assumption that the data does not show any geographical trends. The majority of the data in this study don't reveal any trends. After that, a semivariogram was created to show the dataset's spatial association. The spherical semivariogram model was chosen.

To get a sense of how effectively the model predicts the values at unknown locations, cross-validation was done prior to creating the final surface.

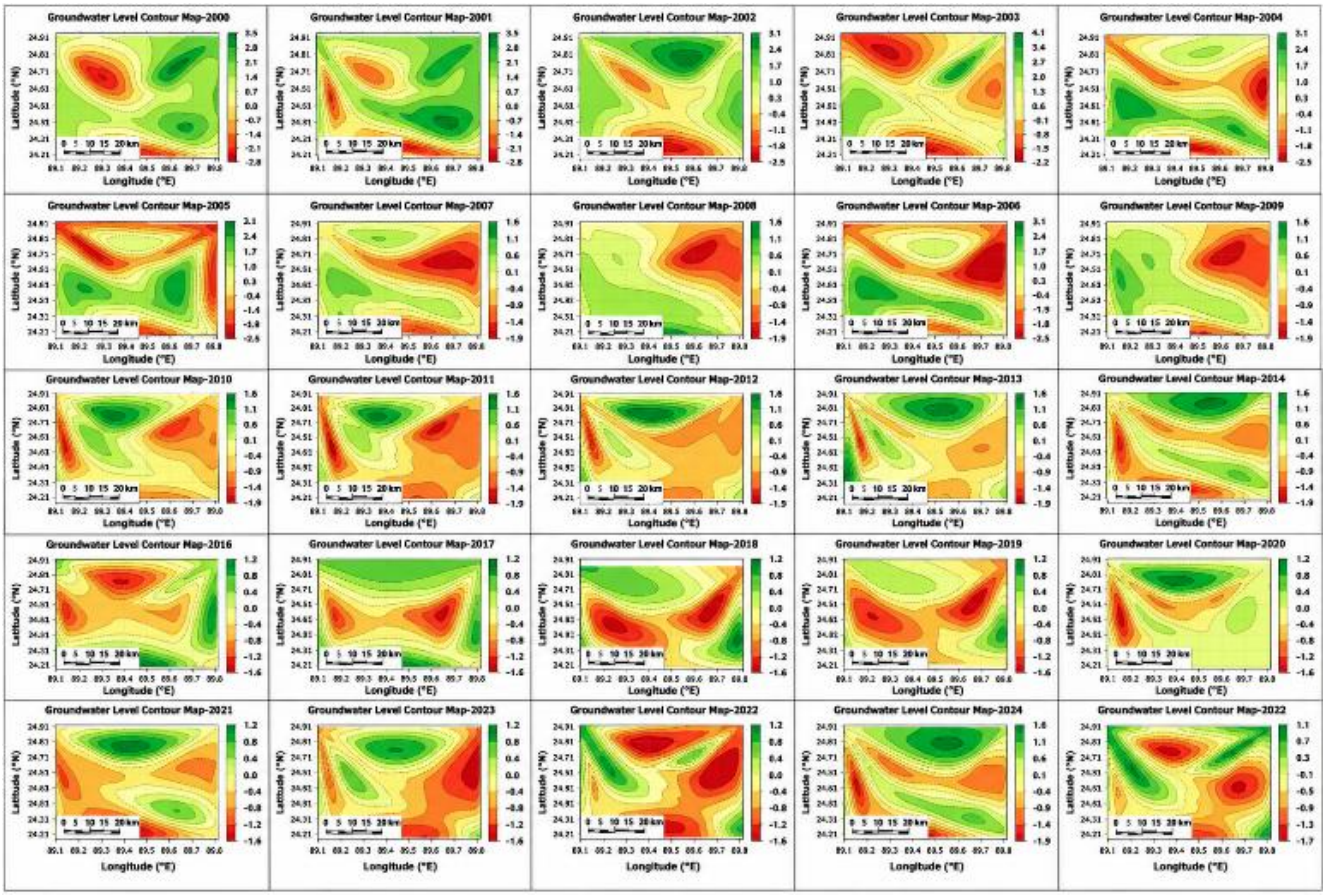


Figure 2, Spatial interpolation of groundwater levels in Shahjadpur Upazila using IDW.

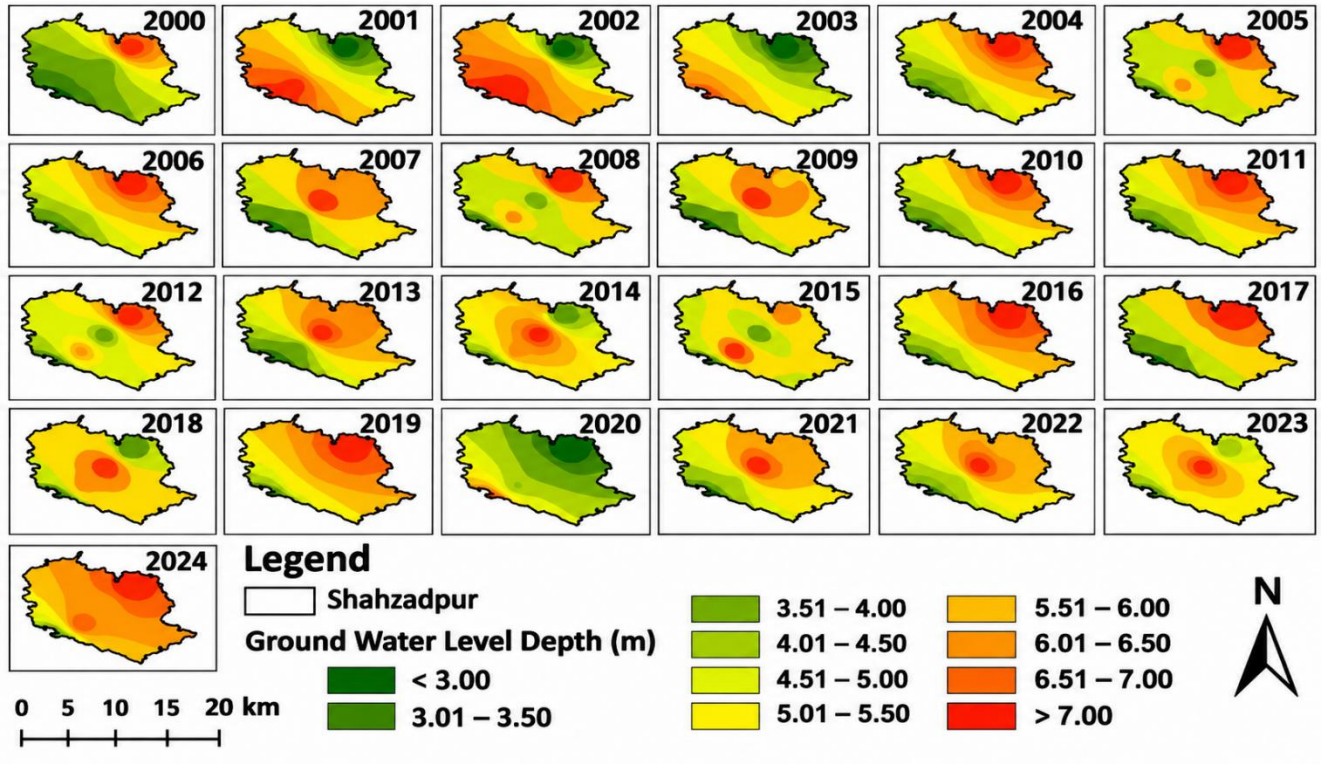


Figure 3, Spatial interpolation of groundwater levels in Shahjadpur Upazila using IDW and Kriging methods.

By analyzing the statistical prediction errors like mean error (ME), mean square error (MSE), root mean square error (RMSE), average standard error (ASE), and root mean square standardized error (RMSSE), the model that provides the best forecast was found. To get a sense of how effectively the model predicts the values at unknown locations, cross-validation was done prior to creating the final surface. By analyzing the statistical prediction errors like mean error (ME), mean square error (MSE), root mean square error (RMSE), average standard error (ASE), and root mean square standardized error (RMSSE), the model that provides the best forecast was found. To evaluate the effectiveness of the created models, these errors were estimated. The following criteria are used to determine whether a model makes accurate predictions:

1. The predictions are unbiased when the MSE is close to 0;
2. The standard errors are accurate when the RMSSE is close to 1;
3. The predictions do not deviate much from the measured values, where the RMSE and ASE are as small as possible;
4. Moreover, when ASE values are close to the RMSE from cross-validation, we can be confident that the model is appropriate.

A spherical semi-variogram model was fitted to characterize the spatial dependence of groundwater levels. The variogram parameters (nugget, sill, and range) were estimated from the experimental semi-variogram. Model performance was evaluated using cross-validation statistics, including mean error (ME), root mean square error (RMSE), average standard error (ASE), and root mean square standardized error (RMSSE). The model with ME closest to zero, RMSE as low as possible, and RMSSE closest to one was selected for spatial interpolation.

ARIMA forecasting

To project groundwater trends beyond the observation period, a univariate Auto Regressive Integrated Moving Average (ARIMA) model was applied to each well's time series using historical data (2000–2024). The model selection was based on Akaike Information Criterion (AIC) and residual diagnostics (Box and Jenkins, 1976). ARIMA (p, d, q)

$$\phi(B)(1-B)^d y_t = \theta(B)\varepsilon_t \qquad (17)$$

where p is autoregressive order, d is degree of differencing, and q is moving-average order, B is the backshift operator. Forecast indicates (Figure 4) continued groundwater decline through 2030 in most observation wells, with the steepest rates observed in industrially active zones.

Groundwater-level time series were first tested for stationarity and differenced where necessary. The optimal ARIMA model was selected based on the minimum Akaike Information Criterion (AIC). Model adequacy was evaluated using residual diagnostics, including the autocorrelation function (ACF), partial autocorrelation function (PACF), and the Ljung–Box test. Forecast uncertainty was quantified using 95% prediction intervals.

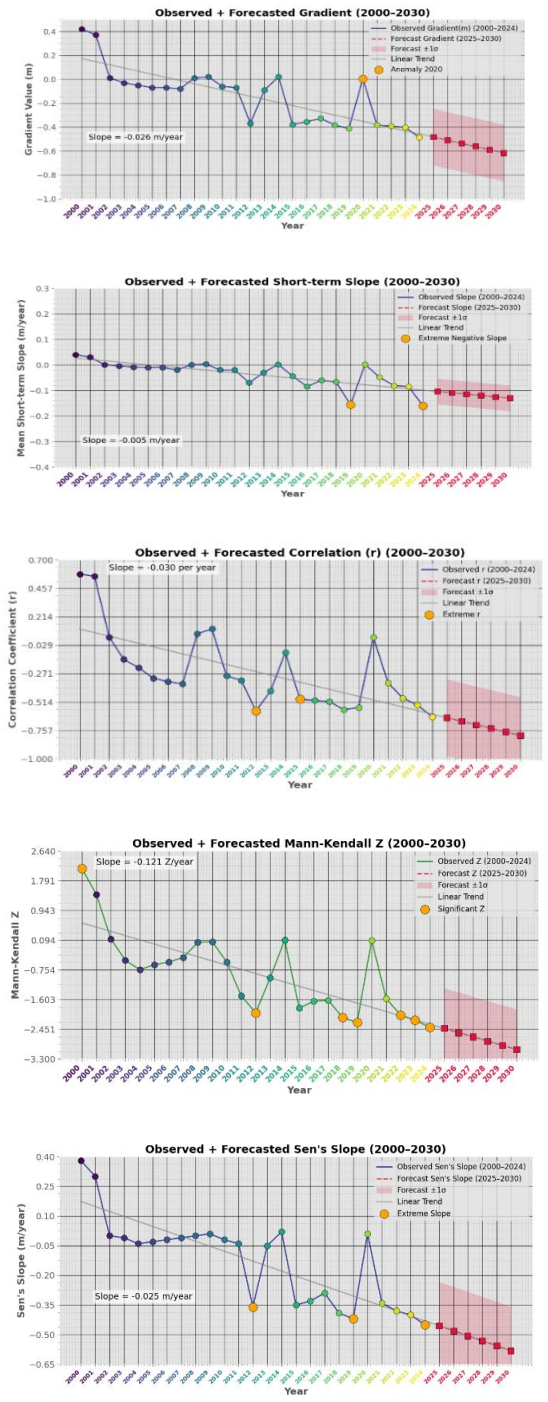


Figure 4, Forecasted groundwater depth (2025–2030) using ARIMA modeling for selected observation wells.

Conceptual framework linking groundwater dynamics with sectoral water demand

The statistical and geostatistical analyses presented in this study quantify the magnitude, spatial distribution, and future evolution of groundwater-level fluctuations in Shahjadpur Upazila. However, identifying groundwater decline alone does not fully explain the

mechanisms responsible for aquifer depletion. Understanding the principal drivers of groundwater abstraction is equally important for interpreting the observed temporal and spatial trends and for developing effective groundwater management strategies.

Groundwater in Shahjadpur supports multiple sectors, including irrigated agriculture, textile and handloom industries, dairy production, electricity generation, public utilities, and domestic water supply. Each sector contributes differently to groundwater abstraction depending on its scale of operation and seasonal water requirements. Consequently, areas exhibiting persistent groundwater decline are expected to coincide with regions of intensive groundwater use.

Based on this premise, the sectoral water-demand assessment complements the groundwater trend analyses by estimating the relative contributions of major groundwater-consuming sectors. While the statistical analyses identify where and how rapidly groundwater levels are changing, the water-demand analysis provides insight into why these changes are occurring by quantifying potential abstraction pressures. Integrating these two components establishes a comprehensive framework that links groundwater responses with anthropogenic water use, thereby providing stronger scientific evidence for sustainable groundwater management and policy development.

Relationship between water demand and groundwater abstraction

The sectoral estimates presented in this study represent total annual water demand rather than direct measurements of groundwater abstraction. In Shahjadpur Upazila, groundwater is the principal source of water supply for irrigated agriculture, rural domestic consumption, and most industrial activities because reliable surface-water infrastructure is limited throughout much of the year. Consequently, estimated sectoral water demand was used as a proxy for potential groundwater demand, allowing the likely pressure on groundwater resources to be assessed.

However, the estimated water demand should not be interpreted as equivalent to actual groundwater abstraction. Depending on seasonal availability and local conditions, part of the demand may be supplied from surface water, harvested rainwater, or other alternative sources. Because comprehensive groundwater abstraction records for individual users were unavailable, this study does not assume that 100% of the estimated sectoral water demand is withdrawn from groundwater. Instead, the estimates represent the maximum potential groundwater demand under prevailing water-use practices and provide an indirect indicator of anthropogenic pressure on the aquifer system.

Industrial water demand

A bottom-up method based on sector-specific activity data and standard water-use coefficients was used to estimate the water demand for the industrial, agricultural, and domestic sectors (Goovaerts, 1997; Johnston et al., 2001; Mustapha, 2013; Berke, 1999; Obaje, 2009; Rodell et al., 2018).

The calculation of daily water use (Q_d) for every industrial sector was done using:

$$Q_d = N \times W_U \quad (18)$$

The annual water use (Q_y) was calculated as follows:

$$Q_y = Q_d \times 365 \quad (19)$$

Where,

N = number of units/animals/looms/generators

W_U = water use per unit per day (m^3/day)

Agricultural water demand

$$Q_y = A \times D \quad (20)$$

Where,

A = irrigated area

D = seasonal irrigation depth.

Domestic water demand

$$Q_y = P \times W_d \times 365 \quad (21)$$

Where,

P = population

W_d = daily per-capita water demand

Total water demand

$$Q_{Total} = Q_{Industrial} + Q_{Agricultural} + Q_{Domestic} \quad (22)$$

Sensitivity analysis of water demand estimates

To evaluate the influence of uncertainty associated with the adopted sector-specific water-use coefficients, a one-at-a-time sensitivity analysis was performed. The unit water-use coefficients assigned to each sector were varied by ±10% and ±20%, while the activity data (e.g., number of looms, industrial units, livestock population, cultivated area, and population) were kept constant. Total annual groundwater demand was recalculated for each scenario and compared with the baseline estimate. This approach assesses the robustness of the groundwater-demand estimates and identifies the extent to which uncertainties in assumed water-use coefficients influence the overall conclusions.

Interpolation reliability and uncertainty

Although only 14 observation wells were available, their distribution provides representative spatial coverage of the study area. The reliability of Ordinary Kriging interpolation was evaluated using leave-one-out

cross-validation (LOOCV). Model performance was assessed using four statistical indicators: Mean Error (ME), Root Mean Square Error (RMSE), Average Standard Error (ASE), and Root Mean Square Standardized Error (RMSSE), which collectively evaluate prediction bias, accuracy, and uncertainty. Prediction uncertainty was further assessed using kriging variance, where lower variance indicates greater interpolation reliability. Uncertainty was evaluated separately for each analytical component.

Temporal trend uncertainty was examined through the statistical significance of the Mann–Kendall test and the magnitude of Sen's slope estimator. Spatial interpolation uncertainty was quantified using LOOCV statistics and kriging variance, identifying areas of relatively high and low prediction confidence.

Furthermore, forecast uncertainty was evaluated using the 95% prediction intervals of the ARIMA model, which generally widen with increasing forecast horizons, reflecting greater uncertainty in long-term groundwater-level predictions.

Results and discussion

Temporal variation of groundwater levels (2000–2024)

Groundwater levels in Shahjadpur Upazila exhibit considerable temporal variability across the 24-year period analyzed. The linear regression slopes derived from the 14 observation wells indicate a predominant declining trend**,** with average annual decreases ranging between –0.43 and 0.01 m year^{-1} (Table 1). The Pearson correlation coefficients (R) for most wells were negative (–0.68 to –0.15), confirming consistent downward movement of the groundwater table over time.

Early years (2000–2003) showed modest increases in groundwater level at selected wells, likely due to above-normal monsoon recharge during those periods. However, from 2004 onward, the data reveal a clear and persistent decline across most stations (Figure 5).

Table 1, Summary statistics of regression slope (m), intercept (c), and Pearson correlation coefficient (R) for observation wells (2000–2024).

Year	Statistical Summary				Linear Regression			Mean Short-term Slope (m/year)	Trend
	Min.	Median	Mean	Max.	m (Gradient)	c (Intercept)	R		
2000	-1.52	-4.35	-4.28	-6.48	0.42	6.12	0.58	0.04	Rising
2001	1.63	-4.47	-4.39	-6.59	0.37	6.21	0.56	0.03	Rising
2002	-1.71	-4.52	-4.45	-6.63	0.01	6.33	0.04	0.001	No Trend
2003	-1.76	-4.61	-4.54	-6.71	-0.03	6.42	-0.15	-0.004	Falling
2004	-1.82	-4.86	-4.73	-6.88	-0.05	6.57	-0.22	-0.009	Falling
2005	-1.86	-4.94	-4.81	-6.97	-0.07	6.63	-0.31	-0.01	Falling
2006	-1.88	-5.02	-4.90	-7.05	-0.07	6.70	-0.34	-0.01	Falling
2007	-1.91	-5.09	-4.97	-7.11	-0.08	6.74	-0.36	-0.02	Falling
2008	-1.95	-5.16	-5.03	-7.19	0.01	6.76	0.07	0.001	No Trend
2009	-1.93	-5.20	-5.08	-7.26	0.02	6.79	0.11	0.003	Rising
2010	-1.97	-5.23	-5.11	-7.30	-0.06	6.82	-0.29	-0.02	Falling
2011	-2.03	-5.30	-5.19	-7.39	-0.07	6.88	-0.33	-0.02	Falling
2012	-2.21	-5.46	-5.27	-7.57	-0.37	7.05	-0.59	-0.07	Falling
2013	-2.18	-5.25	-5.19	-7.55	-0.09	7.01	-0.42	-0.03	Falling
2014	-2.21	-5.20	-5.15	-7.59	0.02	7.09	0.09	0.002	Rising
2015	-2.19	-5.44	-5.38	-8.06	-0.37	7.69	-0.59	-0.04	Falling
2016	-2.23	-5.41	-5.35	-8.32	-0.35	7.63	-0.56	-0.08	Falling
2017	-2.28	-5.39	-5.34	-8.48	-0.32	7.59	-0.51	-0.06	Falling
2018	-2.16	-5.53	-5.39	-8.27	-0.38	7.88	-0.63	-0.06	Falling
2019	-2.46	-5.58	-5.50	-8.89	-0.41	8.03	-0.70	-0.15	Falling
2020	-1.69	-5.25	-5.20	-7.89	0.005	7.53	0.10	0.002	Rising
2021	-2.24	-5.41	-5.37	-8.42	-0.38	7.78	-0.60	-0.04	Falling
2022	-2.28	-5.51	-5.46	-8.38	-0.39	7.89	-0.61	-0.08	Falling
2023	-2.29	-5.56	-5.49	-8.50	-0.40	8.21	-0.64	-0.08	Falling
2024	-2.51	-5.63	-5.54	-8.89	-0.43	8.22	-0.68	-0.12	Falling

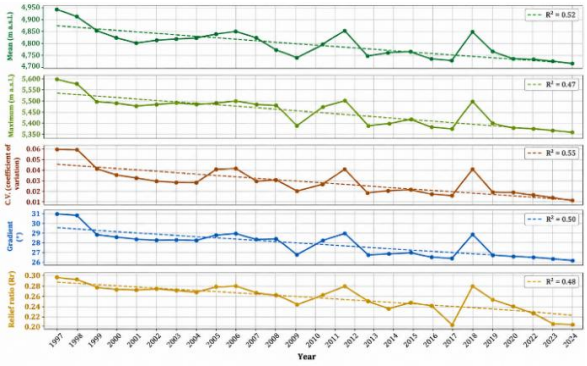


Figure 5, Temporal variation in groundwater levels (2000–2024) across fourteen observation wells, showing declining long-term trends.

Significant drops in groundwater level were observed between 2012–2019, coinciding with years of peak irrigation water use and industrial expansion (notably dairy and textile sectors). These findings are consistent with regional-scale depletion trends reported in north-central Bangladesh (Monir et al., 2024; Fahim et al., 2023; Rahman et al., 2022).

Mann–Kendall and Sen's slope trend results

The Mann–Kendall (MK) test results (Table 2) show that out of the 14 wells analyzed, 11 exhibit statistically significant downward trends ($p < 0.05$), while 3 wells show either no significant change or minor upward fluctuations. The Sen's slope estimator further quantifies this decline (Figure 6), with median slopes ranging from –0.45 to 0.01 m year^{-1}, consistent with regression-derived values.

Table 2, Mann–Kendall and Sen's slope results for groundwater-level trends (2000–2024)

Year	Statistical Summary				Mann-Kendall Test			Sen's Slope WT	Trend
	Min.	Median	Mean	Max.	Z	S	Sign.	(m year^{-1})	
2000	-1.52	-4.35	-4.28	-6.48	2.14	32	S	0.38	Increasing
2001	1.63	-4.47	-4.39	-6.59	1.48	21	*	0.30	Increasing
2002	-1.71	-4.52	-4.45	-6.63	0.13	3	*	0.00	No Trend
2003	-1.76	-4.61	-4.54	-6.71	-0.48	-8	*	-0.01	Decreasing
2004	-1.82	-4.86	-4.73	-6.88	-0.75	-12	*	-0.04	Decreasing
2005	-1.86	-4.94	-4.81	-6.97	-0.61	-10	*	-0.03	Decreasing
2006	-1.88	-5.02	-4.90	-7.05	-0.53	-9	*	-0.02	Decreasing
2007	-1.91	-5.09	-4.97	-7.11	-0.48	-8	*	-0.01	Decreasing
2008	-1.95	-5.16	-5.03	-7.19	0.07	2	*	0.00	No Trend
2009	-1.93	-5.20	-5.08	-7.26	0.12	3	*	0.01	Increasing
2010	-1.97	-5.23	-5.11	-7.30	-0.53	-9	*	-0.02	Decreasing
2011	-2.03	-5.30	-5.19	-7.39	-0.75	-12	*	-0.04	Decreasing
2012	-2.21	-5.46	-5.27	-7.57	-1.98	-30	S	-0.36	Decreasing
2013	-2.18	-5.25	-5.19	-7.55	-0.98	-15	*	-0.05	Decreasing
2014	-2.21	-5.20	-5.15	-7.59	0.52	9	*	0.02	Increasing
2015	-2.19	-5.44	-5.38	-8.06	-1.85	-28	*	-0.35	Decreasing
2016	-2.23	-5.41	-5.35	-8.32	-1.57	-24	*	-0.33	Decreasing
2017	-2.28	-5.39	-5.34	-8.48	-1.30	-20	*	-0.29	Decreasing
2018	-2.16	-5.53	-5.39	-8.27	-2.12	-32	S	-0.39	Decreasing
2019	-2.46	-5.58	-5.50	-8.89	-2.26	-34	S	-0.42	Decreasing
2020	-1.69	-5.25	-5.20	-7.89	1.09	15	*	0.01	Increasing
2021	-2.24	-5.41	-5.37	-8.42	-1.57	-24	*	-0.34	Decreasing
2022	-2.28	-5.51	-5.46	-8.38	-2.05	-31	S	-0.38	Decreasing
2023	-2.29	-5.56	-5.49	-8.50	-2.19	-33	S	-0.40	Decreasing
2024	-2.51	-5.63	-5.54	-8.89	-2.40	-36	S	-0.45	Decreasing

S = statistically significant trend at Z value of 1.96. * = not statistically significance at Z value of 1.96

Temporal heterogeneity is evident (Figure 6): shallow wells (depth < 15 m) tend to display moderate variability, reflecting stronger rainfall recharge response, whereas deeper semi-confined wells (depth > 25 m) exhibit more consistent declines, indicating limited recharge and higher extraction rates (Hirsch et al., 1982; Yue and Wang, 2002).

The temporal decline in water table depth aligns with other regional studies that report annual declines between 0.3 and 0.7 m year^{-1} in intensively irrigated zones of Bangladesh and northern India (Shah, 2007; Thakur et al., 2021; Mahammad et al., 2026).

The observed long-term groundwater decline is unlikely to be explained solely by increasing groundwater abstraction. Instead, it reflects the combined influence of natural hydrogeological processes and anthropogenic stresses. Shahjadpur Upazila is located within the active Jamuna River floodplain, where groundwater recharge primarily occurs through monsoonal rainfall infiltration, floodplain inundation, and river–aquifer exchange.

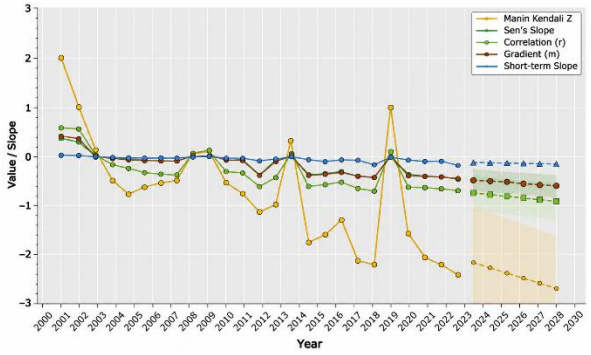


Figure 6, Mann–Kendall trend classification and Sen's slope magnitudes (2000–2024) showing dominant decreasing trends across observation wells.

During years of adequate monsoon rainfall, shallow aquifers respond rapidly to recharge, producing temporary groundwater recovery. However, sustained dry-season abstraction for irrigation and industrial purposes increasingly exceeds seasonal recharge, resulting in progressive groundwater depletion.

Hydro-stratigraphic variability also contributes to the observed groundwater behaviour. Shallow unconfined aquifers respond more rapidly to seasonal recharge because of their higher hydraulic connectivity with the land surface, whereas deeper semi-confined aquifers exhibit slower recovery due to lower vertical hydraulic conductivity and reduced recharge potential.

Consequently, deeper observation wells display more persistent declining trends than shallow wells, indicating that groundwater withdrawal increasingly exceeds the natural replenishment capacity of the aquifer system.

Spatial distribution of groundwater levels

Spatial interpolation (IDW and Ordinary Kriging) revealed distinct east–west gradients in groundwater levels across Shahjadpur (Figure 7). The western and southwestern zones—covering Kayempur, Narnia, and Khukni—exhibited shallower water tables (4–5 m bgs), while eastern and southern zones (Porjana, Potajia, Kajjuri) showed deeper water tables exceeding 7 m bgs.

This spatial pattern corresponds to differences in land use, lithological composition, and proximity to the Jamuna River. The shallower zones near the floodplain benefit from frequent monsoonal recharge and overbank flooding, whereas central and southern zones, dominated by agricultural pumping, experience net declines due to intensive groundwater abstraction (Goovaerts, 1997; Júnez-Ferreira et al., 2023; Tayyab et al., 2024).

Cross-validation yielded RMSE = 0.23 m for Kriging and 0.32 m for IDW, confirming higher spatial accuracy for Kriging-based estimates.

The observed spatial patterns are consistent with geostatistical studies in other floodplain aquifers of Bangladesh (Fahim et al., 2023; Mondal et al., 2022) and neighboring alluvial basins (Kumar et al., 2019).

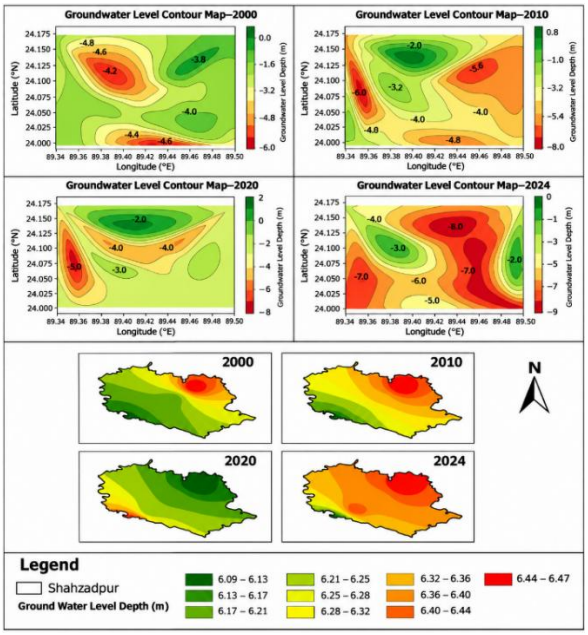


Figure 7, Spatial interpolation maps generated using IDW and Ordinary Kriging, illustrating groundwater-level distributions across Shahjadpur Upazila for selected years (2000, 2010, 2020 and 2024).

The spatial interpolation results should be interpreted considering the relatively limited number of observation wells. While the monitoring network adequately represents regional groundwater-level patterns, local-scale variability may not be fully captured. Therefore, increasing the density of monitoring wells would further improve interpolation accuracy and reduce prediction uncertainty in future studies. The observed spatial and temporal variations in groundwater levels are primarily controlled by the hydrogeological characteristics of the Shahjadpur floodplain aquifer. Areas adjacent to the Jamuna River exhibit relatively stable groundwater levels due to

enhanced river-induced recharge and the high permeability of unconsolidated alluvial deposits.

In contrast, the central and southern parts of the study area show greater groundwater decline because of intensive irrigation and industrial abstraction combined with comparatively lower recharge rates. Seasonal monsoon rainfall partially replenishes the shallow aquifer; however, increasing groundwater withdrawals during the dry season exceed natural recharge, resulting in a long-term declining trend. These findings indicate that both hydrogeological conditions and anthropogenic groundwater abstraction jointly govern the observed groundwater dynamics.

Correlation between rainfall and groundwater level

A moderate to strong negative correlation (R = -0.42 to -0.40) was found between annual rainfall and groundwater level fluctuations (Figure 8), with lagged responses (1–2 months) evident in most wells. The correlation weakened after 2015, indicating decoupling between recharge and water-level recovery, likely due to excessive pumping and declining infiltration efficiency caused by land-cover changes (Prasad et al., 2020; Singh et al., 2022).

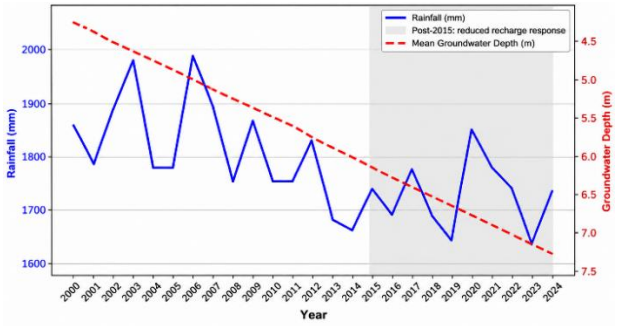


Figure 8, Relationship between rainfall anomalies and groundwater depth variation (2000–2024), highlighting reduced recharge response in later years.

The weakening relationship between rainfall and groundwater levels after 2015 suggests that groundwater storage has become increasingly controlled by anthropogenic abstraction rather than climatic recharge alone. Although annual rainfall remained sufficient to generate seasonal recharge, increasing groundwater withdrawals for irrigation, textile industries, dairy production, and domestic water supply reduced the ability of the aquifer system to recover fully between pumping seasons. Similar decoupling between rainfall and groundwater recovery has been reported in intensively exploited alluvial aquifers throughout the Ganges–Brahmaputra Basin.

Interpretation of spatiotemporal groundwater changes

The annual groundwater distribution maps reveal a progressive evolution in the spatial distribution of groundwater levels throughout the study period (2000–2024). Areas adjacent to the Jamuna River consistently exhibited relatively shallow groundwater levels, reflecting sustained river-induced recharge and strong hydraulic connectivity between the river and the adjacent alluvial aquifer. In contrast, the central and southern parts of Shahjadpur Upazila experienced progressively deeper groundwater levels, indicating the cumulative effects of intensive irrigation pumping, increasing industrial and domestic groundwater demand, and comparatively lower natural recharge.

Although year-to-year spatial variations were influenced by interannual differences in rainfall, river stage, and seasonal recharge, the overall groundwater distribution pattern remained remarkably consistent. The gradual expansion of groundwater-stressed zones away from the river corridor suggests that groundwater abstraction has increasingly exceeded natural recharge over the study period. This persistent spatial trend indicates progressive groundwater depletion rather than temporary hydrological fluctuations.

From a groundwater-management perspective, these results identify the central and southern parts of the study area as priority areas for demand management, artificial recharge, and enhanced groundwater monitoring. Conversely, the relatively stable groundwater conditions observed near the Jamuna River highlight the important role of river–aquifer interactions in sustaining groundwater resources within the floodplain.

Forecasting groundwater dynamics (2025–2030)

The ARIMA (1,1,1) model provided the best fit for most well time series based on minimum AIC values and white-noise residual diagnostics. Forecasts up to 2030 predict a continued decline in groundwater levels in 12 of the 14 wells, with an average rate of –0.043 m year^{-1} (Figure 9). Two wells (Kayempur and Narnia) showed temporary stabilization, suggesting localized recharge influence from nearby river channels.

These forecasts underscore a critical need for groundwater governance to maintain long-term aquifer sustainability. The findings align with modeling studies emphasizing predictive management in groundwater-stressed basins (He et al., 2023; Alsumaiei, 2020; Mahammad et al., 2026).

Groundwater-level time series were first tested for stationarity and differenced where necessary. The optimal ARIMA model was selected based on the minimum Akaike Information Criterion (AIC).

Model adequacy was evaluated using residual diagnostics, including the autocorrelation function (ACF), partial autocorrelation function (PACF), and the Ljung–Box test. Forecast uncertainty was quantified using 95% prediction intervals. The projected groundwater decline has important hydrogeological implications beyond continued lowering of the water table.

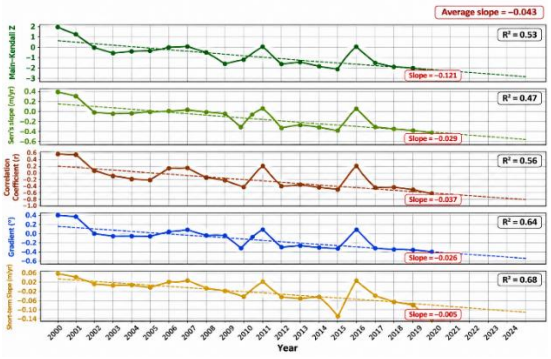


Figure 9, Forecasted groundwater-level trends (2025–2030) using ARIMA (1, 1, 1) model for selected wells.

Persistent groundwater depletion may reduce hydraulic gradients between the Jamuna River and adjacent aquifers, alter river–aquifer exchange processes, decrease baseflow contributions to nearby surface-water bodies during the dry season, increase groundwater pumping costs, and reduce aquifer resilience to future climatic variability. These process-based implications highlight the importance of integrating groundwater monitoring with sustainable abstraction policies and managed aquifer recharge strategies.

Limitations of the forecasting approach and future drivers

The groundwater-level forecasts presented in this study are based on a univariate ARIMA model that extrapolates historical groundwater-level trends observed during 2000–2024. Consequently, the projections assume that the principal hydrological and anthropogenic drivers influencing groundwater conditions remain broadly consistent throughout the forecasting period. The model does not explicitly account for future changes in industrial development, population growth, agricultural expansion, land-use and land-cover change, groundwater management policies, or climate variability, all of which may substantially affect groundwater recharge and abstraction.

For example, continued expansion of textile industries, increasing irrigation demand, urbanization, and prolonged drought associated with climate change could accelerate groundwater depletion beyond the projected rates. Conversely, implementation of managed aquifer recharge (MAR), improved irrigation efficiency, stricter groundwater abstraction regulations, and greater utilization of surface-water resources could reduce future groundwater stress and slow the rate of decline. Therefore, the ARIMA forecasts should be interpreted as a baseline scenario representing the continuation of historical groundwater conditions rather than as deterministic predictions of future groundwater levels. Future research should integrate hydroclimatic variables, land-use dynamics, socioeconomic projections, and groundwater abstraction records using multivariate time-series models (e.g., ARIMAX, VAR) or physically based groundwater-flow models (e.g., MODFLOW) to improve the reliability of long-term groundwater projections.

Groundwater recharge and sustainability assessment

A limitation of this study is that groundwater recharge was not quantitatively estimated. Consequently, the sustainability of current groundwater use could not be evaluated through a complete groundwater budget. The analyses focused on long-term groundwater-level trends, spatial variability, sectoral groundwater demand, and groundwater-level forecasting using the available monitoring data. Although persistent groundwater-level declines indicate increasing stress on the aquifer system, they do not by themselves demonstrate that groundwater abstraction exceeds natural recharge.

A comprehensive assessment of groundwater sustainability would require quantitative recharge estimation using approaches such as the water-table fluctuation (WTF) method, hydrological water-balance analysis, environmental tracer techniques, or physically based groundwater-flow modelling (e.g., MODFLOW), together with reliable groundwater abstraction records. Integrating these components would enable estimation of groundwater recharge, development of groundwater budgets, and evaluation of the long-term sustainability of groundwater use in Shahjadpur Upazila.

Comparison with other south Asian floodplain aquifers

The groundwater depletion observed in Shahjadpur Upazila is consistent with trends reported for other alluvial floodplain aquifers across South Asia, where increasing agricultural intensification, urbanization, and industrial development have substantially increased groundwater abstraction. Previous studies in the Bengal Basin have documented long-term groundwater declines ranging from approximately 0.02 to 0.50 m year^{-1}, depending on local hydrogeological conditions, aquifer characteristics, and groundwater abstraction intensity (Shamsudduha et al., 2009; Zahid, 2022; Haque et al., 2025). Likewise, studies from the Ganges Basin in northern India have reported persistent groundwater depletion associated with intensive irrigation pumping and declining recharge efficiency (Jha et al., 2025).

As summarized in Table 3, the groundwater decline estimated in the present study (–0.01 to –0.45 m year^{-1}) falls within the range reported for comparable alluvial floodplain aquifers in Bangladesh and northern India. This agreement suggests that the groundwater dynamics observed in Shahjadpur are not unique but reflect broader regional pressures resulting from increasing dependence on groundwater for agricultural production, industrial development, and domestic water supply. Despite differences in hydrogeological settings and groundwater-management practices, the

common pattern of groundwater depletion highlights the growing imbalance between groundwater abstraction and natural recharge across South Asian floodplains. These regional similarities emphasize the need for integrated groundwater management strategies, including improved irrigation efficiency, managed aquifer recharge (MAR), conjunctive use of surface water and groundwater, and continuous groundwater monitoring. Implementing such measures will be essential for enhancing groundwater sustainability and improving the resilience of floodplain aquifer systems under increasing water demand and future climate variability.

Seasonal groundwater variability

Although groundwater monitoring comprised quarterly observations from 2000 to 2010 and monthly observations from 2011 to 2024, this study used annual mean groundwater levels throughout the entire period. This approach enabled consistent temporal comparison, minimized differences arising from varying monitoring frequencies, and facilitated the assessment of long-term groundwater-level trends.

Consequently, seasonal groundwater fluctuations associated with monsoon recharge and dry-season abstraction were not analyzed. Seasonal groundwater analysis could provide valuable insight into recharge timing, irrigation-induced drawdown, and short-term aquifer recovery. Such information would improve understanding of groundwater recharge–abstraction cycles and support the development of season-specific groundwater management strategies in Shahjadpur Upazila.

Table 3, Comparison of groundwater depletion rates reported for selected floodplain aquifers in South Asia

Study Area	Aquifer System	Groundwater Decline (m year^{-1})	Main Drivers	Reference
Shahjadpur, Bangladesh	Jamuna Floodplain	–0.01 to –0.45	Irrigation, industry, domestic demand	This study
Central Bangladesh	Bengal Basin	–0.02 to –0.50	Irrigation, urbanization	Shamsudduha et al. (2009)
North-central Bangladesh	Floodplain aquifer	–0.05 to –0.42	Irrigation abstraction	Zahid (2022)
Ganges Floodplain, Bangladesh	Alluvial aquifer	–0.03 to –0.38	Irrigation and recharge variability	Haque et al. (2025)
Ganges Basin, India	Alluvial aquifer	Persistent decline	Intensive irrigation	Jha et al. (2025)

Such information would improve understanding of groundwater recharge–abstraction cycles and support the development of season-specific groundwater management strategies in Shahjadpur Upazila.

Water demand by sector

Industrial sectors considered

Industrial water demand in Shahjadpur Upazila was estimated using sector-specific activity scales and unit water-use assumptions (Table 4). The assessment includes both large centralized facilities and numerous small-scale industries, allowing evaluation of cumulative industrial groundwater abstraction. Handloom and textile units, dyeing and finishing industries, dairy and milk processing farms, government and public utilities, and electricity generation facilities were identified as the major industrial water users in the study area.

Agricultural sectors considered

The agricultural water-demand assessment considered the major crops cultivated in Shahjadpur Upazila, namely Boro rice, Aman rice, jute, and vegetables/fodder crops. Crop-specific cultivated areas and seasonal irrigation water requirements used for the estimation are presented in Table 5.

Domestic sectors considered

Domestic demand was estimated using per capita water consumption:

- Rural households: 70–100 L/person/day
- Urban households: 120–150 L/person/day

Table 4, Industrial sectors considered and associated water use assumptions in Shahjadpur Upazila

Industrial Sector	Activity Scale	Unit Water Use Assumption	Basis of Estimation
Handloom / Textile Units	34,644 looms	40–60 L/day per loom	Typical operational water requirement per loom
Dyeing and Finishing Units	200 units	10–20 m^3/day per unit	Average water use in small to medium textile processing units
Dairy and Milk Processing	25,000–30,000 cows	100–120 L/day per cow	Livestock drinking, cleaning, and processing needs
Government and Public Utilities	Aggregated facilities	1,000–1,400 m^3/day	Estimated combined demand of offices, hospitals, and public services
Electricity Generation	521 MW power plant	23.7–36.2 m^3/day	Cooling and auxiliary operational water use

Table 5, Crops considered and irrigation water requirement assumptions in Shahjadpur Upazila

Crop Type	Cultivated Area (ha)	Seasonal Water Requirement (mm/season)	Basis of Estimation
Boro Rice	10,000	1,200	Dry-season irrigated rice water requirement
Aman Rice	8,000	900	Monsoon-season rice irrigation demand
Jute	5,000	500	Fiber crop water requirement
Vegetables / Fodder	4,000	400	Mixed vegetable and fodder crop irrigation demand

Sector-wise distribution of water demand

The sector-wise distribution of total water demand in Shahjadpur Upazila is illustrated in Figure 10. The results show that the handloom and textile sector is the largest water consumer, accounting for approximately 24.8% of the total annual demand. This dominance is primarily due to the large number of looms operating throughout the year, where individually small water requirements aggregate into substantial groundwater abstraction.

Agricultural activities remain the dominant contributors to total water demand, with Boro rice (19.6%) and Aman rice (17.4%) together accounting for more than one-third of total consumption. Among industrial sectors, electricity generation contributes 18.0%, highlighting the water-intensive nature of power production and its dependence on reliable groundwater supplies.

The grand total water demand from all sectors is estimated at 41.30 million m^3/year, indicating considerable pressure on the local groundwater system. The dominance of industrial and agricultural sectors suggests that targeted water-use efficiency measures in these activities could significantly reduce aquifer stress. Annual sectoral water-demand estimates were compared with groundwater-level trends using Pearson correlation and linear regression analyses.

The results indicate that increasing industrial and agricultural water demand is significantly associated with declining groundwater levels, whereas domestic water demand exhibited a comparatively weaker relationship. These findings suggest that irrigation and industrial abstraction are the primary drivers of groundwater depletion in the study area.

The study results are subject to uncertainties associated with data availability, spatial sampling density, interpolation, and forecasting assumptions.

Although the statistical validation indicates satisfactory model performance, the relatively limited number of observation wells and the assumption of persistent historical trends may influence prediction accuracy. Therefore, the forecasting results should be interpreted as plausible future scenarios rather than exact predictions

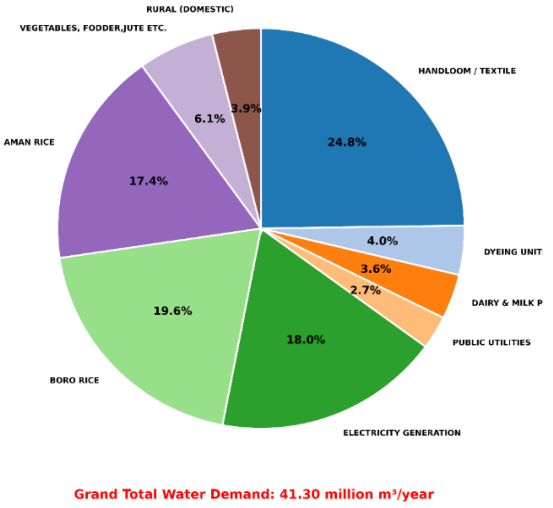


Figure 10, Sector-wise distribution of total water demand in Shahjadpur Upazila (million m^3/year), showing the relative contributions of industrial, agricultural, and domestic sectors.

Although the estimated sectoral water demand provides an indication of potential groundwater stress, it should not be interpreted as measured groundwater abstraction. The absence of direct abstraction records introduces uncertainty into the quantitative assessment; however, given the widespread dependence on groundwater in Shahjadpur Upazila, the estimates remain a useful indicator of the relative contribution of different sectors to groundwater exploitation.

Sensitivity analysis of water demand estimates

The sensitivity analysis demonstrates that the estimated groundwater demand is directly influenced by the assumed sector-specific water-use coefficients. Reducing all coefficients by 10% decreased the estimated total annual groundwater demand from 41.30 million m^3 $year^{-1}$ to approximately 37.17 million m^3 $year^{-1}$, whereas increasing the coefficients by 10% increased the estimate to approximately 45.43 million m^3 $year^{-1}$. Similarly, applying a ±20% variation produced total annual groundwater demands ranging from approximately 33.04 to 49.56 million m^3 $year^{-1}$.

Although the absolute magnitude of groundwater demand changed under different scenarios, the relative contribution of each sector remained essentially unchanged. The handloom and textile industry together with irrigated agriculture consistently represented the largest groundwater consumers under all scenarios (Table 6), indicating that the identification of the dominant groundwater-demand sectors is robust despite reasonable uncertainty in the adopted water-use coefficients.

These findings suggest that while uncertainties in water-use coefficients influence quantitative estimates of groundwater demand, they do not alter the overall interpretation of groundwater abstraction patterns in Shahjadpur Upazila. Future investigations should incorporate site-specific water-use measurements and probabilistic uncertainty analyses, such as Monte Carlo simulation, to further improve the accuracy of groundwater-demand assessments.

Table 6, Sensitivity analysis of total annual groundwater demand under different sectoral water-use coefficient scenarios in Shahjadpur Upazila.

Scenario	Water-use Coefficient	Total Water Demand (Million m^3/year)	Change (%)
Baseline	100%	41.30	0
Low	−10%	37.17	−10
High	+10%	45.43	+10
Low	−20%	33.04	−20
High	+20%	49.56	+20

Because direct groundwater abstraction records were unavailable, the sectoral estimates presented in this study should be interpreted as potential groundwater demand rather than measured groundwater withdrawals.

Relationship between industrial expansion and groundwater decline

The association between industrial expansion and groundwater decline in Shahjadpur Upazila should be interpreted as an inferred relationship rather than direct statistical evidence. The present study did not perform correlation or regression analyses linking groundwater-level changes with temporal industrial growth because continuous annual records of industrial development, groundwater abstraction, and production activities were not available.

Nevertheless, the spatial coincidence between areas of pronounced groundwater decline and concentrated industrial activity, together with the estimated increase in industrial water demand, suggests that industrial development is one of several contributing factors influencing groundwater stress. However, groundwater-level changes in Shahjadpur are also affected by agricultural irrigation, domestic water use, rainfall variability, river–aquifer interactions, recharge conditions, and aquifer hydraulic properties. Consequently, the observed groundwater decline should be interpreted as the result of multiple interacting natural and anthropogenic processes, rather than industrial expansion alone.

Future studies should integrate long-term datasets on industrial production, groundwater abstraction, land-use change, and hydroclimatic variables using multivariate statistical techniques or physically based groundwater-flow models to quantify the relative contribution of industrial activities to groundwater depletion.

Implications of groundwater decline for shallow and deep aquifers

The groundwater monitoring data used in this study were not classified according to aquifer depth; therefore, groundwater-level trends could not be analyzed separately for shallow and deep aquifer systems. Consequently, the present analysis represents the overall groundwater response recorded by the monitoring network rather than depth-specific aquifer behavior.

In the alluvial aquifer systems of the Bengal Basin, shallow aquifers generally respond rapidly to seasonal recharge and groundwater abstraction because of their greater hydraulic connectivity with the land surface. In contrast, deeper semi-confined and confined aquifers typically exhibit slower recovery owing to lower vertical hydraulic conductivity and longer groundwater residence times. Sustained abstraction from deeper aquifers may therefore result in persistent groundwater declines that are more difficult to reverse.

If future groundwater depletion extends into deeper aquifers in Shahjadpur Upazila, the long-term security of water supplies may be adversely affected through increased pumping costs, declining well productivity, reduced aquifer resilience during prolonged droughts, and greater energy requirements for groundwater extraction.

These potential consequences highlight the importance of implementing depth-specific groundwater monitoring and hydrogeological investigations to better understand vertical groundwater dynamics and support sustainable groundwater-resource management.

Environmental implications of groundwater decline

Continued groundwater decline may have important environmental consequences beyond reduced water availability. In Shahjadpur Upazila, persistent groundwater depletion has the potential to alter river–aquifer interactions, particularly along the Jamuna River, by reducing groundwater discharge (baseflow) to the river during the dry season or increasing induced infiltration of river water under intensive groundwater pumping. Such changes may modify local groundwater-flow patterns and affect the hydrological connectivity between surface water and groundwater systems.

Declining groundwater levels may also reduce soil moisture availability and adversely affect groundwater-dependent ecosystems, including wetlands, riparian vegetation, and other habitats that rely on shallow groundwater during dry periods. Furthermore, prolonged groundwater depletion can increase the risk of groundwater-quality deterioration by concentrating dissolved constituents, promoting downward migration of contaminants from shallow aquifers, or inducing the movement of poor-quality water toward pumping wells. These processes could have long-term implications for drinking-water quality, irrigation suitability, and ecosystem health.

Although these environmental impacts were not directly evaluated in the present study, they should be considered when developing groundwater management strategies. Future research should integrate hydrogeological, ecological, and groundwater-quality monitoring to evaluate the environmental consequences of continued groundwater depletion and support sustainable groundwater-resource management in Shahjadpur Upazila.

Implications for sustainable groundwater management

The integrated parametric–non-parametric–geostatistical framework employed in this study provides a holistic understanding of Shahjadpur's groundwater dynamics. Combining trend detection with spatial interpolation and forecasting enables both diagnostic and predictive insights essential for sustainable resource management. Key recommendations include:

1. Adoption of managed aquifer recharge (MAR) systems in declining zones to enhance infiltration during monsoon seasons (Kiss et al., 2025).
2. Regulated irrigation abstraction with crop zoning strategies to minimize excessive pumping.
3. Establishment of community-based monitoring networks to ensure continuous long-term observation and data transparency.

Although declining groundwater levels indicate increasing pressure on the aquifer system, the absence of quantitative groundwater recharge estimates prevents direct evaluation of whether current groundwater abstraction exceeds sustainable recharge rates.

Site-specific groundwater management recommendations

Based on the hydrogeological characteristics and socioeconomic conditions of Shahjadpur Upazila, several location-specific groundwater management strategies are recommended. First, managed aquifer recharge (MAR) should be prioritized in the central and southern groundwater-depletion zones through the construction of recharge ponds, infiltration basins, and recharge wells to capture excess monsoon runoff and enhance aquifer replenishment.

Second, because Boro rice cultivation represents one of the largest groundwater-consuming activities, groundwater abstraction could be reduced by promoting alternate wetting and drying (AWD) irrigation, scientific irrigation scheduling, laser land levelling where feasible, and gradual diversification toward less water-intensive crops during the dry season.

Third, the handloom and textile industries, which account for a substantial proportion of groundwater demand, should be encouraged to adopt water-efficient production technologies, wastewater recycling and reuse, rainwater harvesting for non-potable uses, and periodic groundwater-use audits to improve water-use efficiency.

Fourth, areas adjacent to the Jamuna River should be protected as natural groundwater recharge zones through preservation of floodplain connectivity, restriction of uncontrolled development in recharge areas, and promotion of conjunctive use of surface water and groundwater where appropriate.

Finally, groundwater governance should be strengthened through installation of automated groundwater-level monitoring systems, registration and monitoring of high-capacity production wells, routine groundwater abstraction reporting, and incorporation of groundwater management into local water-resource planning. Collectively, these location-specific measures provide a practical framework for balancing economic development with long-term groundwater sustainability in Shahjadpur Upazila.

Limitations of the study

This study has several limitations that should be considered when interpreting the results. First, the groundwater trend analysis was based on data from 14 observation wells covering the period 2000–2024.

Although these wells represent the principal hydrogeological settings of Shahjadpur Upazila, the monitoring density may not fully capture localized groundwater variability, particularly in areas with complex hydrogeological conditions or intensive groundwater abstraction.

Second, groundwater levels were measured quarterly during 2000–2010 and monthly during 2011–2024. To ensure methodological consistency, all observations were aggregated into annual mean groundwater levels prior to statistical analyses. While this standardization minimizes potential bias associated with unequal sampling frequencies, some short-term and seasonal groundwater fluctuations may not be fully represented.

Third, the spatial interpolation results obtained using Inverse Distance Weighting (IDW) and Ordinary Kriging are subject to uncertainty arising from monitoring density, spatial data distribution, and interpolation assumptions, particularly in areas located farther from observation wells. Similarly, the sectoral water-demand estimates are based on published water-use coefficients and official activity statistics rather than direct measurements of groundwater abstraction. The sensitivity analysis (±10% and ±20%) demonstrated that total annual water demand varied between 33.04 and 49.56 million m^3 $year^{-1}$, whereas the relative dominance of the industrial and agricultural sectors remained unchanged, indicating that the principal conclusions are robust despite uncertainties in the adopted coefficients.

Finally, the ARIMA (1,1,1) forecasting model assumes that historical groundwater trends continue throughout the projection period and does not explicitly incorporate future changes in industrial development, population growth, land-use dynamics, groundwater management policies, or climate variability. Consequently, the forecasts should be interpreted as a baseline scenario rather than deterministic predictions of future groundwater conditions.

Future research should incorporate denser groundwater monitoring networks, direct groundwater abstraction records, hydroclimatic variables, land-use change, and physically based groundwater-flow models to improve the accuracy and reliability of groundwater assessments and long-term forecasts.

A further limitation is that groundwater monitoring wells were not categorized according to aquifer depth, preventing separate evaluation of groundwater-level trends in shallow and deep aquifers. Future investigations should establish depth-specific monitoring networks and undertake detailed aquifer characterization to understand vertical groundwater flow, recharge mechanisms, and the long-term sustainability of groundwater resources.

Additionally, continuous time-series data on industrial growth and groundwater abstraction were unavailable, limiting direct quantification of industrial expansion's contribution to groundwater decline. Consequently, its influence was inferred from spatial groundwater-level patterns and estimated sectoral water demand. Future studies should integrate long-term industrial development records, groundwater abstraction measurements, and depth-specific monitoring data to better distinguish the effects of anthropogenic activities and hydrogeological processes on groundwater depletion and improve the reliability of groundwater sustainability assessments in Shahjadpur Upazila.

Another limitation of this study is that seasonal groundwater dynamics were not investigated. Although quarterly and monthly groundwater observations were available, the data were aggregated into annual mean groundwater levels to facilitate consistent long-term trend analysis across the study period. As a result, seasonal recharge processes, dry-season abstraction effects, and short-term groundwater responses were not evaluated. Future studies should utilize the higher temporal resolution of the monitoring data to quantify seasonal groundwater fluctuations and recharge–abstraction dynamics.

Groundwater abstraction data

Another limitation of this study is the absence of sector-specific groundwater abstraction records for irrigation, municipal, and industrial users. Consequently, groundwater use was estimated from activity statistics and published sector-specific water-use coefficients rather than direct measurements of groundwater pumping. Although this approach provides a reasonable estimate of potential groundwater demand, it cannot fully represent the temporal and spatial variability of actual groundwater abstraction. The lack of pumping records also limits quantitative evaluation of the relationship between groundwater withdrawals and observed groundwater-level decline. Future studies should integrate groundwater abstraction records, pumping-well inventories, metered extraction data, and groundwater-use permits, where available, to improve groundwater-budget assessments, validate water-demand estimates, and quantify the contribution of different sectors to groundwater depletion.

Conclusion

This study integrated parametric, non-parametric, and geostatistical approaches to evaluate the spatiotemporal variability of groundwater levels in Shahjadpur Upazila, Sirajganj District, over a 24-year period (2000–2024). Analysis of fourteen observation wells revealed a predominant declining trend in groundwater levels, with estimated rates of decline ranging from –0.01 to –0.45 m $year^{-1}$.

Spatial interpolation using the Inverse Distance Weighting (IDW) and Kriging methods revealed pronounced east–west variations in groundwater levels, highlighting considerable spatial heterogeneity in aquifer conditions. Shallow aquifer zones adjacent to the Jamuna River appear to benefit from relatively frequent recharge through river–aquifer interactions, whereas deeper aquifers in the central and southern regions, where groundwater extraction for irrigation is intensive, exhibit substantial and persistent groundwater-level declines. These spatial patterns indicate the combined influence of hydrogeological characteristics, proximity to surface-water sources, and human-induced abstraction pressure.

The ARIMA-based forecasting results further suggest that, if existing groundwater abstraction trends continue, groundwater levels could decline by an additional 1.5–2.0 m by 2030. These projections reflect the continuation of historical groundwater-level trends

and should therefore be interpreted as a baseline scenario rather than definitive predictions. Actual future groundwater conditions may vary considerably depending on changes in climatic conditions, rainfall patterns, land-use practices, industrial development, population growth, agricultural intensification, groundwater abstraction rates, and the effectiveness of future water-management interventions.

Nevertheless, the absence of quantitative groundwater recharge estimates represents an important limitation of the present study. Consequently, it is not possible to establish conclusively whether current groundwater abstraction exceeds the aquifer's sustainable recharge capacity. Furthermore, the estimated sectoral water demands represent potential groundwater demand rather than directly measured groundwater abstraction volumes. Therefore, these estimates should be interpreted as indicative of sector-specific groundwater pressure rather than precise measurements of actual extraction. Future research should incorporate spatially distributed recharge estimation, groundwater-budget analysis, and reliable abstraction data to establish a more comprehensive understanding of aquifer sustainability.

The integration of non-parametric trend detection methods (Mann–Kendall and Sen's slope), spatial interpolation techniques (IDW and Kriging), and time-series forecasting (ARIMA) provides a complementary methodological framework for evaluating groundwater-level dynamics. This integrated approach offers considerable potential for replication in other floodplain aquifers across Bangladesh and South Asia, supporting evidence-based groundwater monitoring, water-allocation planning, and sustainable resource management. Further investigations incorporating groundwater–surface water interaction modelling, environmental isotopic tracing, numerical groundwater-flow simulation, and climate-change scenario analysis would strengthen predictive capabilities and provide a more robust scientific basis for developing long-term groundwater management strategies.

Despite the robust analytical framework employed, this study has several limitations. The analysis is based on groundwater-level records from 14 observation wells, which may not fully capture local-scale spatial variability. The statistical trend analyses and geostatistical interpolation rely on assumptions that may introduce uncertainty into the estimated groundwater patterns. Furthermore, the ARIMA forecasts assume that historical groundwater dynamics will continue into the future and do not explicitly account for changes in climate, land use, or groundwater abstraction. Therefore, the forecasted groundwater levels should be interpreted as plausible future scenarios rather than precise predictions. Future studies should incorporate denser monitoring networks, physically based groundwater models, and climate-change scenarios to improve prediction accuracy and support sustainable groundwater management.

Beyond reducing groundwater availability, continued groundwater depletion may alter river–aquifer interactions, degrade groundwater-dependent ecosystems, and increase the risk of groundwater-quality deterioration, emphasizing the need for integrated groundwater management and environmental monitoring.

Sustainable groundwater management in Shahjadpur will require coordinated implementation of managed aquifer recharge, water-efficient irrigation practices, industrial water conservation, protection of natural recharge zones, and strengthened groundwater monitoring and regulation.

Future groundwater management should prioritize depth-specific monitoring to evaluate whether groundwater depletion is confined to shallow aquifers or is progressively affecting deeper groundwater resources that are critical for long-term water-supply security. Future research should investigate seasonal groundwater dynamics using the available monthly monitoring records to improve understanding of recharge processes and seasonal groundwater management.

Future groundwater assessments should incorporate sector-specific groundwater abstraction records to improve groundwater-budget analyses and strengthen the quantitative evaluation of groundwater sustainability.

Acknowledgments

Special thanks to two anonymous reviewers for their comments and suggestions, which helped to rectify the manuscript. The author also expresses sincere gratitude to University of Rajshahi for its continuous support.

Author contributions

Data analysis and the preparation of the initial manuscript were conducted by Md. Nazmul Islam Hasan. Khondaker Emamul Haque contributed through conceptualization, supervision, and visualization. Shamim Ahmed led the software-related efforts, while Md Mahedi Hasan also revised the article. All authors reviewed the final manuscript.

Funding statement

No specific grants were provided for this research by public, commercial, or not-for-profit organizations.

Data availability

The data that support the findings of this study are accessible by contacting the corresponding author.

Declarations

The authors state that there are no conflicts of financial interest or personal relationships that could have impacted the results or interpretation of this study.

Article note

This article is a full-length paper developed from **Extended Abstract #116**, entitled "**Evaluation of Groundwater Level Fluctuation and Its Effects on Industries in Shahjadpur, Sirajganj, Bangladesh**" which was presented at the 15th Asian Regional Conference of the International Association for Engineering Geology and the Environment (ARC-15 of **IAEG**), held in Kathmandu, Nepal, from 27 to 29 November 2025.

References

Alsumaiei, A. A. (2020). A nonlinear autoregressive modeling approach for forecasting groundwater level fluctuation in urban aquifers. Water, 12(3), 820. https://doi.org/10.3390/w12030820

Berke, O. (1999). Estimation and prediction in the spatial linear model. Water, Air and Soil Pollution, 110, 215–237. https://doi.org/10.1023/A:1005035509922

Box, G. E. P., and Jenkins, G. M. (1976). Time series analysis: Forecasting and control. Holden-Day, San Francisco.

Cay, T., and Uyan, M. (2009). Spatial and temporal groundwater level variation: Geostatistical modeling in the city of Konya, Turkey. Water Environment Research, 81, 2460–2470. https://doi.org/10.2175/106143009X442961

de Silva, S., Jirasinha, R., Mondal, M. S., and McCartney, M. P. (2024). Policy and institutional study on the strategic role of water storage in Bangladesh. https://doi.org/10.5337/2025.206

Edmunds, W. M., Ahmed, K. M., and Whitehead, P. G. (2015). A review of arsenic and its impacts in groundwater of the Ganges–Brahmaputra–Meghna Delta, Bangladesh. Environmental Science: Processes and Impacts, 17(6), 1032–1046. https://doi.org/10.1039/c4em00673a

Faruqa, N. N., Kamal, M. A., Jabeen, S., and Hossain, F. (2025). 3-D voxel modeling of near-surface sediments: Insights into depositional environments and geotechnical properties - A case study of Barishal Town and its surroundings, Bangladesh. Asian Journal of Engineering Geology, 2(Special Issue), 67–70. https://doi.org/10.64862/ajeg.2025.2sp.32.130

Fahim, A. K. F., Kamal, A. M., and Shahid, S. (2023). Spatiotemporal change in groundwater sustainability of Bangladesh and its major causes. Stochastic Environmental Research and Risk Assessment, 37(2), 665–680. https://doi.org/10.1007/s00477-022-02294-z

Gleeson, T., Wada, Y., Bierkens, M. F. P., and van Beek, L. P. H. (2012). Water balance of global aquifers revealed by groundwater footprint. Nature, 488, 197–200. https://doi.org/10.1038/nature11295

Goovaerts, P. (1997). Geostatistics for natural resources evaluation. Oxford University Press, New York.

Hamed, K. H., and Rao, A. R. (1998). A modified Mann–Kendall trend test for autocorrelated data. Journal of Hydrology, 204(1–4), 182–196. https://doi.org/10.1016/S0022-1694(97)00125-X

Haque, S. E., Snigdho, F. S., and Tasneem, N. (2025). Water sustainability: a review of advances in water quality management technologies. Computational Automation for Water Security, 195-214. https://doi.org/10.1016/B978-0-443-33321-7.00018-4

He, L., Liu, J., Lei, S., and Chen, L. (2023). A hybrid coupling model of groundwater level simulation considering hydrogeological parameter: A case study of Nantong City in Eastern China. Water Supply, 23(10), 4286–4302. https://doi.org/10.2166/ws.2023.248

Helsel, D. R., Hirsch, R. M., Ryberg, K. R., Archfield, S. A., and Gilroy, E. J. (2020). Statistical methods in water resources. USGS Techniques and Methods, Book 4. https://doi.org/10.3133/tm4A3

Hirsch, R. M., Slack, J. R., and Smith, R. A. (1982). Techniques of trend analysis for monthly water quality data. Water Resources Research, 18, 107–121. https://doi.org/10.1029/WR018i001p00107

Hyndman, R. J., and Athanasopoulos, G. (2018). Forecasting: Principles and practice. OTexts, Melbourne.

Jha, S., Das, V. K., Debnath, K., Chaudhuri, S., and Banerjee, S. (2025). Assessment of the planform evolution of the Lower Ganga River: Meander migration and the causative factors. Journal of Earth System Science, 134(4), 236. https://doi.org/10.1007/s12040-025-02696-x

Johnston, K., Van Hoef, J. M., Krivoruchko, K., and Lucas, N. (2001). Using ArcGIS geostatistical analyst. ESRI Press, Redlands, CA.

Júnez-Ferreira, H. E., Hernández-Hernández, M. A., Herrera, G. S., González-Trinidad, J., Cappello, C., Maggio, S., and De Iaco, S. (2023). Assessment of changes in regional groundwater levels through spatio-temporal kriging: Application to the southern Basin of Mexico aquifer system. Hydrogeology Journal, 31(6), 1405–1423. https://doi.org/10.1007/s10040-023-02681-y

Kiss, S., Nemes-Kókai, Z., Bácsi, I., Lukács, Á., Márton, K., T-Krasznai, E., Borics, G., Stenger-Kovács, C.,

Szeles, J., Török, P., and B-Béres, V. (2025). Structure and biodiversity of benthic diatoms shaped by water availability in streams of the Pannonian Ecoregion. Global Ecology and Conservation, 62, e03858. https://doi.org/10.1016/j.gecco.2025.e03858

Kumar, P. S., Suganya, S., Srinivas, S., Priyadharshini, S., Karthika, M., Karishma Sri, R., ... and Lichtfouse, E. (2019). Treatment of fluoride-contaminated water. A review. Environmental Chemistry Letters, 17(4), 1707-1726. https://doi.org/10.1007/s10311-019-00906-9

MacDonald, A. M., Bonsor, H. C., Ahmed, K. M., Burgess, W. G., Basharat, M., Calow, R. C., Dixit, A., Foster, S. S. D., Gopal, K., Lapworth, D. J., Lark, R. M., Moench, M., Mukherjee, A., Rao, M. S., Shamsudduha, M., Smith, L., Taylor, R. G., Tucker, J., Steenbergen, F., and Yadav, S. K. (2016). Groundwater quality and depletion in the Indo-Gangetic Basin mapped from in situ observations. Nature Geoscience, 9(10), 762–766. https://doi.org/10.1038/ngeo2791

Mahammad, S., Islam, A., Das, B. C., Sarkar, B., Islam, A. R. M. T., and Pal, S. C. (2026). Modelling extraction-induced water table decline and potential relationship with arsenic mobilization in the Western Bengal Delta. Theoretical and Applied Climatology, 157(7), 443. https://doi.org/10.1007/s00704-026-06320-w

Mann, H. B. (1945). Nonparametric tests against trend. Econometrica, 13, 245–259. https://doi.org/10.2307/1907187

Mondal, B. K., Sahoo, S., Das, R., Mishra, P. K., Abdelrahman, K., Acharya, A., Lee, M. A., Tiwari, A., and Fnais, M. S. (2022). Assessing groundwater dynamics and potentiality in the Lower Ganga Plain, India. Water, 14(14), 2180. https://doi.org/10.3390/w14142180

Monir, M. M., Sarker, S. C., and Islam, M. N. (2024). Assessing the changing trends of groundwater level with spatiotemporal scale at the northern part of Bangladesh integrating the MAKESENS and ARIMA models. Modeling Earth Systems and Environment, 10(1), 443–464. https://doi.org/10.1007/s40808-023-01794-3

Mustapha, A. (2013). Detecting surface water quality trends using Mann–Kendall tests and Sen's slope estimates. International Journal of Advanced Research, 1, 108–114.

Obaje, N. G. (2009). Geology and mineral resources of Nigeria. Lecture Notes in Earth Sciences, Vol. 120. Springer, Berlin and Heidelberg. https://doi.org/10.1007/978-3-540-92685-6

Pearson, K. (1895). Contributions to the mathematical theory of evolution. II. Skew variation in homogeneous material. Philosophical Transactions of the Royal Society of London. Series A, 186, 343-414.https://doi.org/10.1098/rsta.1895.0010

Prasad, S., Saluja, R., Joshi, V., and Garg, J. K. (2020). Heavy metal pollution in surface water of the Upper Ganga River, India: human health risk assessment. Environmental Monitoring and Assessment, 192(11), 742. https://doi.org/10.1007/s10661-020-08701-8

Rahman, A., Kumar, P., and Dominguez, F. (2022). Increasing freshwater supply to sustainably address global water security at scale. Scientific Reports, 12(1), 20262. https://doi.org/10.1038/s41598-022-24314-2

Ribeiro, L., and Macedo, M. E. (1995). Application of multivariate statistics, trend and cluster analysis to groundwater quality in the Tejo and Sado aquifer. IAHS Publications, 225, 39–48.

Rodell, M., Famiglietti, J. S., Wiese, D. N., Reager, J. T., Beaudoing, H. K., Landerer, F. W., and Lo, M. H. (2018). Emerging trends in global freshwater availability. Nature, 557(7707), 651–659. https://doi.org/10.1038/s41586-018-0123-1

Sen, P. K. (1968). Estimates of the regression coefficient based on Kendall's tau. Journal of the American Statistical Association, 63, 1379–1389. https://doi.org/10.1080/01621459.1968.10480934

Shah, T. (2007). The groundwater economy of South Asia: an assessment of size, significance and socio-ecological impacts. The agricultural groundwater revolution: Opportunities and threats to development, 7-36.

Shamsudduha, M., Chandler, R. E., Taylor, R. G., and Ahmed, K. M. (2009). Recent trends in groundwater levels in a highly seasonal hydrological system: The Ganges–Brahmaputra–Meghna Delta. Hydrology and Earth System Sciences, 13(12), 2373–2385. https://doi.org/10.5194/hess-13-2373-2009

Singh, A. K., Kaur, R., Verma, S., and Singh, S. (2022). Antimicrobials and antibiotic resistance genes in water bodies: pollution, risk, and control. Frontiers in Environmental Science, 10, 830861. https://doi.org/10.3389/fenvs.2022.830861

Suter, G. W. (2008). Ecological risk assessment in the United States Environmental Protection Agency: A historical overview. Integrated environmental assessment and management, 4(3), 285-289. https://doi.org/10.1897/IEAM_2007-062.1

Taylor, R. G., Scanlon, B., Döll, P., et al. (2013). Groundwater and climate change. Nature Climate Change, 3, 322–329. https://doi.org/10.1038/nclimate1744

Tayyab, M., Aslam, R. A., Farooq, U., Ali, S., Khan, S. N., Iqbal, M., Khan, M. I., and Saddique, N. (2024). Comparative study of geospatial techniques for interpolating groundwater quality data in agricultural areas of Punjab, Pakistan. Water, 16(1), 139. https://doi.org/10.3390/w16010139

Thakur, P. K., Nikam, B. R., Srivastav, S. K., Khaing, T. W. W., Zaw, T., Garg, V., Dhote, P. R., Sharma, V., and Aggarwal, S. P. (2021). Groundwater modeling with inputs from geospatial technology for assessing the sustainability of water use in the Solani watershed, Ganga River Basin (India). Groundwater for Sustainable Development, 12, 100511. https://doi.org/10.1016/j.gsd.2020.100511

Todd, D. K., and Mays, L. W. (2005). Groundwater Hydrology. 3rd Edition, John Wiley and Sons, Inc., Hoboken, 652p.

Yue, S., and Wang, C. Y. (2002). Applicability of prewhitening to eliminate the influence of serial correlation on the Mann–Kendall test. Water Resources Research, 38(6), 4-1. https://doi.org/10.1029/2001WR000861

Zahid, A. (2022). Groundwater resources, challenges and governance in the Bengal Basin, Bangladesh. In Bangladesh geosciences and resources potential (pp. 399–436). CRC Press.

Zar, J. H. (2010). Biostatistical analysis (5th ed.). Prentice Hall, New Jersey.

Asian Journal of Engineering Geology

Volume 3, No. 1

Table of Content

Original Articles

1. **Numerical Evaluation of Post-Earthquake Stability and Rehabilitation of Mountain Trails 'Unnat Goreto' in Gorkha and Rasuwa Districts, Nepal**
   Bikash Adhikari, Ram Chandra Tiwari, and Aanchal Tiwari 1

2. **Engineering Geological Characterization and Mapping of Aleta Wondo Town for Urban Development in Southern Ethiopia**
   Deginet Tesfaye and Ephrem Getahun Gure 17

3. **Landslide Susceptibility Assessment along the Hilly Coastal Corridor of Cox's Bazar-Teknaf, Bangladesh**
   Muqit Ajmain Shahriyar, Md. Abdul Malek, Md. Younus Hider, Tasmim Banu, and Md. Mahedi Hasan 37

4. **Fuzzy Overlay-Based Groundwater Quality Assessment for Drinking and Irrigation Purposes, Hydro geochemical Evaluation and Health Risk Assessment in the Coastal Aquifer of Lakshmipur District, Bangladesh**
   Md. Mahedi Hasan, Khondaker Emamul Haque, Shamim Ahmed, and Md. Nazmul Islam Hasan 55

5. **Spatiotemporal Analysis and Forecasting of Groundwater Level Fluctuations with Sectoral Water Demand Assessment in Shahjadpur, Sirajganj, Bangladesh**
   Md. Nazmul Islam Hasan, Khondaker Emamul Haque, Shamim Ahmed, and Md. Mahedi Hasan 79

Official Journal of Nepal Society of Engineering Geology (NSEG)
Dhobighat, Lalitpur, Nepal
For Online Submission: https://ajeg.nseg.org.np